National Library of Canada
Bibliothèque nationale du Canada

Canadian Theses Service
Service des thèses canadiennes

Ottawa, Canada
K1A 0N4

NOTICE

The quality of this microform is heavily dependent upon the quality of the original thesis submitted for microfilming. Every effort has been made to ensure the highest quality of reproduction possible.

If pages are missing, contact the university which granted the degree.

Some pages may have indistinct print especially if the original pages were typed with a poor typewriter ribbon or if the university sent us an inferior photocopy.

Reproduction in full or in part of this microform is governed by the Canadian Copyright Act, R.S.C. 1970, c. C-30, and subsequent amendments.

AVIS

La qualité de cette microforme dépend grandement de la qualité de la thèse soumise au microfilmage. Nous avons tout fait pour assurer une qualité supérieure de reproduction.

S'il manque des pages, veuillez communiquer avec l'université qui a conféré le grade.

La qualité d'impression de certaines pages peut laisser à désirer, surtout si les pages originales ont été dactylographiées à l'aide d'un ruban usé ou si l'université nous a fait parvenir une photocopie de qualité inférieure.

La reproduction, même partielle, de cette microforme est soumise à la Loi canadienne sur le droit d'auteur, SRC 1970, c. C-30, et ses amendements subséquents.

NL-339 (r. 88/04) c

Canada

THE UNIVERSITY OF ALBERTA

MODEL PILE LOAD TESTS IN FROZEN SALINE SILTY SAND

by

DOUGLAS JEAN HUTCHINSON

A THESIS

SUBMITTED TO THE FACULTY OF GRADUATE STUDIES AND RESEARCH

IN PARTIAL FULFILMENT OF THE REQUIREMENTS FOR THE DEGREE

OF MASTER OF SCIENCE

CIVIL ENGINEERING

EDMONTON, ALBERTA

SPRING 1989

Permission has been granted to the National Library of Canada to microfilm this thesis and to lend or sell copies of the film.

The author (copyright owner) has reserved other publication rights, and neither the thesis nor extensive extracts from it may be printed or otherwise reproduced without his/her written permission.

L'autorisation a été accordée à la Bibliothèque nationale du Canada de microfilmer cette thèse et de prêter ou de vendre des exemplaires du film.

L'auteur (titulaire du droit d'auteur) se réserve les autres droits de publication; ni la thèse ni de longs extraits de celle-ci ne doivent être imprimés ou autrement reproduits sans son autorisation écrite.

ISBN 0-315-52818-4

THE UNIVERSITY OF ALBERTA

RELEASE FORM

NAME OF AUTHOR DOUGLAS JEAN HUTCHINSON

TITLE OF THESIS MODEL PILE LOAD TESTS IN FROZEN SALINE SILTY SAND

DEGREE FOR WHICH THESIS WAS PRESENTED MASTER OF SCIENCE

YEAR THIS DEGREE GRANTED SPRING 1989

Permission is hereby granted to THE UNIVERSITY OF ALBERTA LIBRARY to reproduce single copies of this thesis and to lend or sell such copies for private, scholarly or scientific research purposes only.

The author reserves other publication rights, and neither the thesis nor extensive extracts from it may be printed or otherwise reproduced without the author's written permission.

(SIGNED) D. Jean Hutchinson

PERMANENT ADDRESS:

105 WILLIAM ST W.

WATERLOO ONTARIO

N2L 1J8

DATED OCTOBER 14 1988

THE UNIVERSITY OF ALBERTA

FACULTY OF GRADUATE STUDIES AND RESEARCH

The undersigned certify that they have read, and recommend to the Faculty of Graduate Studies and Research, for acceptance, a thesis entitled MODEL PILE LOAD TESTS IN FROZEN SALINE SILTY SAND submitted by DOUGLAS JEAN HUTCHINSON in partial fulfilment of the requirements for the degree of MASTER OF SCIENCE.

.....

Supervisor

.....

.....

.....

Date..OCTOBER..14,1988.....

Abstract

The presence of saline pore fluid in frozen soils leads to a significant reduction in the resistance of the soil to load. Data from laboratory tests and field pile load tests in frozen saline soils is limited, so that the design of piles in such soils is quite tenuous.

Model pile load tests were undertaken to define some general trends in the behaviour of these soils. The effect of changing pore fluid salinity, temperature and magnitude of load upon the time dependent deformation of model piles in frozen silty sand was examined. The tests were designed to simulate the conditions encountered at such sites as Pond Inlet, Tuktoyaktuk, Pangnintung and Eskimo Point.

The analysis of the test results predicts the long term adfreeze resistance of piles in this soil at -5°C, using the Vyalov (1962) equation, and Weaver's correlation with shear strength from uniaxial compression tests.

Current theory predicts that saline ice-poor soils will exhibit time dependent behaviour similar to that of an ice-rich material. Therefore Nixon and Lem (1984) propose that the design of piles in saline frozen soils be based upon a flow law relating pile velocity to an applied stress. This theory was used to predict the behaviour of the model piles under load for each given salinity and temperature. The normalized pile velocities determined from this study are much higher than those predicted by Nixon and Lem (1984) from the results of their laboratory compression tests on

similar soils. The results of field load tests of piles installed in native saline soil backfill reported by Nixon (1988), match the model pile data very well. On the other hand, a comparison to limited field pile load test data in sand slurry indicates that the model piles may overestimate the resistance of full scale piles.

The results of the testing indicate that the frozen saline soil behaves as a 'structured soil': generally showing no time dependent response to load until the application of the failure stress. Therefore analysis of the data using the flow law for ice-rich soils alone is inappropriate. Soils of this type should be analysed using a theory which accounts for the elastic response to load, followed by creep failure at the higher stresses.

It is evident from the results that the presence of saline pore fluid drastically reduces the strength of the soil, particularly at temperatures between -5 and -8°C.

Acknowledgements

The author would like to thank Dr. D. Sego for his invaluable guidance, support and patience during the work on this thesis.

The excellent suggestions and work by Gerry Cyre, Steve Gamble, and Christine Hurley made the laboratory portion of this work run as smoothly as possible.

My parents provided a great deal of love, moral support and guidance, without which this work would have been much more difficult.

Special thanks are due to Elisabeth Hivon for her tremendous friendship and support and for her half of the frequent brainstorming sessions both technical and personal.

The friendship, help and sense of humour of my fellow graduate students and their wives is very much appreciated as well.

Finally thanks are due to NSERC for personal funding for this thesis.

Table of Contents

Chapter		Page
1.	Introduction	1
	1.1 General	1
	1.2 Scope of the thesis	3
2.	Frozen Soil Strength and Creep Behaviour	4
	2.1 Introduction	4
	2.2 Creep Deformation	5
	2.2.1 Microscopic Soil Behaviour	6
	2.2.2 Unfrozen Water Content	9
	2.3 Creep Deformation Equations	14
	2.3.1 Unified Creep Models	17
	2.3.2 Primary Creep Equations	21
	2.3.3 Secondary Creep Equations	24
	2.3.3.1 Minimum Strain Rate	27
	2.3.4 Tertiary Creep Equations	28
	2.3.5 Conclusions	29
3.	A Review of Current Research and Theory for the Design of Piles in Permafrost	35
	3.1 Introduction	35
	3.2 Pile Velocity Equations	36
	3.3 Piles in non-Saline Ice-Poor Permafrost	39
	3.4 Piles in non-Saline Ice-Rich Permafrost	42
	3.5 Piles in Saline Permafrost	46
4.	Laboratory Procedure for Testing of Model Piles	52
	4.1 Test Objectives	52
	4.2 Material Preparation	52
	4.3 Description of Apparatus	53
	4.4 Test Procedure	57

4.4.1 Preparation of Model Pile and Apparatus ..58

4.4.2 Preparation of Frozen Saline Soil Sample .58

4.4.3 Testing of the Model Piles 60

5. Analysis of the Model Pile Creep Test Results 66

5.1 Presentation and Discussion of Test Results 66

5.1.1 Time dependent deformation 66

5.1.2 Consolidation 67

5.1.3 Density and Salinity measurements 68

5.2 Presentation and Discussion of Analysis of Test Results 70

5.2.1 Basic test parameters 71

5.2.2 Pile Velocity equations 72

5.2.2.1 Best fit curves 73

5.2.2.2 Determination of B for n=3 and n=5 75

5.2.2.3 Comparison to other test data 76

5.2.2.4 Influence of Salinity and Temperature on the parameters B and n 78

5.2.3 Prediction of Phase Composition Curves ...79

5.2.4 Relationship between failure pile shaft stress and time to failure 81

5.2.5 Relationship between adfreeze strength and unconfined compressive strength 83

5.2.6 Hereditary creep 84

5.3 Summary 87

6. Conclusions and Recommendations 126

6.1 Conclusions 126

6.2 Recommendations 127

7. Bibliography 129

A. *Appendix A*
Test results 141

B. *Appendix B*
Photographs 214

C. *Appendix C*
Detailed Laboratory Procedure for Testing of Model Piles 218

C.1 Introduction 218

C.2 Material Preparation 218

C.2.1 Dry Soil Preparation 218

C.2.2 Wet Soil Preparation 218

C.2.3 Pile Preparation 218

C.3 Bucket Preparation 219

C.4 Soil Placement 219

C.5 Consolidation 219

C.6 Freezing 220

C.7 Establishing Temperature Equilibrium 220

C.8 Loading 221

C.9 Removal of Frozen Soil 221

C.10 Measurement of Soil Characteristics 222

List of Tables

Table		Page
5.1	Results of model pile creep tests in frozen silty sand	88
5.2	Creep parameters from best fit lines for saline silty sand	90
5.3	Relationship between normalized pile velocity and shaft stress from best fit lines for saline silty sand at -5°C	91
5.4	Creep parameters for saline silty sand	92
5.5	Relationship between normalized pile velocity and shaft stress for n=5 for saline silty sand at -5°C	93
5.6	Prediction of parameters B and β for the Vyalov equation	94
5.7	Allowable pile shaft stress for piles in saline silty sand at -5°C for 25 year design life using the Vyalov method.	95
5.8	Data from unconfined compression (Hivon, 1988) and model pile load tests on saline silty sand at -5°C	96
5.9	Determination of parameter m from unconfined compressive strength and adfreeze strength testing of silty sand at -5°C	97
A.1	Density and Salinity measurements for frozen silty sand	142
A.2	Roughness profiles of the sand blasted model piles	144

List of Figures

Figure		Page
2.1	Typical creep curve, after Ladanyi (1972).	31
2.2	Creep behaviour of frozen soil, after Ting (1983b).	32
2.3	Position of unfrozen water within a single pore space, after Sheeran and Yong (1975).	33
2.4	Incremental load tests, after Ladanyi (1972).	34
3.1	Shearing of concentric rings, after Nixon and McRoberts (1976).	51
4.1	Grain size distribution	62
4.2	Schematic layout of model pile testing apparatus.	63
4.3	Dimensions of the cell in centimetres	64
4.4	Freezing apparatus	65
5.1	Summary of pile shaft stress and normalized pile velocity results from constant load tests of sand blasted model piles in frozen silty sand	98
5.2	Pile shaft stress to normalized pile velocity results from constant load tests of sand blasted model piles in silty sand at -13°C	99
5.3	Pile shaft stress to normalized pile velocity results from constant load tests of sand blasted model piles in silty sand at -10°C	100
5.4	Pile shaft stress to normalized pile velocity results from constant load tests of sand blasted model piles in silty sand at -5°C	101
5.5	The relationship between the parameter n and salinity for sand at -7°C, Sego et al, 1982, and silty sand at -5°C	102

Figure Page

5.6 Determination of parameter B for n=3 and n=5 from results of constant load tests of sand blasted model piles in silty sand at -13°C 103

5.7 Determination of parameter B for n=3 and n=5 from results of constant load tests of sand blasted model piles in silty sand at -10°C 104

5.8 Determination of parameter B for n=3 and n=5 from results of constant load tests of sand blasted model piles in silty sand at -5°C 105

5.9 Relationship between the parameter B and salinity for silty sand with n=3 106

5.10 Relationship between the parameter B and temperature for silty sand with n=3 107

5.11 Relationship between the parameter B and salinity for silty sand with n=5 108

5.12 Relationship between the parameter B and temperature for silty sand with n=5 109

5.13 Relationship between the parameter B, salinity and temperature for n=3, after Nixon and Lem (1984) 110

5.14 Pile shaft stress to normalized pile velocity results from saline silty sand; from uniaxial compression tests, after Nixon and Lem (1984), and from model pile load tests 111

5.15 Pile shaft stress to normalized pile velocity from constant displacement rate tests on sand backfilled sand blasted model piles at -5 to -6 degrees C (Parameswaran, 1978 and Thurber, 1988) 112

5.16 Pile shaft stress to normalized pile velocity results from field load tests on piles backfilled with sand slurry, after Hoggan (1985), Nixon (1988), and Thurber (1983) 113

Figure Page

5.17 Pile shaft stress to normalized pile velocity from constant load tests on sand blasted model piles in silty sand of salinity 5 ppt. Parameter n assumed to be 5. 114

5.18 Pile shaft stress to normalized pile velocity from constant load tests on sand blasted model piles in silty sand of salinity 10 ppt. Parameter n assumed to be 5. 115

5.19 Pile shaft stress to normalized pile velocity from constant load tests on sand blasted model piles in silty sand of salinity 15 ppt. Parameter n assumed to be 5. 116

5.20 Liquid limit flow curve for non-saline silty sand 117

5.21 Unfrozen water content versus temperature for non-saline silty sand, determined from liquid limit tests, using the method of Tice et al (1976). 118

5.22 Unfrozen water content versus temperature for non-saline silty sand, using data determined from liquid limit tests, and the methods of Tice et al (1976), and Patterson and Smith (1983). 119

5.23 Relationship between the inverse pile shaft stress and the time to failure for silty sand at -5°C 120

5.24 Prediction of the ultimate pile shaft stress for silty sand at -5°C, using the Vyalov method, and time to minimum data 121

5.25 Prediction of the ultimate pile shaft stress for silty sand at -5°C, using the Vyalov method, and time to onset of tertiary data 122

5.26 Prediction of pile shaft stress for model piles in saline silty sand at -5°C for a minimum strain rate of 0.027 (mm/min). Best fit lines and fitted for parameter n = 5. 123

Figure Page

5.27 Pile shaft stress to normalized pile velocity from constant load tests on sand blasted model piles in silty sand. Data from single load tests and the last load step of incremental tests. 124

5.28 Pile shaft stress to normalized pile velocity from constant load tests on sand blasted model piles in silty sand. Data from single load tests. 125

A.1 Temperature, stress and displacement data for sample 1.1: fresh water silty sand at -13°C 145

A.2 Temperature, stress and displacement data for sample 1.2: silty sand of salinity 5 ppt at -13°C 146

A.3 Temperature, stress and displacement data for sample 1.3: silty sand of salinity 10 ppt at -12.5°C 147

A.4 Temperature, stress and displacement data for sample 1.4: silty sand of salinity 15 ppt at -12°C 148

A.5 Temperature, stress and displacement data for sample 1.5: silty sand of salinity 15 ppt at -12°C 149

A.6 Temperature, stress and displacement data for sample 2.1: fresh water silty sand at -10°C 150

A.7 Temperature, stress and displacement data for sample 2.2: silty sand of salinity 5 ppt at -10°C 151

A.8 Temperature, stress and displacement data for sample 2.3: silty sand of salinity 10 ppt at -10°C 152

A.9 Temperature, stress and displacement data for sample 2.4: silty sand of salinity 10 ppt at -10°C 153

A.10 Temperature, stress and displacement data for sample 2.5: silty sand of salinity 15 ppt at -10°C 154

Figure Page

A.11 Temperature, stress and displacement data for sample 2.6: silty sand of salinity 15 ppt at -10°C 155

A.12 Temperature, stress and displacement data for sample 3.1: fresh water silty sand at -5.1°C 156

A.13 Temperature, stress and displacement data for sample 3.2: silty sand of salinity 5 ppt at -5°C 157

A.14 Temperature, stress and displacement data for sample 3.3: silty sand of salinity 10 ppt at -5°C 158

A.15 Temperature, stress and displacement data for sample 3.4: silty sand of salinity 10 ppt at -5°C 159

A.16 Temperature, stress and displacement data for sample 3.5: silty sand of salinity 15 ppt at -5°C 160

A.17 Temperature, stress and displacement data for sample 3.6: silty sand of salinity 15 ppt at -5°C 161

A.18 Temperature, stress and displacement data for sample 4.1: silty sand of salinity 5 ppt at -4.7°C 162

A.19 Temperature, stress and displacement data for sample 4.2: silty sand of salinity 5 ppt at -4.8°C 163

A.20 Temperature, stress and displacement data for sample 4.3: silty sand of salinity 10 ppt at -4.7°C 164

A.21 Temperature, stress and displacement data for sample 4.4: silty sand of salinity 10 ppt at -4.6°C 165

A.22 Temperature, stress and displacement data for sample 4.5: silty sand of salinity 15 ppt at -4.6°C 166

A.23 Temperature, stress and displacement data for sample 4.6: silty sand of salinity 15 ppt at -4.6°C 167

Figure Page

A.24 Pile displacement with time for sample 1.1: fresh water silty sand at -13°C 168

A.25 Pile displacement with time for sample 1.2: silty sand of salinity 5 ppt at -13°C 169

A.26 Pile displacement with time for sample 1.3: silty sand of salinity 10 ppt at -12.5°C 170

A.27 Pile displacement with time for sample 1.4: silty sand of salinity 15 ppt at -12°C 171

A.28 Pile displacement with time for sample 1.5: silty sand of salinity 15 ppt at -12°C 172

A.29 Pile displacement with time for sample 2.1: fresh water silty sand at -10°C 173

A.30 Pile displacement with time for sample 2.2: silty sand of salinity 5 ppt at -10°C 174

A.31 Pile displacement with time for sample 2.3: silty sand of salinity 10 ppt at -10°C 175

A.32 Pile displacement with time for sample 2.4: silty sand of salinity 10 ppt at -10°C 176

A.33 Pile displacement with time for sample 2.5: silty sand of salinity 15 ppt at -10°C 177

A.34 Pile displacement with time for sample 2.6: silty sand of salinity 15 ppt at -10°C 178

A.35 Pile displacement with time for sample 3.1: fresh water silty sand at -5.1°C 179

A.36 Pile displacement with time for sample 3.2: silty sand of salinity 5 ppt at -5°C 180

A.37 Pile displacement with time for sample 3.3: silty sand of salinity 10 ppt at -5°C 181

Figure Page

A.38 Pile displacement with time for sample 3.4: silty sand of salinity 10 ppt at -5°C 182

A.39 Pile displacement with time for sample 3.5: silty sand of salinity 15 ppt at -5°C 183

A.40 Pile displacement with time for sample 3.6: silty sand of salinity 15 ppt at -5°C 184

A.41 Pile displacement with time for sample 4.1: silty sand of salinity 5 ppt at -4.7°C 185

A.42 Pile displacement with time for sample 4.2: silty sand of salinity 5 ppt at -5°C 186

A.43 Pile displacement with time for sample 4.3: silty sand of salinity 10 ppt at -4.7°C 187

A.44 Pile displacement with time for sample 4.4: silty sand of salinity 10 ppt at -4.6°C 188

A.45 Pile displacement with time for sample 4.5: silty sand of salinity 15 ppt at -4.5°C 189

A.46 Pile displacement with time for sample 4.6: silty sand of salinity 15 ppt at -4.6°C 190

A.47 Consolidation of silty sand sample 1.1 191

A.48 Consolidation of silty sand sample 1.2 192

A.49 Consolidation of silty sand sample 1.3 193

A.50 Consolidation of silty sand sample 1.4 194

A.51 Consolidation of silty sand sample 1.5 195

A.52 Consolidation of silty sand sample 2.1 196

A.53 Consolidation of silty sand sample 2.2 197

A.54 Consolidation of silty sand sample 2.3 198

A.55 Consolidation of silty sand sample 2.4 199

Figure Page

A.56 Consolidation of silty sand sample 2.5 200

A.57 Consolidation of silty sand sample 2.6 201

A.58 Consolidation of silty sand sample 3.1 202

A.59 Consolidation of silty sand sample 3.2 203

A.60 Consolidation of silty sand sample 3.3 204

A.61 Consolidation of silty sand sample 3.4 205

A.62 Consolidation of silty sand sample 3.5 206

A.63 Consolidation of silty sand sample 3.6 207

A.64 Consolidation of silty sand sample 4.1 208

A.65 Consolidation of silty sand sample 4.2 209

A.66 Consolidation of silty sand sample 4.3 210

A.67 Consolidation of silty sand sample 4.4 211

A.68 Consolidation of silty sand sample 4.5 212

A.69 Consolidation of silty sand sample 4.6 213

B.1 Consolidation of the soil 215

B.2 Application of load to the pile 216

B.3 Pile in Frozen Soil 217

List of symbols

a = pile radius.

d_f = deflection at failure.

L = embedded length of the pile.

P = load applied to the pile.

r = distance from the center of the pile.

S = nominal soil salinity.

S_m = measured soil salinity.

t = time.

t_f = time to failure.

T = temperature.

u = displacement.

u_a = pile displacment.

$\dot{u}$ = displacement rate.

$\dot{u}_a$ = pile displacement rate.

ϵ = engineering strain.

$\dot{\epsilon}$ = engineering strain rate.

$\dot{\epsilon}_c$ = proof strain rate.

ϵ_e = equivalent strain.

γ = shear strain.

$\dot{\gamma}$ = shear strain rate.

θ = temperature below freezing.

ρ_{dry} = dry density.

σ = stress applied.

σ_c = proof stress.

σ_e = equivalent stress.

σ_m = mean stress.

σ_u = ultimate compressive stress.

τ = shear stress.

τ_a = applied shaft stress or adfreeze strength of the pile.

τ_{lt} = long term adfreeze strength.

τ_u = unconfined compressive shear strength.

1. Introduction

1.1 General

Design of piles in saline permafrost is a key concern for Arctic construction. Until recently the drastic reduction of frozen soil strength due to the presence of saline pore fluid was not fully appreciated. Consequently pile load tests conducted in the Arctic have not been supported by determination of the salinity of the soil pore fluid in most cases. In addition results from laboratory investigations of the creep behaviour of saline frozen soils are fairly limited. Due to this lack of data, constitutive relationships are poorly defined, and piles in saline permafrost have been designed using methods for piles in fresh water soils with a large factor of safety being applied. Nixon and Lem (1984) discovered that the creep rate of frozen soil may be increased as much as 10 to 100 times by the presence of saline pore water fluid in concentrations equal to or less than that of sea water. Field pile load tests in saline permafrost reported by Nixon (1988) provided an allowable pile shaft stress one half to one third that predicted by non-saline pile theory.

Model pile testing is undertaken in this research to define some general trends in the creep behaviour of piles loaded under different combinations of salinity and temperature within the ranges commonly encountered in the Arctic. Model testing provides preliminary results generated

in a controlled environment, free of much of the expense and difficulties of field testing. Eventually the laboratory observations must be compared with results from field pile load tests in saline permafrost to provide practical design guidelines.

The objective of this thesis is to measure the effects of changing temperature, pore fluid salinity and magnitude of load upon the creep behaviour of model steel piles. The thesis describes a series of tests designed to simulate the conditions encountered at such sites as Pond Inlet, Tuktoyaktuk, Pangnintung and Eskimo Point. The results of these tests are analysed using current theories (Nixon and Lem, 1984, Nixon and Neukirchner, 1985, and Neukirchner, 1985) which assume that the behaviour of saline ice-poor soils is similar to the time dependent deformation of ice-rich soils. The results are compared with recently reported laboratory and field data. The validity of theories predicting ultimate strength proposed by Weaver (1979) and Vyalov (1962) are examined as well. The thesis is also useful for the discussion of model pile test apparatus, and the exploration of the feasibility of model pile tests for this type of comparative study of creep and strength behaviour.

1.2 Scope of the thesis

The creep behaviour of frozen soils is examined in Chapter 2. The physical mechanisms controlling deformation are discussed, and the creep and strength theories arising from laboratory testing are presented.

Current research and guidelines for the design of piles in permafrost are reviewed in Chapter 3. Piles in non-saline and saline soils are discussed separately. Laboratory creep and model pile test results are discussed. Current pile design guidelines for permafrost are examined.

The laboratory testing program undertaken for this thesis is discussed in Chapter 4. The materials, apparatus and test procedure are outlined.

The results of the laboratory tests are summarized in Chapter 5. The methods of analysis of the deformation time data are discussed and an interpretation provided of the effects of temperature, salinity and magnitude of load upon the time dependent deformation of model piles in frozen soil. The applicability of the theory of hereditary creep is examined as well.

Conclusions drawn from the model pile testing are presented in Chapter 6. The results of this testing are discussed with respect to the design of piles in saline permafrost. Recommendations for further study leading to the development of a set of realistic design guidelines are presented.

2. Frozen Soil Strength and Creep Behaviour

2.1 Introduction

Pile design methods for permafrost evolve from a combination of laboratory testing and field observations. The expense of field pile testing is often prohibitive while laboratory tests provide an inexpensive convenient method of examining the creep or strength behaviour of frozen soils. Laboratory test results indicate the trends in material behaviour, which must be verified by field results.

Laboratory strength and deformation testing may take one of several forms, with either a constant displacement rate or a constant stress being applied to a frozen soil sample under uniaxial or multiaxial stress conditions. Model pile tests can also be conducted using these test configurations. Creep tests conducted for this thesis consisted of the application of a constant load to a model pile while monitoring the pile displacement with time.

This chapter reviews the literature which describes the mechanics of deformation of frozen soil and the methods used to analyse the results of laboratory tests on frozen soils. These topics are discussed for both non-saline and saline soils. Extensive literature discussing non-saline frozen soil is available, while investigations of saline frozen soil characteristics have been undertaken only recently. Theories specific to the design of piles in permafrost will be outlined in Chapter 3.

2.2 Creep Deformation

The time dependent deformation of permafrost under load can be described in two ways. Ladanyi (1972) suggested that the creep progresses through three stages: primary or decelerating, secondary or steady state, and tertiary or accelerating creep. The failure of a frozen soil can be defined as the end of the secondary regime, when the creep begins to accelerate, as shown in Figure 2.1. More recently, Ting et al (1983) indicated that the creep goes through an inflection point at the transition from decelerating to accelerating creep. Failure is defined as point where the minimum strain rate is observed, as in Figure 2.2. Further discussion of these definitions is made in Section 2.3.3.

Many theories have been proposed to describe the behaviour of frozen materials under load. Micromechanistic theories describing the creep of crystals in metal have been developed. The creep of these materials is similar to that observed in frozen soil. Therefore phenominalogical models for soil based upon such micromechanistic theories were presented by Vyalov (1962) and Ladanyi (1972). Ladanyi (1972) suggests that micromechanistic theories are valid for intermediate and high levels of stress, while the phenominalogical models are valid for low or intermediate stress levels.

2.2.1 Microscopic Soil Behaviour

Frozen soil is composed of water, ice, gas and the mineral soil grain. Saline soils also contain dissolved salts in the pore fluid. The response of individual constituent materials of the frozen soil to load has been discussed by several authors in an attempt to understand the microscopic physical behaviour of frozen soil as it contributes to the macroscopically observed creep and strength characteristics.

Roggensack and Morgenstern (1978) discuss the response of a frozen soil sample to load. They state that the strength of the ice matrix must be overcome before any strain of the sample is observed. Gradual deformation of the soil and ice permits frictional strength to be mobilized at the soil particle contacts. Under long term loading conditions, time dependent deformation causes the resistance of the ice to diminish, and the applied stress is carried solely by the particle contacts.

Weaver (1979) discusses the geotechnical properties of both ice and frozen soil, A sample of ice under load will exhibit an instantaneous elastic response, followed by time dependent plastic deformations in the three creep regimes. Where the ice has large crystals, deformation is governed by the mobility of dislocations within their glide planes. Crystal boundaries are obstacles to this dislocation movement so reductions in crystal size result in reductions of the creep rate. In fine grained ice, creep is dominated

by a diffusional process.

When soil is added to the ice, the creep mechanisms may be completely changed. In general the soil particles reduce the creep rate by impeding dislocation movement and causing reductions in the average grain size of the ice crystals. The creep mechanism of warm fine grained permafrost soils is further complicated by the presence of unfrozen water within the pore space (Weaver, 1979).

The physical process of creep can be explained through consideration of a fluid phase transport model. Load applied to frozen soil creates stress concentrations at the contact between the soil particle and the pore ice, leading to pressure melting of the ice. The melted pore fluid then migrates to areas of lower stress where it refreezes. For additional details, the reader is referred to Parameswaran (1980), Yuanlin et al (1983), and Orth and Meissner (1982).

Recrystallization of ice and the development of a preferred crystal fabric contribute to the creep deformation of the frozen material as well. Sego and Morgenstern (1983) suggest that under load the basal plane of each crystal in a pure ice sample becomes aligned with the direction of the shear stress. The ice becomes increasingly more deformable as total strain increases due to this gradual crystal realignment. Deformation within single ice crystals is much faster if the shear stress is aligned parallel to the basal plane. They observed that the majority of the strain occurs in the primary creep zone and the resistance of the ice to

deformation under load reduces beyond about one percent accumulated strain, reaching a constant resistance beyond ten percent strain.

Primary creep is observed while there is movement of the unfrozen water through the soil (Yuanlin et al, 1983) and while the soil pores are compressing due to the closure of microscopic cracks, size reduction of open cavities and irreversible shear of particles relative to one another (Tsytovich, 1975). In this phase, the load is largely supported by the pore ice. Secondary creep is associated with pressure melting and recrystallization of the ice (Yuanlin et al, 1983) and reorientation of the soil grains (Parameswaran, 1980 and Tsytovich, 1975). The long term deformation behaviour of the soil is influenced by the migration of ice toward the shear induced fabric in the soil (Roggensack and Morgenstern, 1978). Weaver and Morgenstern (1981) attribute primary creep to deformation in the mineral layers and secondary creep to the behaviour of the ice component of the soil.

Goughnour and Andersland (1968) compared the strengths of a pure ice sample and a sand ice sample. They propose that the addition of sand to ice creates a strength increase for several reasons. Sand particles are not deformable under the loads considered, so a larger deformation rate is imposed on the ice matrix. In addition, strength is provided by the friction at the contacts between the soil grains and the prevention of dilation of the sand grains by the ice

matrix.

Ting et al (1983) note that some of these strength mechanisms for frozen sand apply to frozen fine grained soil which has not been subjected to segregational freezing, in which case it can be assumed that the particle to particle contacts are maintained. The strength developed comes from the ice, soil and structural hindrance between the soil and ice matrix. Roggensack (1977) and Ting et al (1983) suggest that during creep deformation the frictional component of strength remains the same while the cohesive component decreases with time.

2.2.2 Unfrozen Water Content

In general the creep response of a frozen soil is dependent upon the ice content, the amount of unfrozen water, the temperature, the stress applied, the length of time since the application of load, and the soil type. All other test conditions being the same, the difference in the creep behaviour of saline and non-saline soils can be attributed to the enhanced unfrozen water content of saline soils. Berggren and Furuberg (1985) stated that the unfrozen water content defines the temperature dependency of the creep of frozen soils. Ogata et al (1983) observed from uniaxial creep testing of frozen sands that an increase in the volume ot the unfrozen water due to the presence of salt in the pore fluid lead to reductions in the compressive strength and accelerated creep rates. Stuckert and Mahar

(1984) assumed that the predominant source of frozen soil strength is the adhesive force provided by the ice bonding the particles. The presence of unfrozen saline pore fluid reduces the volumetric ice content of the soil, thereby decreasing this adhesion and therefore the strength.

In fresh water soils the unfrozen water is either strongly or loosely bonded to the particles. The strongly bound water is subject to high intermolecular forces which cause a small freezing point suppression. The loosely bound water has lower intermolecular forces as it is further removed from the soil grain surface, and therefore can undergo phase change easily. Ice will begin to form within a single pore near 0°C, and all free water will be converted to ice with a slight decrease in the temperature below 0°C. The adsorbed or strongly bound layer freezes as the temperature continues to decrease. In fresh water soil, unfrozen water is encountered only in fine grained soils close to 0°C. For additional detail, see Weaver (1979).

The amount of unfrozen water at a given temperature in non-saline soils depends upon the specific surface area of the soil particles (Anderson and Tice, 1972) and roughly upon the liquid limit of the soil (Anderson et al, 1973). Tice et al (1976) conducted a series of tests to determine the liquid limit of various soils. The water content and corresponding number of blows were plotted on logarithmic linear axes, and the liquid limit flow curves fitted through the data. From the fitted line, the moisture content

corresponding to blow counts, N = 25 and N = 100 were found. The authors postulate that these moisture contents can be used to predict the unfrozen water content at -1 and -2°C respectively, with the equations;

$$w_{(u\theta=1)} = 0.346 \cdot w_{(N=25)} - 3.01$$

and

$$w_{(u\theta=2)} = 0.338 \cdot w_{(N=100)} - 3.72 \qquad (2.1)$$

where $w_{(u\theta=1)}$ = unfrozen water content at -1°C

$w_{(N=25)}$ = water content at N=25

$w_{(u\theta=2)}$ = unfrozen water content at -2°C

$w_{(N=100)}$ = water content at N=100.

Good correlations between the unfrozen water predicted from the equations and measured using an isothermal calorimeter were found. The results of this analysis were plotted on double logarithmic axes of temperature to unfrozen water content, w_u, and a straight line fitted through the data. The straight line was then used to determine the temperature and unfrozen water content points for a typical phase composition curve for the non-saline soil.

A different physical theory governs the volume of unfrozen water present in saline soil. Saline soil is composed of water, salt, gas and the mineral soil grain. As the soil begins to freeze, ice crystals begin to grow once the freezing point of the saline fluid is reached. The ice crystals are formed of nearly pure water, forcing the salt

molecules into a progressively more concentrated saline pore fluid solution within the pore space and between the growing ice crystals. The enriched brine leads to a continuing freezing point depression, and consequent decrease in the thickness of the adsorbed water film on the fine grained particles. As the temperature drops, the adsorbed water layer undergoes phase change and the brine pocket shrinks. At temperatures warmer than -21.3°C, the eutectic temperature for salt water, some unfrozen water will remain within the soil pores (Ogata et al, 1983). Hence, the unfrozen water content at a given temperature is significantly increased by the presence of saline pore fluids. Figure 2.3 demonstrates the effects of the addition of salt to the pore fluid upon the position of the unfrozen water within the soil pore space. For additional detail, the reader is referred to Sheeran and Yong (1975).

The effect of the saline pore fluid on the unfrozen water content depends on the granulometric composition of the soil as well. In coarse-grained soils, the unfrozen water is contained in pockets between the ice covered soil grains. Here the particle contacts are surrounded by ice, and the unfrozen saline fluid is isolated in the pore space. In fine-grained soils, a layer of unfrozen water surrounds the mineral particle due to the intermolecular forces between the soil grains, and the ice occupies the central pore space.

Tsytovich et al (1973) noted that the addition of silt and clay sized particles to a sand sample reduced the effect of saline pore fluid on the strength of the frozen soil. The authors suggested that while the salinity reduced the ice cement strength, the cohesion between the finer grained particles provided strength. For a more detailed review of the mechanics of freezing of saline soils, see Sheeran and Yong (1975), Akimov et al (1983), Nixon and Lem (1984), Stuckert and Mahar (1984) and Nixon (1988).

Patterson and Smith (1983) postulate that the freezing point depression caused by saline pore fluids can be calculated if a phase composition curve relating the unfrozen water content to temperature for a single salinity is known. The results are expressed in terms of the change in temperature for a given unfrozen water content, due to the change in salinity. The equation is;

$$T_n = T_i + \frac{S_o \cdot \delta}{\theta_i / \theta_o} \qquad (2.2)$$

where T_n= new temperature at which unfrozen water content θ_i will occur

θ_i= unfrozen water content at temperature T_i

θ_o= water content of thawed soil

S_o= pore water salinity (g NaCl/g) of the thawed sample

δ= -0.058675 °C/(g NaCl/g).

In this equation it is assumed that only NaCl is contained

in the pore water, and the water contents are expressed on a volumetric basis. The authors found good correlation between the unfrozen water contents measured using time domain reflectometry and those predicted using this equation, for clay and silty clay. The correlation was best at the lower salinities.

The strength and creep deformation of permafrost is dependent upon many factors. However the single factor which affects the comparative performance of non-saline and saline frozen soil is the volume of unfrozen water contained in the soil pore space.

2.3 Creep Deformation Equations

The creep behaviour of permafrost has been researched extensively. The analytical equations to describe the time dependent deformation and reduction of the strength of frozen materials as well as the time dependent deformation of piles have been developed from laboratory testing of model piles, and uniaxial testing of ice and frozen soil.

The application of load to frozen soil or model piles in laboratory research takes one of two forms: either constant displacement rate or constant load testing. For the former the load required to generate a certain constant displacement rate is measured. Failure occurs at the peak observed on the load displacement curve. Parameswaran (1980) observed a double peak in samples of frozen soil tested at low temperatures and high constant strain rates. The first

peak, corresponding to the initial yield of the ice matrix is followed by a drop in the stress required to maintain the specified strain rate. The stress then increases again as the frictional component of the resistance develops. A second peak in the curve is observed when secondary yield occurs.

In constant load testing, the deformation of the soil with time is measured. Mellor and Cole (1983) observed an initial yield point in constant load testing of ice at -5°C, although it was more difficult to define than in constant strain rate tests. As in the work by Parameswaran, at higher strain rates the initial yield point converged with the secondary yield point, generally observed at one percent strain.

It has been suggested that the point of maximum stress in a constant displacement rate test corresponds to the point of minimum strain rate in a constant stress test. At these points the ratio of stress to strain rate is a maximum. Hence Sego and Morgenstern (1983) and Mellor and Cole (1982, 1983) state that the physical behaviour of the ice at these points is comparable irrespective of the method of load application. Mellor and Cole found that the behaviour of ice tested at -5°C under constant load and constant strain rate compared well at the point of minimum strain rate and maximum stress respectively, so long as brittle fracture at the initial yield point was not the controlling failure process.

Another method of comparing the results of testing of frozen soils is to examine the behaviour at a certain percentage of strain. Goughnour and Andersland (1968) observed the same accumulated strain to peak in testing of frozen sands independent of the ultimate stress or strain rate. Ladanyi (1972) found approximately constant permanent strain at the start of tertiary creep for a given temperature and type of test. Nixon and Pharr (1984) arbitrarily selected ten percent strain to be the comparison point for their tests on frozen saline gravel as they did not observe a secondary state creep phase. Mellor and Cole (1983) also selected ten percent strain as a convenient point for comparison of the behaviour of ice in the tertiary regime.

Long term constant load testing of frozen soils is most applicable to the development of pile deformation design methods. Extrapolation from shorter term or constant displacement rate testing often leads to overestimation of the strength of the soil due to removal of load prior to the development of the true minimum strain rate and due to rate effects. Parameswaran (1985) has observed this fact from a comparison of the results of short and long term laboratory testing.

Step load testing is a common procedure adopted to maximize the data obtained from a single test. Here a constant load is applied to the pile or frozen soil sample. Once steady state creep is observed, an additional load is

applied. In this way, several stresses can be applied to a single sample prior to its failure. Ladanyi (1972) proposed that the strain of the sample in a step loading test could be obtained from a summation procedure which accounted for the loading and temperature history of the soil. It was predicted that the steady state creep displacement rate developed under a particular stress would be independent of the preceeding stress history, even though the absolute strain under the load would not be comparable. Figure 2.4 modified from Ladanyi (1972) demonstrates this postulate.

2.3.1 Unified Creep Models

Unified constitutive models to describe the deformation of frozen materials over a range of state parameters have been proposed by several researchers. The models are based upon the principle of superposition which states that the present material response can be deduced from summation of the preceeding responses to load increments.

Mellor and Cole (1983) developed a unified creep theory from the examination of several identifiable points on the deformation-time curves resulting from both constant load and constant displacement rate tests on ice at -5°C. They postulated that ice should deform and fail in the same manner irrespective of the method of loading. In order to examine this theory the initial yield point, ductile yield point and axial strain of ten percent were selected for comparison. These points were intended to give more

sensitive indications of the variations of strain rate with time than the traditional creep curve provides. Equations based on the simple power creep law;

$$\dot{\varepsilon} = B \cdot \sigma^n \qquad (2.3)$$

where $\dot{\varepsilon}$ = engineering strain rate

σ = applied stress

n = coefficient dependent on temperature

were presented for each of these comparison points, and showed reasonable fit to the data from both types of tests. The three relations converged as the stress and strain decreased. It was noted however that the material properties change with strain and time and the stress/strain/time relations differ for the two types of test conducted. Attempts to generate creep curves from stress-strain curves and vice versa were not very successful, due to differences in the stress/strain/time paths of the two tests. Systematic comparison of the strain rates at these identifiable points indicated that the creep curves are not geometrically similar. Hence a model describing constitutive relations and failure criterion cannot be completely general, but instead should be considered separately for various levels of stress and creep regimes.

Vinogradav (1985) suggested a linear viscoelastic theory in which the behaviour of ice under low stress would be completely defined by the longitudinal and lateral

components of stress. However data from uniaxial static creep tests indicated a strong dependence of the material behaviour on the initial stress history and rate of loading at the time of application. Therefore it was concluded that the development of constitutive laws must be confined to a limited range of parameters.

Berggren and Furuberg (1985) provide equations to predict the three creep stages of an idealized soil. The theory is derived from definition of the time dependency of creep in terms of a time resistance principle, and stress dependence in terms of a degree of mobilization. The time resistance value R is defined as the change in cause or load duration divided by the change in effect or the strain. The degree of mobilization is the ratio between the applied stress level and a temperature specific reference strength. The temperature dependence is accounted for by determination of the unfrozen water content, which is then related to the strength of the material at that temperature. These parameters can be defined from two strength tests at different temperatures, two creep tests at different temperatures and stresses, and one test for unfrozen water content. Once these parameters have been determined, it is postulated that the creep behaviour of the soil can be completely predicted. Prediction of the tertiary creep behaviour is not made since it is postulated that once secondary creep has commenced, it is inevitable that failure will occur after some time. Hence the failure criterion used

is one that delineates the end of primary or the onset of secondary creep. For further details as to the exact method of determining the parameters, the reader is referred to Berggren and Furuberg (1985).

Ting (1983) analysed the results of unconfined compressive creep tests on frozen sands, using primary, secondary and tertiary creep laws. It was observed that the primary creep law fit the early time data, but significantly underestimated the strain and strain rate at large times. The secondary model was useful only in the middle section of the test, considerably overestimating the strain and underestimating the strain rate initially and slightly underestimating the strain and strain rate at large times. The tertiary creep model provided an accurate fit for most of the test data, only slightly underestimating the strain rate at large times. These results are presented graphically in Figure 5 of his paper. Ting proposes that the tertiary creep equation provides a unified approach to the prediction of creep behaviour, at least for frozen sands in the range of stresses considered.

In general, it seems that development of constitutive relations and failure criterion for creep of frozen materials should be confined to limited ranges of stress and to the individual creep regimes. Equations developed to describe the creep behaviour of frozen materials in each of the decelerating, pseudo-steady state and accelerating phases of deformation are discussed below.

2.3.2 Primary Creep Equations

Primary creep is composed of a recoverable delayed elastic strain portion and an irreversible viscous strain component.

Weaver and Morgenstern (1981) postulate that the long term time dependent behaviour of ice-poor soils will be characterised by primary creep. The creep of ice-poor frozen soil can be modelled by the equation proposed by Vyalov (1962);

$$\epsilon = \left[\frac{1}{w(\theta+1)^k}\right]^c \sigma^c t^b \qquad (2.4)$$

where σ= applied stress (kPa)

t= time since the application of load (hours)

θ= temperature below freezing (°C)

w, b, c, k= constants dependent upon the material properties.

The use of this equation assumes the validity of the hereditary creep theory, presented by Ladanyi (1972), as discussed in Section 2.3.

Weaver and Morgenstern (1981) modified this equation to account for the effect of mean normal pressure, σ_m using the theory presented by Ladanyi (1972). Using the Mohr-Coulomb failure theory to model the influence of hydrostatic

pressure on non-steady state creep rates, the equation becomes;

$$\epsilon_1 = D(\sigma_1 - j\sigma_3)^c t^b \qquad (2.5)$$

where $j = (1+\sin\phi)/(1-\sin\phi)$

$$D = \left[\frac{1}{w(\theta+1)^k}\right]$$

ϕ = internal angle of friction.

The validity of this equation has been verified by Weaver (1979) for both short and long term behaviour through his analysis of the confined compression test data for various frozen soils reported by Sayles (1973). Reasonable agreement between the predicted and observed behaviour was noted.

To account for multi-axial states of stress Ladanyi (1972), using the von Mises failure criterion, presented the non-steady state creep equation as;

$$\epsilon_e = D\left[\left[\frac{j+2}{3}\right]\sigma_e + (1-j)\sigma_m\right]^c t^b \qquad (2.6)$$

where σ_e = equivalent stress

ϵ_e = equivalent strain

σ_m = mean normal pressure

$$= \frac{\sigma_1+\sigma_2+\sigma_3}{2}$$

The equivalent stress and strain are defined in terms of stress and strain invariants from the principal stresses and

strains, as follows (Ladanyi, 1972);

$$\sigma_e^2 = \frac{1}{2}\left[(\sigma_1-\sigma_2)^2+(\sigma_2-\sigma_3)^2+(\sigma_3-\sigma_1)^2\right]$$

$$\epsilon_e^2 = \frac{2}{9}\left[(\epsilon_1-\epsilon_2)^2+(\epsilon_2-\epsilon_3)^2+(\epsilon_3-\epsilon_1)^2\right] \qquad (2.7)$$

Due to the lack of multiaxial test data on frozen soils, Weaver and Morgenstern (1981) were unable to verify the validity of this equation.

It is assumed that the value of the ratio $\sigma_1/j\sigma_3$ is usually less than 1.25 for ice-poor soils, allowing the constitutive relationship to be simplified to;

$$\epsilon_e = D\cdot\sigma_e^{\,c}t^b \qquad (2.8)$$

The time resistance principle proposed by Berggren and Furuberg (1985) theorizes that primary creep deformation is uniquely described by the slope of the line defined by the data points plotted on axes of inverse creep rate to time. The model has been used to analyse the results of laboratory tests on clay. The authors state that the method of analysis must be verified for soils other than clays, and for long term behaviour. The influence of excess ice on the soil response must also be examined.

2.3.3 Secondary Creep Equations

Often time dependent deformation in the primary regime is not considered in the development of creep equations, as it is assumed that it contributes only a small portion of the total deformation. According to Vyalov (1962) deformation in the primary phase accounts for less than ten percent of the total strain. Yuanlin et al (1983) found from confined compression testing of ice and frozen soils that one third to one fifth of the total deformation occurred during the primary stage.

The flow law developed by Glen (1955) to portray secondary creep of polycrystalline ice;

$$\dot{\epsilon} = B \cdot \sigma^n \qquad (2.9)$$

is the basis for much of the following work on the time dependent deformation of frozen materials. Using the relationship between the equivalent and principle stresses and strains presented in equation 2.7, this flow law can be written as;

$$\dot{\epsilon}_e = B \cdot \sigma_e^n \qquad (2.10)$$

Subsequently, the power creep law has been modified by introducing a proof stress σ_c required to maintain a given proof strain rate $\dot{\epsilon}_c$. The equation is then;

$$\frac{\dot{\epsilon}}{\dot{\epsilon}_c} = \left[\frac{\sigma}{\sigma_c}\right]^n \qquad (2.11)$$

where the proof stress and exponent are temperature dependent (Ladanyi, 1972).

The results of constant displacement rate unconfined compression testing of frozen saline sand by Sego et al (1982) showed that the proof stress σ_c and exponent n changed significantly as the salinity increased due to the increasing unfrozen water content and corresponding decrease in soil strength. Yuanlin et al (1983) suggested that the exponent was also dependent on the initial moisture content, temperature and applied pressure.

From low stress constant displacement rate testing of polycrystalline ice, Sego and Morgenstern (1983) delineated two flow laws: one describing the behaviour below one percent strain and the other valid at strains greater than ten percent. At small deformations there is no recrystallization of the ice, while longer term loads result in large deformations which are associated with recrystallization of the ice and accelerating strain rates. Analysis of pile and ice data by Morgenstern (1987) indicated that for small strains the power coefficient is 2.5, while for larger strains the value of n becomes 3.

The effect of temperature on the creep rate and strength of frozen material is often examined from the perspective of work on thermally activated creep in metals (Ladanyi, 1972). This theory is termed the rate process

theory and is based upon the Arrhenius equation;

$$\dot{\epsilon} = B \cdot \sigma^n \exp^{-Q/RT} \qquad (2.12)$$

where Q= activation energy

R= universal gas constant

T= temperature.

The use of the theory assumes a single activation energy governs the dependence of strain behaviour on temperature, and that steady state conditions exist (Goughnour and Andersland, 1968). It has been found that the use of this theory is difficult since there are several mechanisms governing the deformation of the material, each having a different activation energy (Parameswaran, 1980). Ladanyi (1972) suggests that there are two processes ongoing: the thermal energy of moving molecules is changing and a gradual phase change is occurring. In addition the assumption of steady state behaviour is violated by the primary and tertiary creep phases. Sego and Morgenstern (1983) propose that the Arrhenius equation is valid at temperatures lower than -10°C. At temperatures close to 0°C they suggest that an empirical equation presented by Voytkovskiy (1960) relating strain rate and temperature;

$$\dot{\epsilon} \propto \left[\frac{1}{1+T}\right] \qquad (2.13)$$

is more applicable.

2.3.3.1 Minimum Strain Rate

In the secondary creep equations, failure is assumed to occur at the point where accelerating creep commences. Here the time dependent deformation in the secondary regime is considered to be completely steady state. However Mellor and Cole (1982, 1983) and Ting (1983) propose that the development of theories should be based on the definition of the inflection point of the creep curve. They recognize that the period of approximate constant strain rate can be quite long, while in reality the strain rate continuously decreases from the start of the test until it reaches a minimum, then continuously increases until creep rupture occurs. The minimum point is most readily visible on a plot of logarithmic strain rate to logarithmic time (Orth and Meissner, 1982, Ting, 1983), as shown in Figure 2.2. Figure 2.1 shows data plotted on the same axes for purely steady state behaviour. The definition of the inflection point or minimum strain rate is precise, while the determination of the end of the secondary creep regime at the onset of tertiary creep is insensitive.

Ting (1983) noted a strong log-linear correlation between minimum strain rate and time to minimum results for ice, soil and frozen soil. The slope of contours drawn through the minimum points was -1, indicating that the strain at the minimum point is approximately constant.

Yuanlin and Carbee (1983) define failure as the point of minimum strain rate. A series of constant stress and

constant temperature unconfined compression tests on silt was conducted from which the creep failure strain and time to mimimum were found. A plot of logarithmic minimum strain rate to inverse stress defined a family of bilinear curves breaking at a critical strain rate. The authors suggest that this critical strain rate delineates different deformation mechanisms: short term being dislocational creep and long term controlled by glide creep. From these results equations relating the state parameters to one another were derived and lead to the development of a strength loss equation which will predict the ultimate strength of the frozen soil at a given time. It was observed that the creep failure strain is basically independent of the strain rate and temperature, while it is affected by changing the initial water content of the soil. A creep model after Assur (1980) was examined and found to match the primary and short term creep behaviour. However the model provides at best a first approximation to the long term behaviour of the soil and should not be considered a reliable indicator.

2.3.4 Tertiary Creep Equations

Equations incorporating the time to the onset of tertiary creep have been used to predict the ultimate stress a soil can withstand. Sayles (1968), Long (1978) and Parameswaran (1985, 1986) have used Vyalov's time to failure equation to predict the ultimate soil stress from laboratory creep testing of soils taken to failure.

Vyalov's (1959) time to failure equation;

$$\sigma_u \beta = \ln\left[\frac{t_f}{B}\right] \tag{2.14}$$

predicts the ultimate compressive stress σ_u for a given time to failure t_f. The parameters β and B vary with the soil type and temperature and are determined from a plot of the inverse stress against the time to failure at a given temperature for the specific soil, density and moisture content variation (Long, 1978).

The tertiary creep model proposed by Ting (1983) is discussed briefly in the Unified Creep Theory section above. The equation presented is;

$$\dot{\epsilon} = A \cdot e^{\beta t} t^{-m} \tag{2.15}$$

where A, m, β= experimentally determined constants.

These constants are calculated from the strain, strain rate and time at an initial non-zero time and at the point of minimum strain rate. Ting's analysis of creep tests on frozen sand indicated a good fit of the equation to the experimental data, throughout the three stages of deformation.

2.3.5 Conclusions

It is evident from the literature review contained in this section that many theories have been presented to

describe the time dependent deformation of ice and frozen soils. The use of each analysis method depends upon the temperature, salinity and soil type in question, which in turn determines the resistance of the material to load. The validity of these equations must be verified individually for a particular set of test results.

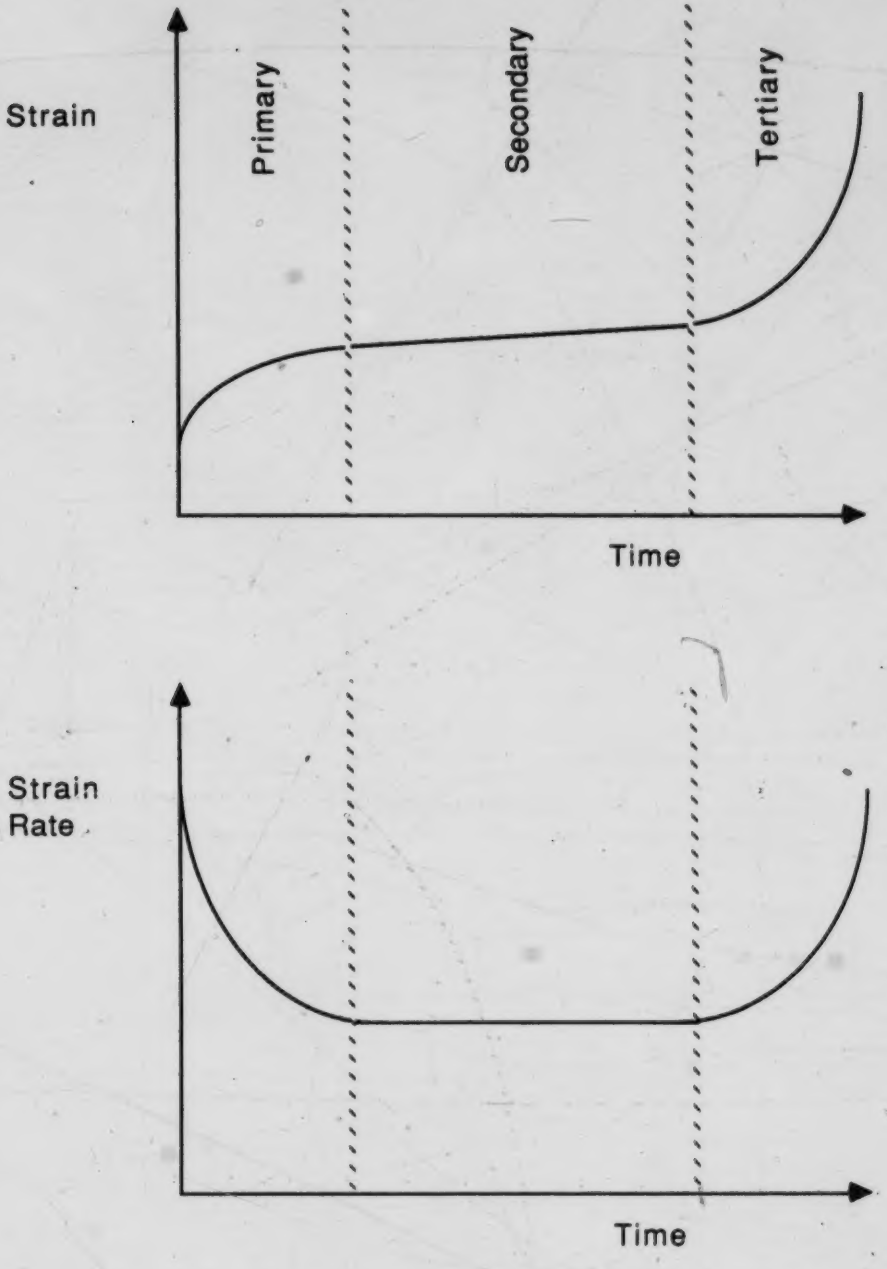

Figure 2.1: Typical creep curve, after Ladanyi (1972).

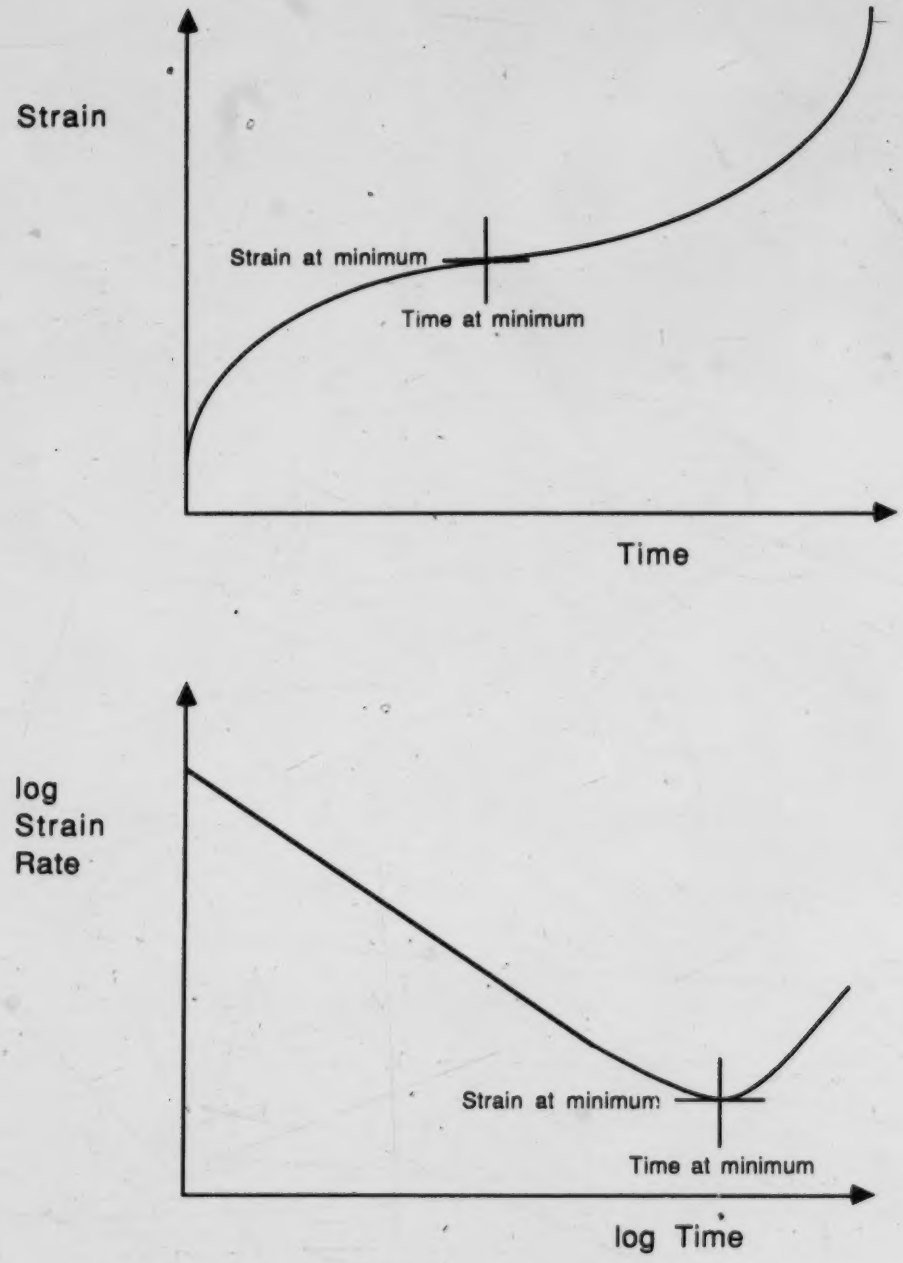

Figure 2.2: Creep behaviour of frozen soil, after Ting (1983b).

a) Low concentration saline pore water

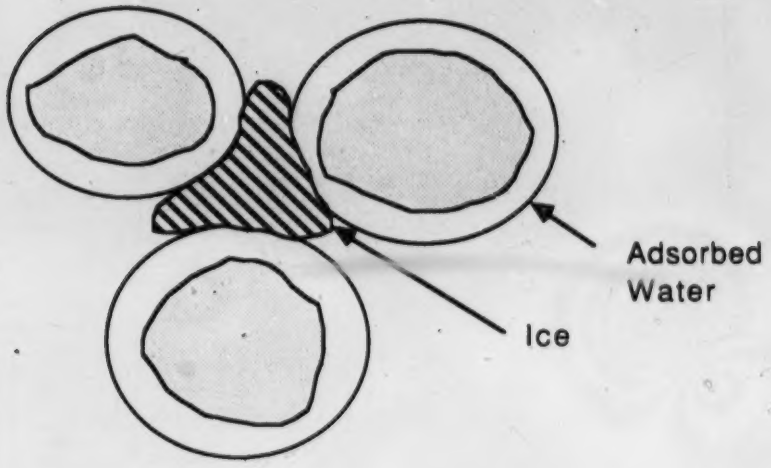

b) High concentration saline pore water

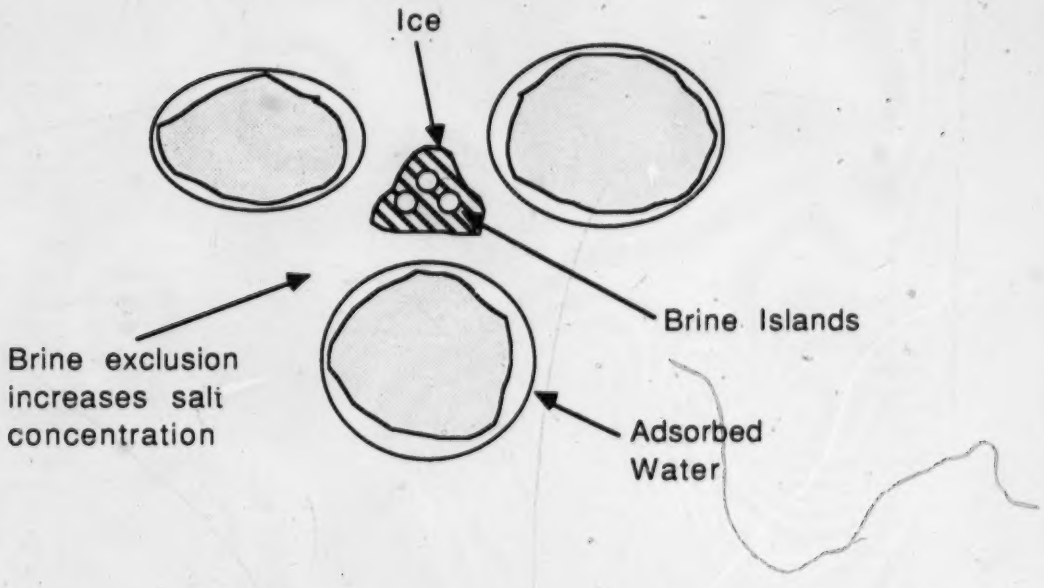

Figure 2.3: Position of unfrozen water within a single pore space, after Sheeran and Yong (1975).

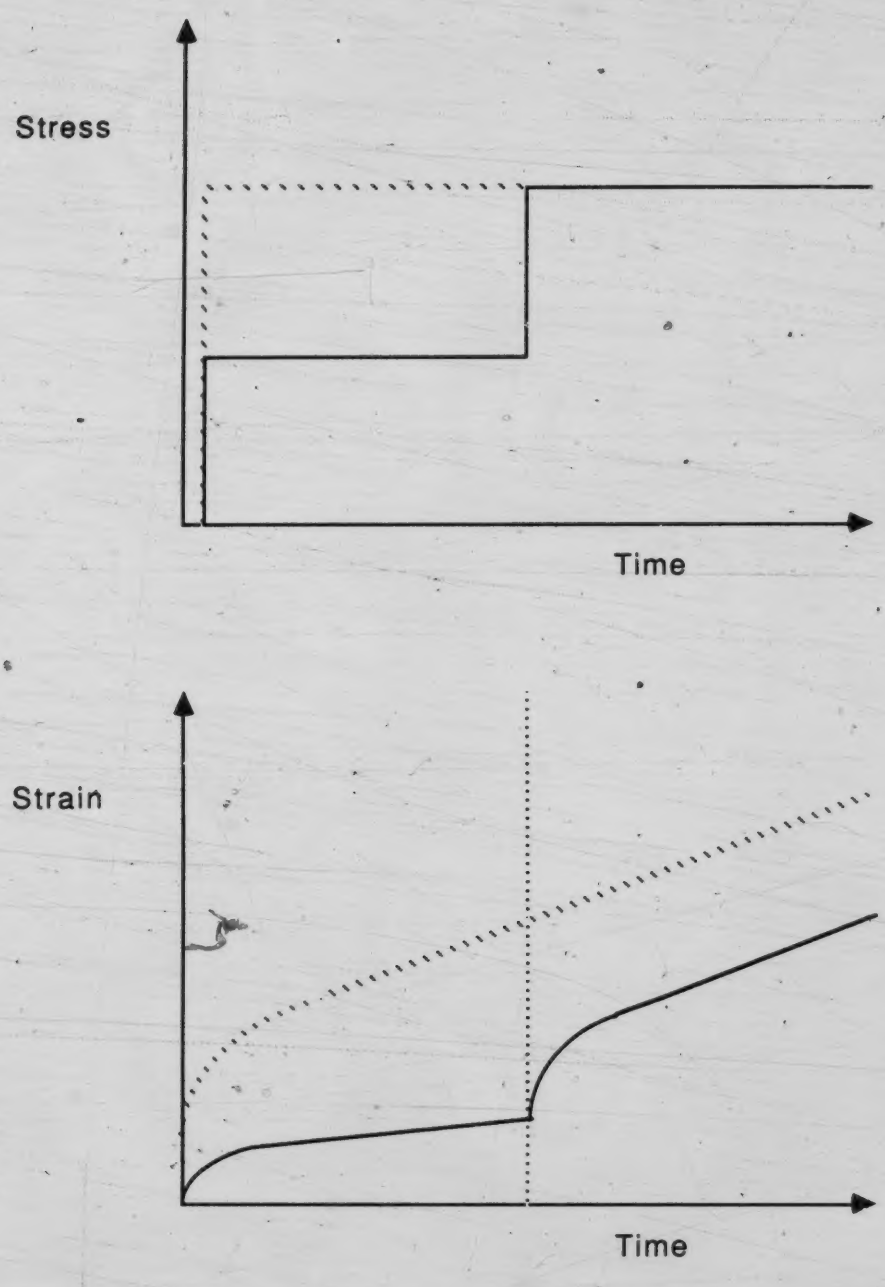

Figure 2.4: Incremental load tests, after Ladanyi (1972).

3. A Review of Current Research and Theory for the Design of Piles in Permafrost

3.1 Introduction

A pile fails when the adfreeze bond between the pile and the frozen soil ruptures or when the pile settles excessively.

Methods for the design of piles in permafrost depend upon the behaviour of the frozen soil. Phukan (1984) noted that the deformation of ice-poor soils under low stress is confined to the primary creep regime since these are "structured soils", the behaviour of which is influenced by the soil grain to grain contact. This soil behaviour is frictional, so design is governed by the allowable adfreeze resistance.

In ice-rich soils the pile behaviour is controlled by the time dependent deformation of the ice separating the soil particles. Design is based on the prediction of a stress small enough to limit the creep deformation (Weaver and Morgenstern, 1981).

Testing by Nixon and Lem (1984) indicated that saline soils deform predominantly in the secondary creep regime, and so design must seek to limit the deformation, as with ice-rich soils. Here the presence of unfrozen water leads to greater time dependent deformations and lower resistances than observed in non-saline soils (Nixon and Lem, 1984, and Nixon, 1988).

3.2 Pile Velocity Equations

Design methods which predict the time dependent deformation of piles in frozen soil were derived (Nixon and McRoberts, 1976) from the combination of equations describing the deformation rate of the frozen material and the geometry of the pile.

Johnston and Ladanyi (1972) presented a method for the design of piles in permafrost resulting from their back analysis of the field tests of grouted anchors in frozen silts and clays, carried out at Thompson, Manitoba. They considered the deformation of soil around a loaded anchor as the shearing of concentric cylinders. The geometry of this model is shown in Figure 3.1, modified from Nixon and McRoberts (1976). The assumptions inherent in this analysis are that the pile is cylindrical, the shear stress is uniformly distributed along the embedded length of the pile, the soil is homogeneous, isotropic and at a constant temperature and that the force of gravity can be neglected. In addition it must be assumed that there is no slip at the pile soil interface and that the analysis is insensitive to changes in the normal stress acting along the pile surface. The effect of normal stress on the steady state creep rate of ice or ice-rich soil is negligible. The normal stress, however, alters the behaviour of ice-poor soils. Since the normal stress acting on the pile is less than 200 kPa this effect can be neglected (Weaver and Morgenstern, 1981).

The creep equation for a general state of stress and an incompressible material obeying the von Mises failure criterion was given by Johnston and Ladanyi (1972) as;

$$\dot{\epsilon}_e = B \cdot \sigma_e^n \qquad (3.1)$$

where $\dot{\epsilon}_e$ = equivalent strain rate

σ_e = equivalent stress

as previously discussed in Section 2.3.3.

The tangential strains around a vertically loaded pile in frozen soil are zero. Hence each element deforms under plane strain conditions. For frozen soil subjected to simple shear under plane strain conditions, it was shown by Johnston and Ladanyi (1972) that the flow law above reduces to;

$$\dot{\gamma} = 3^{(n+1)/2} B \tau^n \qquad (3.2)$$

where $\dot{\gamma}$ = shear strain rate

τ = shear stress.

The equation describing the time dependent strain of ice-poor soils was presented by Weaver and Morgenstern (1981) as;

$$\epsilon_e = D \cdot \sigma_e^c t^b \qquad (3.3)$$

Additional detail regarding this equation is presented in Chapter 2.3.2. The strain of ice-poor soils can then be

represented as;

$$\frac{\gamma}{t^b} = 3^{(c+1)/2} D\tau^c \qquad (3.4)$$

The shear stress on a pile is given by the equation;

$$\tau_a = \frac{P}{2\pi aL} \qquad (3.5)$$

where τ_a= applied shaft stress

P= load on the pile

a= pile radius

L= embedded length of the pile.

Ladanyi (1963) showed that for a weightless soil;

$$\tau = \tau_a(a/r) \qquad (3.6)$$

where r= distance from the pile center.

As shown in Figure 3.1, the shear strain is related to the displacement u at any radius r by the equation;

$$\gamma = \frac{-du}{dr} \qquad (3.7)$$

Hence the shear strain rate $\dot{\gamma}$ is related to the displacement rate $\dot{u}$ by;

$$\dot{\gamma} = \frac{-d\dot{u}}{dr} \qquad (3.8)$$

Substituting the preceeding two equations into the flow law for ice or ice-rich soils gives;

$$\frac{d\dot{u}}{dr} = -3^{(n+1)/2} B \left[\frac{\tau_a a}{r}\right]^n \qquad (3.9)$$

Integration of the equation, with the boundary conditions that at r=a, $\dot{u}=\dot{u}_a$ and $\dot{u}=0$, at $r=\infty$ gives;

$$\frac{\dot{u}_a}{a} = \frac{3^{(n+1)/2} B \tau_a^{\,n}}{n-1} \qquad (3.10)$$

where $\frac{\dot{u}_a}{a}$ = normalized pile velocity.

Similarly, the pile deformation in an ice-poor soil is given by;

$$\frac{u_a}{at^b} = \frac{3^{(c+1)/2} D \tau_a^{\,c}}{c-1} \qquad (3.11)$$

The deformation of piles in ice-rich and ice-poor frozen soils can be described by equations 3.10 and 3.11 respectively.

3.3 Piles in non-Saline Ice-Poor Permafrost

Weaver and Morgenstern (1981) state that the design of piles in ice-poor frozen soils must prevent the rupture of the adfreeze bond between the pile and the frozen soil.

The adfreeze resistance at the interface depends upon the pile roughness and the area of the pile bounded by the shear plane. Weaver (1979) proposes that the adfreeze strength of the pile can be related to the long term adfreeze strength;

$$\tau_a = m \cdot \tau_{lt} \qquad (3.12)$$

where τ_a= adfreeze strength of the pile

τ_{lt}= long term adfreeze strength

m= coefficient dependent upon the pile type and installation method.

Typical values of the coefficient m and the long term adfreeze strength τ_{lt} are presented by Weaver and Morgenstern (1981). The contribution of friction to the adfreeze strength is neglected in their analysis, since the normal pressure acting on the pile is small.

Weaver (1979) postulates that the time dependent deformation of piles in ice-poor frozen soils can be predicted from laboratory creep data of these soils, except in frozen fine-grained soils at temperatures close to the melting point, where unfrozen water influences the soil behaviour.

As discussed above, the time dependent deformation of piles in these soils can be predicted using the equation;

$$\frac{u_a}{at^b} = \frac{3^{(c+1)/2} D \tau_a^{\,c}}{c-1} \qquad (3.13)$$

presented by Weaver and Morgenstern (1981).

Design charts for piles in ice-poor frozen soils based upon this equation and the creep constants found from laboratory tests on such soils are presented by Weaver and Morgenstern (1981). These charts contain the predicted pile displacement response to a given applied shaft stress for piles in frozen soils at different temperatures. The adfreeze resistance of the piles, which depends upon the applied shaft stress and temperature, is also presented. It is noted from these charts that the design of piles in ice-poor soils is governed by criteria which require the prevention of the rupture of the adfreeze bond at the pile-soil interface.

The prediction of long term settlement from short term static tests in ice-poor soils is based upon the assumption that the long term primary creep behaviour of piles loaded statically or with a sequence of steps will be similar if the final total load increment is the same as under the static load (Weaver, 1979). This assumption can lead to errors in the value determined for the time exponent b when the soil behaviour is influenced by stress history. To minimize such errors, large load increments applied for long times should be utilized, thereby allowing the pile to compress elastically and the shear stress distribution along the pile shaft to become representative of the long term

applied load.

Neukirchner and Nyman (1985) analysed field pile load test data for ice-poor permafrost using the pile velocity equation generally utilized for the prediction of pile behaviour in ice-rich permafrost, with good results. Further details are provided in the following section.

3.4 Piles in non-Saline Ice-Rich Permafrost

Ice and "warm" frozen ice-rich soils deform predominantly in the secondary creep regime, where the relationship between strain rate and stress is;

$$\dot{\epsilon} = B \cdot \sigma^n \tag{3.14}$$

As discussed previously, this equation, in conjunction with pile deformation theory, (Nixon and McRoberts, 1976) yields;

$$\dot{u}_a = \frac{a 3^{(n+1)/2} B \tau_a^{\,n}}{n-1} \tag{3.15}$$

where B, n= temperature dependent coefficients

a= pile radius

$\dot{u}_a$= pile velocity

τ_a= applied shaft stress.

DiPasquale et al (1983) found values of n = 2.67 from uniaxial creep testing of ice-rich frozen silt at temperatures warmer than -2°C. Other researchers have consistently determined a value of 3 for n from testing of

ice-rich soils (McRoberts et al, 1978) and ice at low stresses (Morgenstern et al, 1981) and warm temperatures (Sego and Morgenstern, 1983).

Morgenstern et al (1980) provide a summary of the creep parameters n and B for ice at temperatures between -1 and -10°C based upon the analysis of the results of several researchers. Morgenstern (1987) stated that the parameter B for ice must be reduced by a factor of 6 to model the creep of a slope in warm frozen glaciolacustrine clay studied by Savigny (1980).

Neukirchner and Nyman (1985) examined field pile load test data for piles driven and slurried in silty sands and sandy silts. The soil is assumed to be non-saline, although no salinity measurements were made on these soils. A value of 3 was assumed for n, so the pile velocity equation became;

$$\dot{u}_a = 4.5 \cdot B \cdot a \cdot \tau^3 \qquad (3.16)$$

To facilitate their analysis, the creep data was adjusted to a common temperature of -9.4°C and data for piles not truly in the secondary creep regime was not considered. The remaining pile shaft stress and corresponding normalized pile velocity using a double logarithmic plot defines a band parallel to that of ice or ice-rich frozen soil and providing a value of n = 3. Expressions for B, dependent upon temperature, were found to be;

$$B = \frac{1.8 * 10^{-7}}{(1-T)^2} \qquad (3.17)$$

valid over the ranges -2°C to -1°C and;

$$B = \frac{6.1 * 10^{-8}}{(1-T)} \left[kPa^{-3} yr^{-1} \right] \qquad (3.18)$$

for temperatures less than -2°C.

It was concluded from a comparison of the test data for the various pile types that the pile creep prior to the rupture of the adfreeze bond is controlled by the soil properties and not the pile characteristics or the installation technique. Neukirchner (1985) noted that changes in the ice content or soil type or the introduction of soil salinity would alter this equation.

Design charts for friction piles based upon the pile velocity equation and the creep characteristics of ice are presented by Weaver and Morgenstern (1981) in Figures 8 to 11. They postulate that the design of piles in ice-rich frozen soils is bounded in the upper limit by the behaviour of piles in ice. Therefore the design of piles in ice-rich frozen soils based upon the creep characteristics of ice will be conservative (Nixon and McRoberts, 1976, Sego and Morgenstern, 1983).

Creep testing of model piles under low loads in various ice-rich soils at average temperatures of -2°C by Parameswaran (1985) indicated that more than fifty percent of the deformation to the onset of tertiary creep occurs in

the primary or decelerating creep regime, especially for wooden model piles. The comparison of the test results and equations describing primary creep in visco-elastic materials lead to the conclusion that a power creep law relating strain, ϵ, to time provided the best fit to the data;

$$\epsilon = A \cdot t^m \qquad (3.19)$$

The exponent m which is dependent upon the temperature and characteristic of the soil type, was found to be 0.46 on average. This value 0.33, the value found for ice, indicating that creep of ice-rich frozen soil at temperatures near the melting point of ice is similar to the time dependent behaviour of ice. However it was noted that the scatter in the magnitude of m was large, especially in the low stress range. Hence it was concluded that a general equation could not be determined which would predict pile behavior with accuracy.

Parameswaran (1985) also advocated the use of the time to failure equation (2.14) presented by Vyalov (1962), as this method accounts for the total creep curve from the beginning of the test until the onset of tertiary creep. In this way, the assumption of negligible primary creep made in theories based upon the use of secondary creep rates is avoided. It was concluded that the most conservative estimate of the long term bearing capacity of piles in

permafrost was provided by Vyalov's time to failure equation.

3.5 Piles in Saline Permafrost

The creep behaviour of saline permafrost is of critical importance for the design of piles, as the presence of salt in the pore water of the soil can lead to reductions of pile capacity by a factor of two to three (Nixon, 1988) and increases in the creep rate of 10 to 100 times depending upon the salinity (Nixon and Lem, 1984). Stehle (1970b) found that the tangential adfreeze strength of piles with sea water backfill was about one-third that of fresh water backfill.

Nixon and Lem (1984), Nixon and Neukirchner (1985) and Nixon (1985) postulate that the constitutive relation for saline soil is the same as that presented above for ice and ice-rich frozen soils. Nixon and Lem (1984) note that the the value of n can range between the values of 3 and 7 depending upon the stress range and type of soil, and that B is dependent upon the temperature and salinity of the soil.

Several authors (Bro, 1985, Neukirchner, 1985, Nixon and Neukirchner, 1985, Nixon, 1988) have determined that the secondary creep law with the exponent $n = 3$ remains valid when saline permafrost is considered. Nixon and Lem (1984) found a value of 3 as well from laboratory creep testing of frozen saline silt and clay.

Sego et al (1982) conducted a series of controlled strain rate unconfined compression tests on frozen saline sand at -7°C. The salinities investigated varied from 0 to 100 ppt. The analysis of this data provided a range of values for the creep exponent n and the proof stress required to maintain a specified proof strain rate. It is evident from the data presented in Figure 9 of their paper that n is dependent upon the salinity, especially so at low salt contents.

Nixon and Lem (1984) presented values of B from the analysis of their laboratory test data in Figure 10 of their paper and found that the parameter varied widely dependent upon the temperature and soil salinity.

Neukirchner (1985) postulated that changes in the soil type and salinity would result in an offset of the lines defining the velocity of the material with no effect upon the slope. To quantify this offset, he introduced a relative creep stiffness parameter, N_B, being the ratio between the theoretical deformation rate of ice, $\dot{u}_{ice}$, and the measured deformation rate of the soil, $\dot{u}$, determined for the same pile geometry, temperature and applied stress;

$$N_B = \frac{\dot{u}_{ice}}{\dot{u}} \qquad (3.20)$$

The definition of this parameter assumes that N_B is independent of the applied stress and soil temperature, that the assumption of a value of 3 for the creep exponent

describes the time dependent behaviour of frozen saline soils and that the values of B quoted in equation 3.11 define the relationship between the creep rate and temperature. The pile velocity equation then becomes;

$$\dot{u} = 4.5a\left[\frac{B}{N_B}\right]\tau^3 \qquad (3.21)$$

Neukirchner (1985) cautioned that the assumption of the value of the stress exponent n = 3 may not be valid for saline soils since the creep behaviour depends upon the unfrozen water content which varies with temperature. Hence temperature specific evaluations of N_B must be made for frozen saline soils.

Nixon and Neukirchner (1984) presented guidelines in Figure 4 of their paper for the design of piles in saline permafrost at various temperatures and salinities. This chart is based upon the creep characteristics of ice and icy permafrost reported by Morgenstern et al (1980) and the test results of Nixon and Lem (1984).

Nixon and Neukirchner (1984) note that full scale field testing is required to validate laboratory results to provide some confidence in pile design for saline permafrost. Due to the limited volume of data from laboratory testing of saline frozen soils and the lack of field measurements of salinity in conjunction with in-situ pile load tests, methods to design piles in saline permafrost are quite uncertain. Therefore it is essential

that pile design for saline permafrost be verified by on-site field pile load testing.

Nixon (1988) reports the results of field pile load tests in Clyde River, NWT. The salinity of the soil was found to be between 10 to 15 ppt and the ground temperature over the length of the pile averaged -5°C. The allowable pile shaft stress determined from the field load testing was one half to one third of that predicted from the equations presented by Morgenstern et al (1981) and Nixon and Neukirchner (1984). It is suggested that the pile installation method and the salinity of the soil have a significant effect upon the pile behaviour. The backfill salinity is presumed to equal that of the surrounding soil due to mixing of the soil with the slurry and to salt diffusion.

The field data was compared with that of Nixon and Lem (1984) on a plot of applied stress to normalized pile velocity, shown in Figure 11 of Nixon's paper (1988). The Clyde River pile load tests plot at points representative of laboratory creep tests on frozen saline soils at a temperature of -5°C and 35 ppt salinity. The temperature is comparable, but it is unclear why the comparative salinity should be so high, unless there were local increases in brine content due to the redistribution of the salt.

It is evident that much additional work must be done before the designer will feel confident about the prediction of the behaviour of piles in saline permafrost. The pile

velocity charts provided by Nixon and Lem (1984) and Nixon (1988) provide a starting point for design, but this data must be verified by additional field and laboratory testing.

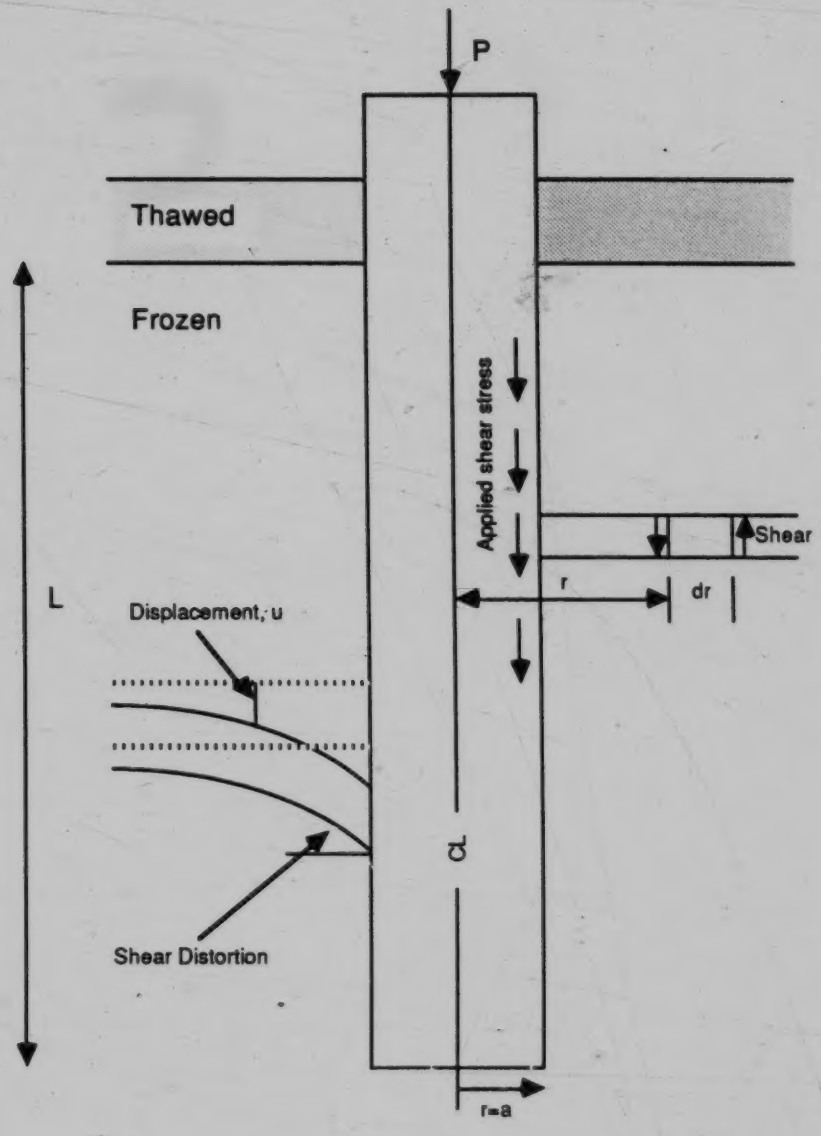

Figure 3.1: Shearing of concentric rings, after Nixon and McRoberts (1976).

4. Laboratory Procedure for Testing of Model Piles

4.1 Test Objectives

The main objective of the laboratory test program was to investigate the effects of changing temperature, salinity and load magnitude on the creep of model piles in contact with frozen soils. The salinities, temperature and soil were selected to cover the range of conditions encountered in certain coastal Arctic communities. The research also explored the feasibility of model pile testing for a comparative study of the creep response of saline permafrost.

4.2 Material Preparation

The soil used in these experiments was chosen to be comparable to soil found in such Arctic communities as Pond Inlet, Tuktoyaktuk, Pangnirtung and Eskimo Point. The grain size distribution curves of soils from these communities provided by Thurber Consultants (1987), suggested the following match points: 100 percent passing the #4 seive, 20 to 30 percent passing the #200 seive and 0 to 10 percent of 0.002 mm diameter clay sized particles. The moisture content of these soils was reported between 3 and 22 percent.

The test soil was prepared using sand and silty sand obtained from sites around Edmonton. These materials were dried in a 55°C oven for 24 hours. To remove all lumps from the soil, the sand was vibrated through a #10 seive, and the

sandy silt was crushed. The soils were then mixed in equal proportions by weight to produce a material with the average grain size curve shown in Figure 4.1. It can be seen from this diagram that the material used in the tests was somewhat finer than the Arctic soils.

4.3 Description of Apparatus

The apparatus developed comprised six identical systems to facilitate simultaneous testing of the four salinities, 0, 5, 10, and 15 ppt, and the two methods of load application at each temperature. Each set consisted of a bucket with two chambers: one for the soil and the other accomodating the circulation of cooling fluid. A temperature bath, a model pile, a load cell, a linear voltage displacement transducer (LVDT) and positioning collar, three thermistors, a loading frame, a bellofram driven by pressurized air/oil reservoir system, a pressure regulator, a loading cap, a cedar base plate, an insulating styrofoam cap, and a freezing plate made up the additional equipment of each test apparatus. The data was collected by a Helios data acquisition system consisting of an Operand XT and a Helios Fluke box. A schematic of the apparatus is shown in Figure 4.2. A detailed drawing of the cell is contained in Figure 4.3.

The test cell was constructed of two 30 centimetre long steel cylinders of average diameters 30 and 48 centimetres, welded to a steel base plate. Copper tubing coils were

inserted into the space between the two cylinders, with inlet and outlet tubes cut through the outer wall near the top of the bucket, thereby providing a conduit for the circulation of cooling fluid. In the center of each base plate, a 3 centimeter diameter hole was drilled. Teflon plastic was machined to fit into this hole, to act as a guide during the preparation of the sample and during load testing. The inner surface was machined to receive a rubber O-ring which fitted snuggly against the base of the pile. The O-ring and teflon insert provided a guide for the centering of the pile, and a seal against the loss of pore fluid during consolidation and freezing of each sample. Two small steel plates were welded to the top of each cell to provide handles for lifting the cell, and to provide a fixed point against which the LVDT could be positioned. A drain was provided at the base of the outer wall of the cell, to facilitate removal of the coolant between experiments.

Three constant temperature baths were used in portions of this research. The baths were calibrated for each temperature investigated. A bath consisted of a reservoir for the antifreeze, a heating and refrigeration unit, and a pump. Each bath pumped antifreeze coolant through the coil of copper tubing in two of the buckets, returning through Tygon tubing to the bath reservoir. Fluctuations of the temperature of the frozen soil were stabilized by the circulation of fluid from the bath to within ± 0.5°C. This system insulated the soil from the temperature fluctuations

of the cold room in which each apparatus was contained.

The model piles were cut from a tube of grade B black steel pipe without any specialized coating, selected to match that used in full scale piles used in Arctic construction. The piles were machined to smooth the outer walls. A load cap was machined to fit into the top of each pile, and receive a ball bearing for uniform load transfer.

The load cells were designed and constructed at the university. Each cell screwed onto the end of the Bellofram ram, and a load transfer dimple was machined into the end of the cell. The cells were machined of 6061 aluminum with a length to diameter ratio of four to one. Eight strain guages were mounted in a temperature compensating full bridge configuration on the barrel.

A 7 volt LVDT with five centimeter travel was inserted into a collar which was fastened to the ram of the Bellofram load system. The tip of the LVDT rested against the stationary horizontal handles on the outside of the bucket. As the ram moved downward, the LVDT recorded the deformation of the pile. It was essential that the LVDTs were positioned to give an initial voltage output within its linear range.

Three thermistors were inserted into each soil sample prior to freezing. The thermistors recorded temperature at one third points of the height of the soil column, at the point midway between the pile and the inner bucket wall. The thermistors were calibrated in an ice water bath at 0°C prior to each test series.

The rigid load frame was constructed of six inch channel iron. Each Bellofram was bolted through the horizontal top crosspiece, thereby ensuring vertical movement of the load ram. The load was applied to the Bellofram with a pressurized air/oil system. The pressure was controlled with a regulator, and monitored using a pressure transducer. The air line entered an oil reservoir, and the oil transferred the pressure to the diaphragm in the Bellofram. In this way, any moisture in the air line would not enter the interior of the Bellofram. Tests of the regulators indicated that the pressure remained fairly constant throughout the test. The maximum variation of the average shaft shear stress was ± 10 kPa.

Load caps were required to consolidate the soil prior to freezing to ensure uniform density and saturation throughout testing. They were machined of aluminum to fit within the inner bucket with holes for drainage, the three RTDs, and the pile. The pile protruded through a hole in the top of the plate, and a three inch collar fitted on top of the plate to allow downward movement of the cap as consolidation of the soil around the pile progressed. A cap machined to accept a load ball bearing was centered over the collar.

A cedar base plate with a hole in the center was used to raise the bucket above the load frame, and allow at least 2 centimetres of displacement of the pile.

An aluminum freezing plate was designed to control the flow of liquid nitrogen beneath the bucket. Conduits of depth and width of one centimeter, machined into the aluminum base plate, directed the flow between the inlet and exhaust ports of the plate. The liquid nitrogen, stored in a dewar, flowed into and exhausted out of the plate through copper tubing.

A Helios data acquisition system connected to an Operand XT was used to record the results. Labtech Notebook, the program controlling the data logging, allowed the user to specify the recording time increment, the number of decimals to be read, and to order the organization of the output data in any convenient manner. The current program contains 64 data recording channels, with the potential for division of these channels into as many as 4 blocks. Each of these blocks can be assigned to a different user, with individual recording intervals and specifications. The data stored by this program was directly compatible with Lotus 123, providing for rapid and efficient data analysis.

4.4 Test Procedure

The schematic of the apparatus used in this series of experiments is shown in Figure 4.2, with details of the cell given in Figure 4.3. Figure 4.4 depicts the apparatus used to freeze the sample. Appendix B contains photographs of the equipment. For a more detailed presentation of the laboratory procedure, the reader is referred to Appendix C.

4.4.1 Preparation of Model Pile and Apparatus

Prior to each creep test the piles were roughened by sand blasting, using size 5 industrial glass beads, in order to remove rust accumulated during the preceding test, to provide surface roughness, and to achieve similarity of surface texture throughout the testing program. The bottom two centimetres of each pile were not roughened to prevent damage to the Teflon guide insert and O-ring. Surface profiles of each pile, presented in Table A.2, were made after sand blasting using a Hobson Talysurf Profiler which indicated that the roughness remained fairly constant throughout the testing.

The smooth end of the roughened model pile was inserted into the teflon guide collar at the base of the bucket. An O-ring mounted in the guide fitted snuggly against the pile, thereby ensuring no leakage of the pore fluid from the bucket prior to freezing. The top of the pile was centered in the bucket and held in place by a guide, consisting of a bar across the top of the bucket with a protruding hollow tube which fit around the top of the pile.

A layer of filter paper was placed along the walls of the bucket to provide a radial drainage surface, thereby reducing the time for the consolidation of the soil.

4.4.2 Preparation of Frozen Saline Soil Sample

The soil was prepared as discussed in the Section 4.2. The pore fluid was prepared for the particular salinity

required, using distilled water and pure sodium chloride. The soil and saline water were mixed to a stiff consistency using a heavy industrial beater. This partially saturated, well mixed soil was placed a spoonful at a time into the bucket. The soil was well rodded to minimize the occurrence of air pockets in the soil. The upper layer of saline silty sand was levelled to within three centimetres of the top of the bucket. A double layer of filter paper was placed on the soil, followed by a layer of well graded gravelly sand to fill the bucket, providing a free draining upper surface and a stable base for the top loading cap.

The soil filled bucket was placed in the loading frame in a cold room set at 0°C, and the temperature allowed to stabilize for 24 hours. The loading cap was lowered into place, and a pressure applied to the Bellofram to provide a consolidation pressure of 80 kPa. This load was applied for an average of 30 hours to ensure at least 95 percent consolidation. The consolidation curves generated from the 80 kPa pressure applied to the buckets of soil are presented in Appendix A.

The bucket containing the consolidated soil was placed on the freezing plate and the top loading plate removed. The RTDs were zeroed and inserted into the soil. The dewar containing liquid nitrogen was connected to the plate for approximately four hours, until the RTDs indicated that the soil was completely frozen. Once all of the buckets were frozen, the cold room and temperature baths were set to the

desired test temperature.

The temperature baths were unable to control temperatures below -9 or -10°C. Therefore the four of the six cells in the first group of tests were not connected to the temperature baths. It was determined from these cells, that the glycol coolant in the cell annulus, and the thermal mass of the soil was sufficient to prevent undue temperature fluctuations at the pile surface. Hence the temperature baths were not used in a majority of the tests.

4.4.3 Testing of the Model Piles

The buckets were placed in the cold room for 24 hours to allow the frozen soil to stabilize to the test temperature. The LVDT collar was fixed to the Bellofram ram, and the load cell screwed onto the end. The ram was lowered to touch the ball bearing resting in the dimple on the pile load cap. The LVDT collar was positioned to allow the core to rest on the horizontal handle on the bucket, ensuring that the voltage output was within the linear range of behaviour. The air pressure regulator was set using the pressure transducer to apply the required load to each pile.

The deformation response to each load increment was computed from the data logger record of the LVDT and load cell output. When constant time dependent response was observed, an additional load increment was applied. The voltage output of each RTD was converted to degrees to monitor compliance to within ± 0.5°C of the desired test

temperature.

The results of each test can be found on summary plots in Appendix A. Appendix C contains a more detailed discussion of the procedure. Analysis of the data recorded is discussed in Chapter 5, and conclusions drawn in Chapter 6.

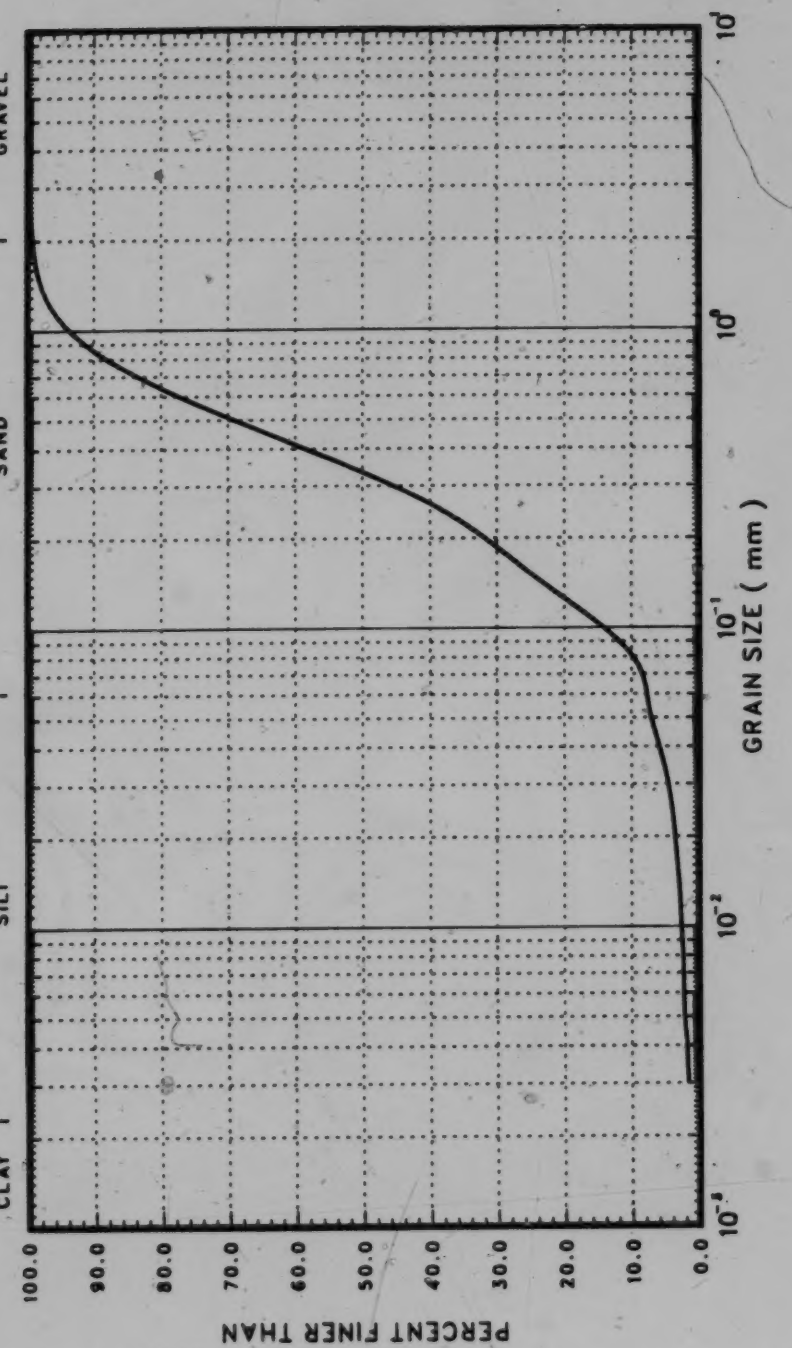

Figure 4.1: Grain Size Distribution

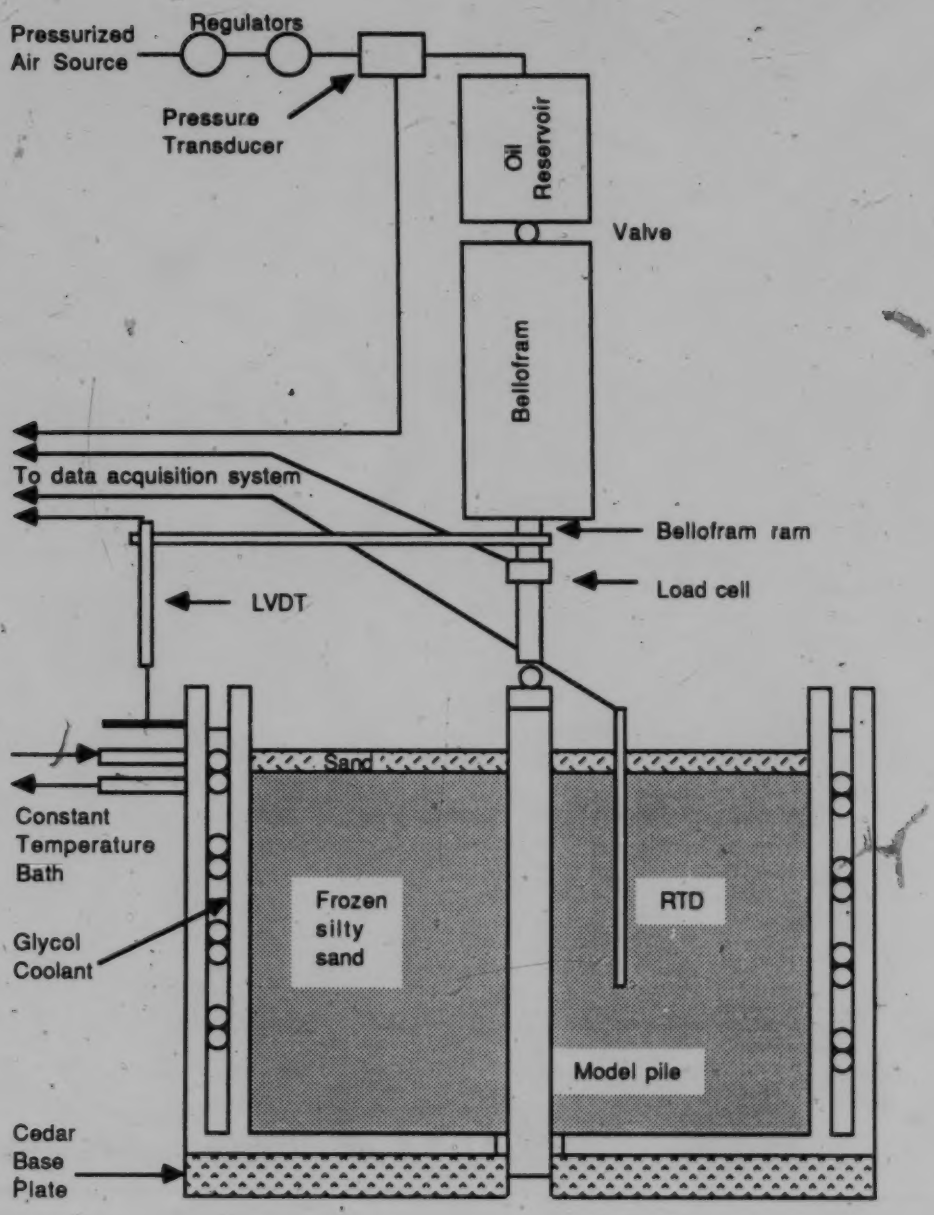

Figure 4.2: Schematic layout of model pile testing apparatus.

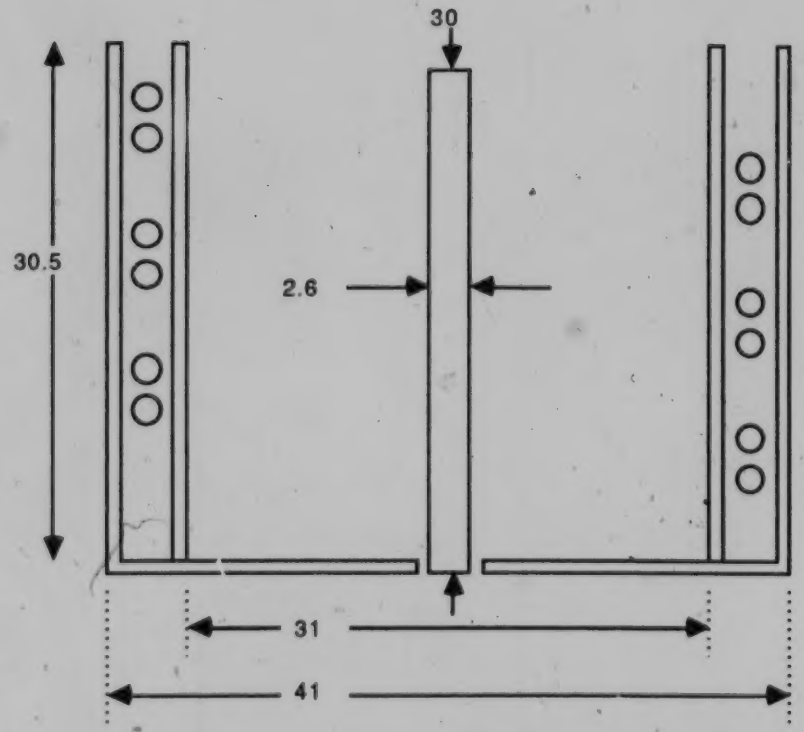

Figure 4.3: Dimensions of cell in centimeters

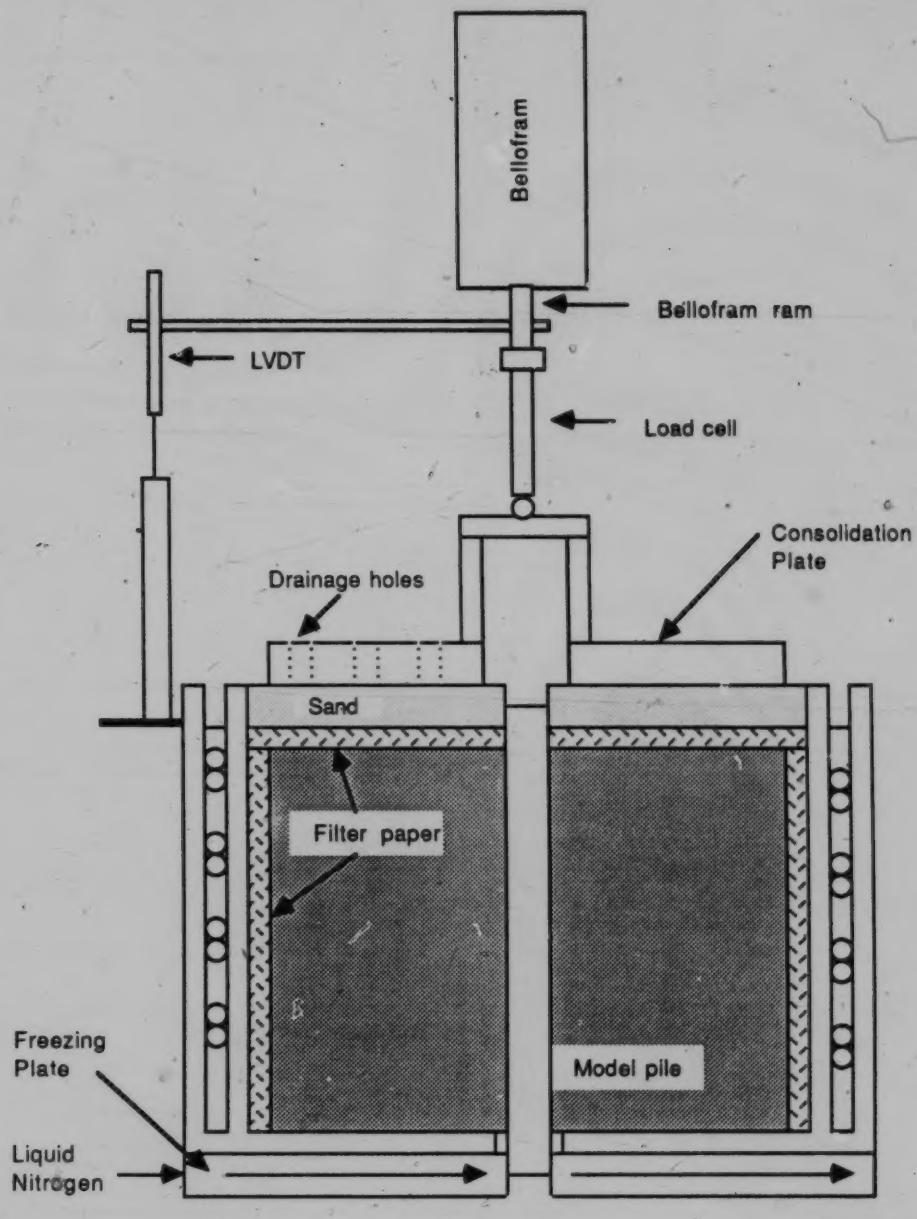

Figure 4.4: Consolidation and Freezing Apparatus

5. Analysis of the Model Pile Creep Test Results

5.1 Presentation and Discussion of Test Results

The results of the constant load tests of sand blasted model piles in silty sand are presented in Appendix A. For each test sample three figures are presented: one showing the temperature, applied shaft stress and deformation, another the time dependent deformation of the pile under load, and the final plot showing the consolidation behaviour of the soil.

5.1.1 Time dependent deformation

The plots in Figures A.1 to A.23 show the variation of temperature and shaft stress and the corresponding pile deformation for the sequence of loads applied during each test. It will be noted that the variation in temperature over the duration of any test was ±0.5°C, with the exception of the tests run at -10°C. These tests show a rapid decline in the temperature from an average of -9°C to -10°C near the beginning of the test. Failure of each pile occurred after the drop in temperature, so this initial test temperature was ignored. At the end of the test on Sample 2.1, after the point of minimum strain rate had been reached, the cold room cooling system failed, and the sample melted. The results of this test are included since all of the relevant data was collected prior to the failure of the cold room.

The shaft stress was constant during each load step, with a maximum deviation of ± 5 kPa from the average stress applied, which is presented on the graphs and in the tables.

The pile shaft stress and normalized pile velocity data for all load increments are summarized in Table 5.1. As can be seen from this summary and the displacement to time plots contained in Figures A.24 to A.46, many of the initial increments of load on the piles result in an elastic response with no measurable displacement over time. In a majority of the tests, increasing strain with time was observed only during the final load increment.

These results indicate that the soil behaves as a "structured soil" where load is carried at the soil particle contacts. The density of the soil indicates an ice-poor soil (Morgenstern et al, 1980).

However, current theory suggests that saline ice-poor soil will deform under load in the same manner as would an ice-rich soil. Therefore the analysis of the data was conducted following the methods proposed by Nixon and Lem (1984). Hence the analysis of the test data discussed in the following sections makes use of the response of the piles to the load steps only when typical creep is observed.

5.1.2 Consolidation

Perusal of the consolidation results in Figures A.47 to A.69 reveals that the consolidation of the soil was complete, prior to the start of freezing. The consolidation

deformation ranged between 7 and 20 mm, dependent upon the moisture content of the prepared soil and the length of time between the soil placement and the application of the constant 80 kPa consolidation stress.

5.1.3 Density and Salinity measurements

The density and salinity of each sample were determined after the completion of the pile creep test. The detailed density and salinity results can be found in Table A.1, while a summary is presented in Table 5.1.

The samples used for the density and salinity measurements for all of the samples, except those in group one, were cut from a wedge of soil that was sawed from the still frozen soil mass at the end of each test. The wedge was cut into six equally sized pieces, and each alternate slice reserved for either salinity or density testing.

The average density for all of the tests was calculated to be 1.69 Mg/m^3. The density varied between 1.76 and 1.61 Mg/m^3. The variation in density over the height of the sample was quite random.

The largest densities were determined from the group of samples tested at -13°C. This deviation may be due to the fact that the block samples used for the density measurements for this group were removed from the thawed soil as it was excavated by hand from the bucket. Every attempt was made to remove the soil without disturbance, however, it is apparent that the method was imperfect. The

cubes for the determination of the density for the following tests were cut from wedges sawed from completely frozen soil samples.

The salinity measurements were not conducted for the tests at -13°C, as the pore water extraction cell was obtained after the completion of this group of tests.

The three frozen soil cubes contained in tightly sealed bags which were reserved for the salinity measurements were allowed to thaw in a moisture room. The thawed samples were then placed in a thoroughly cleaned and dried pore water extraction cell. Load was applied to the cell, and the extruded water collected in syringes. The water collected generally contained a lot of fine particles. The syringes were sealed, and set on end to allow the particles to settle. Once the pore water was clear, a hand refractometer was used to determine the salinity. The individual salinity measurements for each sample are contained in Table A.1.

Variation in the salinity with depth would be observed if the rate of freezing of a sample were slow enough to allow the rejection of brine ahead of the advancing freezing front. In this case the salinity measured would increase with increasing distance from the freezing source at the base of the bucket. Examination of the test data in Table A.1 reveals fairly uniform salinity measurements over the height of the sample. Some variation in salinity is noted, but it is of a random nature. Hence it may be assumed that the rate of freezing was sufficiently rapid to prevent the

exclusion of brine in front of the freezing front.

A single salinity reading of the three taken for each of the tests 2.4, 3.2 and 3.5 was significantly different than the other two. These variations are attributed to dessication of the soil sample, or to the improper cleaning of the porous stone in the pore water extraction cell. In this case saline pore fluid would remain in the porous stone, giving the high salinity readings.

Whenever possible the soil was re-used from test to test. Concern developed as salinity measurements became available that this procedure would create variation in the pore water salinity throughout the test program. The salinity measurements presented in Table 5.1 are accompanied by a letter R or N indicating re-used or newly mixed soil. The results of the salinity determination for the samples from group four indicate that the re-use of the 5 ppt soil has no effect on the measured salinity. However, the nominal soil salinities of the 10 and 15 ppt soils were increased by 2 to 3 ppt when re-used. Therefore in future tests, it is suggested that the soil be freshly mixed prior to each test.

5.2 Presentation and Discussion of Analysis of Test Results

The test data contained in Appendix A was analyzed using several theories for the prediction of the long term resistance of piles from short term test data. These theories include the correlation of the pile velocity to applied shaft stress, a prediction of the long term failure

resistance, and estimates of the pile adfreeze resistance from the peak resistance found during unconfined compression tests on frozen saline silty sand. In addition the validity of the theory of hereditary creep as presented by Ladanyi (1972) will be discussed.

The unfrozen water content dependent upon salinity and temperature was calculated using the results of liquid limit testing of the soil. The results of this analysis will be discussed in this section as well.

In the analysis, the term, t_f, time to failure, will be defined as the time to the point of minimum strain rate, unless otherwise specified. In addition the soil salinities given are the nominal mixing salinities and not the values measured from the extracted pore water, to facilitate comparison of the test data.

5.2.1 Basic test parameters

The point of minimum pile velocity corresponding to a specific pile shaft stress was determined from the plots of pile displacement versus time of loading, Figures A.24 to A.46. The point of minimum strain rate was calculated visually from enlarged plots of the deformation time data for each test. The time to and deformation at this failure point were recorded, whenever time dependent deformation was observed solely during the final load step. The minimum pile velocity, $\dot{u}_{min}$ (mm/min), was converted to $\dot{u}_a/a$ (1/year), the pile velocity normalized to the pile radius, so as to be

compatible with data presented in the literature. A summary of the data measured from the tests is contained in Table 5.1. In this table, the calculated normalized pile velocities are quoted. To convert to the minimum pile velocity measured, multiply by the pile radius, 13.5 mm and convert the time units to minutes.

It will be noted that there are several sets of data for given combinations of temperature and salinity reported in this table. In several instances, the strength of the piles tested incrementally are higher than piles which failed under a single load increment. This can be attributed to the apparent strain hardening behaviour which is discussed in Section 5.2.6.

5.2.2 Pile Velocity equations

The equation relating the steady state pile velocity to the average applied pile shaft stress, as presented by Nixon and McRoberts (1976);

$$\frac{\dot{u}_a}{a} = \frac{3^{(n+1)/2} B \tau_a^{\,n}}{(n-1)} \qquad (5.1)$$

is the basis of this portion of the analysis of the test results. This equation provides a phenomenological model for the behaviour of saline silty sand as observed by Nixon and Lem (1984). The equation describes a quasi flow law for a pile penetrating into frozen soil. The normalized pile velocity is related to the applied stress by the parameters

B and n. A plot of the pile shaft stress versus the normalized pile velocity for all of the test data, from which the creep parameters B and n can be determined, is found in Figure 5.1.

5.2.2.1 Best fit curves

The parameters B and n were determined for each set of data at a given temperature and salinity. For ease of analysis, Figures 5.2 to 5.4 present the data for each test temperature on a distinct plot. Straight lines were visually fitted to the data, as shown on these figures, and the creep parameters contained in Table 5.2 were calculated. The data obtained from tests at -13°C was insufficient for the evaluation of the parameters B and n. The data found at -10°C was more extensive, and permitted the definition of lines for salinities of 5 and 15 ppt. The slopes of these lines were 5.5 and 4.7 respectively. An average value of n=5 was utilized to fit lines through the data points at 0 and 10 ppt. The experimental data base was most complete at -5°C. The slope of the lines fitted through this data varied quite drastically, as shown on Figure 5.4.

It is evident that there is not a great deal of data on Figure 5.4 for each salinity at -5°C. Therefore a slight change in the determination of the value of the minimum strain rate for a given stress could alter the slope of the best fit line and the value of n quite significantly. A small change in slope can lead to a large change in the value of n determined. Hence caution must be exercised in

the determination of n due to the strong influence of the value of the minimum pile velocity.

The review of current literature contained in Section 3.5 indicates that most researchers use a value of n=3. The exception to this rule is the data presented by Sego et al (1982), wherein the value of n found from testing of frozen saline sand at -7°C varies between n=5 for 0 ppt samples to n=1.25 for a salinity of 100 ppt. The results of this study are presented in Figure 5.5, and compared with the test data generated during the testing for this thesis. As can be seen on Figure 5.5, the slope varies from n=25 at 5 ppt to n=2 at 15 ppt. It is evident that the variation in n with increasing salinity is far greater for the silty sand than for the sand. It should be noted that the comparison is being made between different soils at different temperatures.

For purposes of discussion, the magnitude of the pile shaft stress required to initiate two specific pile velocities, 1 and 100 (1/year), at -5°C have been determined from Figure 5.4, and are contained in Table 5.3. These results indicate that increasing salinity reduces the resistance remarkably, with the greatest change between 5 and 10 ppt. In addition, the increment in applied shaft stress required to change the pile velocity by this value increases with increasing soil salinity. From these observations it may be concluded that increasing salinity reduces the resistance, both in terms of the absolute

magnitude of stress corresponding to a given pile velocity, and with regard to the greater increases in pile velocity with increments in the applied pile shaft stress.

5.2.2.2 Determination of B for n=3 and n=5

Lines of slope n=3 and n=5 were fitted visually through the data in an attempt to facilitate comparison of the data to that presented in the literature. These lines are shown in Figures 5.6 to 5.8. The parameters resulting from the curve fitting calculations are presented in Table 5.4, and the variation of B with salinity shown in Figures 5.9 and 5.11.

Table 5.5 contains the pile shaft stresses required to initiate normalized pile velocities of 1 and 100 (1/year), for curves of constant slope n=5 at -5°C, to correspond with the data from the best fit lines given in Table 5.3. These results again demonstrate a drastic reduction in the adfreeze strength with increasing salinity. In this case, however, the increment in applied shaft stress to increase the normalized pile velocity to a specific value is much greater for the lower salinity samples.

The use of a constant slope for the analysis of data for soils of differing salinities at a given temperature has the result that the increase in stress required to cause a specific increase in pile velocity, when divided by the value of the initial stress, will give the same ratio independent of the salinity. Hence it can be concluded that an increase in salinity will decrease the absolute magnitude

of stress required to initiate a given pile velocity and will have no effect upon the proportional increase in stress required to increase the pile velocity.

5.2.2.3 Comparison to other test data

In an effort to determine the validity of the parameters B and n, the data was compared with the results of different authors. The parameters found by Nixon and Lem (1984) from tests on saline silty sand are included in Figure 5.13, and are used to predict the pile velocity for a given shaft stress in Figure 5.14. Figure 5.13 includes the data determined from the lines of slope n=3 fitted to the model pile load tests for each salinity at -5°C and for 15 ppt at each temperature. This figure indicates that the values of B found from the research for this thesis are greater than those found by Nixon and Lem (1984). Hence the results of the unconfined compression tests on this soil will predict a lower strain rate for a specific stress than will the results of the model pile load tests.

Figure 5.14 contains the results of the model pile tests and the pile velocity for an applied stress predicted by Nixon and Lem. Examination of this plot indicates that the data for 0 ppt corresponds well at both -5 and -10°C. However the model pile results for 5 ppt at both temperatures fall on the line given by Nixon and Lem for 35 ppt. Model pile tests conducted in soils of salinity greater than 5 ppt at these temperatures indicated a much reduced resistance to load. It can be concluded that the influence

of saline pore fluid upon the resistance of the adfreeze bond, predicted by the results of Nixon and Lem, is significantly less than that found from the model pile load tests, for any given pile shaft stress.

Figure 5.14 contains data presented by Nixon (1988) from field pile load tests at Clyde River. These points are assumed to represent a native soil slurry backfill of salinity 10 to 15 ppt at a ground temperature of -10°C. As can be seen in the figure, the field results compare well with the results of the laboratory tests for the same temperature and salinity.

The results of constant displacement rate tests by Parameswaran (1978b) and the University of Alberta (1988) on sandblasted model piles in sand and sand slurry backfill respectively are given in Figure 5.15. These results provide an upper limit to the data from the model pile creep tests conducted for this thesis. The data from the piles in sand at -5 to -6°C falls in the range of the data for piles in fresh water silty sand at -13 and -10°C. This is a reasonable observation, as sand blasted piles in non-saline sand would be expected to be more resistant to load than sand blasted model piles in non-saline silty sand. For this data the parameters are n=6.4 and B=2.43E-08 ($kPa^{-n}year^{-1}$).

Figure 5.16 summarizes the results of field pile load tests on sand slurry backfilled piles, conducted by several consultants in the Arctic. The data was presented in the reports of Hoggan (1985), Nixon (1988) and Thurber (1983).

All of these tests are considered to represent the failure of piles in sand of minimal salinity (0 to 1 ppt) at temperatures of -5 to -6°C. This data compares favourably with the model pile test results at -5°C, lying in the range of 0 to 5 ppt. A line fitted through the field data provides the parameters; n=3.5 and B=4.45E-08 ($kPa^{-n}year^{-1}$). Since the results of the model piles at 5 ppt can correspond with the field data at 0 ppt, the model pile tests may overestimate the resistance of full scale piles. However, this observation is based upon a comparison of sandblasted model piles in silty sand to untreated piles in the field, backfilled with a sand slurry.

5.2.2.4 Influence of Salinity and Temperature on the parameters B and n

The influence of salinity and temperature on the parameters B and n determined from the model pile tests has been discussed to a certain extent in the preceeding section. The The best fit lines to the data at -5°C presented a decreasing value of n with increasing salinity. This trend, although not so extreme, was observed by Sego et al (1982) from tests on saline sand at -7°C.

It should be noted that the slope of the best fit lines through the data plotted on double logarithmic axes of pile shaft stress to minimum pile velocity is very sensitive to the determination of the minimum pile velocity. A slight change in the rate of strain observed for a given stress could alter the position of the fitted curves significantly.

The creep parameter B was also determined for lines of slope n=3 and n=5 fitted through the data. Figures 5.9 and 5.11 present the influence of salinity on the creep parameter B.

It should be noted that the slope of the best fit lines

A pictoral presentation of the influence of salinity for a given temperature is given in Figures 5.6 to 5.8. Similarly the influence of temperature on a specific nominal soil salinity is presented in Figures 5.17 to 5.19. Examination of these plots shows that the change in salinity from 0 to 15 ppt or change in temperature from -5 through -10 to -13°C results in an equal offset in the fitted lines for equal changes in salinity or temperature. This observation is also made from the generally straight lines through the data points shown in Figures 5.9 to 5.12; the plots of parameter B versus salinity and temperature.

5.2.3 Prediction of Phase Composition Curves

The unfrozen water content for non-saline silty sand was determined using the method presented by Tice et al (1976), as discussed in Section 2.2.2.

Liquid limit tests were conducted on the silty sand. The individual test results are shown in Figure 5.20. The low percentage of clay in the soil prevented the determination of the liquid limit at moisture contents below 17.5 precent. Hence the extrapolation of the liquid limit flow curve to N = 100, in Figure 5.20 is tenuous, given the

narrow range of data between N = 6 and N = 18. The moisture content at blow counts of N = 25 and N = 100 were calculated from this plot to be 17.15 and 15.48 percent respectively. The unfrozen water content at -1 and -2°C was then calculated using equations 2.1. The unfrozen water content for these two temperatures defines a straight line on double logarithmic axes, as shown in Figure 5.21. This line can then be utilized to calculate the predicted unfrozen water content for other temperatures, thereby developing a typical phase compostion curve as shown in Figure 5.22 for 0 ppt.

Figure 5.22 also contains phase composition curves for the other test salinities. These curves were calculated using the equations presented by Patterson and Smith (1983), which were also discussed in Section 2.2.2. It is evident from these curves that the unfrozen water content of a soil depends very strongly upon the salinity. In general, these curves show that for a given temperature, the unfrozen water content basically doubles for each 5 ppt increase in salinity. In addition, most of the decrease in the unfrozen water content with temperature occurs between 0 and -5°C for 0 ppt and 0 and -8°C for 15 ppt.

The results of the model pile load tests plotted in Figure 5.1 show that the data at -13 and -10°C for all salinities falls within a fairly narrow band. The -5°C data for the 10 and 15 ppt samples shows a significantly lower resistance. This is to be expected as the change in resistance of the piles is dependent upon the unfrozen water

content, and the largest variation in unfrozen water content occurs between 0 and -8°C.

The phase composition curves in Figure 5.22 begin at an unfrozen water content of five percent. This is the volumetric unfrozen water content of non-saline silty sand at -1°C. The unfrozen water content for saline soils near 0°C must be determined before the curves can be extended further.

5.2.4 Relationship between failure pile shaft stress and time to failure

The shaft stress at failure for the given design life of a pile can be predicted from short term test data, using the method of Vyalov. The equation upon which this method is based was presented by Vyalov (1962) in the form:

$$\sigma_u \beta = \ln\left[\frac{t_f}{B}\right] \qquad (5.2)$$

where σ_u= ultimate stress

t_f= time to failure

β, B= experimentally determined parameters.

The time to failure was originally defined as the time to onset of tertiary creep in unconfined constant stress compression tests. The analysis presented examines two definitions of the time to failure; the time to onset of tertiary, and the time to minimum strain rate. The applied

pile shaft stress τ_s is substituted for the ultimate stress σ_u in the equations used in this analysis.

The use of this theory requires at least two determinations of the time to failure for pile shaft stress for each salinity and temperature. In addition, the data points must be derived from single increment tests free of the possible effects of load history. These restrictions on the data preclude the analysis of the -10 and -13°C data. However, sufficient data at -5°C is available to predict the long term resistance of piles in saline soil using this procedure.

The parameter β was determined from the slope of lines defined by a plot of the inverse pile shaft stress to the time to failure on linear logarithmic axes. This graph is shown in Figure 5.23. It will be noted that the data for both the time to minimum and the time to onset of tertiary are included. The slope of the lines for salinities of 15 and 10 ppt are parallel, while the slope is different for the 5 ppt results. From this plot, the pile shaft stress at 1 hour can also be found. Using the equation;

$$\log\left[\frac{1}{B}\right] = \frac{\beta}{\tau_1} \qquad (5.3)$$

where $1/\beta$= the slope of the plot of inverse shaft stress to the log of time to failure

τ_1= the shaft stress at 1 hour.

the parameter B was calculated for each temperature and salinity. The results of this analysis are summarized in Table 5.6. It is evident from Figure 5.23 that additional data is required to truly quantify this behaviour.

The Vyalov equation was then utilized to predict the long term pile behaviour as shown in Figures 5.24 and 5.25 for the time to minimum, t_{min}, and the time to onset of tertiary, t_{tert}, respectively. Comparison of the two plots shows that the curves for 10 and 15 ppt are very similar for the two definitions of the time to failure. The time to minimum data predicts a higher allowable pile shaft stress at a given time than does the time to onset of tertiary data for the 5 ppt data.

Table 5.7 contains the estimate of the allowable shaft stress for a reasonable design life from these plots. The application of a factor of safety to these values produces very low allowable pile shaft stresses for design.

5.2.5 Relationship between adfreeze strength and unconfined compressive strength

Weaver (1979) postulated that the adfreeze strength of a pile, τ_a could be estimated from the shear strength in unconfined compression tests, τ_u using the equation;

$$\tau_a = m \cdot \tau_u \qquad (5.4)$$

where m= 0.6 for steel piles.

Unconfined compression tests on saline silty sand are being conducted at the University of Alberta by Hivon. At the time of writing, data for tests at -5°C was available (Hivon, personal communication). The results of the unconfined compression tests and model pile tests are summarized in Table 5.8.

The pile shaft stress to minimum pile velocity results of the model pile load tests at -5°C are plotted in Figure 5.26. Straight lines were fitted visually through the data at random slopes, for n=3 and for n=5. These lines were used to estimate the pile shaft stress at the strain rate of 0.027 mm/min, used by Hivon in her constant displacement rate tests. The shaft stresses determined at this rate are tabluated in Table 5.9. Also included in this table are the values of m calculated from this data.

The results of this analysis are comparable to Weaver's postulate, with the exception of m=1.91 for the 5 ppt, n=3 and n=5 data points. Excluding these points, the average value of m for these sand blasted model piles in found to be approximately 0.4. Weaver predicted that m for piles in non-saline frozen soil would be 0.6, which would overpredict the strength obtained from these model pile tests.

5.2.6 Hereditary creep

Incremental load tests were undertaken in this research in an attempt to produce more data from a single test sample. Inherent in the use of step loading procedure is the

assumption that the pile deformation response to a particular load is independent of the stress history of the soil. This assumption was presented formally by Ladanyi (1972), as discussed in Section 2.3.

The unconfined compression test data provided by Hivon (1988) indicates that the saline silty sand undergoes strain hardening behaviour. If the soil in the pile load tests is also exhibiting strain hardening behaviour, the assumption of hereditary creep is no longer valid. Strain hardening could affect the response in two ways: the pile displacement rate for a given applied stress could be the same, but the displacement to failure would increase with the application of successive load steps, or the pile displacement rate for a given pile shaft stress would be greater for a single load step test than for an incremental strain hardening test.

Figures 5.1, 5.27 and 5.28 summarize the test results for all of the temperatures and salinities. These plots allow an evaluation of the validity of the assumption of hereditary creep.

The first figure in the series shows all of the data points. The results of tests in which incremental load steps lead to the observation of time dependent deformation in more than one step, are omitted from Figure 5.27. Figure 5.28 shows only those data points from single increment tests.

It can be seen in Figure 5.1 that there is a great deal of scatter in the data points at 5 ppt at -13°C, and 0 ppt

at -10 and -5°C, preventing any prediction of the pile velocity equation parameters. On the other hand, the data for 5 and 15 ppt at -10°C defines a line which follows the trend defined by the data. These points are all derived from tests in which time dependent deformation was observed before the final load step.

A comparison of Figures 5.27 and 5.28 reveals that the tests at 15 ppt and -13°C could exhibit strain hardening. The data from the last load step of the incremental test indicates a much greater resistance to load, than was found in the single step test. In comparison, the tests at 10 ppt and -5°C are apparently not affected by strain hardening, as the data from incremental tests lie on the straight line defined by the data from the single increment tests.

It is evident from Figure 5.28 that the data from the single load step tests alone is insufficient to quantify the soil behaviour for most of the combinations of salinity and temperature.

On each plot, there are data points which support and which negate the theory of hereditary creep. Obviously, additional test data is required to determine the validity of this theory.

As was noted previously, the response of the soil to load does not follow a typical creep configuration. Instead the response is that of a structured soil, for which the hereditary creep theory would not be expected to apply.

5.3 Summary

The results of the model pile constant load tests on saline silty sand are discussed in the preceding sections. It is evident that the test data are valuable as indicators of the effect of salinity, temperature and magnitude of load on the pile response, but are insufficient to permit the development of a definitive theory.

In addition it is apparent that the theories based upon a minimum strain rate which assume typical creep behaviour are inappropriate for such structured soils.

Table 5.1 Results of model pile creep tests in frozen silty sand

	T_t	S	τ_a	$\dot{u}_a/a$	t_f	d_f	ρ_{dry}	S_w	
	°C	(ppt)	(kPa)	(year^{-1})	(min)	(mm)	$\frac{Mg}{m^3}$	(ppt)	
1.1	-13	0	15	0			1.72		N
			44	0					
			71	0					
			182	0					
			345	0					
			426	0					
			606	FAILURE	400	0.1			
1.2	-13	5	19	0			1.73		N
			57	0.029					
			93	0.047					
			193	0.028					
			433	1.518		1.3			
1.3	-13	10	15	0			1.71		N
			45	0					
			74	0					
			189	0					
			356	45.94	30	0.1			
1.4	-13	15	15	0			1.71		N,S*
			45	0					
			60	0					
			178	0					
			337	194.7	20	1.0			
1.5	-13	15	216	1206.9	1.5	0.2	1.73		R
2.1	-10	0	24	0.060			1.71		R
			200	0.135					
			349	0.154		0.9			
2.2	-10	5	26	0			1.65	5.7	N
			52	0					
			78	0.034					
			156	1.386		0.6			
2.3	-10	10	29	0			1.69	10.9	
			129	0					
			200	36.01	40	0.1			
2.4	-10	10	19	0			1.66	11	
			43	0					
			72	0					
			148	104.7	15	0.3			
2.5	-10	15	16	0			1.59	16.4	S*
			40	0.210					
			57	3.410		1.0			
2.6	-10	15	20	0			1.72	16	
			50	0					
			79	0					
			156	63.46	50	0.5			

	T_t	S	τ_a	$\dot{u}_a/a$	t_f	d_f	ρ_{dry}	S_m	
	°C	(ppt)	(kPa)	(year^{-1})	(min)	(mm)	$\frac{Mg}{m^3}$	(ppt)	
3.1	-5	0	78	0.412			1.71		R
			97	0.084					
			115	0.142					
			135	0.114					
			158	0.069					
			193	0.285		0.7			
3.2	-5	5	40	0			1.70	5	R
			64	0					
			85	0.662	1600	0.2			
4.1	-5	5	71	10.2	100	1.0	1.72	5	R
4.2	-5	5	96	9.5	20	.07	1.72	5	N
3.3	-5	10	36	121.9	25	0.4	1.68	11.3	R
3.4	-5	10	10	0			1.65	11.7	R
			17	0					
			27	2.48	500	1.3			
4.3	-5	10	26	0.807	400	0.6	1.71	10	N
4.4	-5	10	42	52.1	20	0.3	1.70	12	R
3.5	-5	15	7.5	58.4	250	1.5	1.68	16.8	R
3.6	-5	15	25	568.4	5	2.2	1.71	17.9	R
4.5	-5	15	12	97.2	8	0.9	1.71	16	R
4.6	-5	15	19	241.0	6	0.6	1.69	18	R

T_t = test temperature measured in soil mass
S^t = soil salinity
τ_a = applied pile shaft stress
$\dot{u}_a/a$ = minimum pile displacement rate normalized to pile radius
t_f = time to minimum strain rate, where failure occurs during the last load step
d_f = displacement at point of minimum strain rate from start of test
ρ_{dry} = dry density of the soil
S_m = average salinity measured after the test

NOTES: Results for the sample at 5 ppt and -13°C may be affected by glycol contamination of the soil.
S* denotes piles to which strain guages were applied.
N denotes freshly mixed soil.
R denotes re-used soil.
Additional detail for the density and salinity measurements can be found in table A.1.

Table 5.2 Creep parameters from best fit lines for saline silty sand

$$\dot{u}_a/a = \frac{3^{(n+1)/2} B \tau_a^{\,n}}{n-1}$$

Salinity ppt	n	B $kPa*10^{-n}yr^{-1}$
Temperature = -5°C		
5	25	$5.44*10^{-53}$
10	13.5	$2.04*10^{-22}$
15	2	0.193
Temperature = -10°C		
0	5	$1.91*10^{-14}$
5	5.5	$2.52*10^{-13}$
10	5	$3.99*10^{-11}$
15	4.7	$1.95*10^{-09}$

Table 5.3 Relationship between normalized pile velocity and shaft stress from best fit lines for saline silty sand at -5°C

$$\frac{\dot{u}_a}{a} = \frac{3^{(n+1)/2} B \tau_a^{\,n}}{n-1}$$

	τ_a (kPa)		
$\dot{u}_a/a$	Salinity		
($year^{-1}$)	5 ppt	10 ppt	15 ppt
1	80	25	1
100	86	33	14
δ	6	8	13
δ/τ_{a1}	0.075	0.32	13

δ = increment in applied shaft stress to increase the pile velocity from 1 to 100 ($year^{-1}$).

τ_{a1} = shaft stress required to initiate pile velocity of 1 ($year^{-1}$).

Table 5.4 Creep parameters for saline silty sand

$$\dot{u}_a/a = \frac{3^{(n+1)/2} B \tau_a^{\,n}}{n-1}$$

	Creep parameter B			
T_t	Salinity (ppt)			
(°C)	15	10	5	0
n = 5				
-5	$2.51*10^{-05}$	$2.82*10^{-08}$	$5.95*10^{-11}$	$4.42*10^{-13}$
-10	$1.64*10^{-10}$	$3.99*10^{-11}$	$1.86*10^{-12}$	$1.91*10^{-14}$
-13	$2.75*10^{-11}$	$7.22*10^{-13}$	$1.75*10^{-14}$	
n = 3				
-5	$8.00*10^{-03}$	$3.62*10^{-05}$	$4.39*10^{-07}$	$1.29*10^{-08}$
-10	$1.83*10^{-06}$	$1.83*10^{-06}$	$3.89*10^{-08}$	$2.09*10^{-09}$
-13	$4.52*10^{-06}$	$1.89*10^{-07}$	$4.52*10^{-09}$	

T_t = nominal test temperature

Table 5.5 Relationship between normalized pile velocity and shaft stress for n=5 for saline silty sand at -5°C

$$\frac{\dot{u}_a}{a} = \frac{3^{(n+1)/2} B \tau_a^{\,n}}{n-1}$$

	τ_a (kPa)		
$\dot{u}_a/a$	Salinity		
$year^{-1}$	5 ppt	10 ppt	15 ppt
1	67	19	5.5
100	160	45	13
δ	93	26	7.5
δ/τ_{a1}	1.39	1.37	1.36

δ = increment in applied shaft stress to increase the normalized pile velocity from 1 to 100 ($year^{-1}$).

τ_{a1} = shaft stress required to initiate normalized pile velocity of 1 ($year^{-1}$).

Table 5.6 Prediction of parameters B and β for the Vyalov equation

$$\tau_a \cdot \beta = \ln\left[\frac{t_f}{B}\right]$$

θ	t_{min} (min)		t_{tert} (min)	
(ppt)	β	B	β	B
5	200	0.00631	133.3	0.2154
10	83.3	0.00562	83.3	0.0147
15	20.4	0.00754	20	0.0263

θ = nominal soil salinity.

t_{min} = time to minimum strain rate.

t_{tert} = time to onset of tertiary creep as defined by Vyalov.

Table 5.7 Allowable pile shaft stress for piles in saline silty sand at -5°C for 25 year design life using the Vyalov method.

Salinity ppt	τ_a kPa
5	17 to 20
10	8.5
15	2

τ_a = allowable pile shaft stress.

Table 5.8 Data from unconfined compression (Hivon, 1988) and model pile load tests on saline silty sand at -5°C

θ	σ_u	ϵ	τ_{aw}	τ_a	$\dot{\epsilon}_m$	t_f
(ppt)	(kPa)	$\left[\frac{mm}{mm}\right]$	(kPa)	(kPa)	$\left[\frac{mm}{min}\right]$	(min)
30	38.9	0.008	11.7			
	39	0.005	11.7			
15				7.5	$1.5*10^{-04}$	400
				25	$1.5*10^{-02}$	10
				12	$2.5*10^{-03}$	11
				20	$6.2*10^{-03}$	6
10	318.5	0.01	95.6	36	$3.1*10^{-03}$	60
				42	$1.3*10^{-03}$	40
5	419.3	0.006	125.8	71	$2.6*10^{-04}$	200
				96	$2.4*10^{-04}$	30

θ = soil salinity.
σ_u = unconfined compressive strength tested at 0.027 mm/min.
ϵ = strain corresponding to σ_u.
τ_{aw} = adfreeze strength calculated from unconfined compressive strength, using the relation; $\tau_a = 0.6*\sigma_u$, after Weaver, 1979.
τ_a = adfreeze strength of the model piles.
$\dot{\epsilon}_m$ = strain rate at minimum corresponding to τ_a.
t_f = time to minimum strain rate.

Table 5.9 Determination of parameter m from unconfined compressive strength and adfreeze strength testing of silty sand at -5°C

θ (ppt)	n	τ_a (kPa)	τ_u (kPa)	m
5	25	110	210	0.52
	5	290		1.38
	3	400		1.91
10	13.5	50	159	0.31
	5	83		0.52
	3	98		0.62
15	2	39	100	0.38
	5	23		0.23
—	3	30		0.30

θ = soil salinity.
n = creep parameter.
τ_a = adfreeze pile strength estimated for strain rate of 0.027 mm/min.
τ_u = unconfined shear strength tested at 0.027 mm/min.
m = strength parameter.

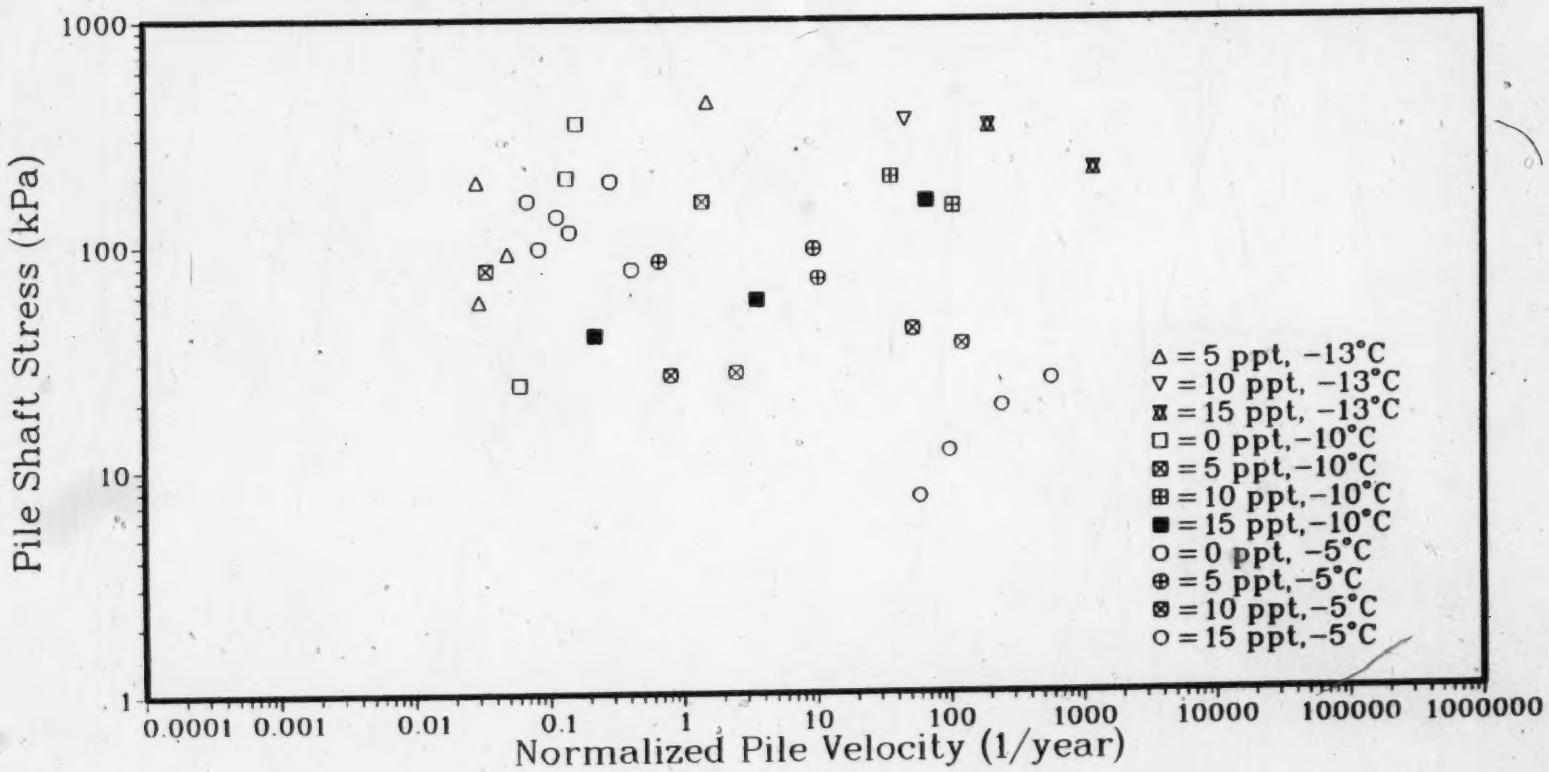

Figure 5.1: Summary of pile shaft stress and normalized pile velocity results from constant load tests of sand blasted model piles in frozen silty sand

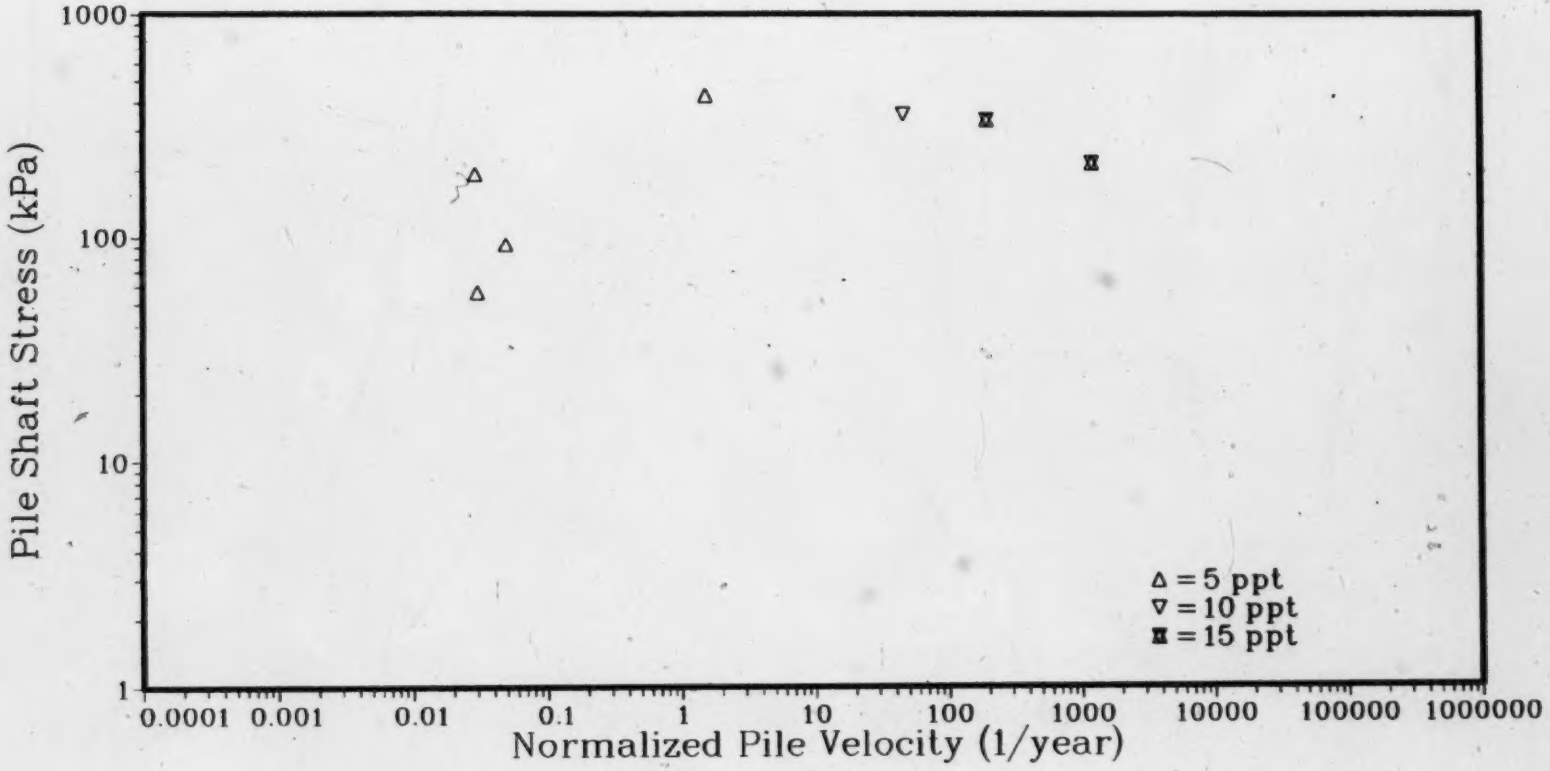

Figure 5.2: Pile shaft stress and normalized pile velocity results from constant load tests of sand blasted model piles in silty sand at −13°C

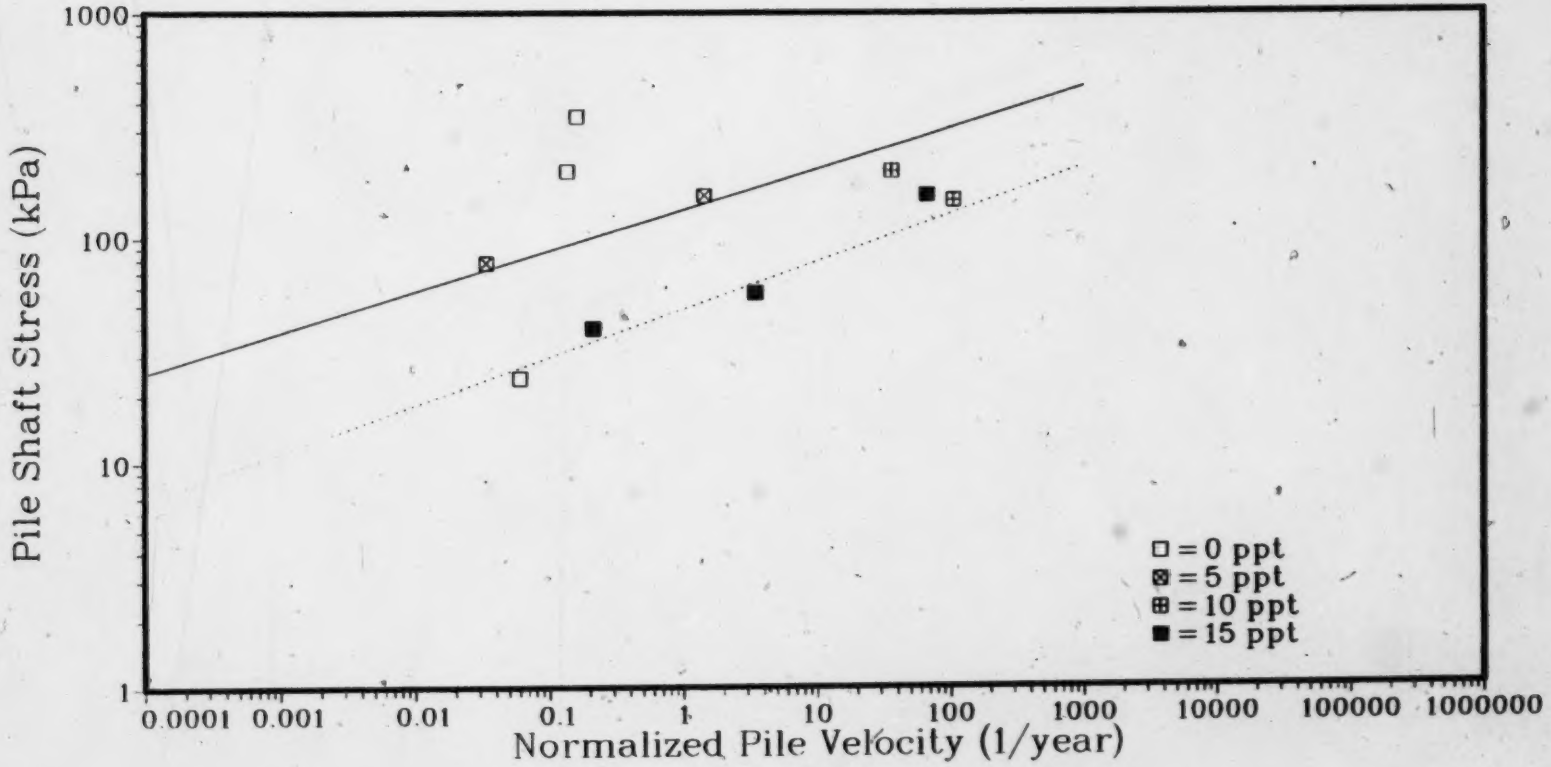

Figure 5.3: Pile shaft stress to normalized pile velocity results from constant load tests of sand blasted model piles in silty sand at −10°C

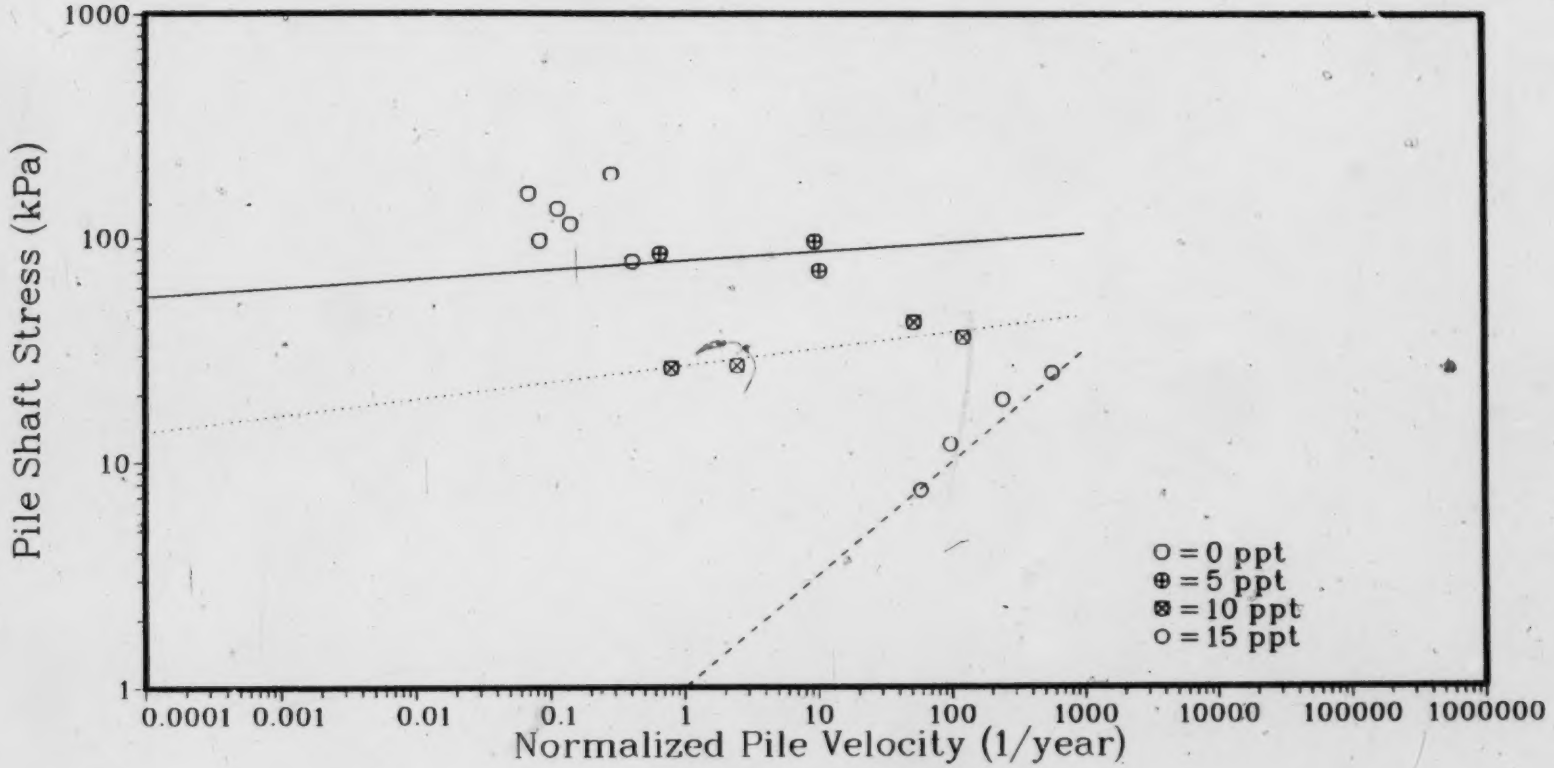

Figure 5.4: Pile shaft stress to normalized pile velocity results from constant load tests of sand blasted model piles in silty sand at −5°C

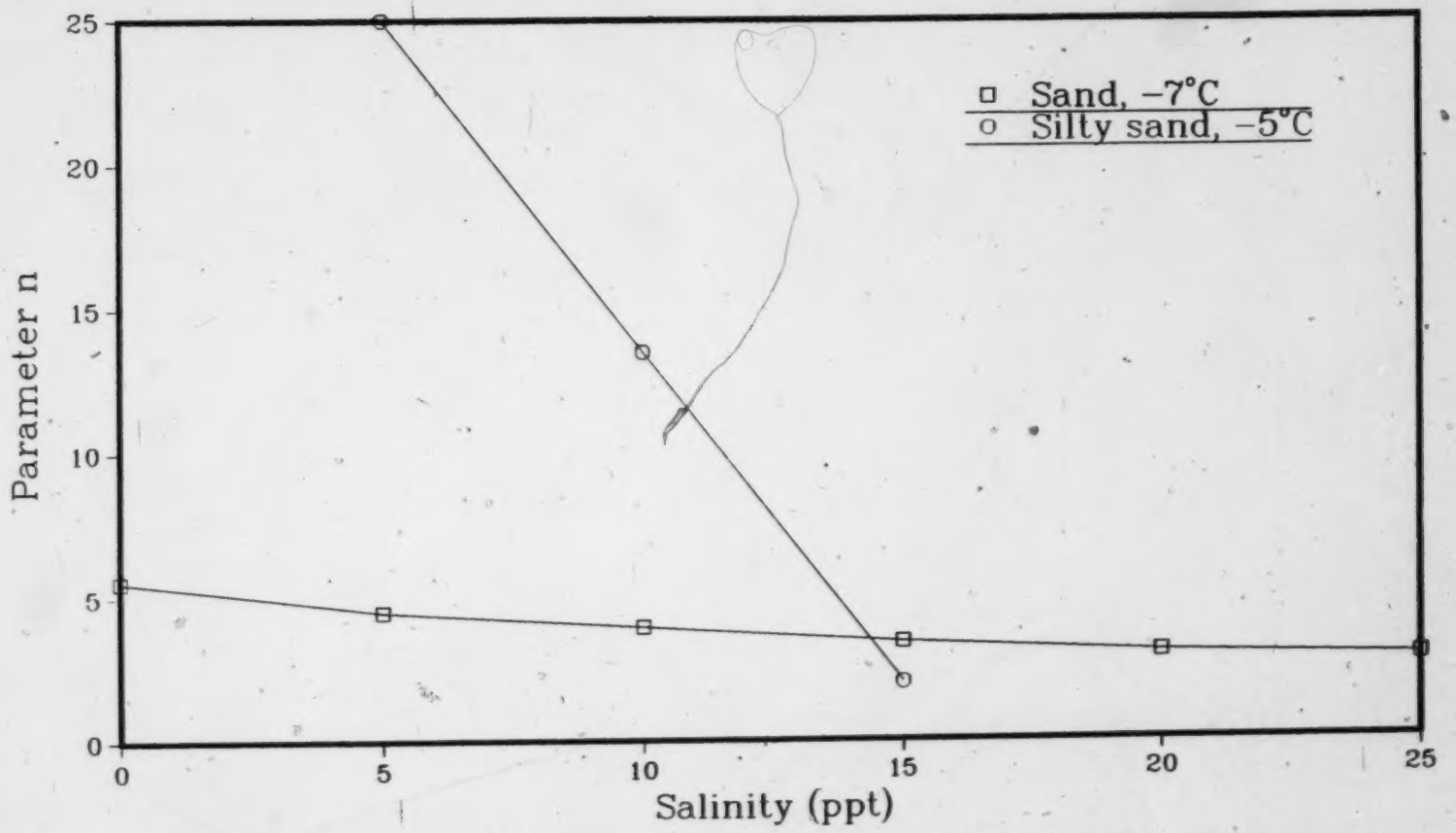

Figure 5.5: The relationship between the parameter n and salinity for sand at −7°C, Sego et al, 1982, and silty sand at −5°C

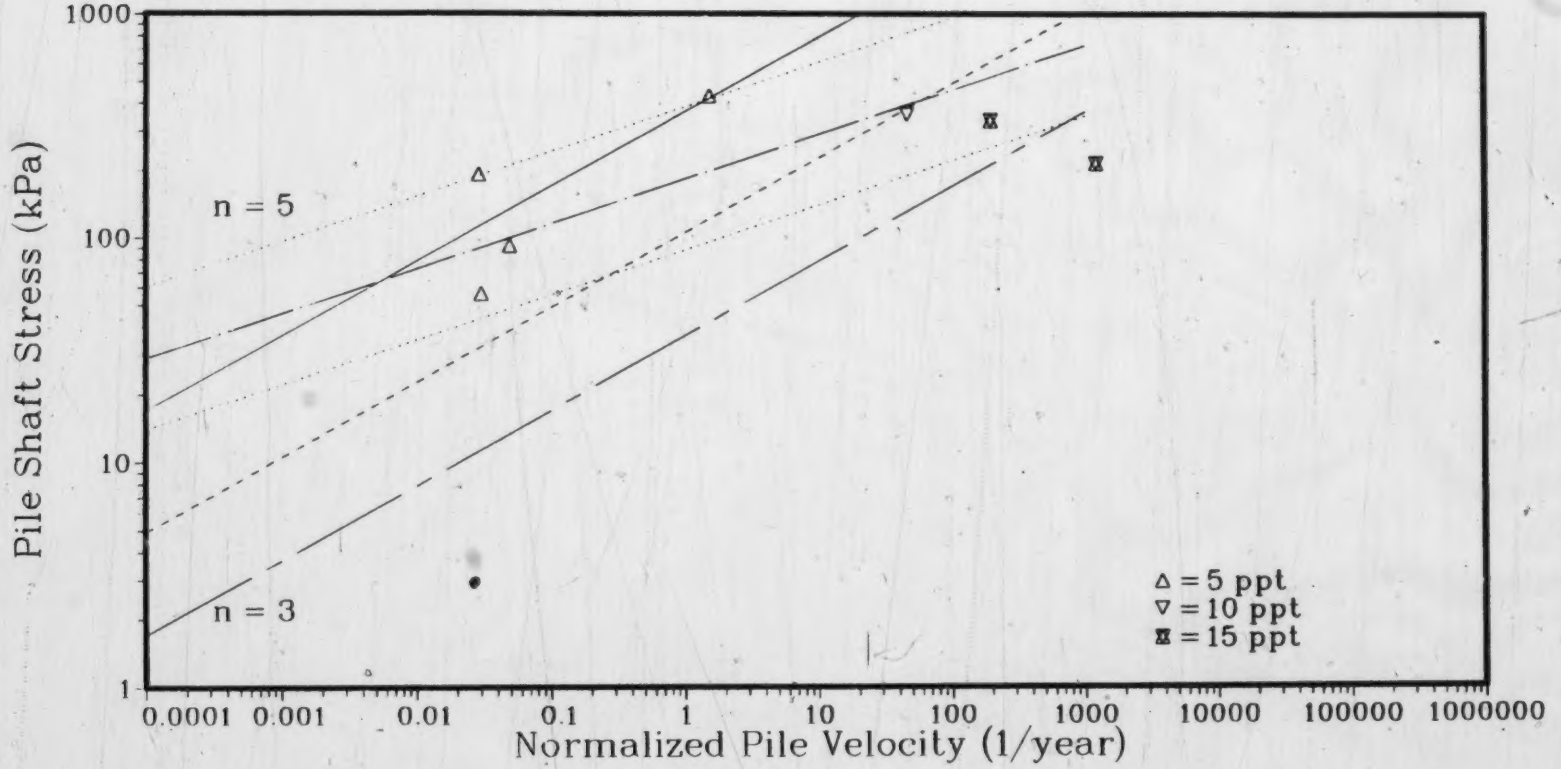

Figure 5.6: Determination of parameter B for n=3 and n=5 from results of constant load tests of sand blasted model piles in silty sand at −13°C

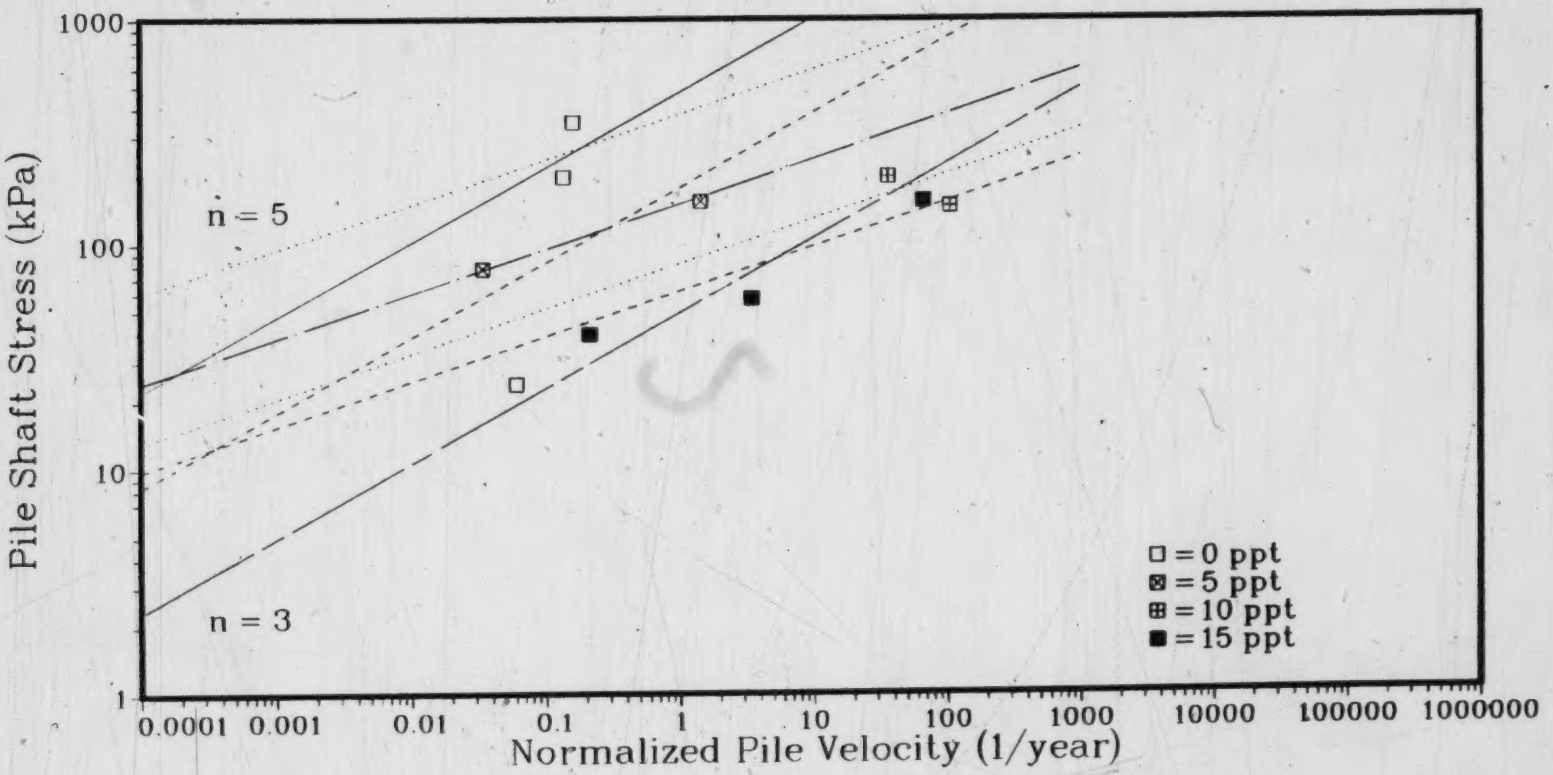

Figure 5.7: Determination of parameter B for n=3 and n=5 from results of constant load tests of sand blasted model piles in silty sand at −10°C

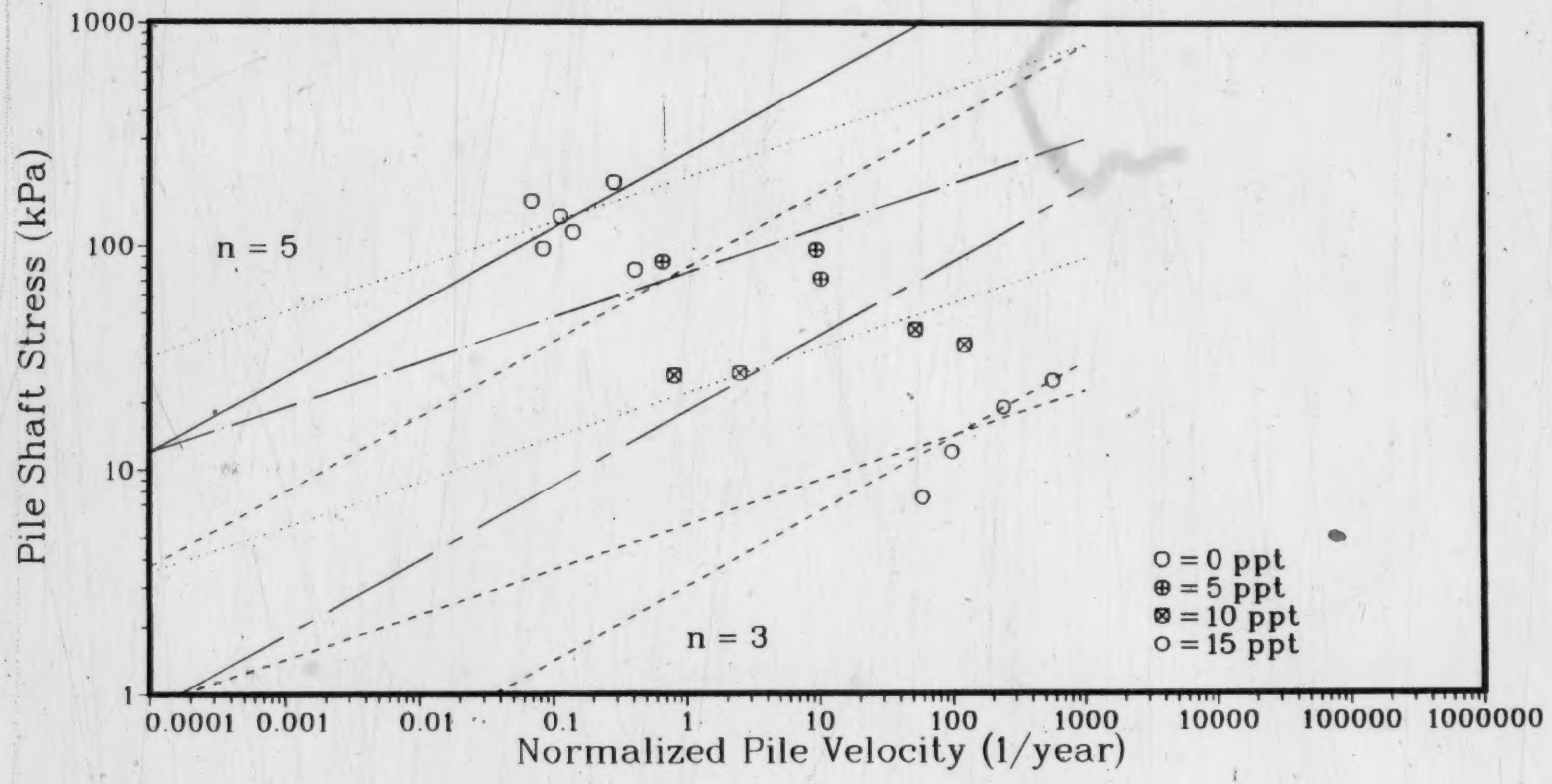

Figure 5.8: Determination of parameter B for n=3 and n=5 from results of constant load tests of sand blasted model piles in silty sand at −5°C

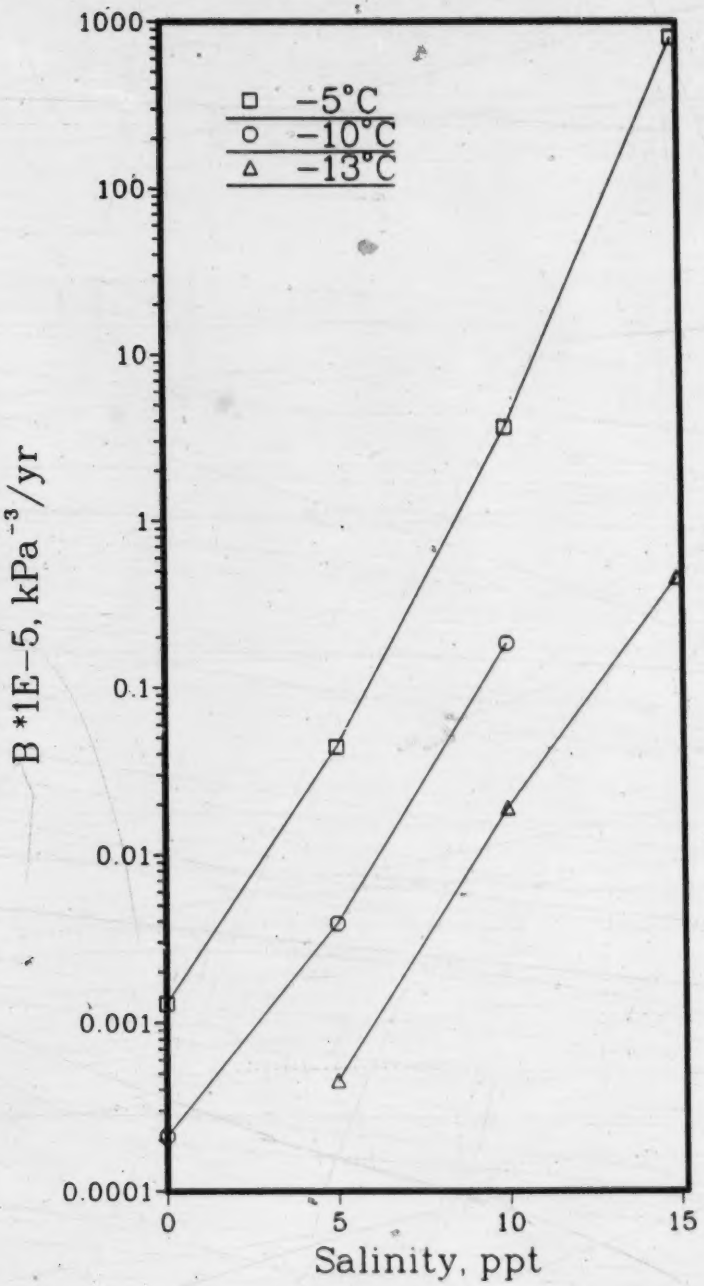

Figure 5.9: Relationship between the parameter B and salinity for silty sand with n = 3

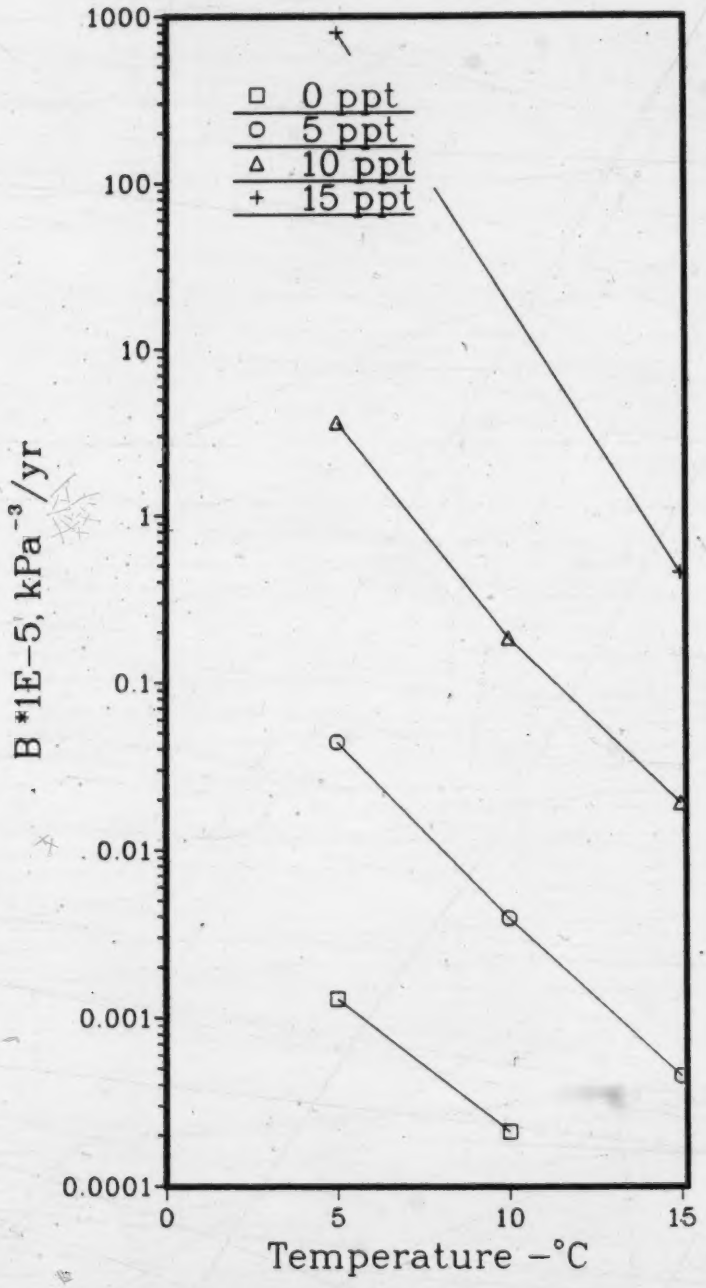

Figure 5.10: Relationship between the parameter B and temperature for silty sand with n =3

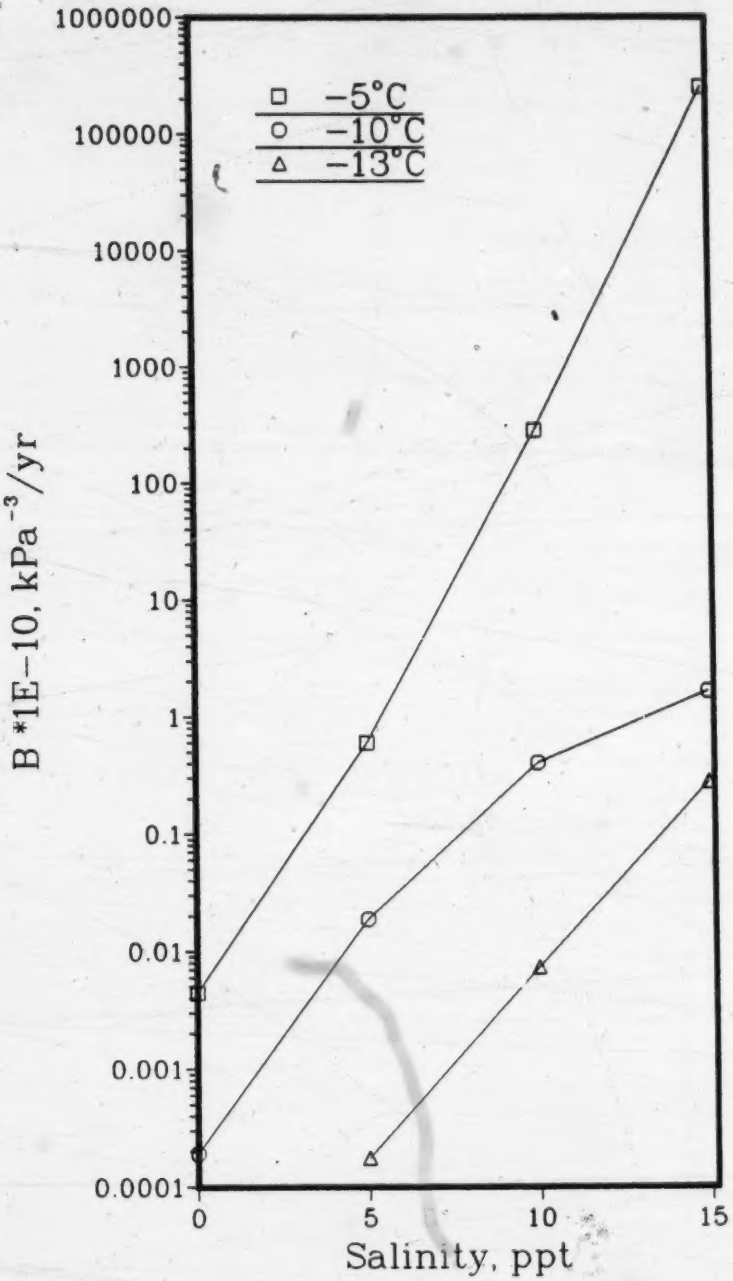

Figure 5.11: Relationship between the parameter B and salinity for silty sand with n = 5

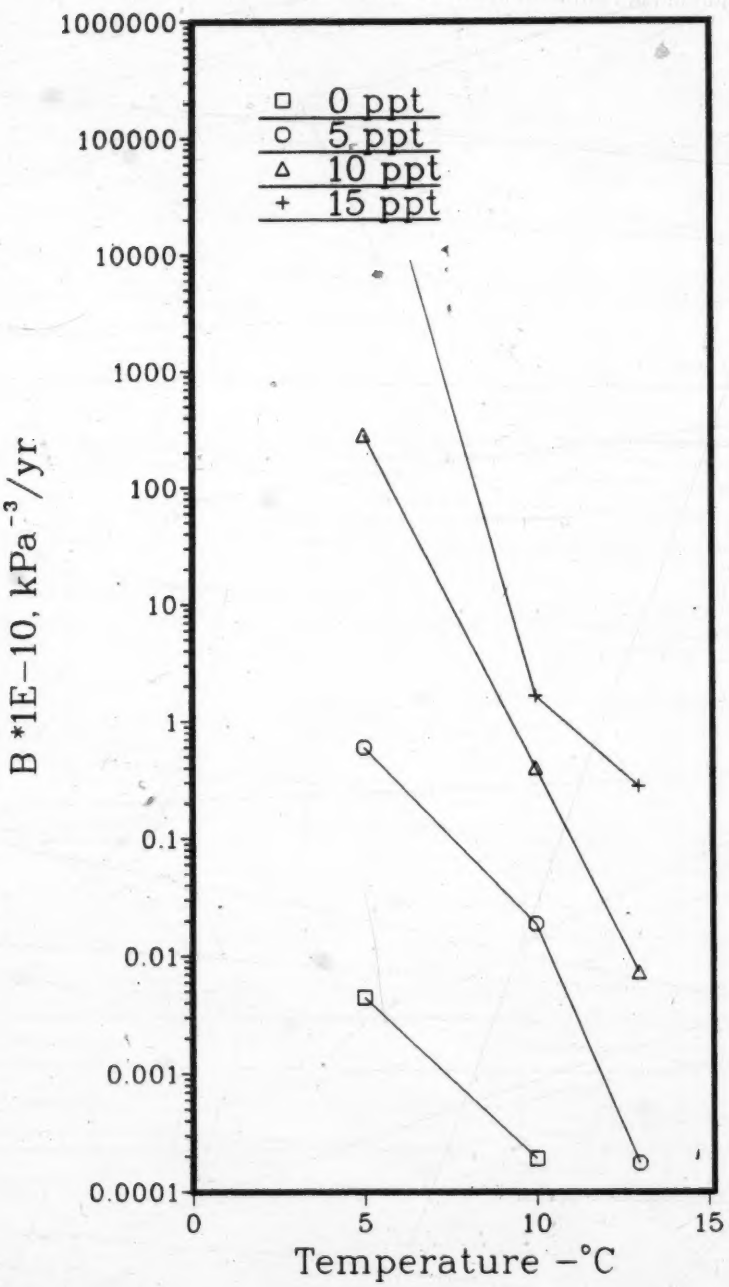

Figure 5.12: Relationship between the parameter B and temperature for silty sand with n = 5

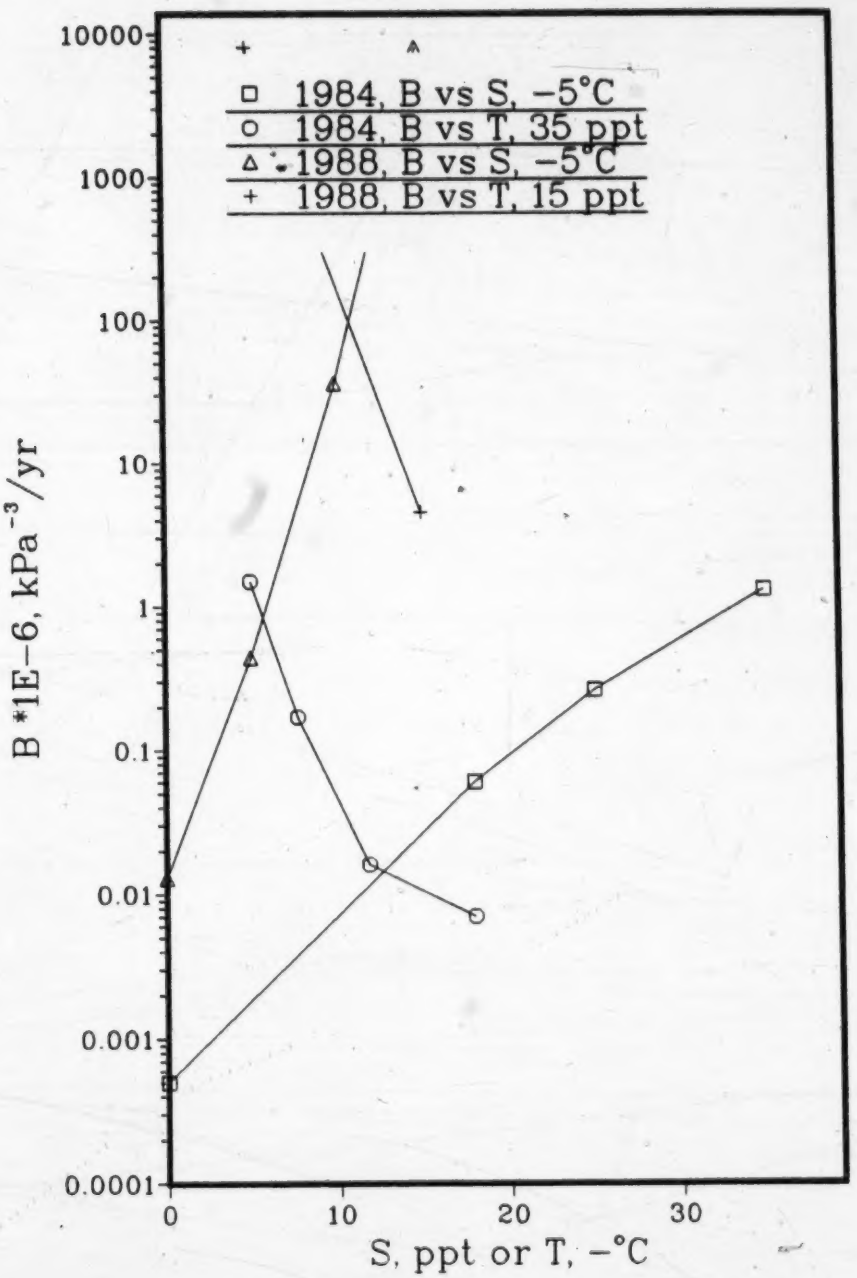

Figure 5.13: Relationship between B, salinity and temperature with n = 3 for silty sand, after Nixon and Lem (1984) and for model pile load tests (1988).

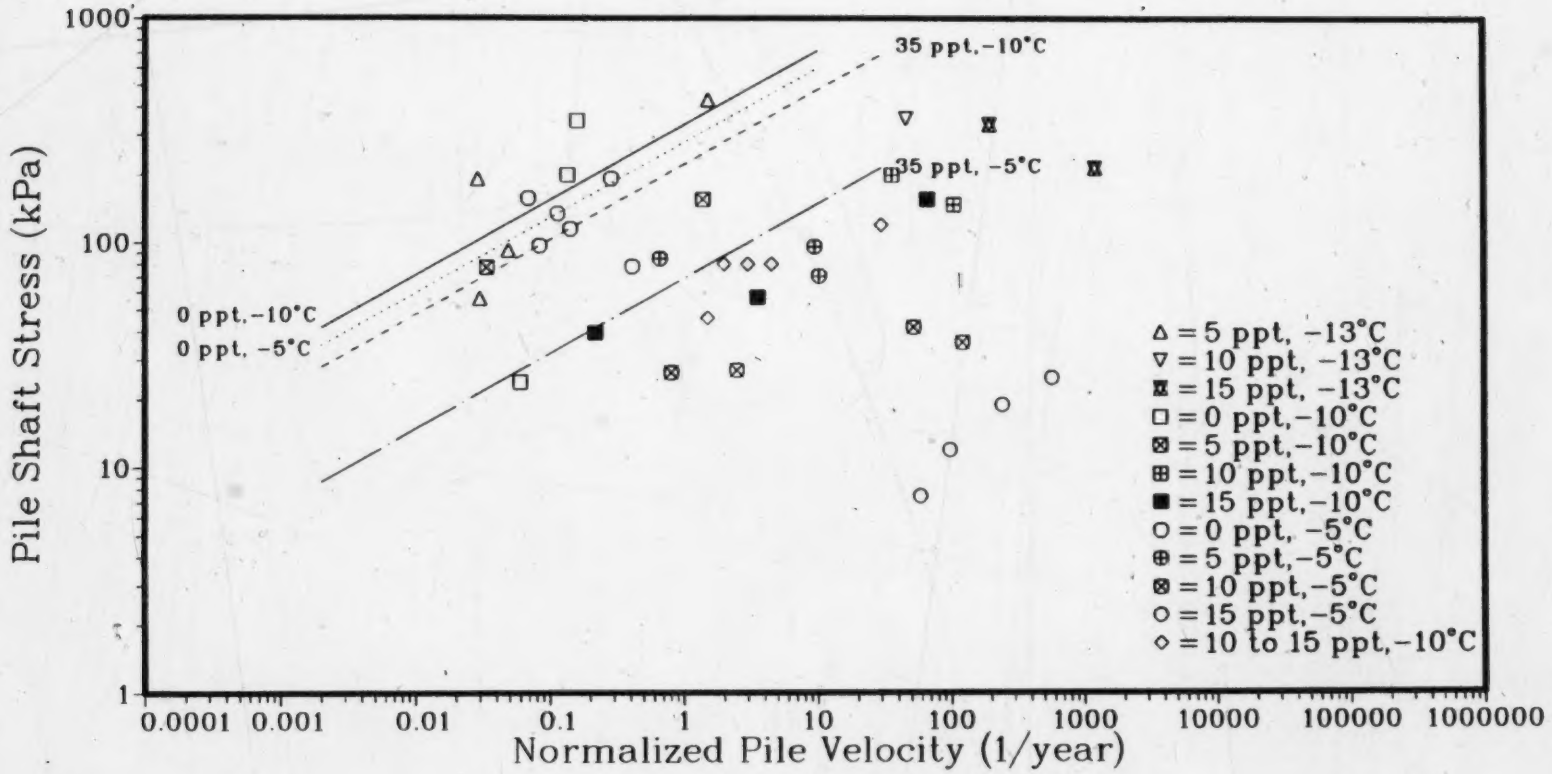

Figure 5.14: Pile shaft stress to normalized pile velocity results for saline silty sand; from uniaxial compression tests (Nixon and Lem, 1984), field load tests (Nixon, 1988) and from model pile load tests.

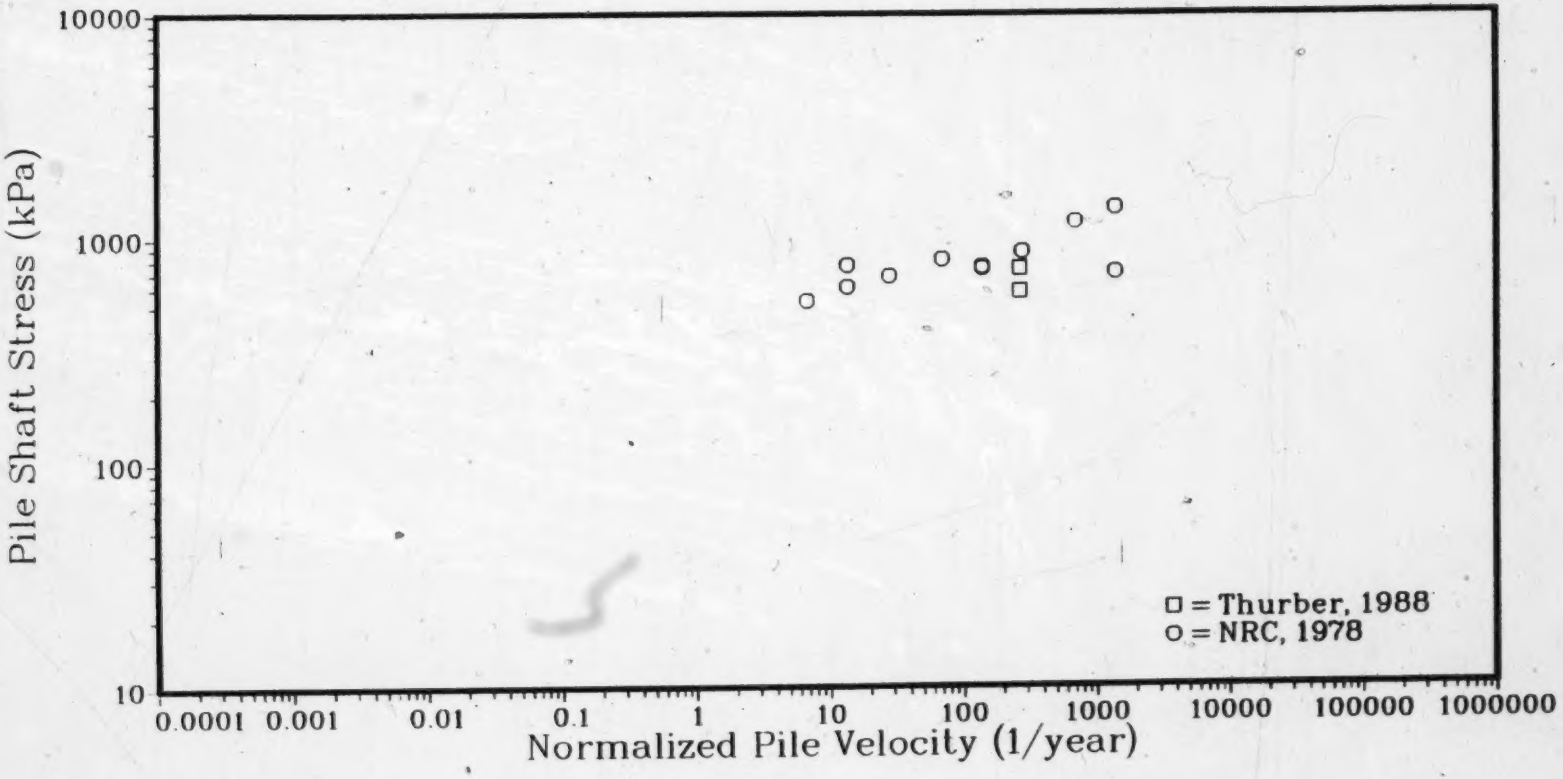

Figure 5.15: Pile shaft stress to normalized pile velocity from constant displacement rate tests on sand backfilled sand blasted model piles at −5 to −6 degrees C (Parameswaran, 1978b, and Thurber, 1988).

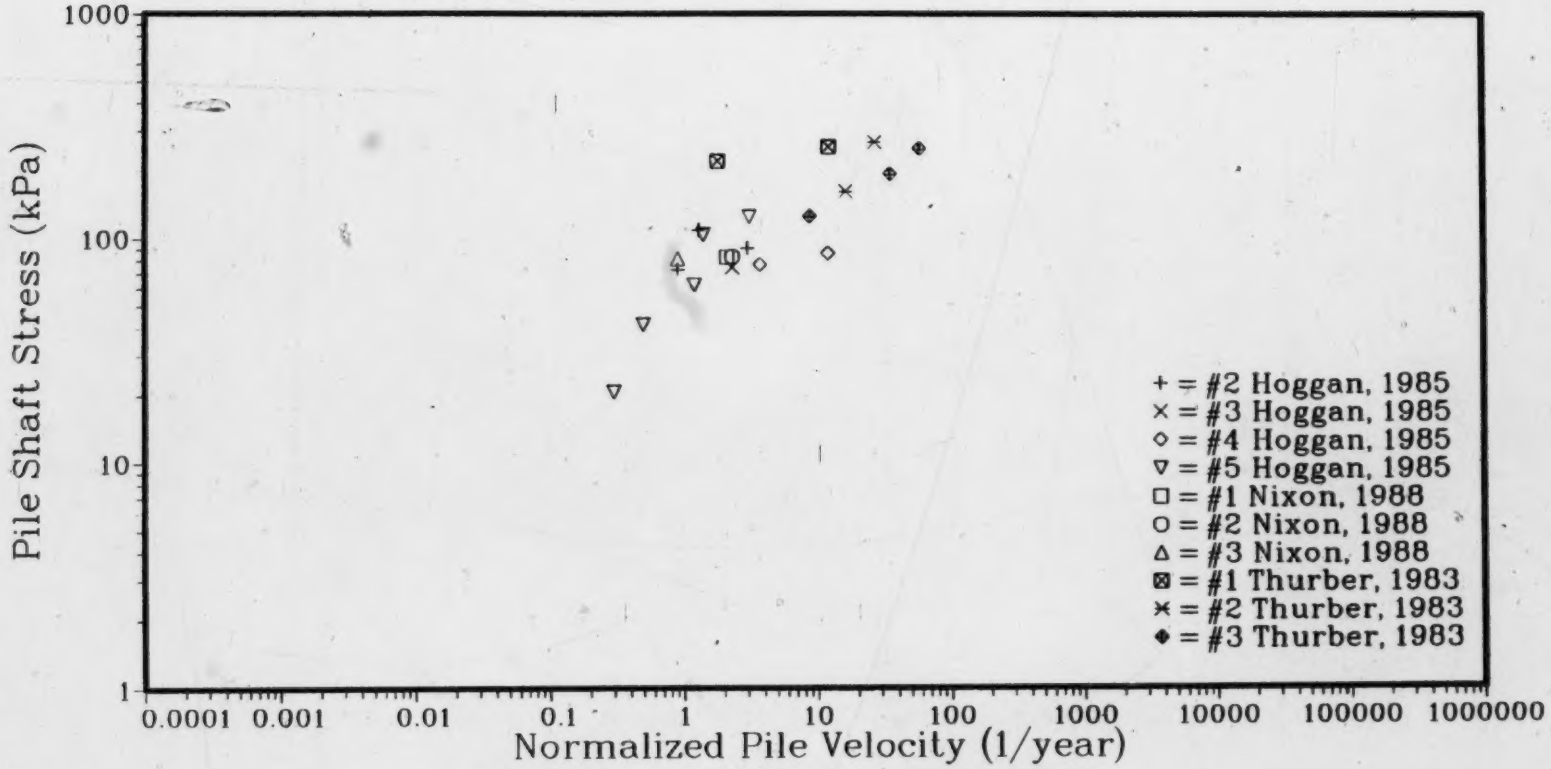

Figure 5.16: Pile shaft stress to normalized pile velocity results from field pile load tests on piles backfilled with sand slurry after Hoggan (1985), Nixon (1988) and Thurber (1983).

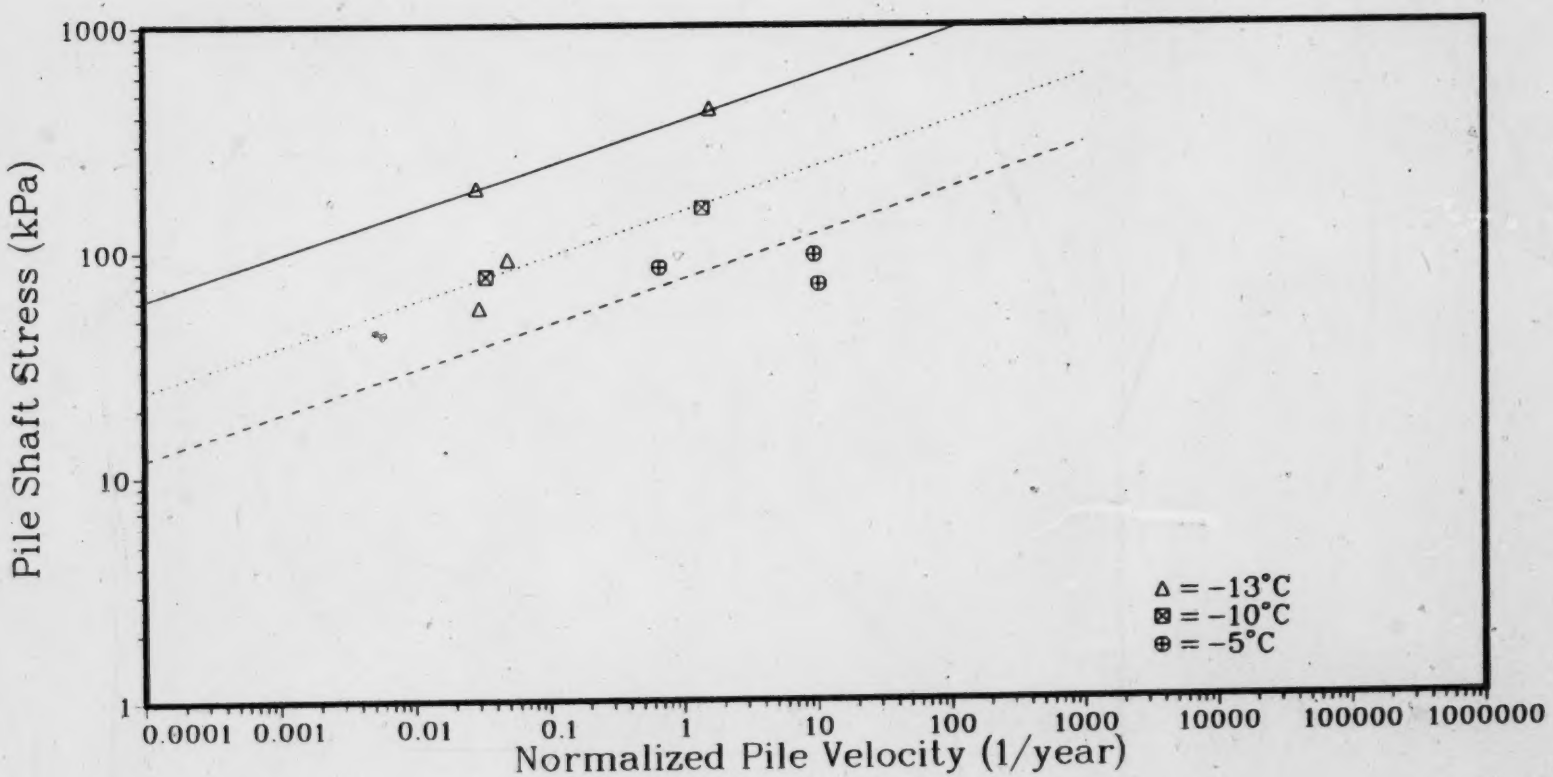

Figure 5.17: Pile shaft stress to normalized pile velocity from constant load tests on sand blasted model piles in silty sand of salinity 5 ppt. Parameter n assumed to be 5.

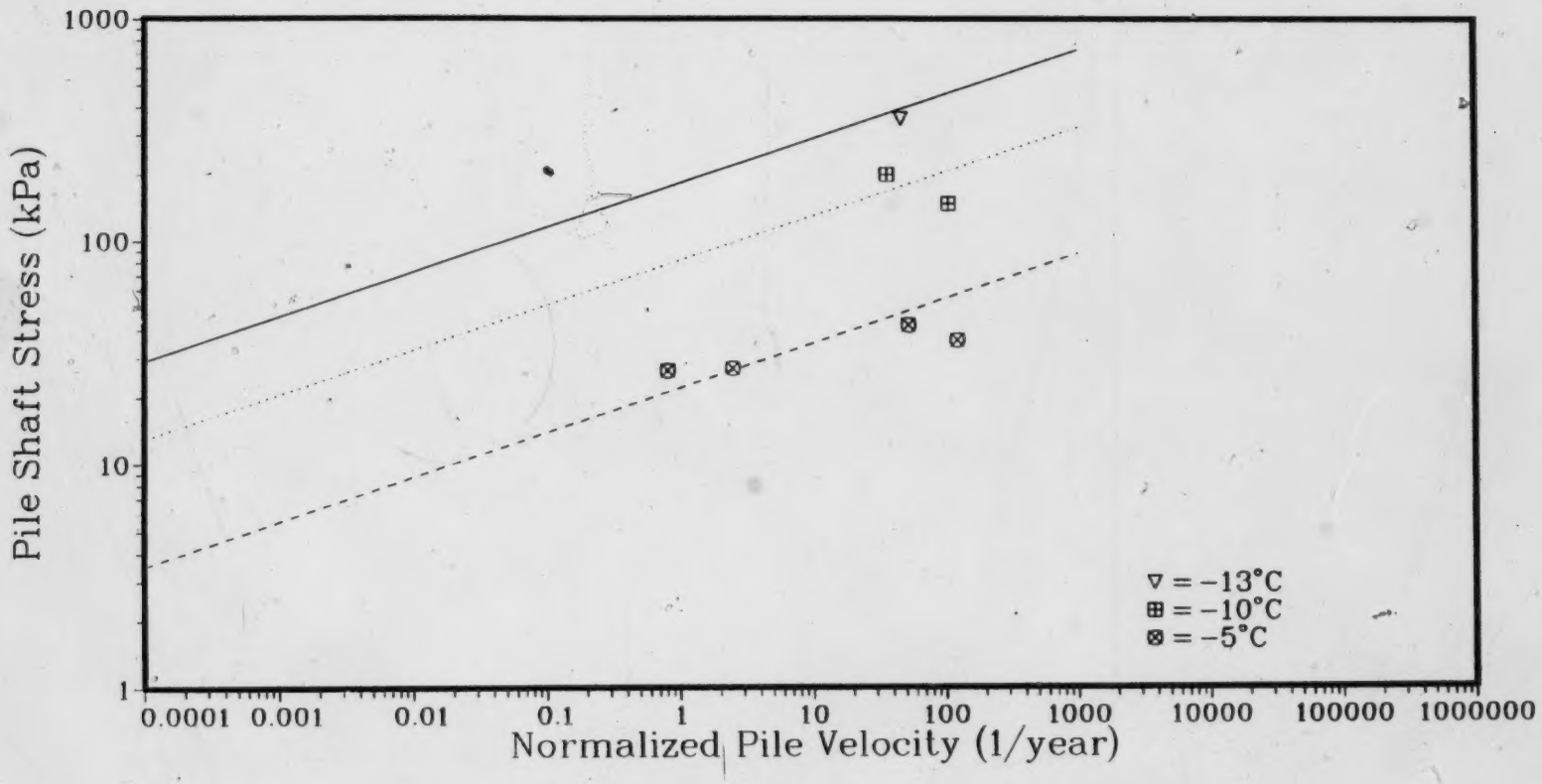

Figure 5.18: Pile shaft stress to normalized pile velocity from constant load tests on sand blasted model piles in silty sand of salinity 10 ppt. Parameter n assumed to be 5.

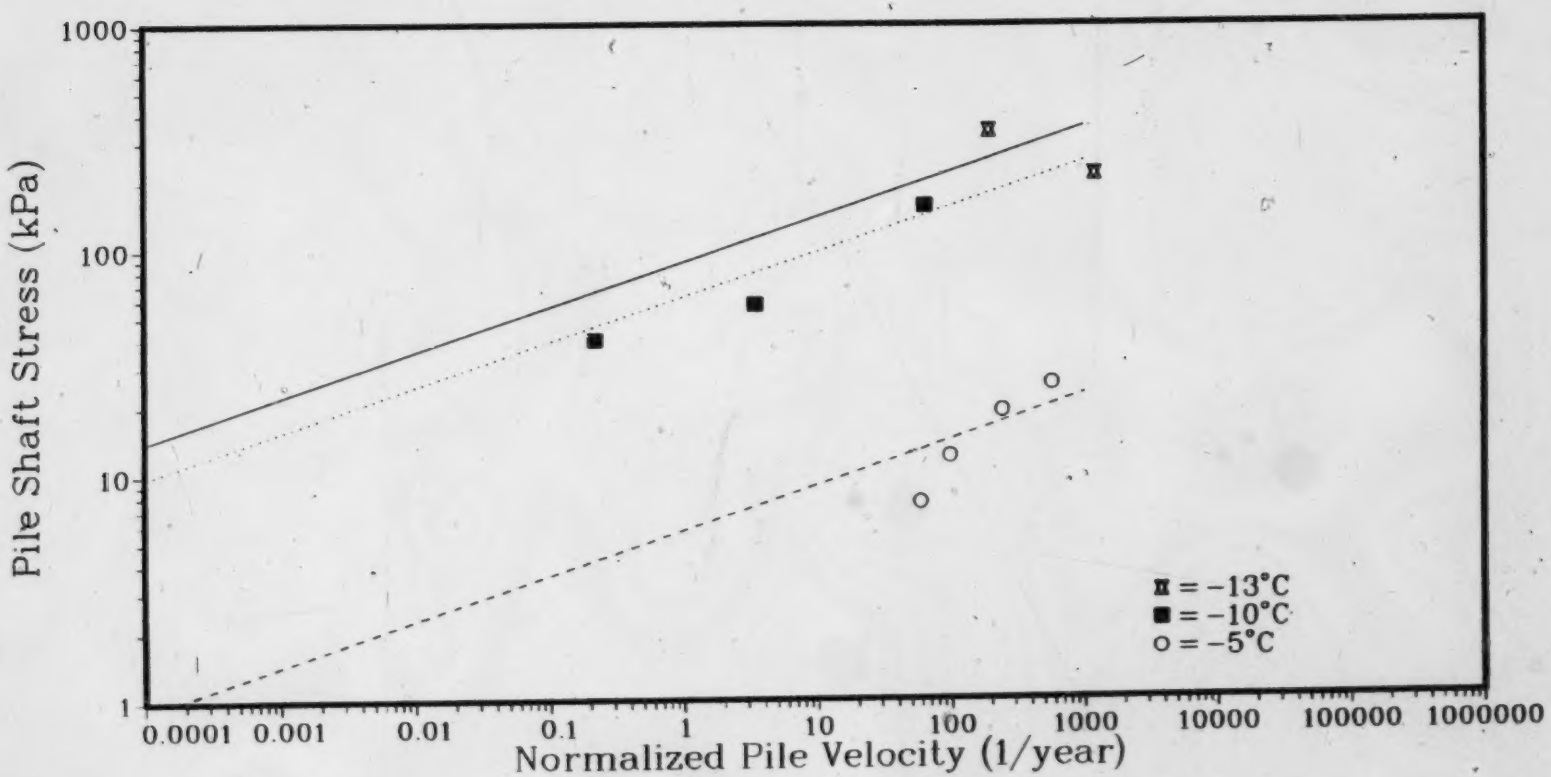

Figure 5.19: Pile shaft stress to normalized pile velocity from constant load tests on sand blasted model piles in silty sand of salinity 15 ppt. Parameter n assumed to be 5.

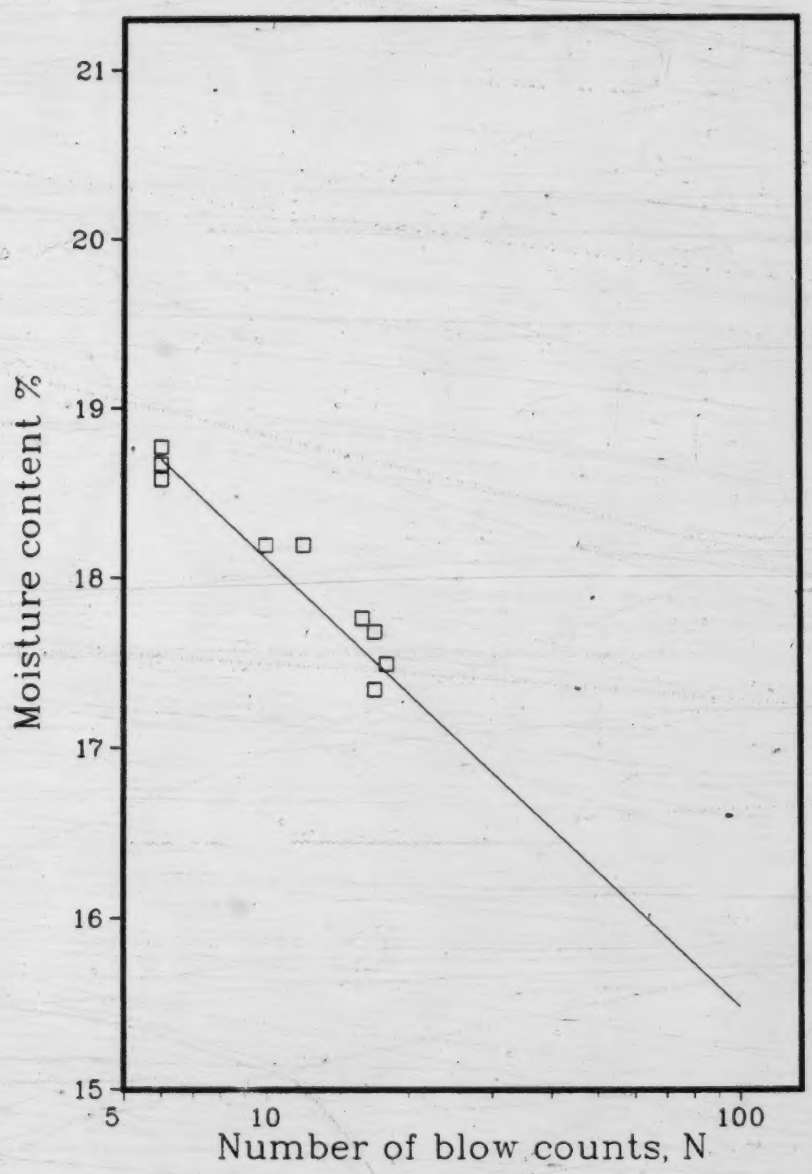

Figure 5.20: Liquid limit flow curve for non-saline silty sand

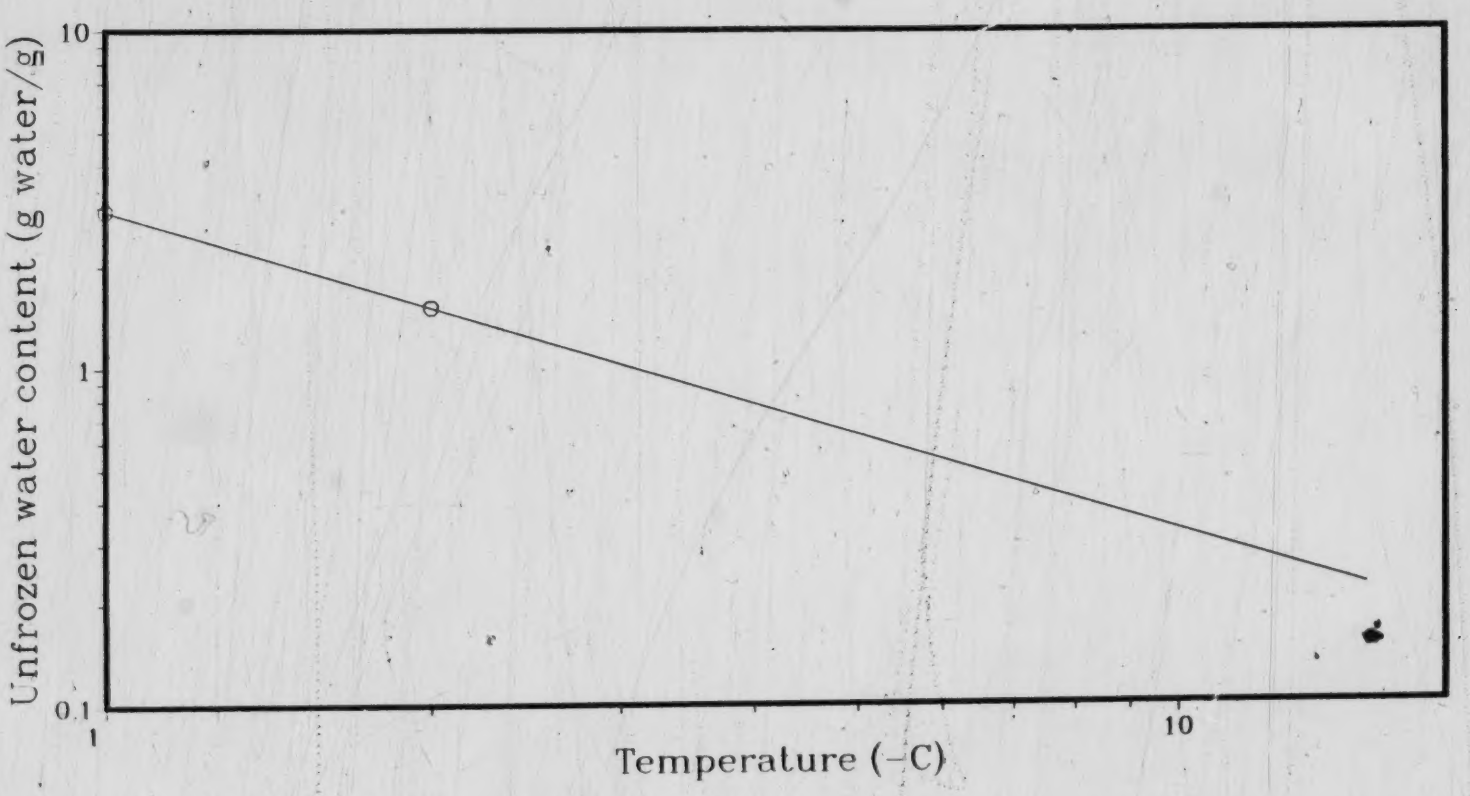

Figure 5.21: Unfrozen water content versus temperature for non-saline silty sand, determined from liquid limit tests, using the method of Tice et al (1976).

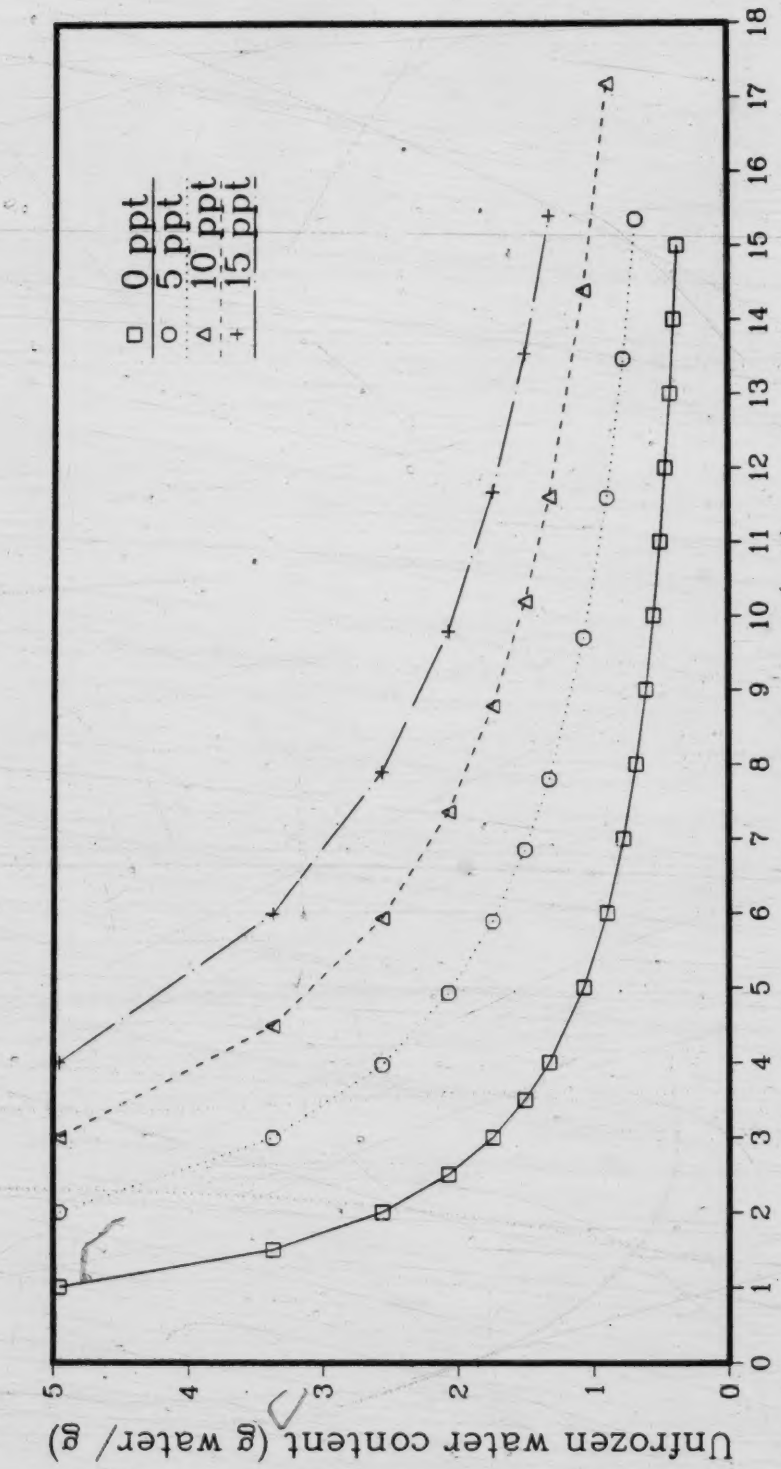

Figure 5.22: Unfrozen water content versus temperature for frozen silty sand, using data determined from liquid limit tests, and the methods of Tice et al (1976), and Patterson and Smith (1983).

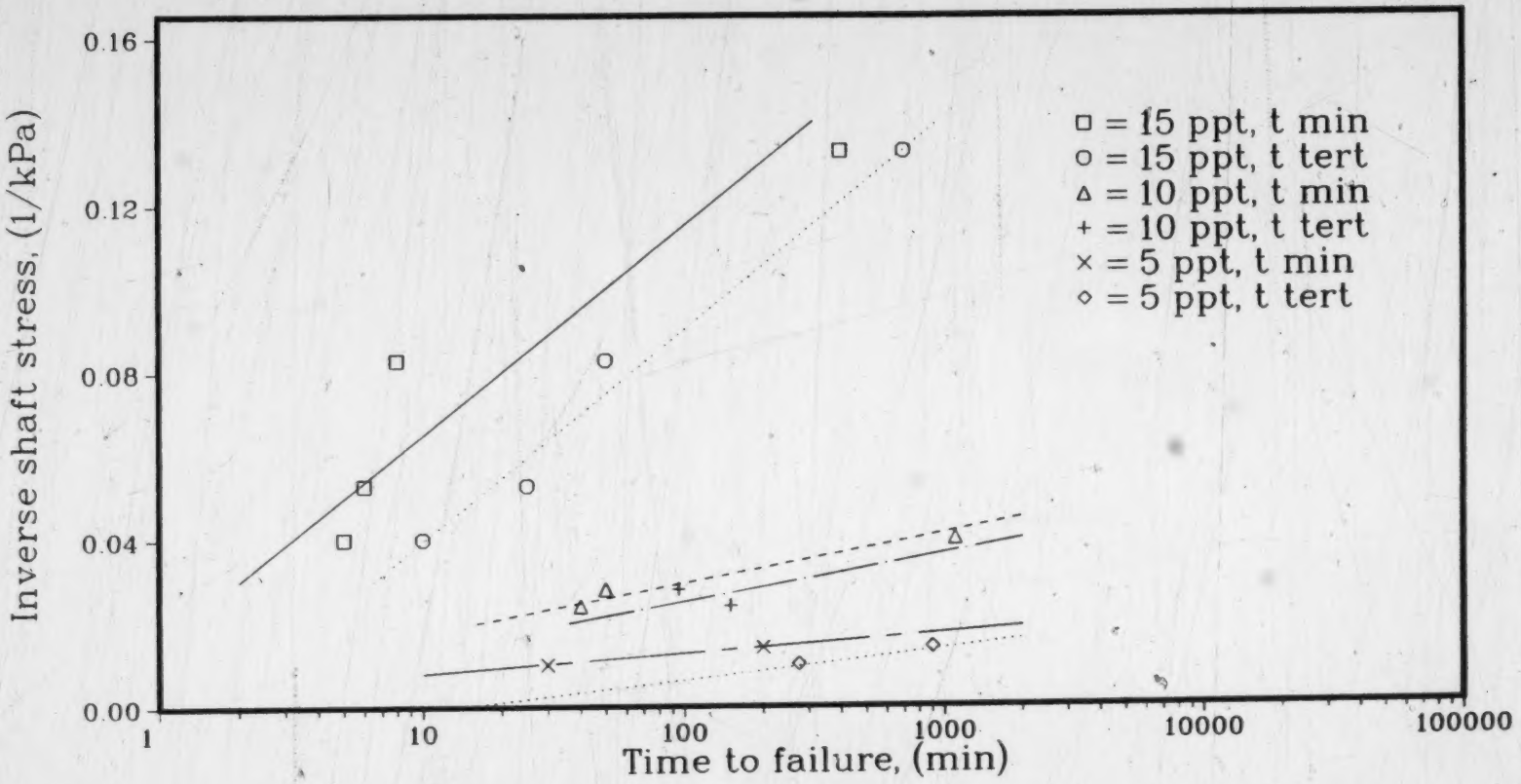

Figure 5.23: Relationship between the inverse pile shaft stress and the time to failure for silty sand at −5°C

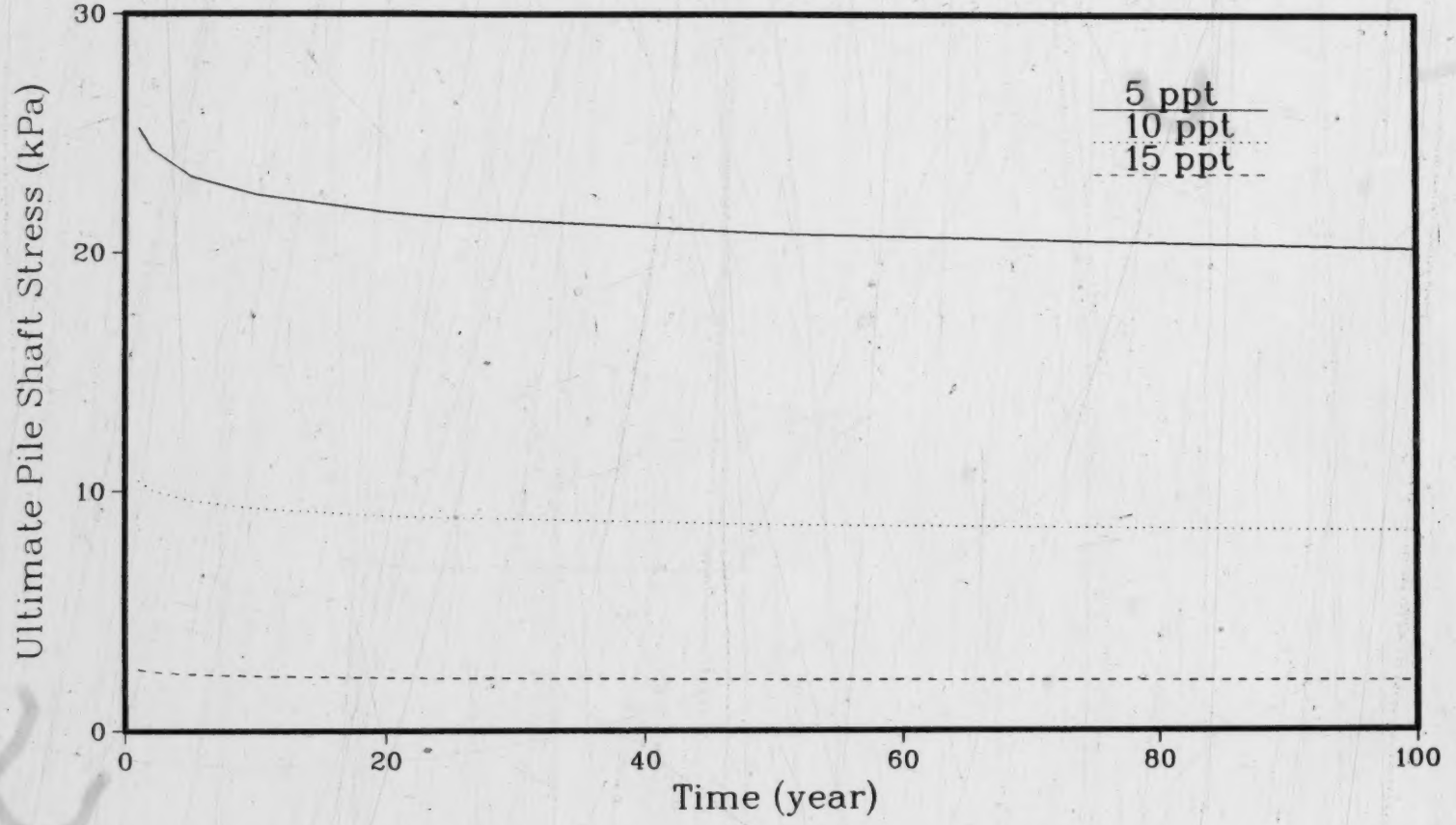

Figure 5.24: Prediction of ultimate pile shaft stress for silty sand at −5°C, using the Vyalov method, and time to minimum data.

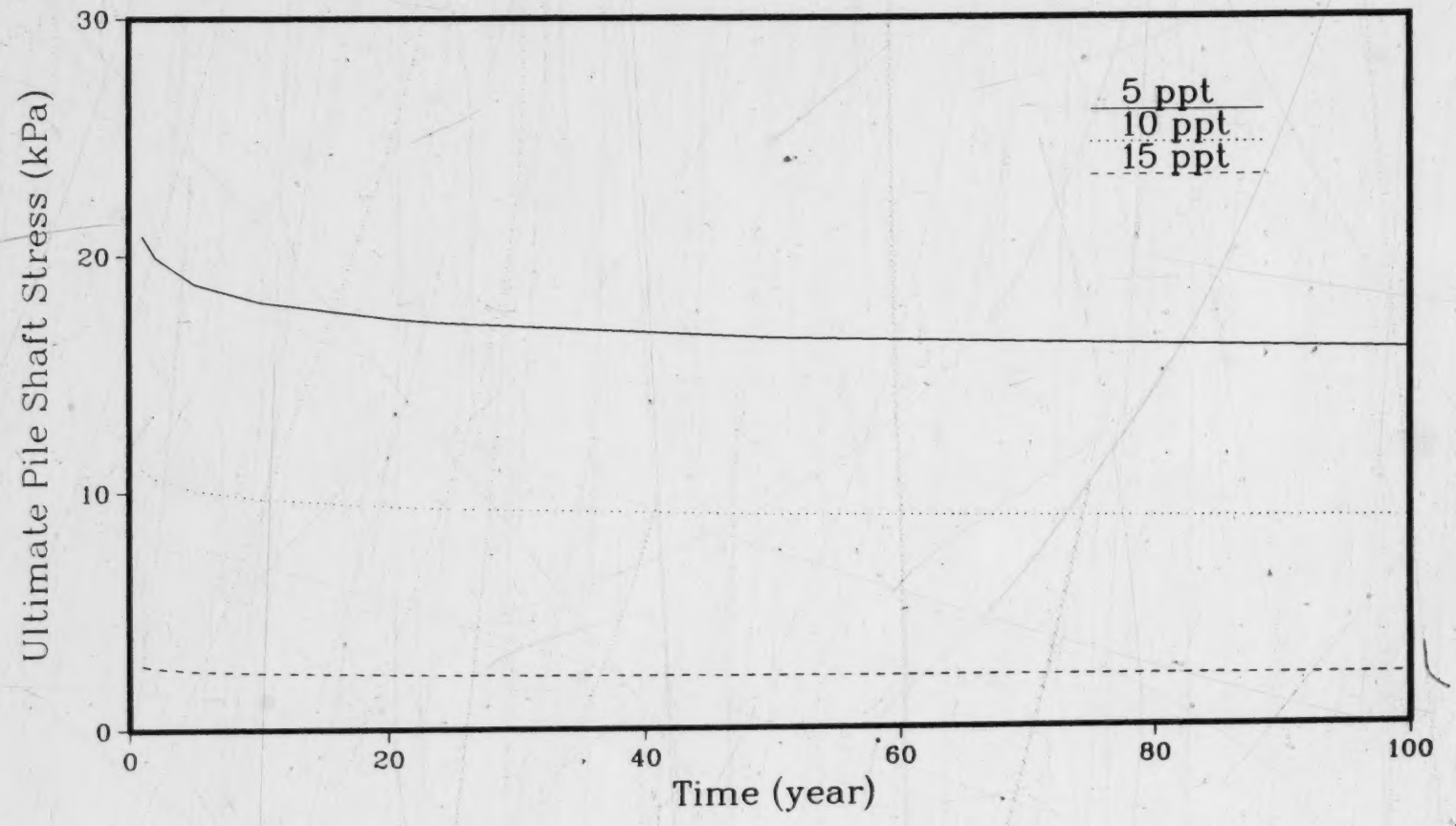

Figure 5.25: Prediction of ultimate pile shaft stress for silty sand at −5°C, using the Vyalov method, and time to onset of tertiary data.

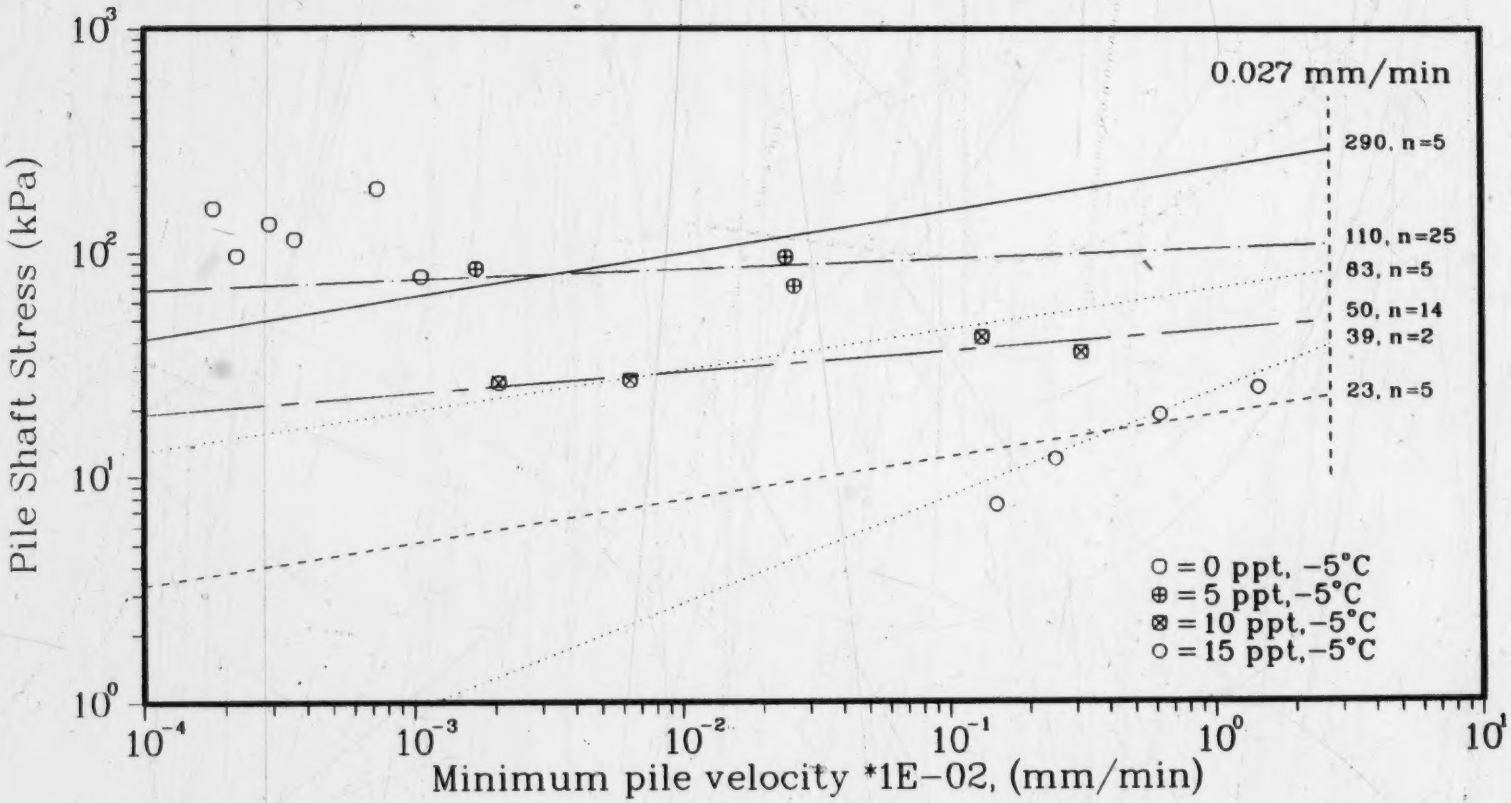

Figure 5.26: Prediction of pile shaft stress for model piles in saline silty sand at −5°C for a minimum strain rate of 0.027 mm/min. Best fit lines and fitted for parameter n = 5.

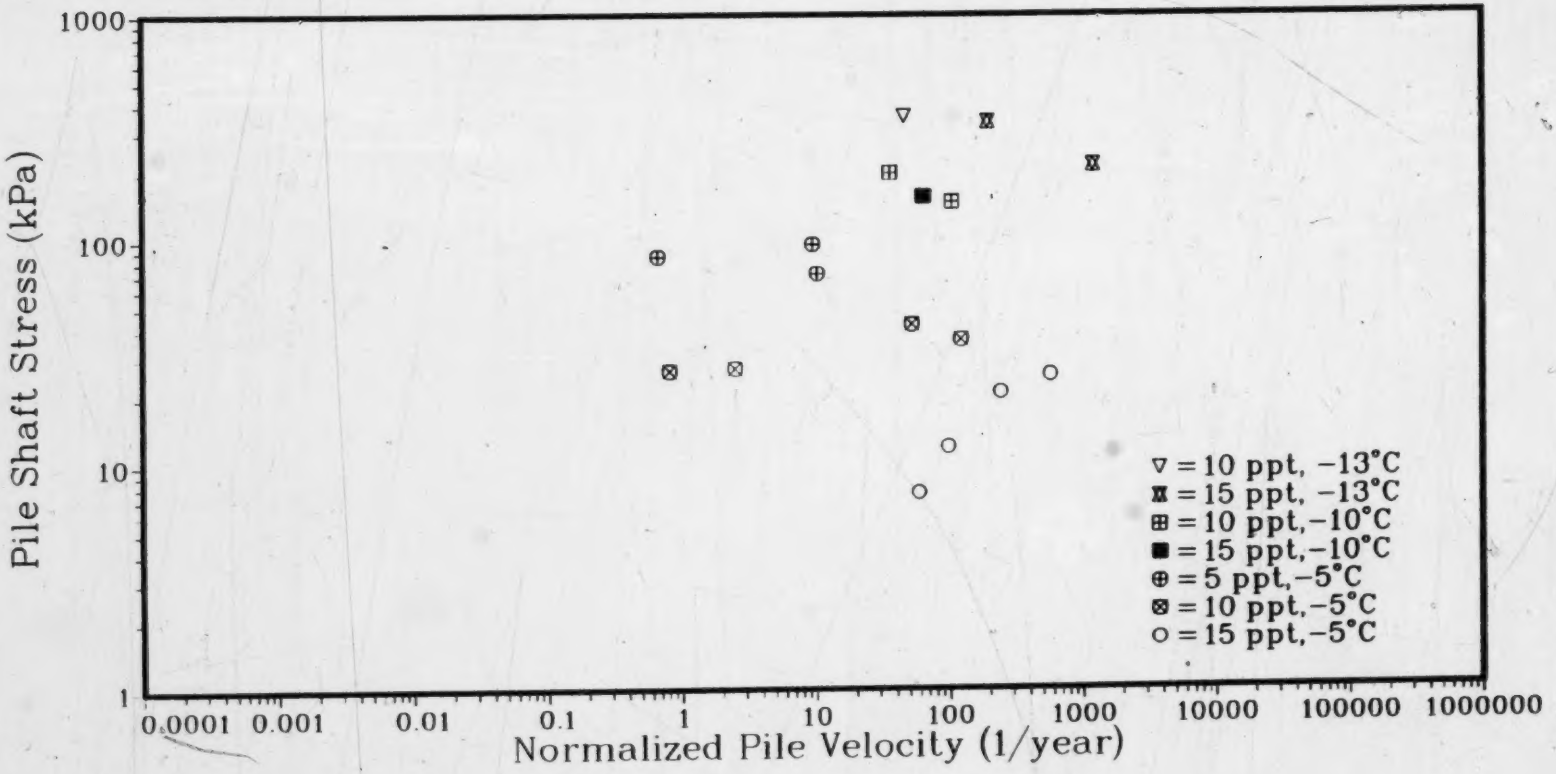

Figure 5.27: Pile shaft stress to normalized pile velocity from constant load tests on sand blasted model piles in silty sand. Data from single load tests and the last load step of incremental tests.

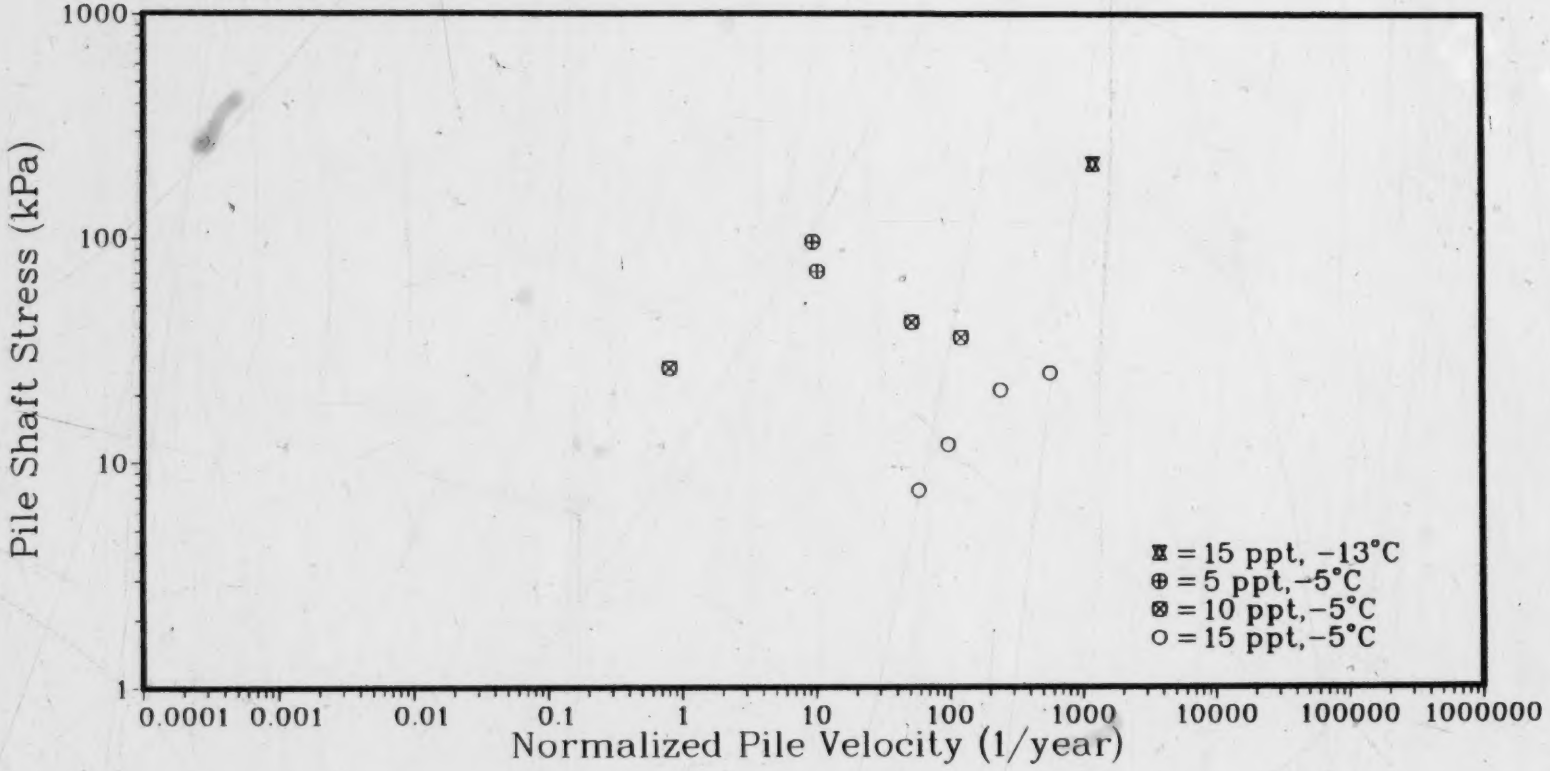

Figure 5.28: Pile shaft stress to normalized pile velocity from constant load tests on sand blasted model piles in silty sand. Data from single load tests.

6. Conclusions and Recommendations

6.1 Conclusions

The material behaviour indicates a "structured soil", which is subject to primary creep at low stresses. The failure stresses are generally the only load which cause a typical creep response. Therefore design of the pile should be based upon a determination of the elastic response of the material to stress, in conjunction with a determination of the creep failure at higher loads. Design based upon predictions of the normalized pile velocity alone is not appropriate.

Predictions of normalized pile velocity, made in accordance with current theory compare favourably with field tests in sand slurry (Hoggan, 1985, Nixon, 1988 and Thurber, 1983) and in saline native soil slurry (Nixon, 1988) and with laboratory model pile tests in sand (Parameswaran, 1978b, and Thurber, 1988.). Predictions of pile velocity from uniaxial laboratory testing of saline soils (Nixon and Lem, 1984) indicate a much higher resistance to load.

The addition of saline pore fluid reduces the resistance of the material drastically.

Failure stresses for a reasonable design life are very low. Therefore the resistance of the pile to load should be augmented by the use of sand backfill or grout slurries.

The parameter m, relating pile adfreeze resistance to uniaxial shear resistance is 0.4, compared to 0.6 reported

by Weaver (1979).

The variation in unfrozen water content with temperature and salinity can be calculated from liquid limit tests on the soil. However, the phase composition curves must be verified with physical measurements of the salinity of the frozen soil.

The use of step load tests is probably improper for this soil since the validity of the theory of hereditary creep is in question. More data is required to answer this question.

The method of freezing is rapid enough to prevent redistribution of the saline pore fluid.

Re-use of saline soil results in an increase in the measured salinity.

6.2 Recommendations

The conclusions drawn above must be verified for a larger data base. The tests conducted in this thesis were sufficient to define general trends, but not extensive enough to permit a great deal of confidence in the conclusions. Therefore further tests of model piles should be conducted at temperatures between 0 and -8°C at the salinities used in this testing. The upper temperature limit will depend upon the test method and the material strength. In addition, the results should be compared to any field pile load test data that becomes available for saline soils.

The theory based upon the assumption of ice-rich behaviour should no longer be used in light of the sensitivity of the parameter n and the fact that this soil behaves in a 'structured' manner. Therefore design should be based upon the prevention of failure under high stress and upon a quantification of the elastic response of piles to applied stress.

Additional step and single load increment tests should be conducted in the laboratory to determine the validity of hereditary creep.

In view of the very low failure stresses calculated using the Vyalov equation, tests on strengthening techniques, such as backfilling with sand or grout should be conducted in the laboratory.

7. Bibliography

Akimov, Y.P., Yershov, E.D., and Cheveryov, V.G. 1983. The physicochemical nature of the formation of unfrozen water in frozen soils. Proceedings: Fourth International Conference on Permafrost, Fairbanks, Alaska, National Academy of Sciences, Washington, D.C., 17-22 July. pp. 195-199.

Andersland, O.B., and AlNouri, I. 1970. Time-dependent strength behaviour of frozen soils. Journal of Soil Mechanics and Foundation Design, ASCE. pp. 1249-1265.

Andersland, O.B., and Alwahhab, M.R.M. 1982. Bond and slip of steel bars in frozen sand. Third International Symposium on Ground Freezing, Hanover, New Hampshire. pp. 27-34.

Andersland, O.B., and Alwahhab, M.R.M. 1983. Lug behaviour for model steel piles in frozen sand. Proceedings: Fourth International Conference on Permafrost, Fairbanks, Alaska, National Academy of Sciences, Washington, D.C., 17-22 July. pp. 16-21.

Andersland, O.B., and Alwahhab, M.R.M. 1984. Load capacity of model piles in frozen ground. Proceedings: Cold Regions Engineering Specialty Conference, Edmonton, Alberta, CSCE, 4-6 April. pp. 29-39.

Andersland, O.B., and Anderson, D.W. 1978. **Geotechnical engineering for cold regions.** McGraw-Hill Inc. p. 566.

Anderson, D.M., and Tice, A.R. 1972. Predicting unfrozen water contents in frozen soils from surface area measurements. Highway Research Board, no. 393. pp. 12-18.

Anderson, D.M., Tice, A.R., and Banin, A. 1973. The water-ice phase composition of clay-water systems. Part 1. The kaolinite-water system. Proc. Soil Science Society of America. 37, no. 6.

Assur, A. 1980. Some promising trends in ice mechanics. in, Physics and Mechanics of Ice, International Symposium. Copenhagen, Springer-Verlag.

Baker, T.H.W. 1979. Strain rate effect on the compressive strength of frozen sand. Journal of Engineering Geology.13, pp. 223-231.

Berggren, A.L., and Furuberg, T. 1985. A new Norwegian creep model and creep equipment. Fourth International Symposium on Ground Freezing, Sapporo, 5-7 August. pp.

181-185.

Bro, A. 1985. Research challenges in frozen ground pile design. Proceedings of Conference Arctic 85: Civil Engineering in the Arctic Offshore, San Francisco, California, ASCE, 25-27 March. pp. 1196-1205.

Crory, F.E. 1963. Pile foundations in permafrost. Proceedings: First International Conference on Permafrost, Lafayette, Indiana, National Academy of Sciences, Washington, D.C., 11-15 November. pp. 467-476.

DiPasquale, L., Gerlek, S., and Phukan, A. 1983. Design and construction of pile foundations in the Yukon-Kuskokwim Delta, Alaska. Proceedings: Fourth International Conference on Permafrost, Fairbanks, Alaska, National Academy of Sciences, Washington, D.C., 17-22 July. pp. 232-237.

Domaschuk, L., Man, C.-S., Shields, D.H., and Yong, E. 1983. Creep behaviour of frozen saline silt under isotropic compression. Proceedings: Fourth International Conference on Permafrost, Fairbanks, Alaska, National Academy of Sciences, Washington, D.C., 17-22 July. pp. 238-243.

Eroshenko, V.N. 1976. Determination of the loading capacity of piles in permafrost by means of static tests. Soil Mechanics and Foundation Engineering. pp. 174-176.

Ersoy, T., and Torgrol, E. 1978. Temperature and strain rate effects on the strength of compacted frozen silty-clay. Proceedings: Third International Conference on Permafrost, Edmonton, Alberta, National Research Council of Canada, 10-13 July.1, pp. 642-647.

Fellenius, B.H. 1975. Test loading of piles and new proof testing procedure. Journal of Geotechnical Engineering Design, ASCE. 101.

Fellenius, B.H. 1980. The analysis of results from routine pile load tests. Ground Engineering, Found. Publ. Ltd., 13, No. 6, pp. 19-31.

Foster,M.L. 1986. Adfreeze strength of ice to steel pipe piles as a function of temperature. Proceedings of the Fourth International Conference on Cold Regions Engineering, Anchorage, Alaska, 24-26 February. pp. 11-20.

Frederking, R., and Karri, J. 1983. Effects of pile material and loading state on adhesive strength of piles in ice. Canadian Geotechnical Journal. 20, pp. 673-680.

Gardner, A.R., Jones, R.H., and Harris, J.S. 1982. Strength and creep testing of frozen soils. Third International Symposium on Ground Freezing, Hanover, New Hampshire. pp. 53-60.

Glen, J.W. 1955. The creep of polycrystalline ice. Proc. Royal Society (London). A228. pp. 519-538.

Goughnour, R.R., and Andersland, O.B. 1968. Mechanical properties of a sand-ice system. Journal of Soil Mechanics and Foundation Design, ASCE. pp. 923-950.

Gregerson, O., Phukan, A., and Johansen, T. 1983. Engineering properties and foundation alternatives in marine Svea clay, Svalbard. Proceedings: Fourth International Conference on Permafrost, Fairbanks, Alaska, National Academy of Sciences, Washington, D.C., 17-22 July. pp. 384-388.

Gupalenko, V.I., and Rudenko, A.A. 1976. Performance of piles cast in predrilled holes and consolidated masses during slump-type settlements of soils surrounding them due to their own weight. Soil Mechanics and Foundation Engineering. pp.126-129.

Hallet, B. 1978. Solute redistribution in freezing ground. Proceedings: Third International Conference on Permafrost, Edmonton, Alberta, National Research Council of Canada, 10-13 July.1, pp. 85-91.

Hoggan Engineering and Testing (1980) Ltd. 1983. Pile foundation design for Kuluak School, Clyde River, N.W.T., report submitted to the Department of Public Works and Highways, Government of the Northwest Territories.

Hoggan Engineering and Testing (1980) Ltd. 1985. Pile load tests, Arctic Bay multi-purpose Hall and School Extension, report submitted to the Department of Public Works and Highways, Government of the Northwest Territories.

Iwata, S. 1985. A mechanism for the existence of unfrozen liquid in the vicinity of a solid surface. Fourth International Symposium on Ground Freezing, Sapporo, 5-7 August. pp. 25-31.

Johnston, G.H., ed. 1981. **Permafrost Engineering Design and Construction.** John Wiley and Sons. p. 483.

Johnston, G.H., and Ladanyi, B. 1972. Field tests of grouted rod anchors in permafrost. Canadian Geotechnical Journal. 9, pp. 176-194.

Kinney, T.C., Santana, B.W., Hawkins, D.M., Long, E.L., and Yarmak, E. 1983. Foundation stabilization of Central Gas injection facilities, Prudhoe Bay, Alaska. Proceedings: Fourth International Conference on Permafrost, Fairbanks, Alaska, National Academy of Sciences, Washington, D.C., 17-22 July. pp. 618-622.

Kinosita, S., and Ishizaki, T. 1980. Freezing point depression in moist soil. Second International Symposium on Ground Freezing, Trondheim, Norway, The Norwegian Institute of Technology, 24-26 June. pp. 640-646.

Ladanyi, B. 1972. An engineering theory of creep of frozen soils. Canadian Geotechnical Journal. 9. pp. 63-80.

Ladanyi, B., and Arteau, J. 1979. Effect of specimen shape on creep response of a frozen sand. Journal of Engineering Geology.13, pp. 207-222.

Ladanyi, B., and Paquin, J. 1978. Creep behavior of frozen sand under a deep circular load. Proceedings: Third International Conference on Permafrost, Edmonton, Alberta, National Research Council of Canada, 10-13 July., pp. 679-686.

Linell, K. and Lobacz, E. 1980. Design and construction of foundations in areas of deep seasonal frost and permafrost. US Army Cold Regions Research and Engineering Lab, Hanover, New Hampshire. Special Report 80-34. p. 320.

Long, E.L. 1973. Designing friction piles for increased stability at lower installed cost in permafrost. Permafrost: The North American Contribution to the Second International Conference, Yakutsk, USSR, National Academy of Sciences, Washington, D.C., 13-28 July. pp. 693-699.

Long, E.L. 1978. Permafrost Foundation Designs. Proceedings: Cold Regions Specialty Conference, Anchorage, Alaska, ASCE, 17-19 May.11, pp. 973-987.

Luscher, U., Black, W.T., and McPhail, J.P. 1983. Results of load tests on temperature-controlled piles in permafrost. Proceedings: Fourth International Conference on Permafrost, Fairbanks, Alaska, National Academy of Sciences, Washington, D.C., 17-22 July. pp 756-761.

Manikian, V. 1983. Pile driving and load tests on permafrost for the Kuparuk pipeline system. Proceedings: Fourth International Conference on Permafrost, Fairbanks, Alaska, National Academy of Sciences, Washington, D.C., 17-22 July. pp. 804-810.

McRoberts, E.C., Law, T.C., and Murray, T.K. 1978. Creep tests on undisturbed ice-rich silt. Proceedings: Third International Conference on Permafrost, Edmonton, Alberta, National Research Council of Canada, 10-13 July. pp. 539-545.

Mellor, M., and Cole, D.M. 1982. Deformation and failure of ice under constant stress or constant strain-rate. Cold Regions Science and Technology.5, pp. 210-219.

Mellor, M., and Cole, D.M. 1983. Stress/strain/time relations for ice under uniaxial compression. Cold Regions Science and Technology.6, pp. 207-230.

Mel'nikov, P.I., Vyalov, S.S., Snezhko, O.V., and Shishkanov, G.F. 1963. Pile foundations in permafrost. Proceedings: First International Conference on Permafrost, Lafayette, Indiana, National Academy of Sciences, Washington, D.C., 11-15 November. pp. 542-547.

Mikheev, V.V., Petrukhin, V.P., and Kronik, Y.A. 1973. Properties of saline soils used in construction. Proceedings of the Eighth International Conference on Soil Mechanics and Foundation Engineering.2, pt. 2, pp. 133-138.

Morgenstern, N.R. 1988. Recent observations on the deformation of ice and ice-rich permafrost. J. Ross Mackay Symposium Volume, ed. by M. Church and O. Slaymaker, University of British Columbia Press. pp. 133-153.

Morgenstern, N.R., Roggensack, W.D., and Weaver, J.S. 1980. The behaviour of friction piles in ice and ice-rich soils. Canadian Geotechnical Journal. 17. pp. 405-415.

Morland, L.W. 1979. Constitutive laws for ice. Cold Regions Science and Technology.1, pp. 101-108.

Morland, L.W., and Spring, U. 1981. Viscoelastic fluid relation for the deformation of ice. Cold Regions Science and Technology.4, pp. 255-268.

Nakajima, H., Koma, N., and Inoue, M. 1981. The ice force acting on a cylindrical pile. Proceedings of the Sixth International Conference on Port and Ocean Engineering under Arctic Conditions, Quebec, Canada.1, pp. 517-525.,3, pp. 1505-1510.

Nawwar, A.M., Nadreau, J.P., and Wang,Y.S. 1983. Triaxial compressive strength of saline ice. Proceedings of the Seventh International Conference on Port and Ocean Engineering under Arctic Conditions, Espoo, Finland.3, pp. 193-202.,4, pp. 876-878.

Nerseova, A. and Tsytovich, N.A. 1963. Unfrozen water in frozen soils. Proceedings: First International Conference on Permafrost, Lafayette, Indiana, National Academy of Sciences, Washington, D.C., 11-15 November. pp. 230-234.

Neukirchner, R.J. 1984. Permafrost temperature profiles for design of piles by creep theory. Proceedings: Cold Regions Engineering Specialty Conference, Edmonton, Alberta, CSCE, 4-6 April. pp. 53-67.

Neukirchner, R.J. 1985. Pile creep designs for frozen layered profiles. Proceedings of Conference Arctic 85: Civil Engineering in the Arctic Offshore, San Francisco, California, ASCE, 25-27 March. pp. 1103-1111.

Neukirchner, R.J., and Nyman, K.J. 1985. Creep rate analysis of pile load test data. Proceedings of Conference Arctic 85: Civil Engineering in the Arctic Offshore, San Francisco, California, ASCE, 25-27 March. pp. 1112-1121.

Nixon, J.F. 1988. Pile load tests in saline permafrost at Clyde River, Northwest Territories. Canadian Geotechnical Journal. 25, pp. 24-32.

Nixon, J.F. and Lem, G. 1984. Creep and strength testing of frozen saline fine-grained soils. Canadian Geotechnical Journal. 21, pp. 518-529.

Nixon, J.F., and McRoberts, E.C. 1976. A design approach for pile foundations in permafrost. Canadian Geotechnical Journal. 13, pp. 40-57.

Nixon, J.F., and Neukirchner, R.J. 1984. Design of vertical and laterally loaded piles in saline permafrost. Proceedings: Cold Regions Engineering Specialty Conference, Edmonton, Alberta, CSCE, 4-6 April. pp. 131-144.

Nixon, M.S., and Pharr, G.M. 1984. The effects of temperature, stress and salinity on the creep of frozen saline soil. Transactions of the ASME Journal of Energy Resources Technology. 106, pp. 344-348.

Nyman, K.J., and Bird, H.W.K. 1984. Design for partially embedded piles in permafrost. Proceedings: Cold Regions Engineering Specialty Conference, Edmonton, Alberta, CSCE, 4-6 April. pp. 145-160.

Ogata, N., Yasuda, M., and Kataoka, T. 1983. Effects of salt concentration on strength and creep behaviour of artifically frozen soils. Cold Regions Science and Technology.8, pp. 139-153.

Orth, W. 1985. Deformation behaviour of frozen sand and its physical interpretation. Fourth International Symposium on Ground Freezing, Sapporo, 5-7 August. pp. 245-253.

Orth, W., and Meissner, H. 1982. Long-term creep of frozen soil in uniaxial and triaxial tests. Third International Symposium on Ground Freezing, Hanover, New Hampshire. pp. 81-87.

Parameswaran, V.R. 1978a. Laboratory studies of the adfreeze bond between small-scale model piles and frozen sand. Proceedings: Third International Conference on Permafrost, Edmonton, Alberta, National Research Council of Canada, 10-13 July.1. pp 715-720.

Parameswaran, V.R. 1978b. Adfreeze strength of frozen sand to model piles. Canadian Geotechnical Journal. 15. pp. 494-500.

Parameswaran, V.R. 1978c. Creep of model piles in frozen soil. Canadian Geotechnical Journal. 16. pp. 69-77.

Parameswaran, V.R. 1980. Deformation behaviour and strength of frozen sand. Canadian Geotechnical Journal. 17. pp. 74-88.

Parameswaran, V.R. 1981. Adfreeze strength of model piles in ice. Canadian Geotechnical Journal. 18.pp. 8-16.

Parameswaran, V.R. 1984. Effect of dynamic loads on piles in frozen soils. Proceedings: Cold Regions Engineering Specialty Conference, Edmonton, Alberta, CSCE, 4-6 April. pp. 41-52.

Parameswaran, V.R. 1985. Attenuating creep of piles in frozen soils. Proceedings: Foundations in Permafrost and Seasonal Frost, ASCE Spring Convention, Denver, Colorado. pp. 16-28.

Parameswaran, V.R. 1986. Bearing capacity calculations for piles in permafrost. Proceedings of the Fourth International Conference on Cold Regions Engineering, Anchorage, Alaska, 24-26 February. pp. 751-759.

Parameswaran, V.R. 1987. Adfreezing strength of ice to model piles. Canadian Geotechnical Journal.24.pp. 446-452.

Patterson, D.E. and Smith, M.W. 1983. Measurement of unfrozen water content in saline permafrost using time domain reflectometry. Proceedings: Fourth International Conference on Permafrost, Fairbanks, Alaska, National Academy of Sciences, Washington, D.C., 17-22 July. pp. 968-972.

Pharr, G.M., and Merwin, J.E. 1985. Effects of brine content on the strength of frozen Ottawa sand. Cold Regions Science and Technology.Vol. 11, pp. 205-212.

Phukan, A. 1984. Frozen ground engineering. Prentice-Hall Inc. p. 336.

Poorooshasb, H.B., and Parameswaran, V.R. 1982. Uplift of rigid vertical piles in frozen sand. Soils and Foundations. 22, no. 2, pp. 82-88.

Rein, R.G., and Hathi, V.V. 1978. The effect of stress on strain at the onset of tertiary creep of frozen soils. Canadian Geotechnical Journal. 15, pp. 424-426.

Research Group on Pile Foundations in Permafrost, Research Institute of Ministry of Railways, The People's Republic of China. 1978. Testing of pile foundations in permafrost areas. Proceedings: Third International Conference on Permafrost, Edmonton, Alberta, National Research Council of Canada, 10-13 July. pp. 179-185.

Roggensack, W.D. 1977. Geotechnical properties of fine-grained permafrost soils. PH.D. thesis, University of Alberta, Edmonton, Alberta. p. 449.

Roggensack, W.D., and Morgenstern, N.R. 1978. Direct shear tests on natural fine-grained permafrost soils. Proceedings: Third International Conference on Permafrost, Edmonton, Alberta, National Research Council of Canada, 10-13 July. pp. 729-735.

Rowley, R.K., Watson, G.H., and Ladanyi, B. 1973. Vertical and lateral pile load tests in permafrost. Permafrost: The North American Contribution to the Second International Conference, Yakutsk, USSR, National Academy of Sciences, Washington, D.C., 13-28 July. pp. 712-721.

Sadovskiy, A.V. 1973. Adfreeze between ground and foundation materials. Permafrost: USSR Contribution to the Second International Conference, Yakutsk, USSR, National Academy of Sciences, Washington, D.C., 13-28 July. pp. 650-653.

Savigny, K.W. 1980. In-situ analysis of naturally occurring creep in ice-rich permafrost soil. PH.D. thesis, The University of Alberta, Edmonton, Alberta. p. 439.

Sayles, F.H. 1968. Creep of frozen sands. CRREL Technical Report 190, Hanover, N.H. p 54.

Sayles, F.H. 1973. Triaxial and creep tests on frozen Ottawa sand. Permafrost: The North American Contribution to the

Second International Conference, Yakutsk, USSR, National Academy of Sciences, Washington, D.C., 13-28 July. pp. 384-391.

Sego, D.C., and Chernenko, D. 1984. Confining pressure influence on the strength of frozen saline sand. Proceedings: Cold Regions Engineering Specialty Conference, Edmonton, Alberta, CSCE, 4-6 April. pp. 565-578.

Sego, D.C., and Morgenstern, N.R. 1983. Deformation of ice under low stresses. Canadian Geotechnical Journal. 20. pp. 587-602.

Sego, D.C., Schultz, T., and Banasch, R. 1982. Strength and deformation behaviour of frozen saline sand. Third International Symposium on Ground Freezing, Hanover, New Hampshire. pp. 11-19.

Sheeran, D.E., and Yong, R.N. 1975. Water and salt redistribution in freezing soils. Proceedings: First International Conference on soil-water problems in Cold Regions, Calgary, Canada, 6-7 May. pp. 58-69.

Shibata, T., Adachi, T., Yashima, A., Takahashi, T., and Yoshioka, I. 1985. Time-dependence and volumetric change characteristic of frozen sand under triaxial stress condition. Fourth International Symposium on Ground Freezing, Sapporo, 5-7 August. pp. 173-179.

Sivanbaev, A.V., Shilin, N.A., Nikhotin, N.I., and Neklyudov, V.S. 1977. Results of field tests on piles in permanently frozen ground. Soil Mechanics and Foundation Engineering. pp. 345-347.

Smith, G.D., and Morland, L.W. 1981. Viscous relations for the steady creep of polycrystalline ice. Cold Regions Science and Technology.5, pp. 141-150.

Stehle, S. 1970a. Adfreezing strength of ice. International Association for Hydraulic Research Symposium: Ice and its Action on Hydraulic Structures, Reykjavik, Iceland. Session 5.3.

Stehle, S. 1970b. Holding strength of piles in ice. US Naval Civil Engineering Laboratory, Port Hueneme, California. Technical Report R-700. p. 38.

Stuckert, B.J.A, and Mahar, L.J. 1984. The role of ice content in the strength of frozen saline coarse grained soils. Proceedings: Cold Regions Engineering Specialty Conference, Edmonton, Alberta, CSCE, 4-6 April. pp. 579-587.

Thomas, H.W., and Mobley, K. 1986. Special pile foundations for a coastal permafrost site. Proceedings of the Fourth International Conference on Cold Regions Engineering, Anchorage, Alaska, 24-26 February. pp. 1-10

Thurber Consultants Limited. 1983. Pile load tests, Baffin Island Correctional Center, report submitted to the Government of the Northwest Territories, Department of Public Works.

Thurber Consultants Limited. 1988. North Warning System, Short Range Radar Sites - Zone 2, Pile Load Test Program, Model Pile Load Tests - Phase 1, report submitted to Stanley Associates Engineering Limited.

Tice, A.R., Anderson, D.M., and Banin,A. 1976. The prediction of unfrozen water contents in frozen soils from liquid limit determinations. CRREL Report 76-8. p. 9.

Ting, J.M. 1983a. On the nature of the minimum creep rate - time correlation for soil, ice, and frozen soil. Canadian Geotechnical Journal. 20, pp. 176-182.

Ting, J.M. 1983b. Tertiary creep model for frozen sands. Journal of Geotechnical Enginnering, ASCE.109. No. 7, pp. 932-945.

Ting, J.M., and Martin, R.T. 1979. Application of the Andrade equation to creep data for ice and frozen soil. Cold Regions Science and Technology.1, pp. 29-36.

Ting, J.M., Martin, R.T., and Ladd, C.C. 1983. Mechanisms of strength for frozen sand. Journal of Geotechnical Enginnering, ASCE.109. pp. 1286-1302.

Tobiasson, W., and Johnson, P. 1978. The details behind a typical Alaskan pile foundation. Proceedings: Third International Conference on Permafrost, Edmonton, Alberta, National Research Council of Canada, 10-13 July.1. pp. 892-897.

Tsytovich, N.A. 1975. The mechanics of frozen ground. McGraw-Hill, New York. p. 426.

Tsytovich, N.A., Kronik, Y.A., Markin, K.F., Aksenov, V.I., and Samuel'son, M.V. 1973. Physical and mechanical properties of saline soils. Permafrost: USSR Contribution to the Second International Conference, Yakutsk, USSR, National Academy of Sciences, Washington, D.C., 13-28 July. pp. 238-247.

Velli, Y.Y., Lenzniiep, and Karpunina, A.A. 1973. Saline permafrost as bearing ground for construction.

Permafrost: USSR Contribution to the Second International Conference, Yakutsk, USSR, National Academy of Sciences, Washington, D.C., 13-28 July. pp. 545-550.

Vershinin, P.V., Deriagin, B.V., and Kirilenko, N.V. 1960. The nonfreezing water in soil. CRREL Translation No 30. pp. 1-10.

Vinogradov, A.M. 1985. Creep properties of ice: Theory and experiment. Proceedings of Conference Arctic 85: Civil Engineering in the Arctic Offshore, San Francisco, California, ASCE, 25-27 March. pp. 447-455.

Voytkovskiy, K.F. 1960. The mechanical properties of ice. Translation Air Force Cambridge Research Laboratories, Bedford, M.A., AFCRC-62-838, AMS-T-R#391. p. 92.

Vyalov, S.S. 1962. The strength and creep of frozen soils and calculations for ice-soil retaining structures. CRREL Translation 76, Hanover, N.H. 1965.

Vyalov, S.S. 1973. Principles of controlling the geocryological conditions during construction in the permafrost region (survey of research in the USSR). Permafrost: USSR Contribution to the Second International Conference, Yakutsk, USSR, National Academy of Sciences, Washington, D.C., 13-28 July. pp. 777-799.

Weaver, J.S. 1979. Pile foundations in permafrost. PH.D. thesis, University of Alberta, Edmonton, Alberta. p. 224.

Weaver, J.S., and Morgenstern, N.R. 1980. Simple shear creep tests on frozen soil. Canadian Geotechnical Journal.18, pp. 217-229.

Weaver, J.S., and Morgenstern, N.R. 1981. Pile design in permafrost. Canadian Geotechnical Journal.18, pp. 357-370.

Yong, R.N., Cheung, C.H., and Sheeran, D.E. 1979. Prediction of salt influence on unfrozen water content in frozen soils. Journal of Engineering Geology.13, pp. 137-155.

Yuanlin, Zhu, and Carbee, D.L. 1983. Creep behaviour of frozen silt under constant uniaxial stress. Proceedings: Fourth International Conference on Permafrost, Fairbanks, Alaska, National Academy of Sciences, Washington, D.C., 17-22 July. pp. 1507-1512.

Yuanlin, Zhu, Zhang Jiayi, and Wu Ziwang. 1982. Elastic and compressive deformation of frozen soils. Third

International Symposium on Ground Freezing, Hanover, New Hampshire. pp. 65-77.

A. Appendix A
Test results

Table A.1 Density and Salinity measurements for frozen silty sand

T_t	S	Water Content	ρ_{dry}	S_m	Sample Number	
°C	(ppt)	(%)	$\frac{Mg}{m^3}$	(ppt)		
-13	0	14.86	1.737		1.1	N
		16.41	1.685			
		17.90	1.728			
	5	16.75	1.715		1.2	N
		16.55	1.760			
		17.24	1.715			
	10	17.20	1.702		1.3	N
		17.20	1.721			
		17.60	1.705			
	15	16.50	1.693		1.4	N
		16.75	1.722			
		17.37	1.729			
		15.81	1.721		1.5	R
		15.44	1.747			
		15.86	1.716			
-10	0	16.15	1.703		2.1	
		16.08	1.713			
	5	17.81	1.691	6	2.2	N
		18.28	1.609	5		
		18.74	1.646	6		
	10	16.89	1.682		2.3	N,R?
		16.62	1.698	10.8		
		17.33	1.673	11		
		17.77	1.686	15.8	2.4	N,R?
		19.65	1.657	12		
		19.17	1.648	10		
	15	19.49	1.616		2.5	N,R?
		21.28	1.550	16		
		19.25	1.608	16.8		
		18.77	1.695	16.8	2.6	N,R?
		17.32	1.728	15.3		
		17.45	1.727	16		
-5	0	17.31	1.705		3.1	R
		16.53	1.741			
		16.82	1.696			
	5	15.70	1.681	5	3.2	R
		15.35	1.715	5		
		16.65	1.708	9		
	10	18.07	1.636	11.5	3.3	R
		15.89	1.709	11.8		
		15.93	1.705	10.8		

		18.54	1.589	12	3.4	R
		16.00	1.668	12		
		16.00	1.702	11		
	15	17.78	1.650	23.5	3.5	R
		16.54	1.700	17.5		
		16.60	1.682	16.4		
		18.26	1.669	18.1	3.6	R
		16.38	1.715	18		
		16.32	1.747	17.5		
-5	5	17.26	1.696	5	4.1	R
		16.61	1.731	5		
		16.48	1.727	5		
		16.77	1.728	5	4.2	N
		16.61	1.747	5		
		16.98	1.697	5		
	10	17.71	1.689	9.5	4.3	N
		16.46	1.724	9.5		
		16.76	1.714	9.5		
		18.32	1.651	13	4.4	R
		17.40	1.720	12		
		17.42	1.716	12		
	15	18.38	1.692	18	4.5	R
		17.65	1.686	16		
		17.05	1.739	15		
		19.01	1.647	18.5	4.6	R
		17.44	1.720	18		
		16.88	1.707	17		

T_t = nominal test temperature
S^t = nominal soil salinity
ρ_{dry} = dry soil density
S^m = average salinity measured after the test
N^m = newly mixed soil
R = reused soil

Table A.2 Roughness profiles of the sand blasted model piles

Pile #		Center line average roughness (micro inches) -12°C	-10°C	-5°C	-5°C
1	Top	97	90	93	98
	Middle	96	92	89	85
	Bottom	74	80	84	80
2	Top	64	70	73	68
	Middle	80	73	89	82
	Bottom	84	80	75	79
3	Top	65	70	80	77
	Middle	84	84	79	82
	Bottom	78	73	83	69
4	Top	64	67	83	78
	Middle	91	82	79	84
	Bottom	93	90	79	87
5	Top	88	92	84	78
	Middle	110	95	99	88
	Bottom	93	78	82	90
6	Top	79	83	91	100
	Middle	111	96	99	89
	Bottom	129	110	99	113

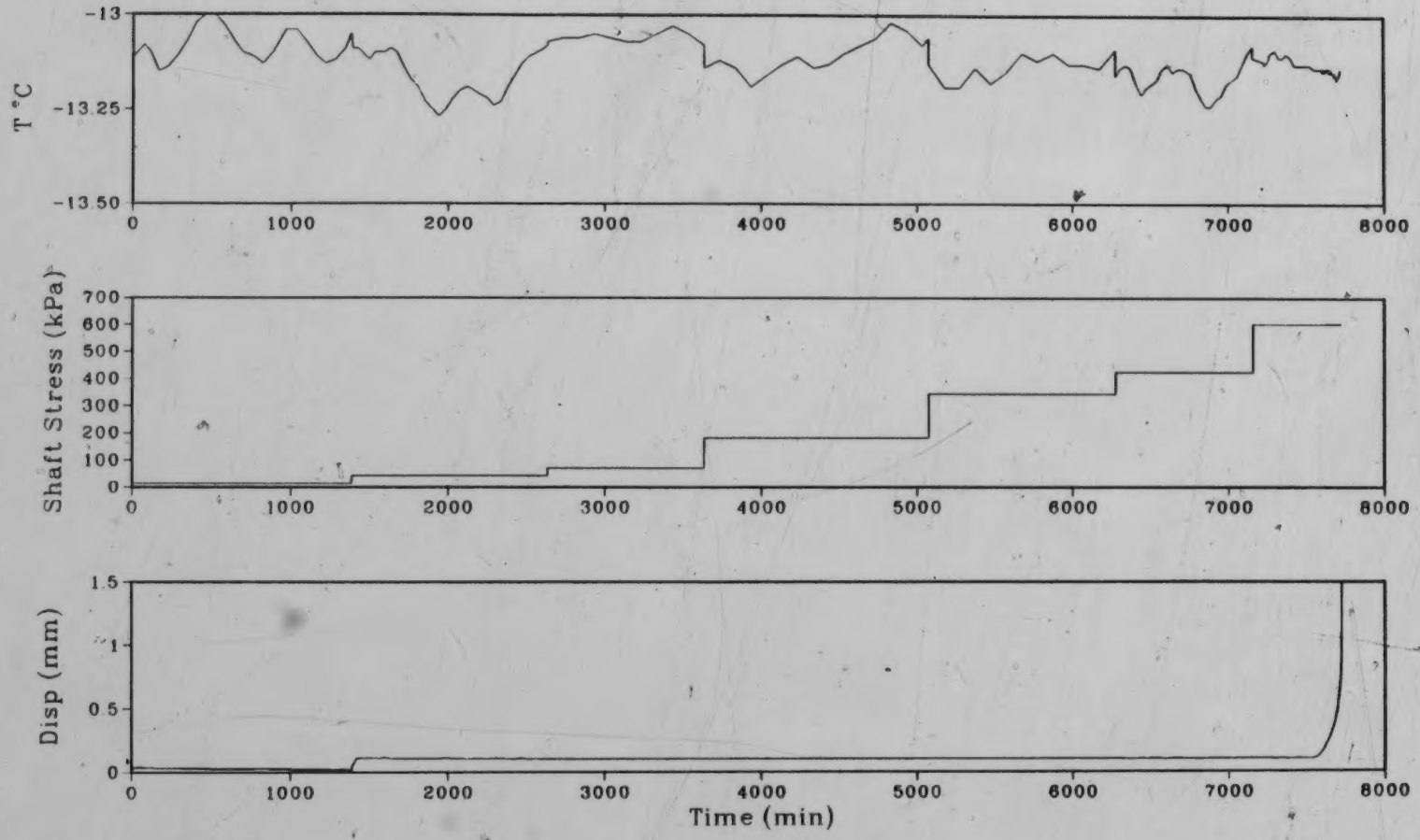

Figure A.1: Temperature, stress and displacement data for sample 1.1: fresh water silty sand at −13°C

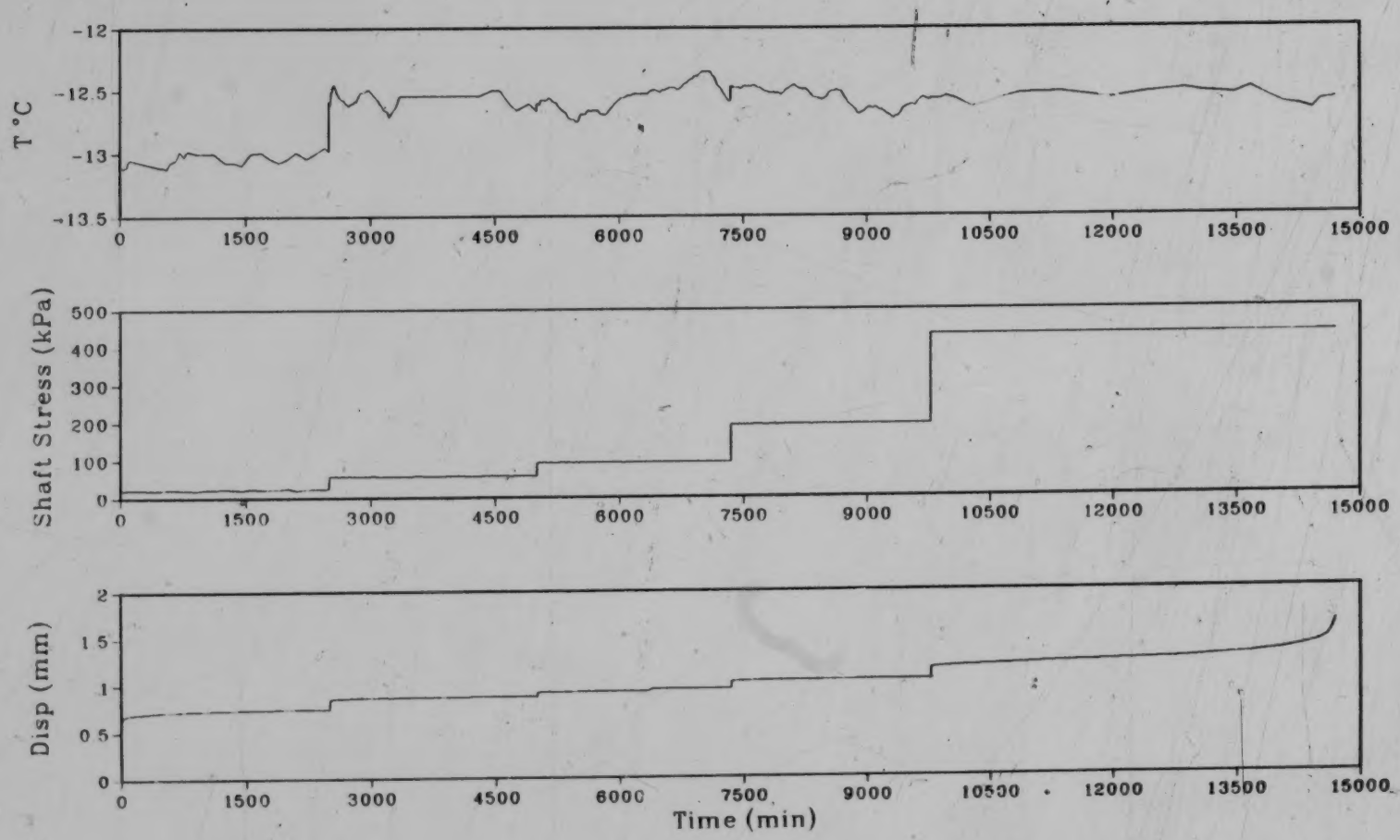

Figure A.2: Temperature, stress and displacement data for sample 1.2: silty sand of salinity 5 ppt at −13°C

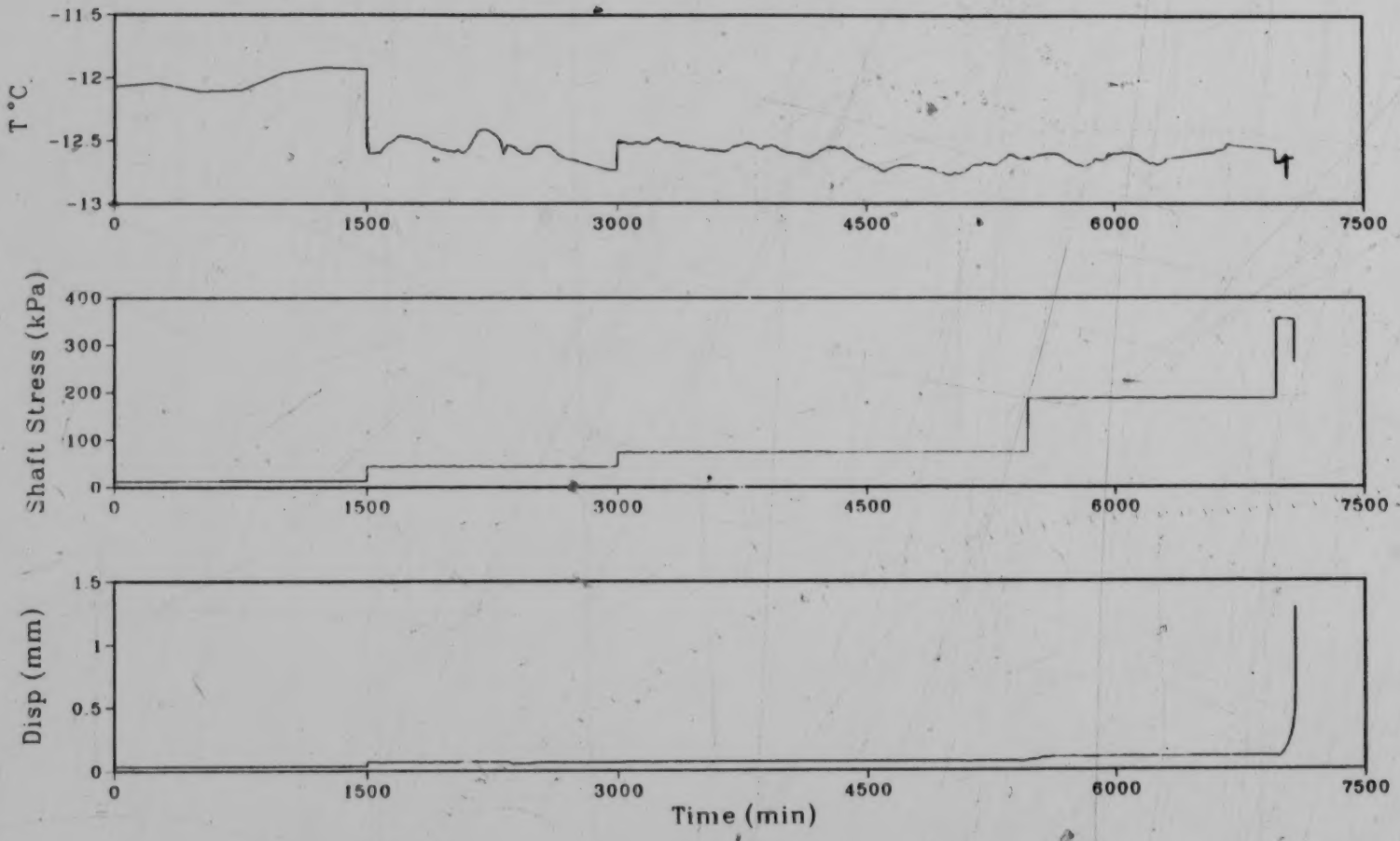

Figure A.3: Temperature, stress and displacement data for sample 1.3: silty sand of salinity 10 ppt at −12.5°C

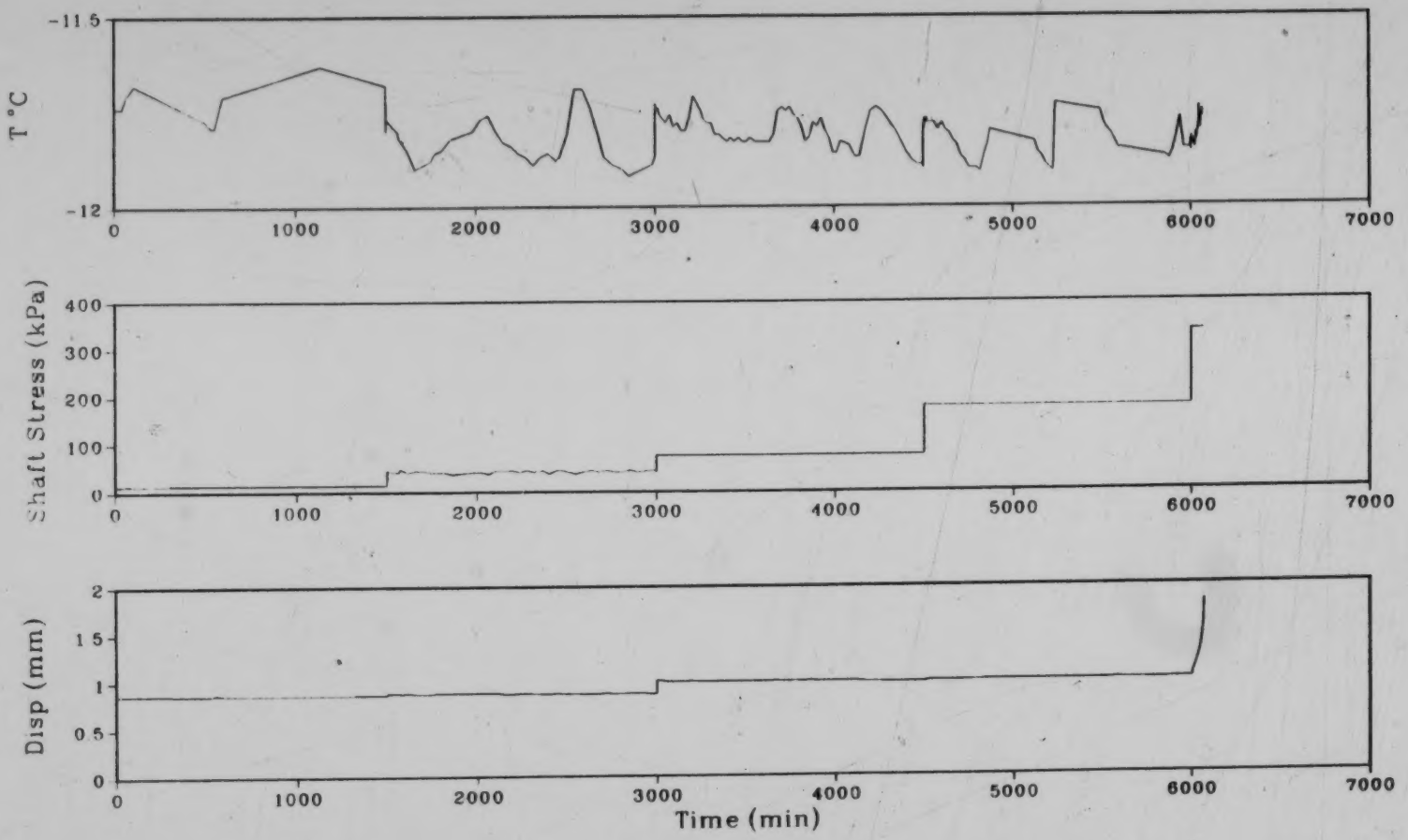

Figure A.4: Temperature, stress and displacement data for sample 1.4: silty sand of salinity 15 ppt at −12°C

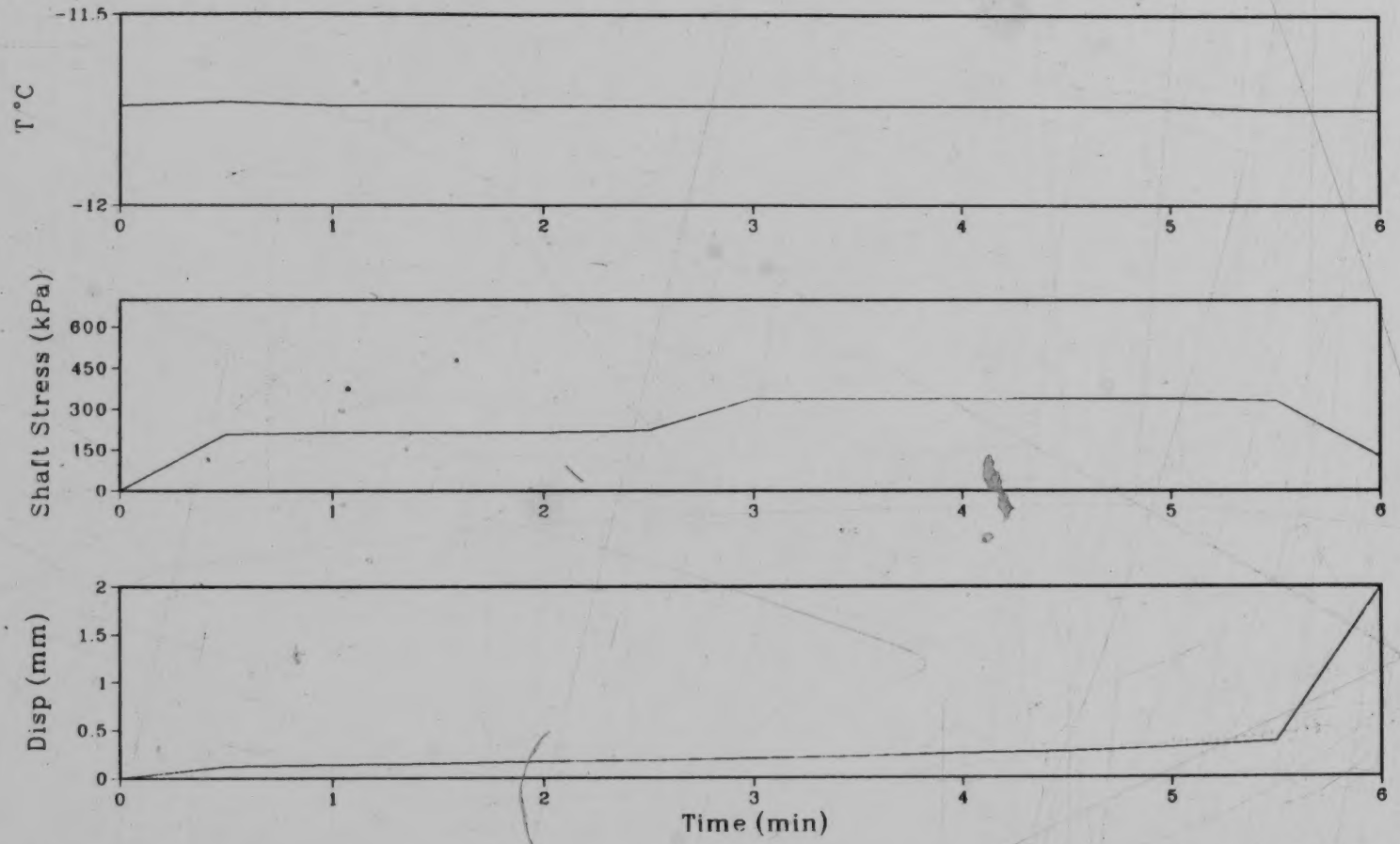

Figure A.5: Temperature, stress and displacement data for sample 1.5: silty sand of salinity 15 ppt at −12°C

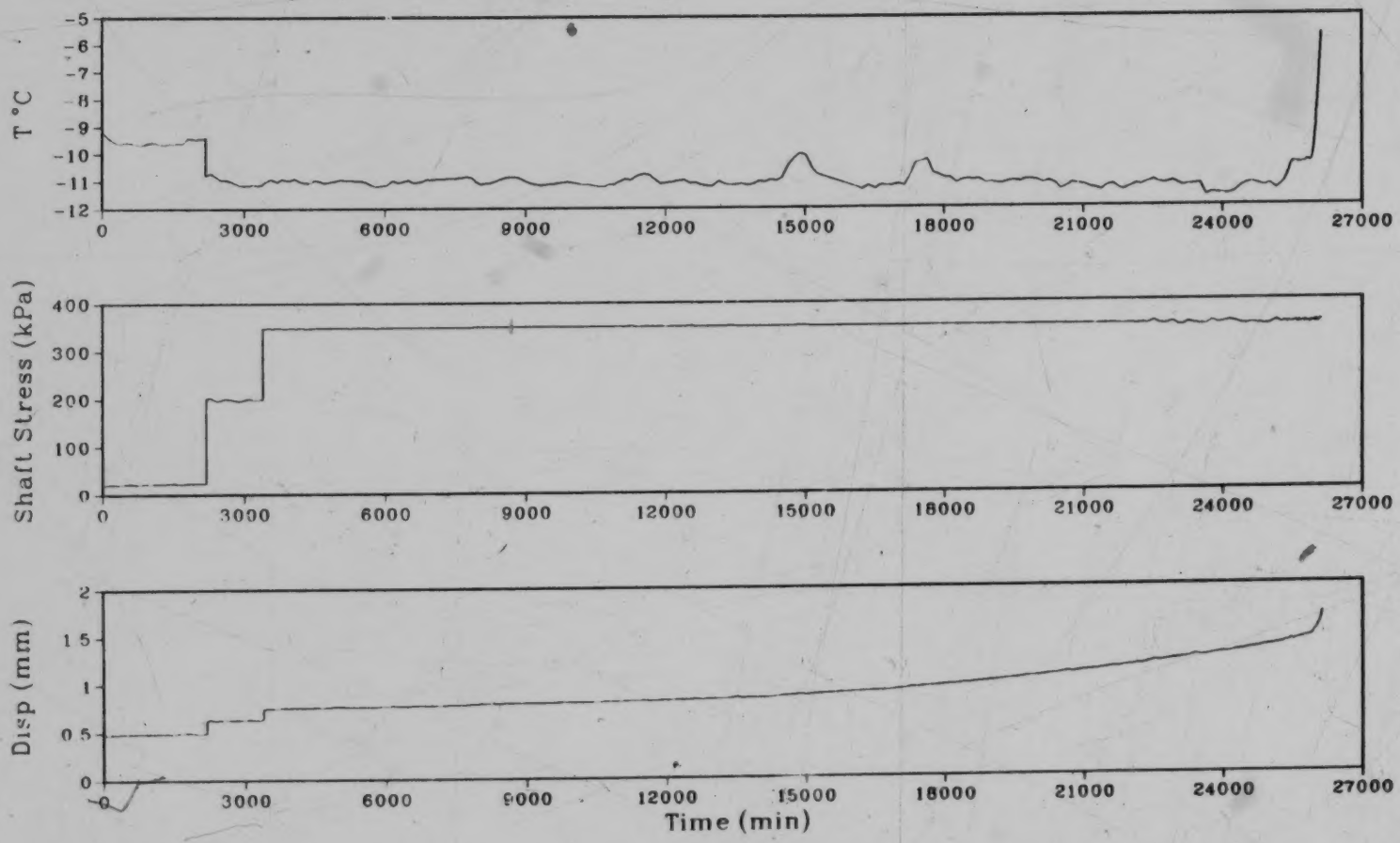

Figure A.6: Temperature, stress and displacement data for sample 2.1: fresh water silty sand at −10 °C

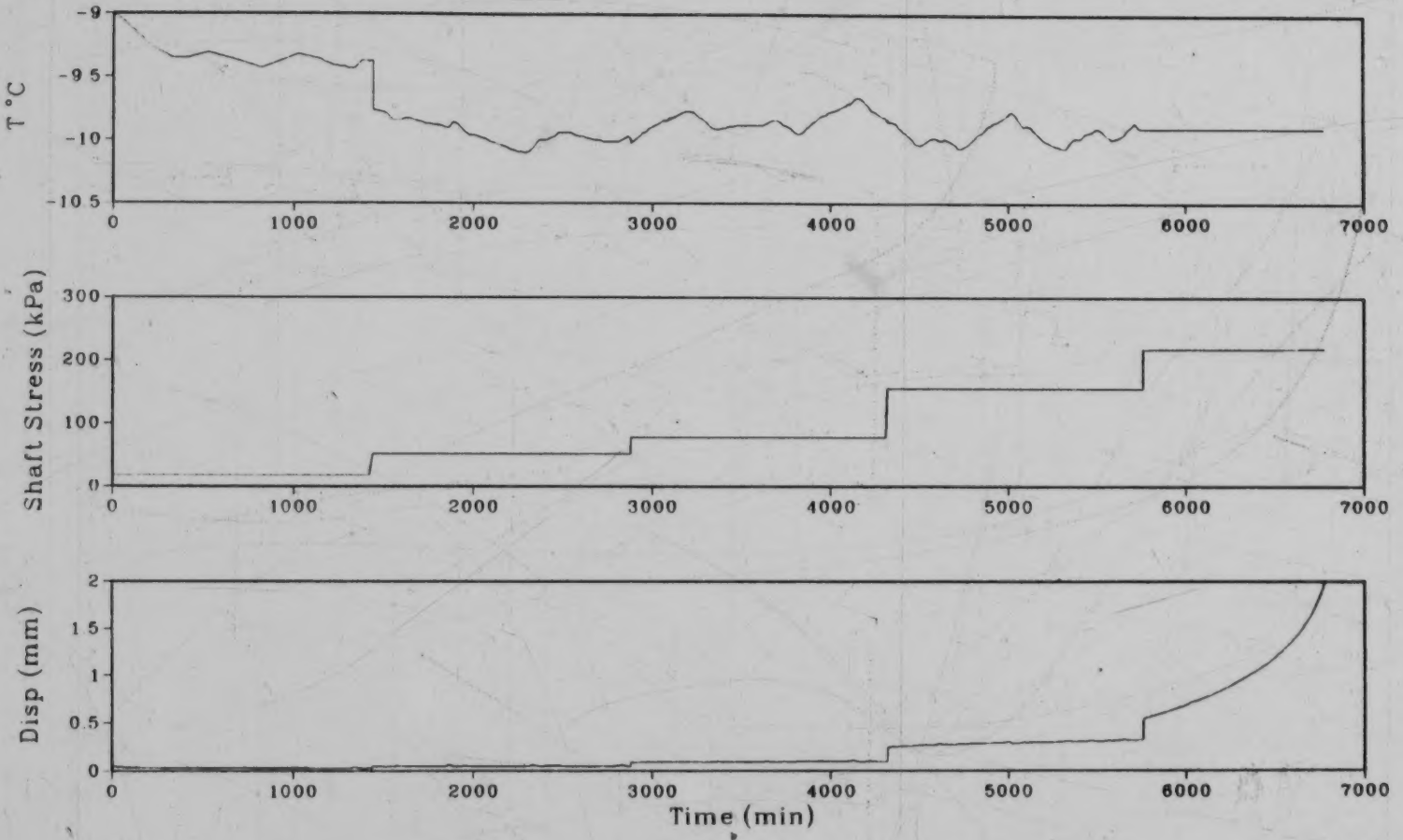

Figure A.7: Temperature, stress and displacement data for sample 2.2: silty sand of salinity 5 ppt at −10°C

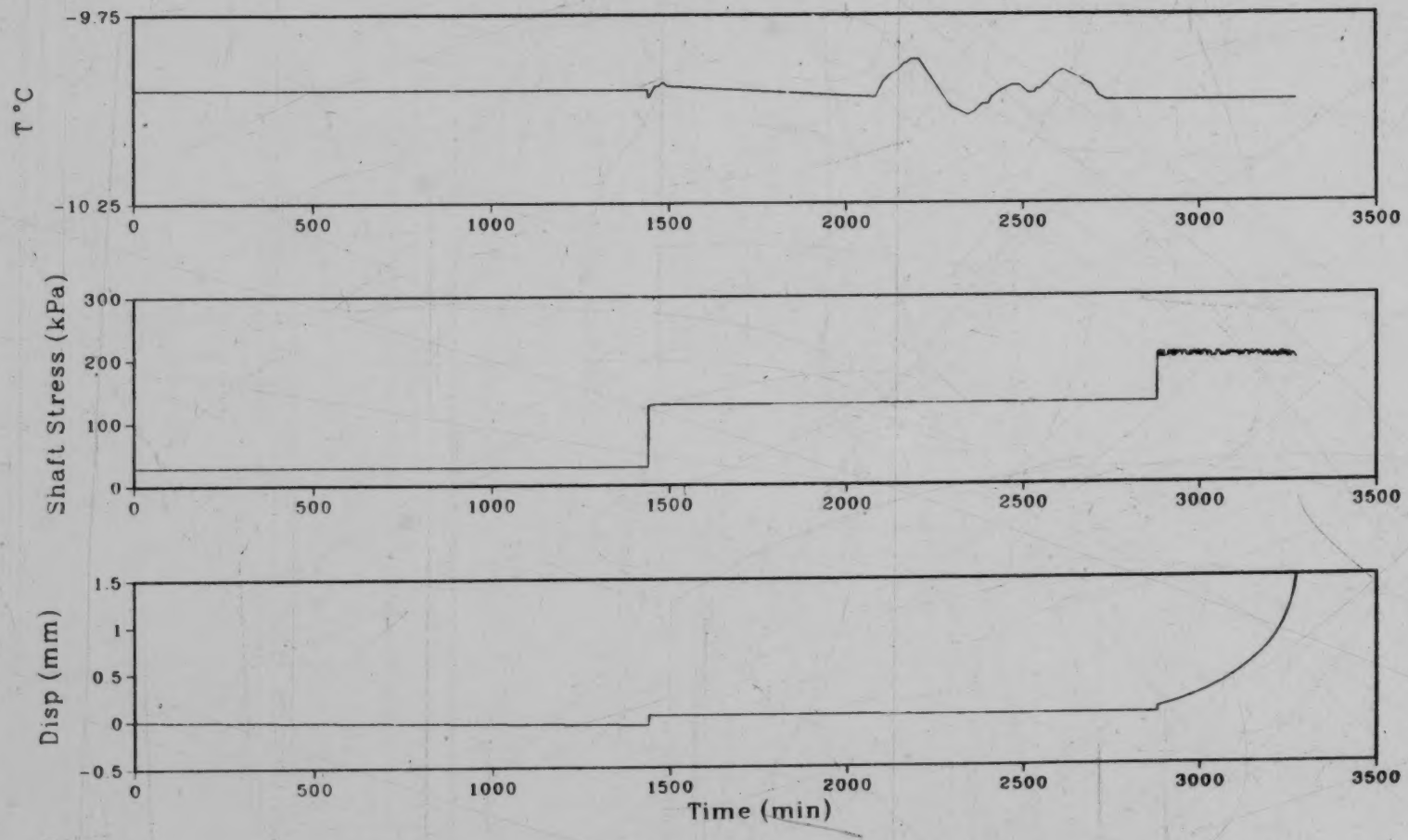

Figure A.8: Temperature, stress and displacement data for sample 2.3: silty sand of salinity 10 ppt at −10°C

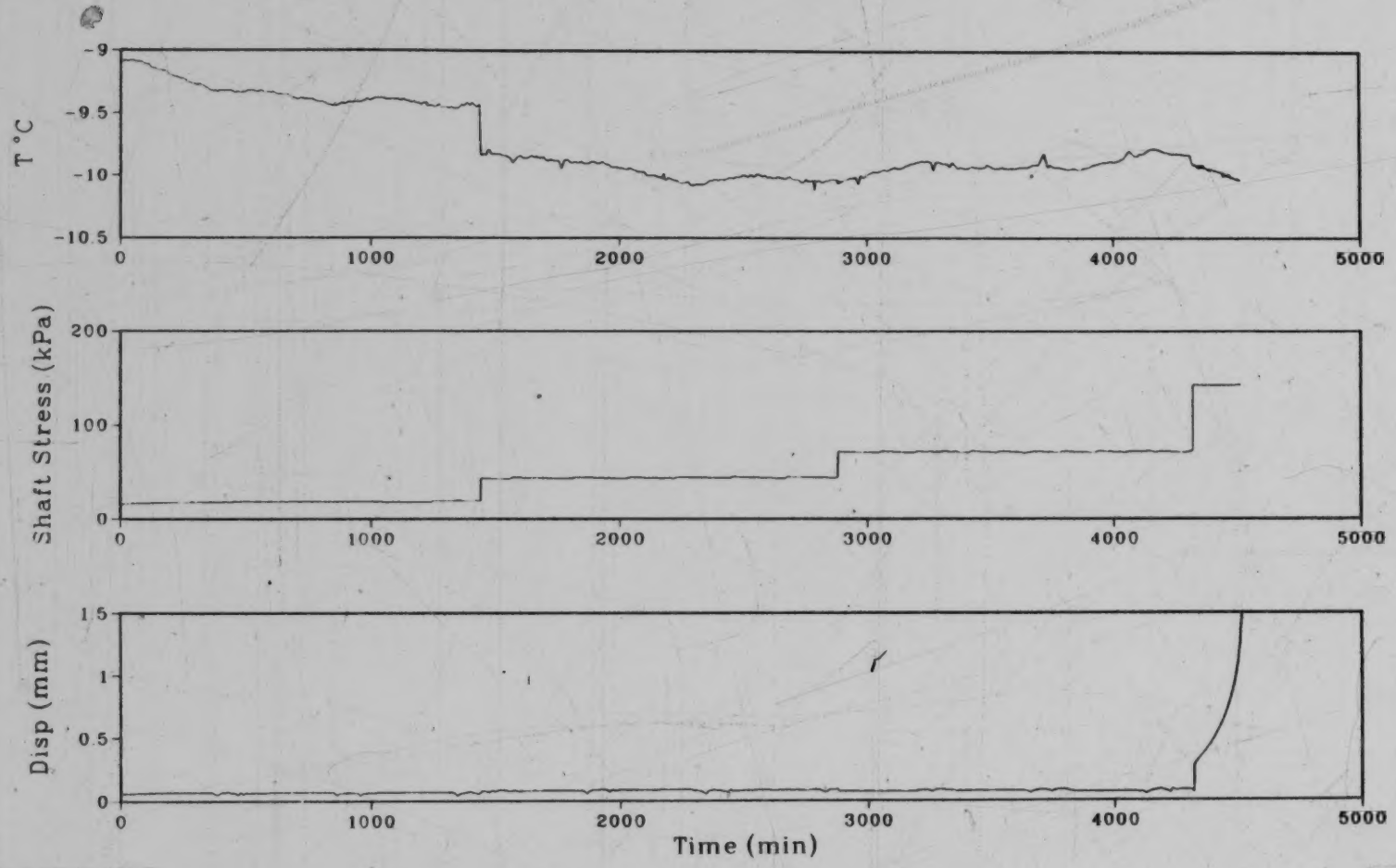

Figure A.9: Temperature, stress and displacement data for sample 2.4: silty sand of salinity 10 ppt at −10°C

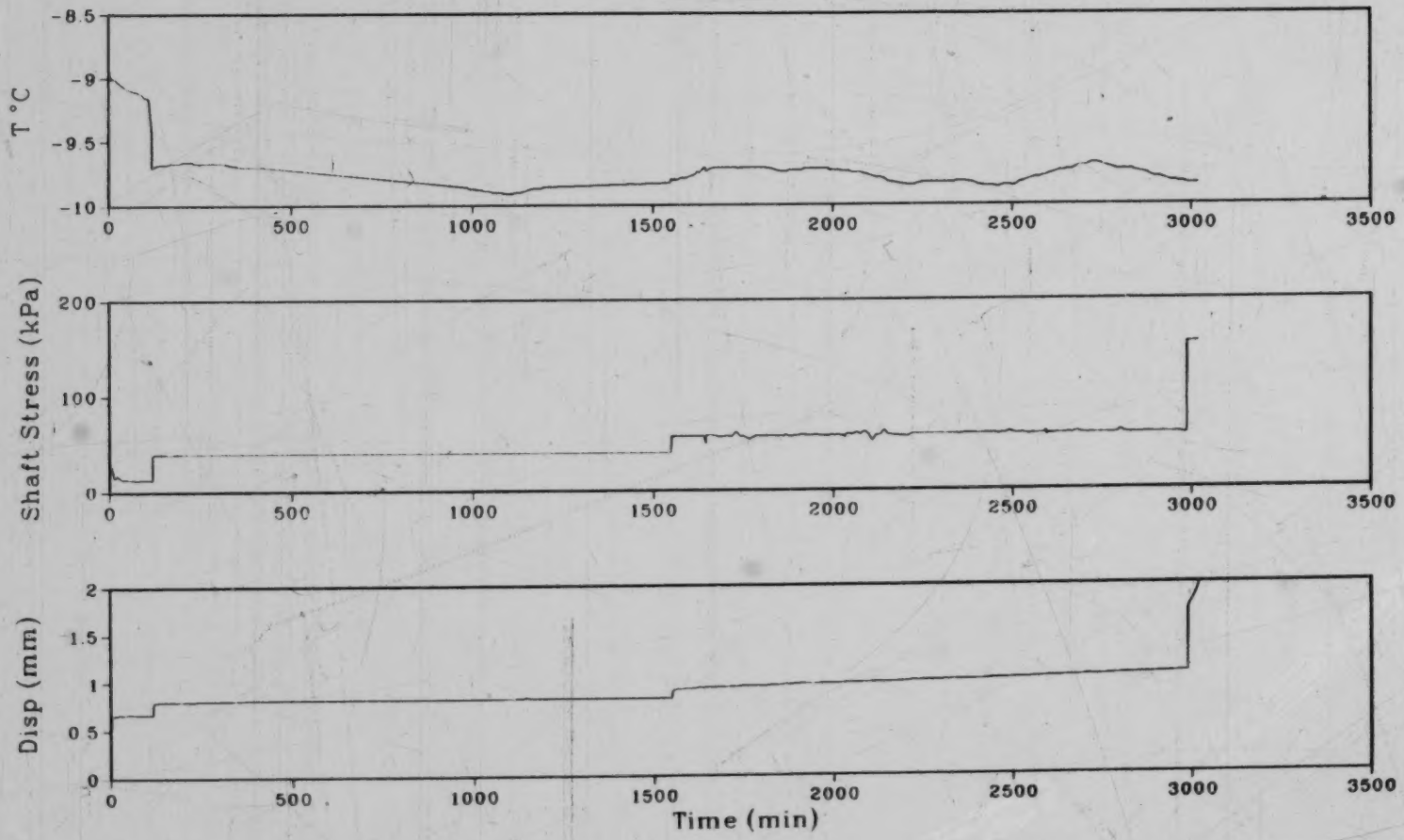

Figure A.10: Temperature, stress and displacement data for sample 2.5: silty sand of salinity 15 ppt at −10°C

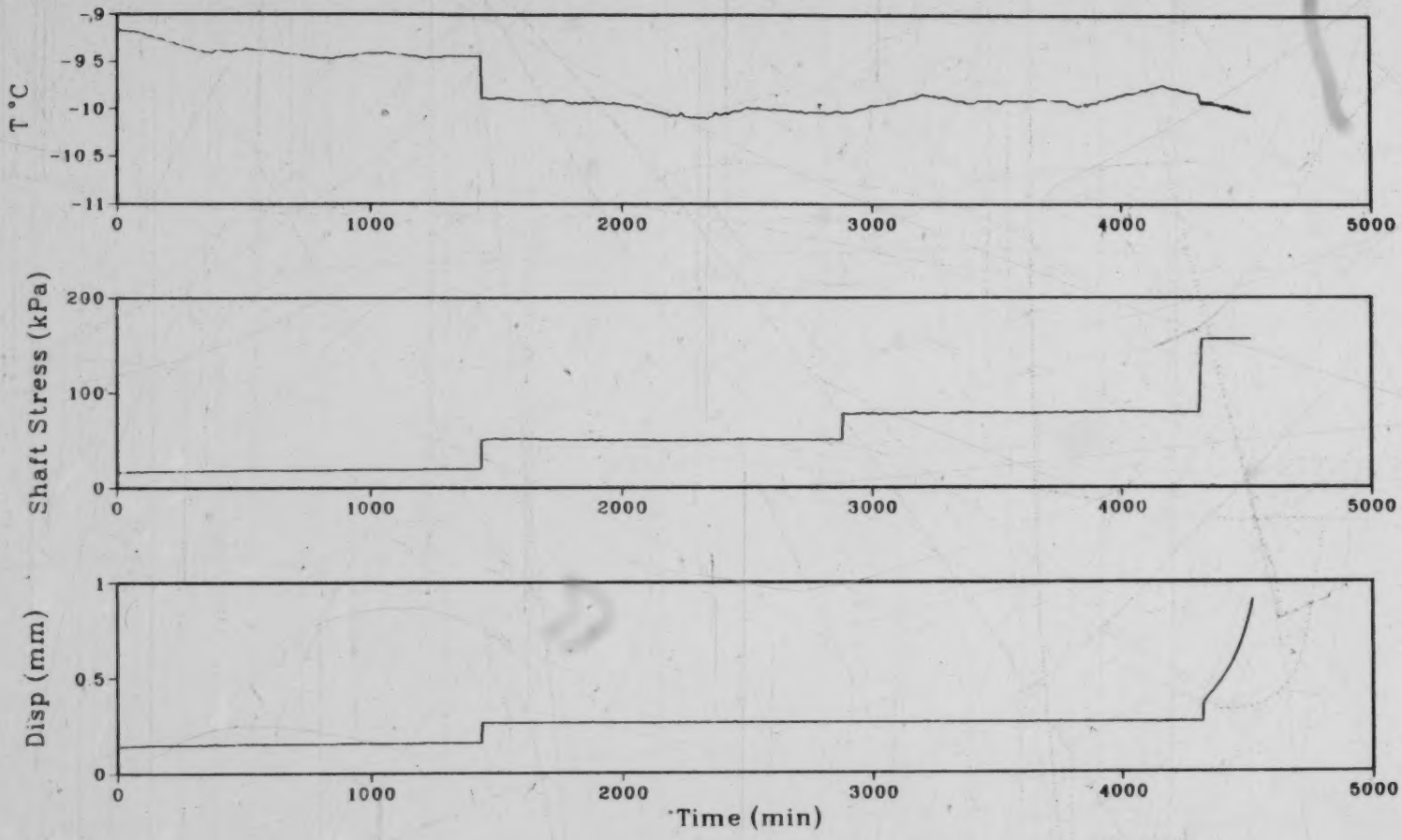

Figure A.11: Temperature, stress and displacement data for sample 2.6: silty sand of salinity 15 ppt at −10°C

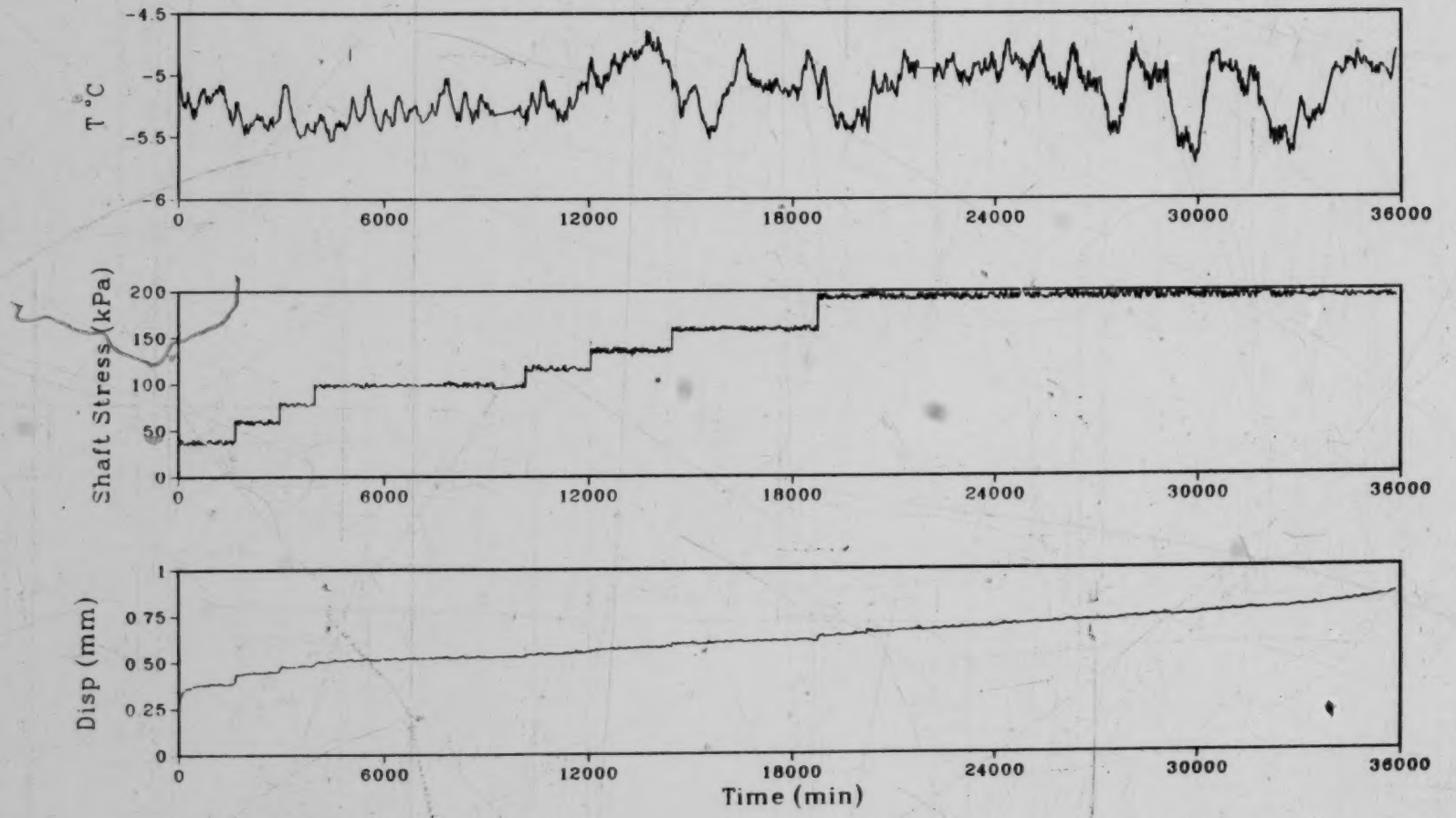

Figure A.12: Temperature, stress and displacement data for sample 3.1: fresh water silty sand at −5.1°C

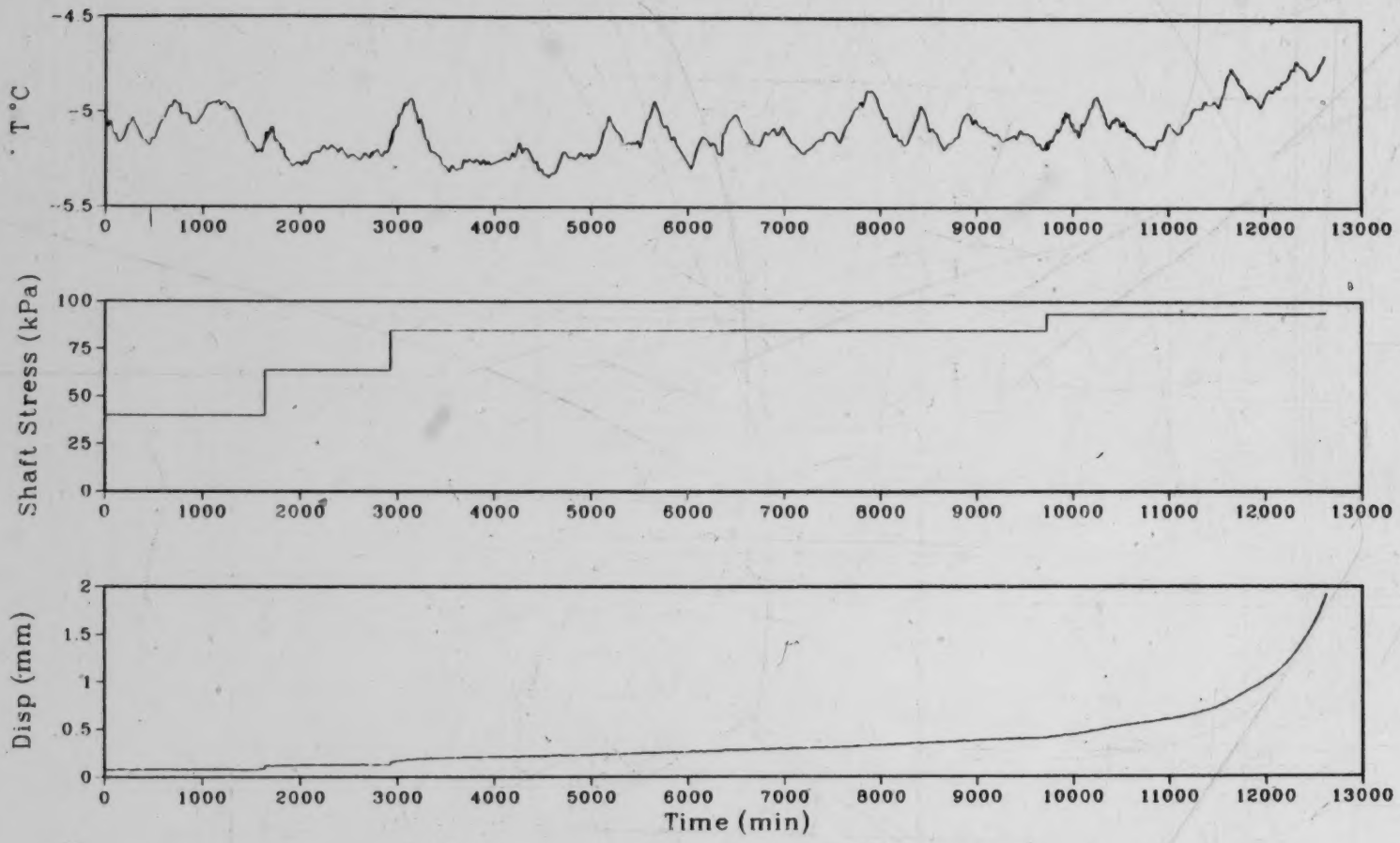

Figure A.13: Temperature, stress and displacement data for sample 3.2: silty sand of salinity 5 ppt at −5°C

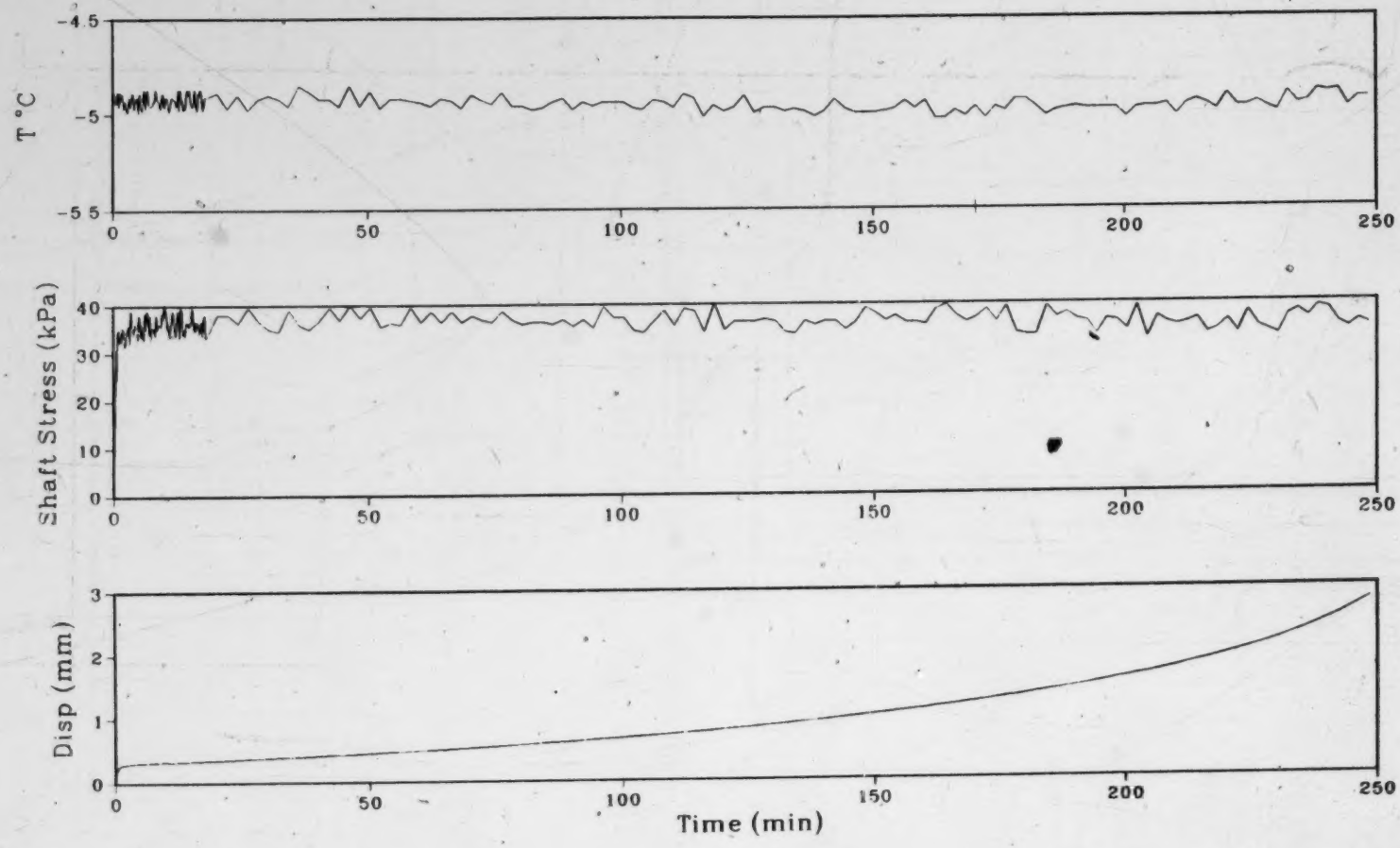

Figure A.14: Temperature, stress and displacement data for sample 3.3: silty sand of salinity 10 ppt at −5°C

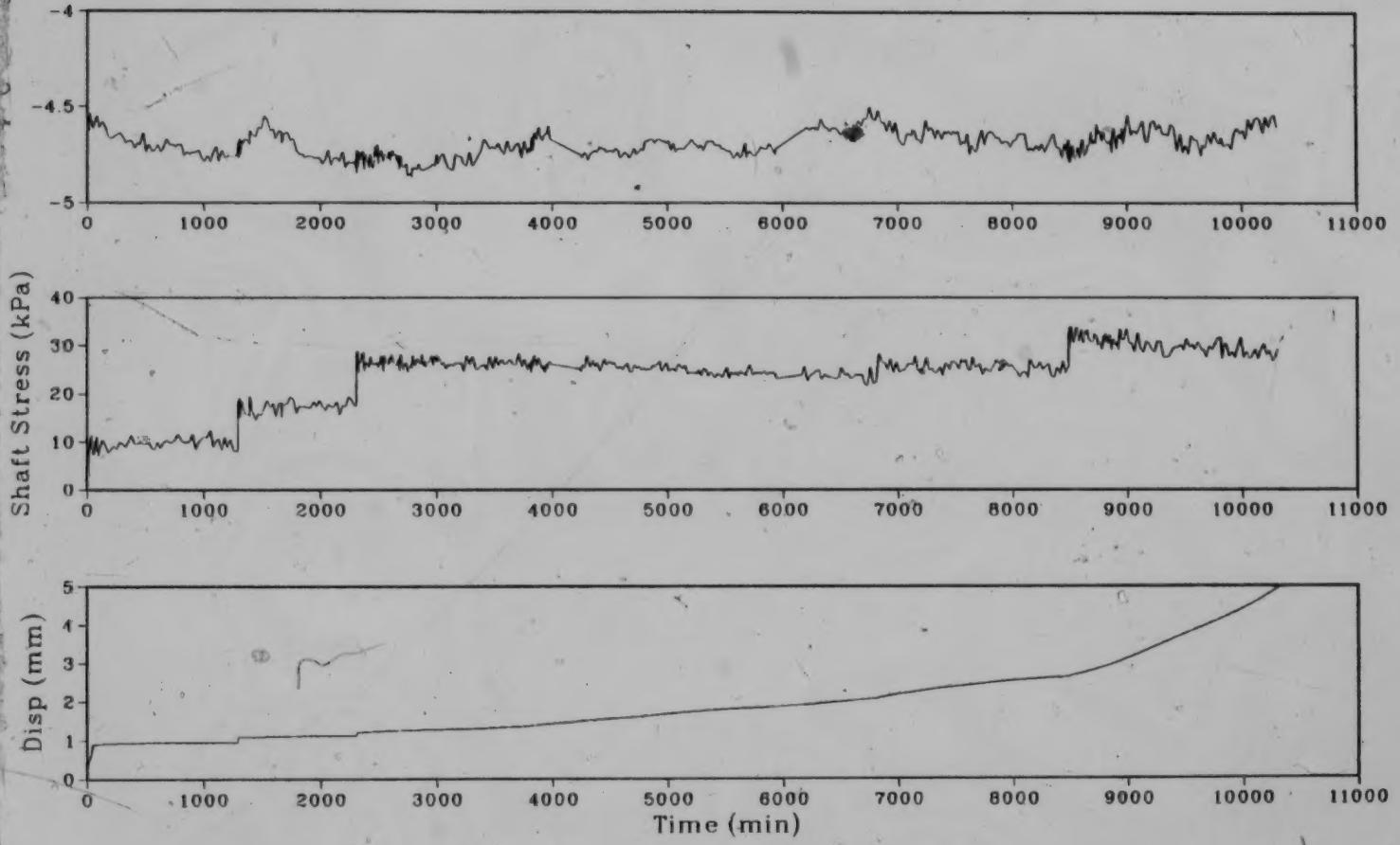

Figure A.15: Temperature, stress and displacement data for sample 3.4: silty sand of salinity 10 ppt at −5°C

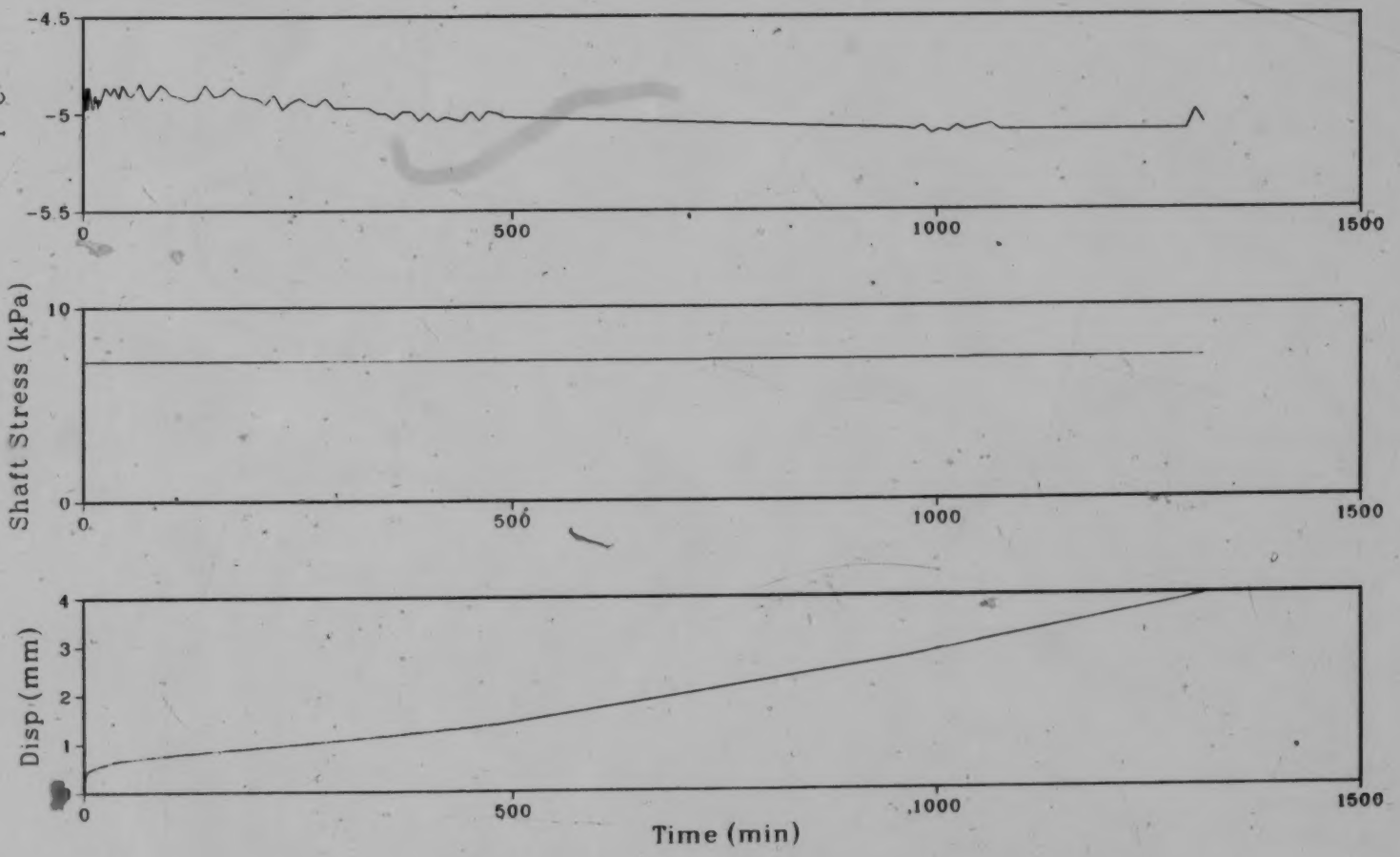

Figure A.16: Temperature, stress and displacement data for sample 3.5: silty sand of salinty 15 ppt at −5°C

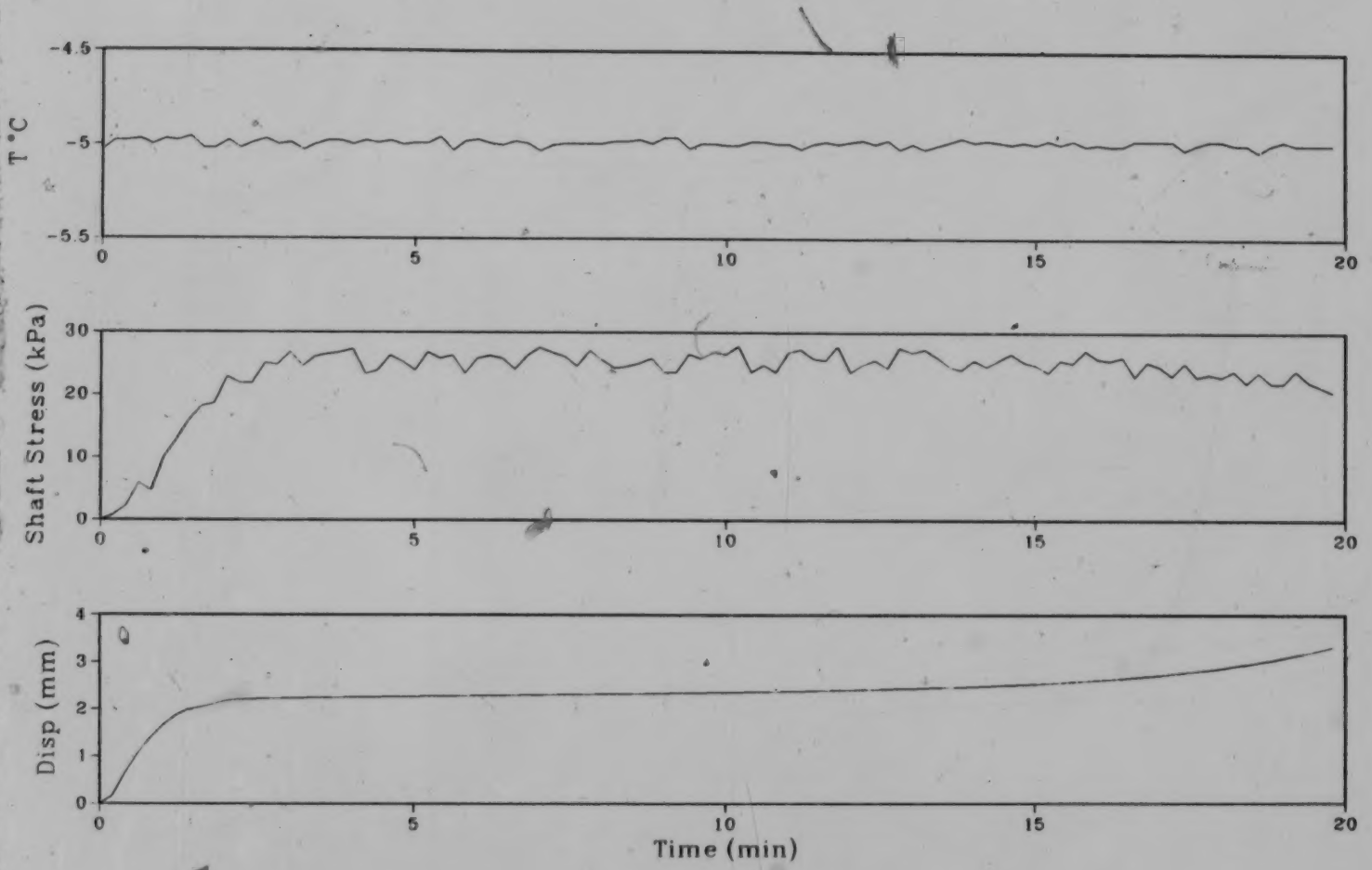

Figure A.17: Temperature, stress and displacement data for sample 3.6: silty sand of salinity 15 ppt at −5°C

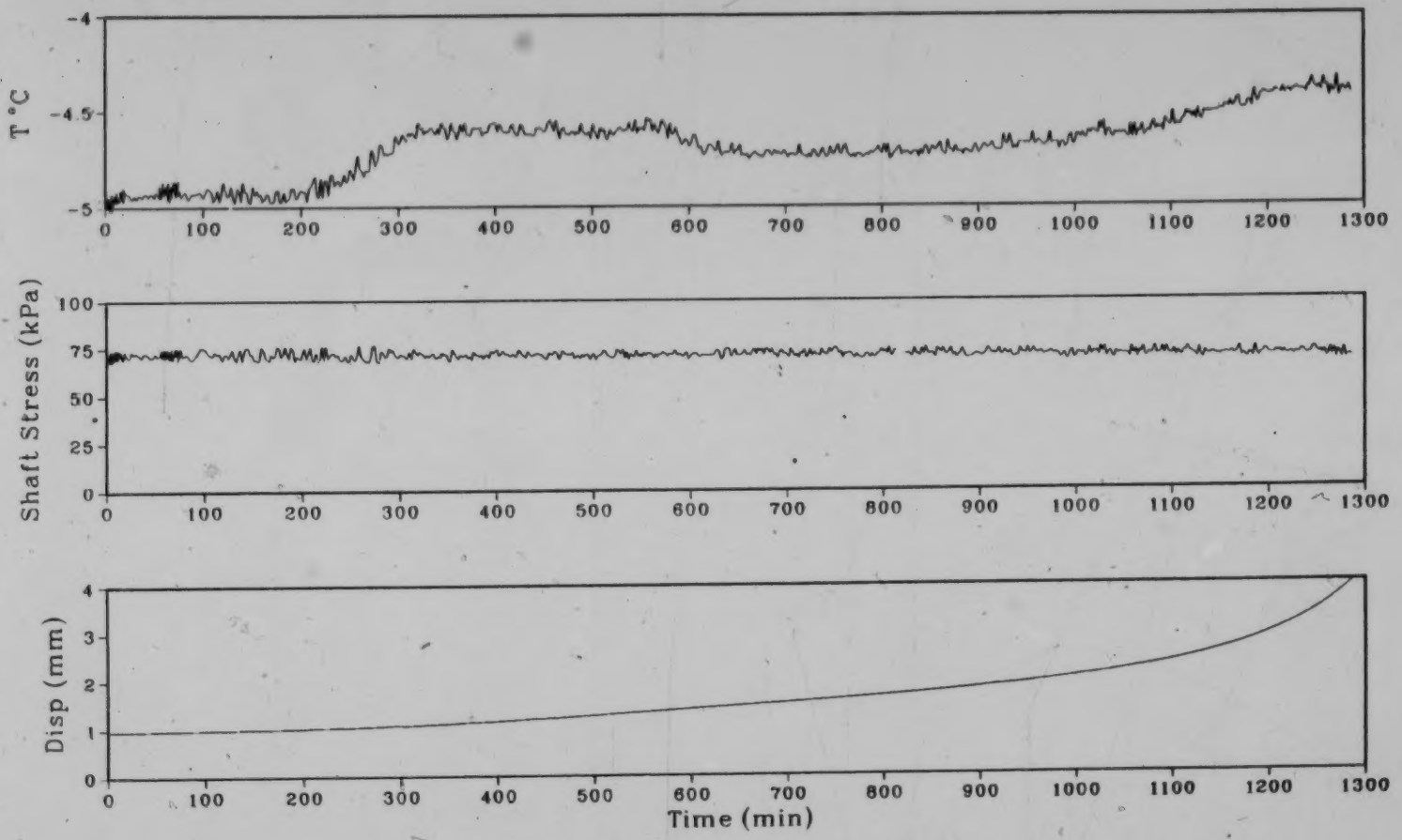

Figure A.18: Temperature, stress and displacement data for sample 4.1: silty sand of salinity 5 ppt at −4.7°C

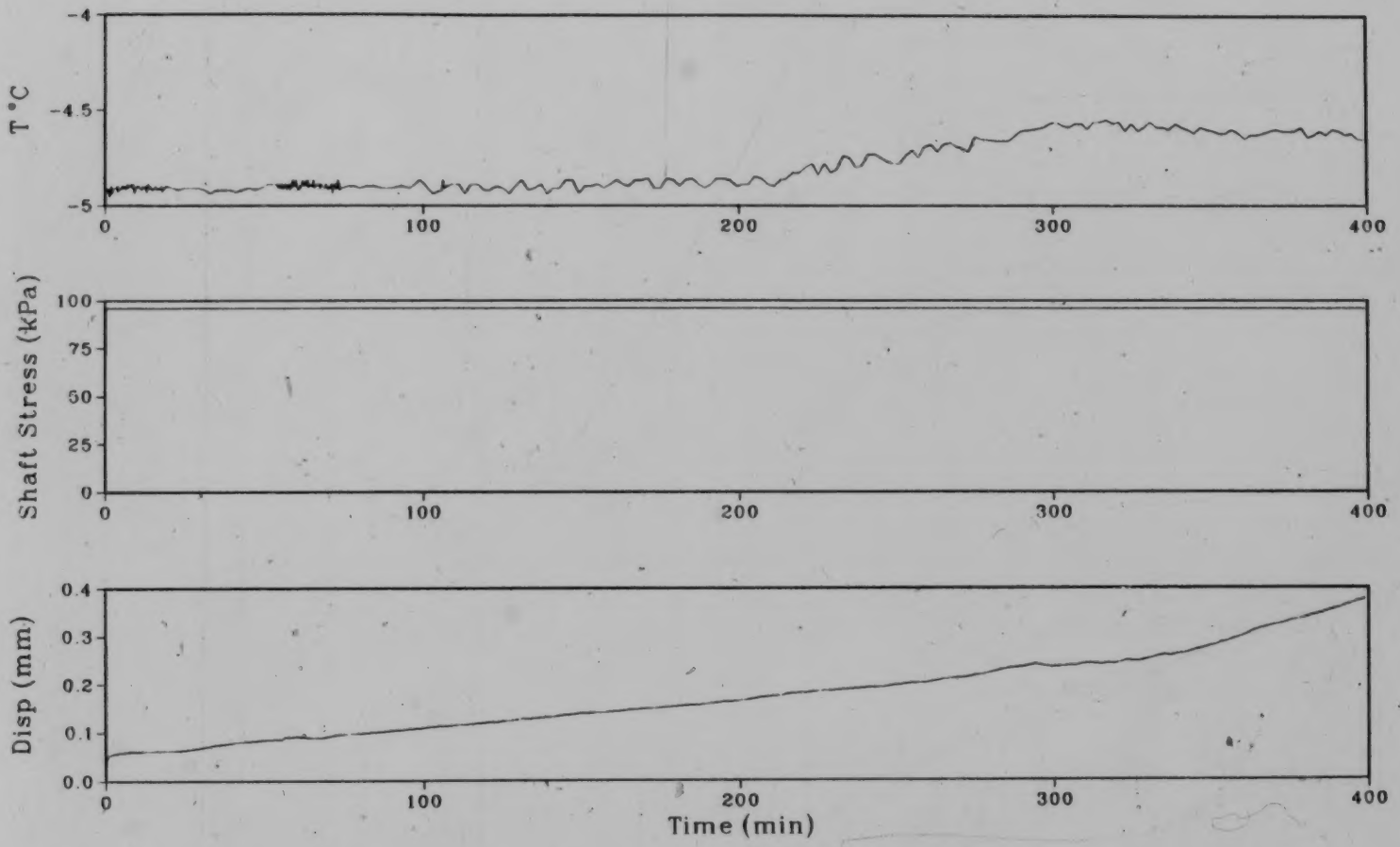

Figure A.19: Temperature, stress and displacement data for sample 4.2: silty sand of salinity 5 ppt at −4.8°C

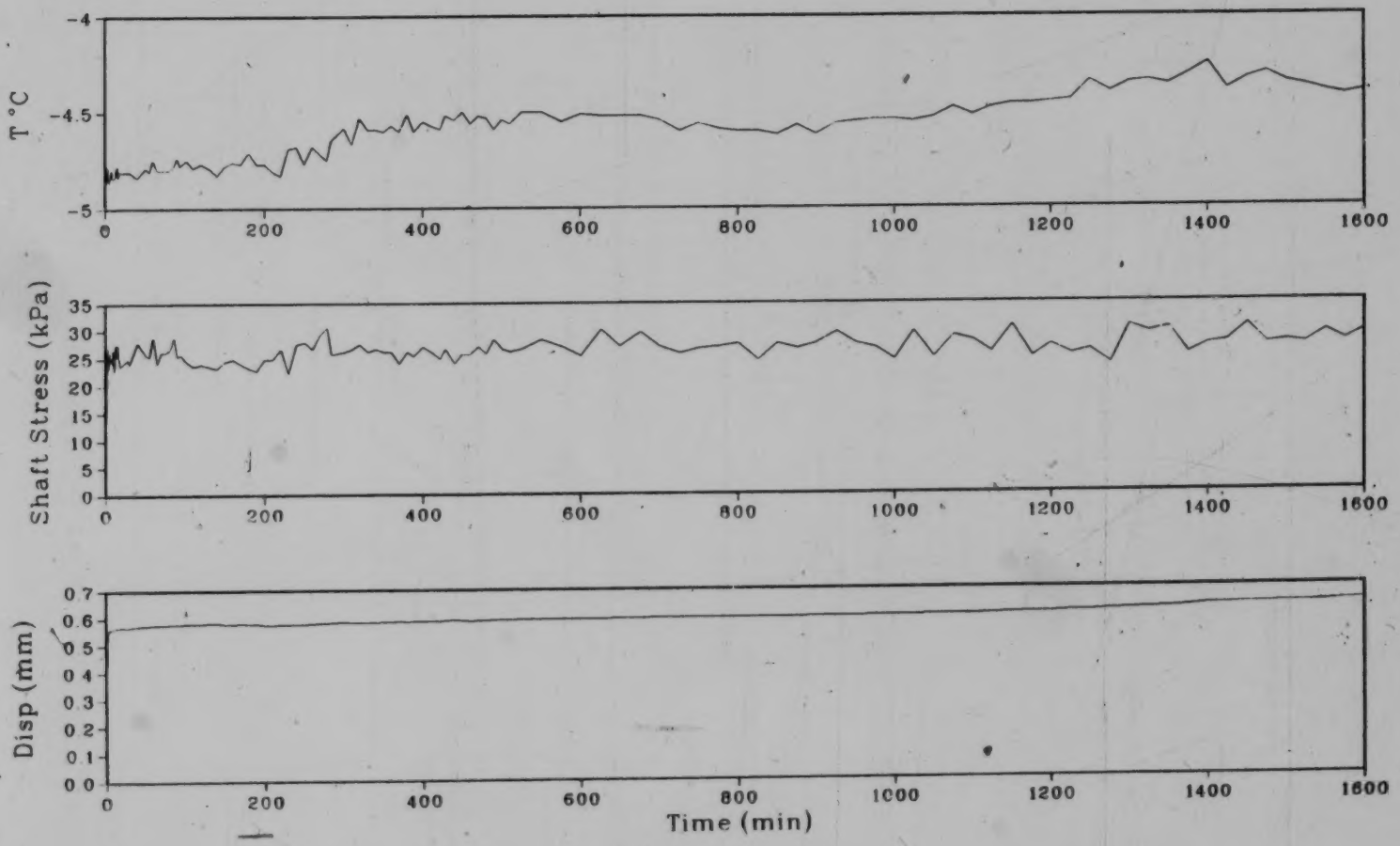

Figure A.20: Temperature, stress and displacement data for sample 4.3: silty sand of salinity 10 ppt at −4.7°C

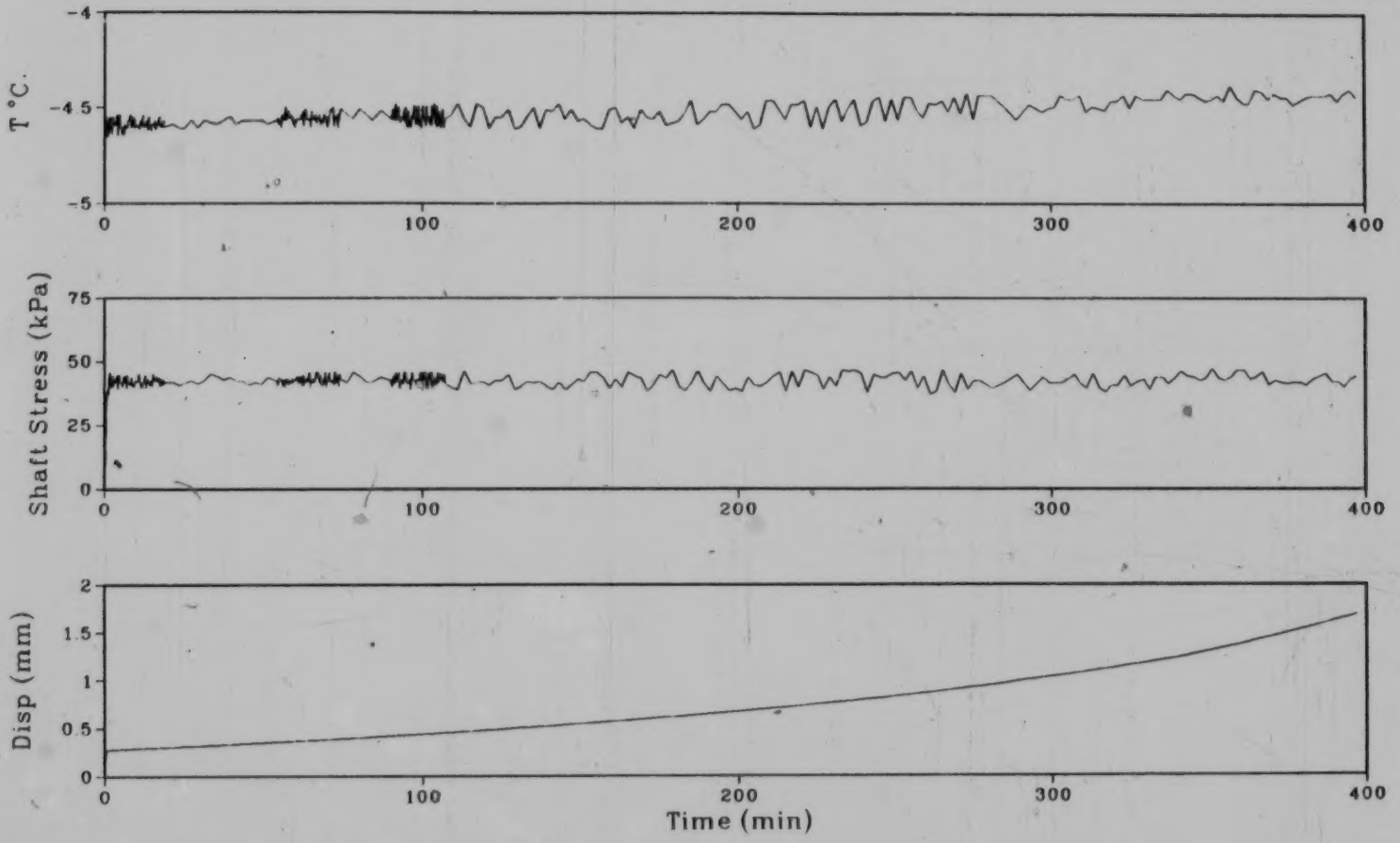

Figure A.21: Temperature, stress and displacement data for sample 4.4: silty sand of salinity 10 ppt at −4.6°C

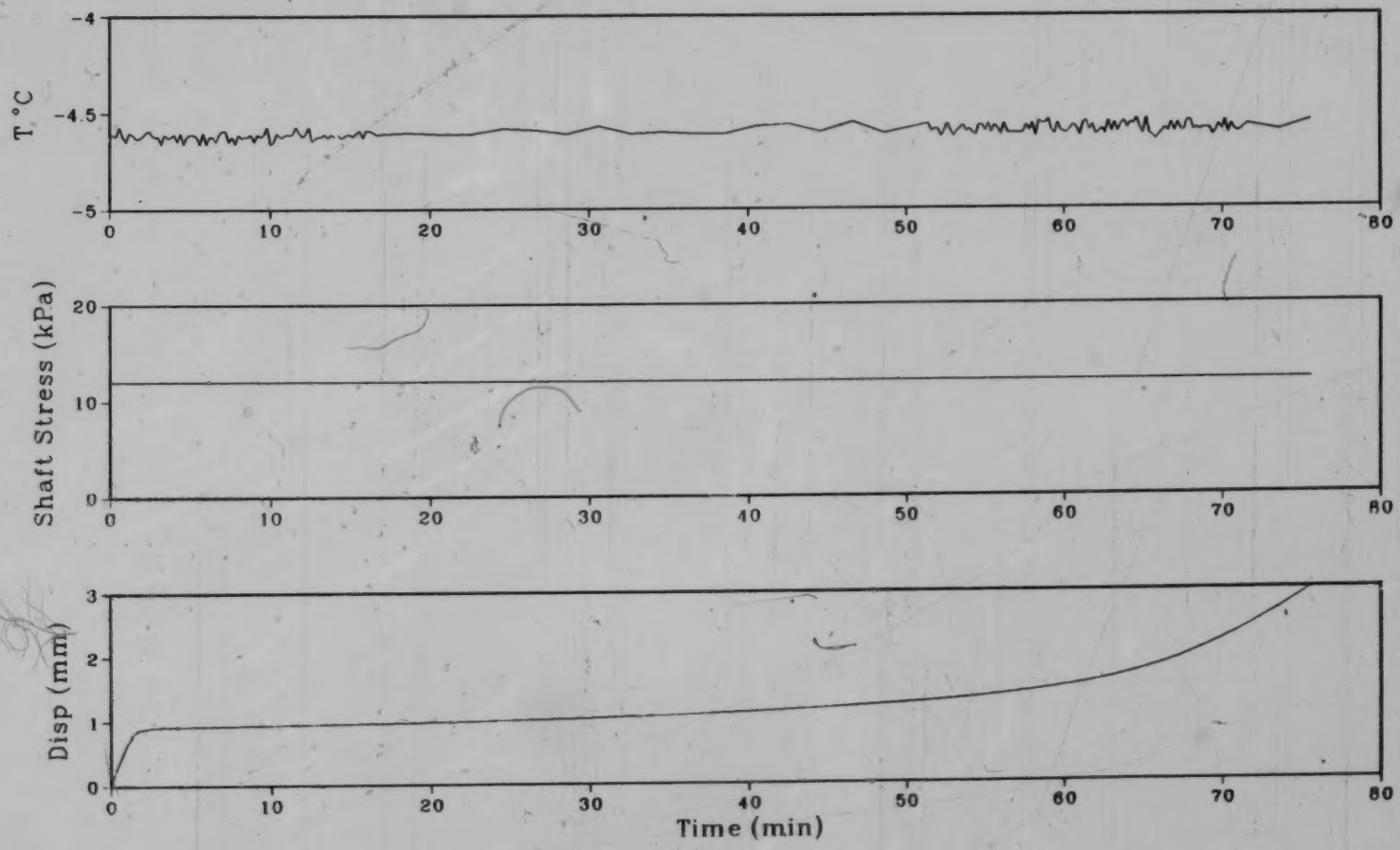

Figure A.22: Temperature, stress and displacement data for sample 4.5: silty sand of salinity 15 ppt at −4.6°C

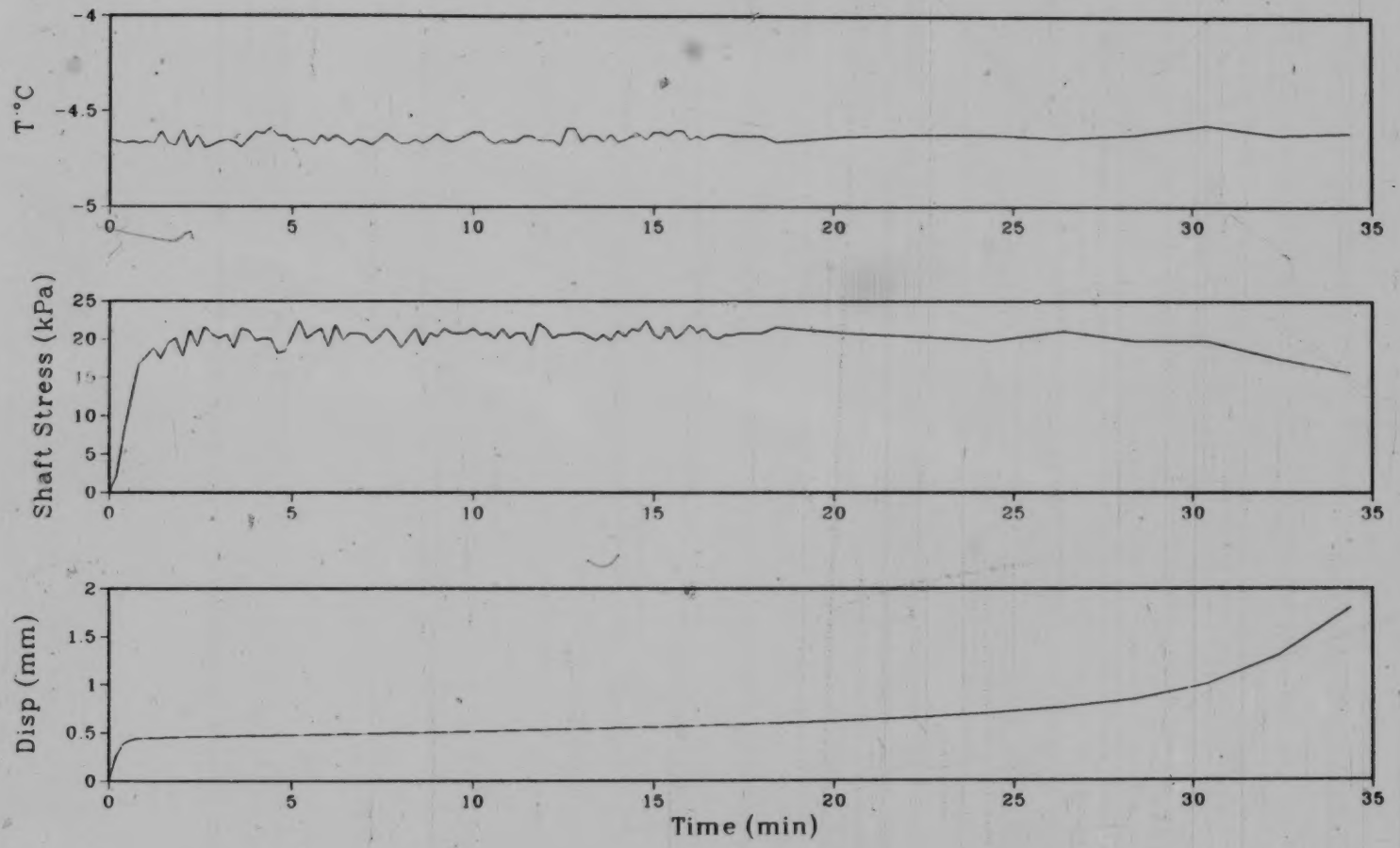

Figure A.23: Temperature, stress and displacement data for sample 4.6: silty sand of salinity 15 ppt at −4.6°C

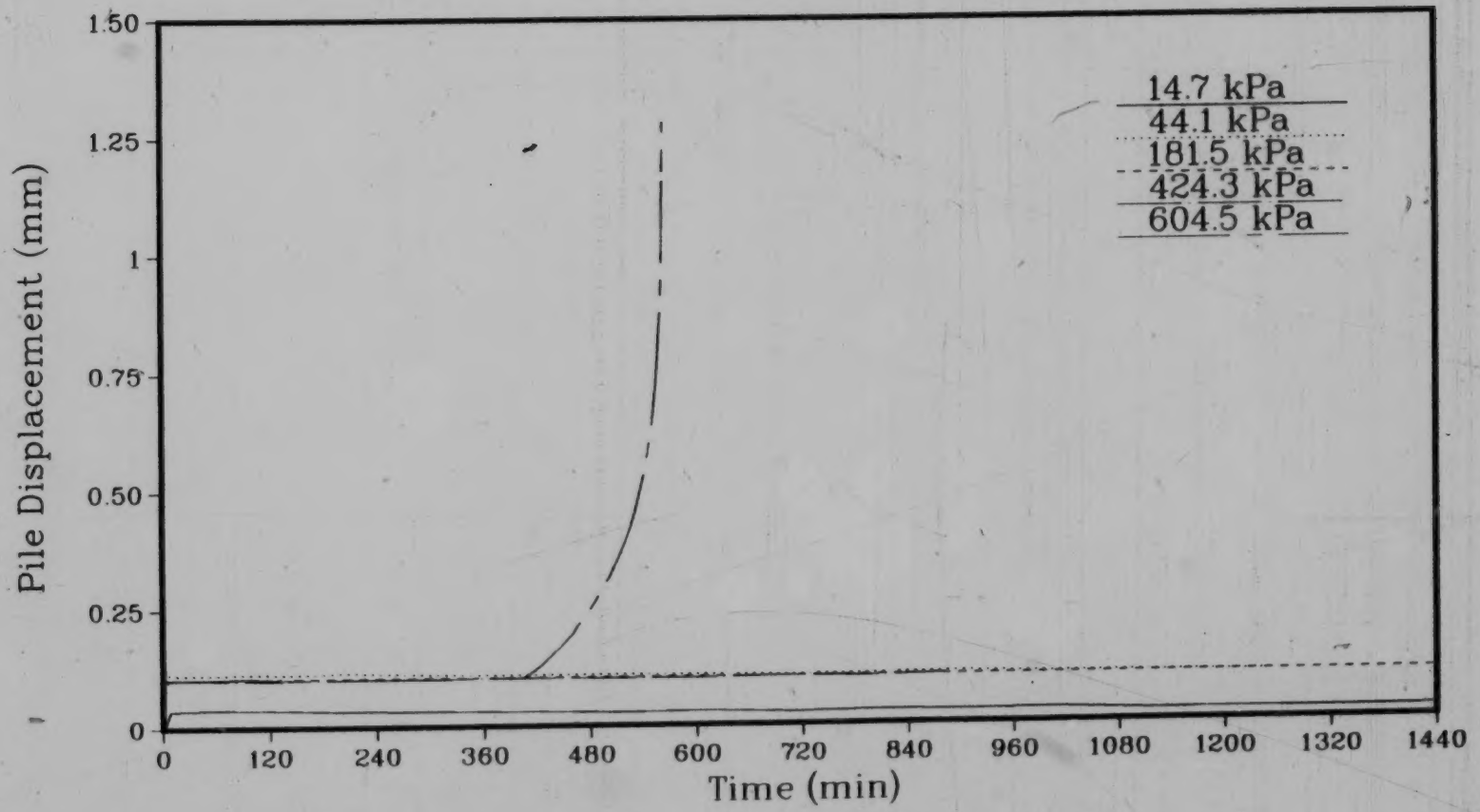

Figure A.24: Pile displacement with time for sample 1.1: fresh water silty sand at −13°C

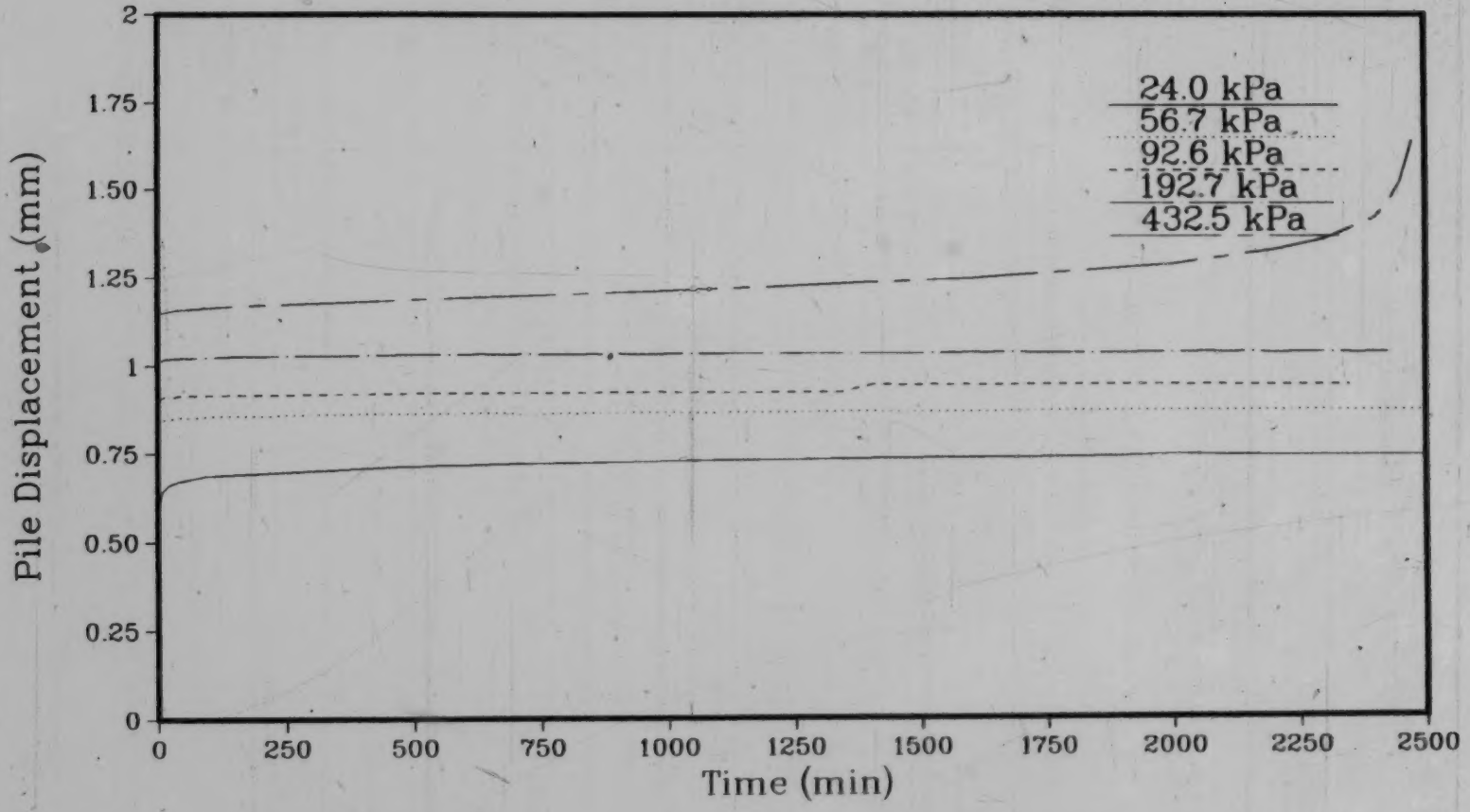

Figure A.25: Pile displacement with time for sample 1.2: silty sand of salinity 5 ppt at −13°C

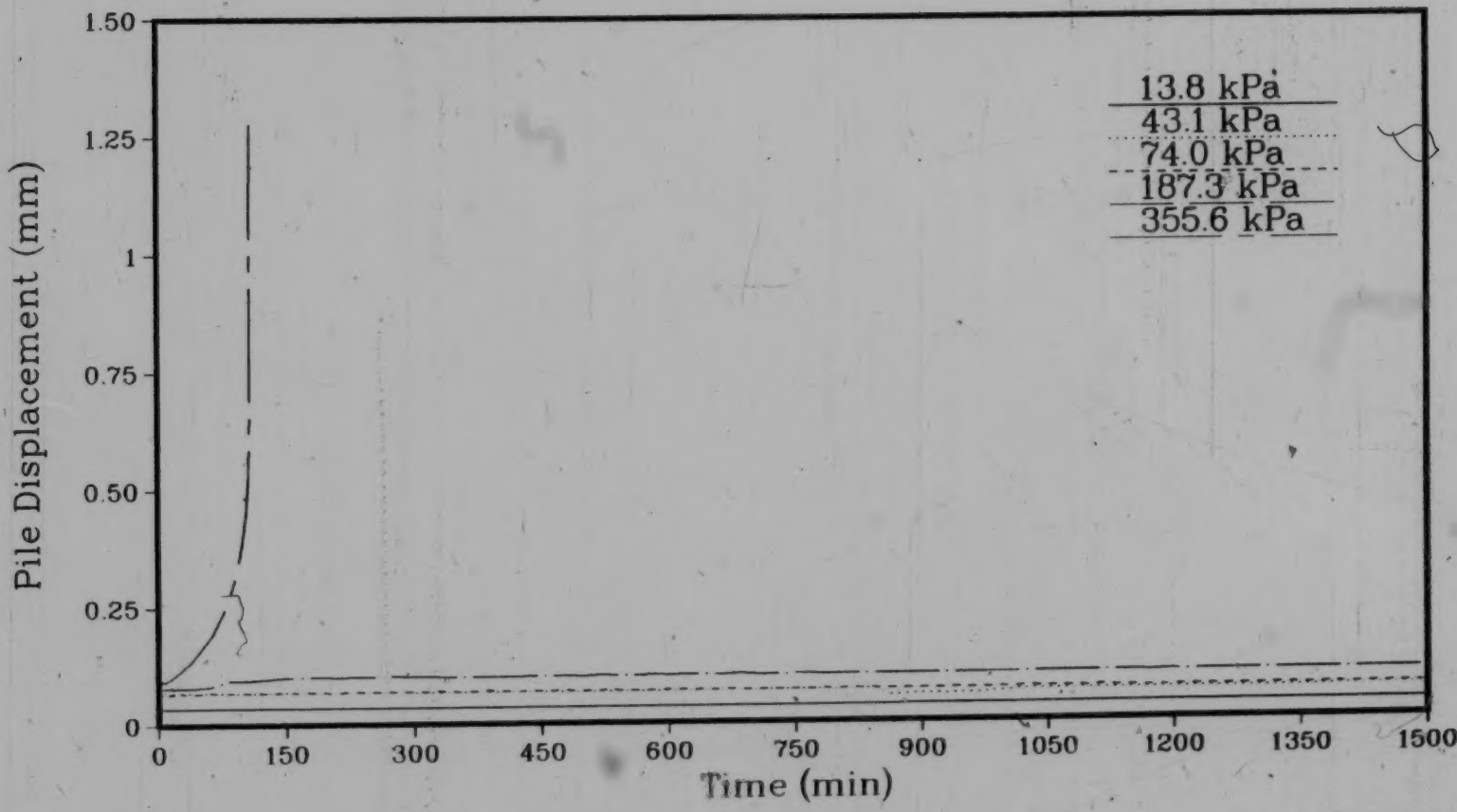

Figure A.26: Pile displacement with time for sample 1.3: silty sand of salinity 10 ppt at −12.5°C

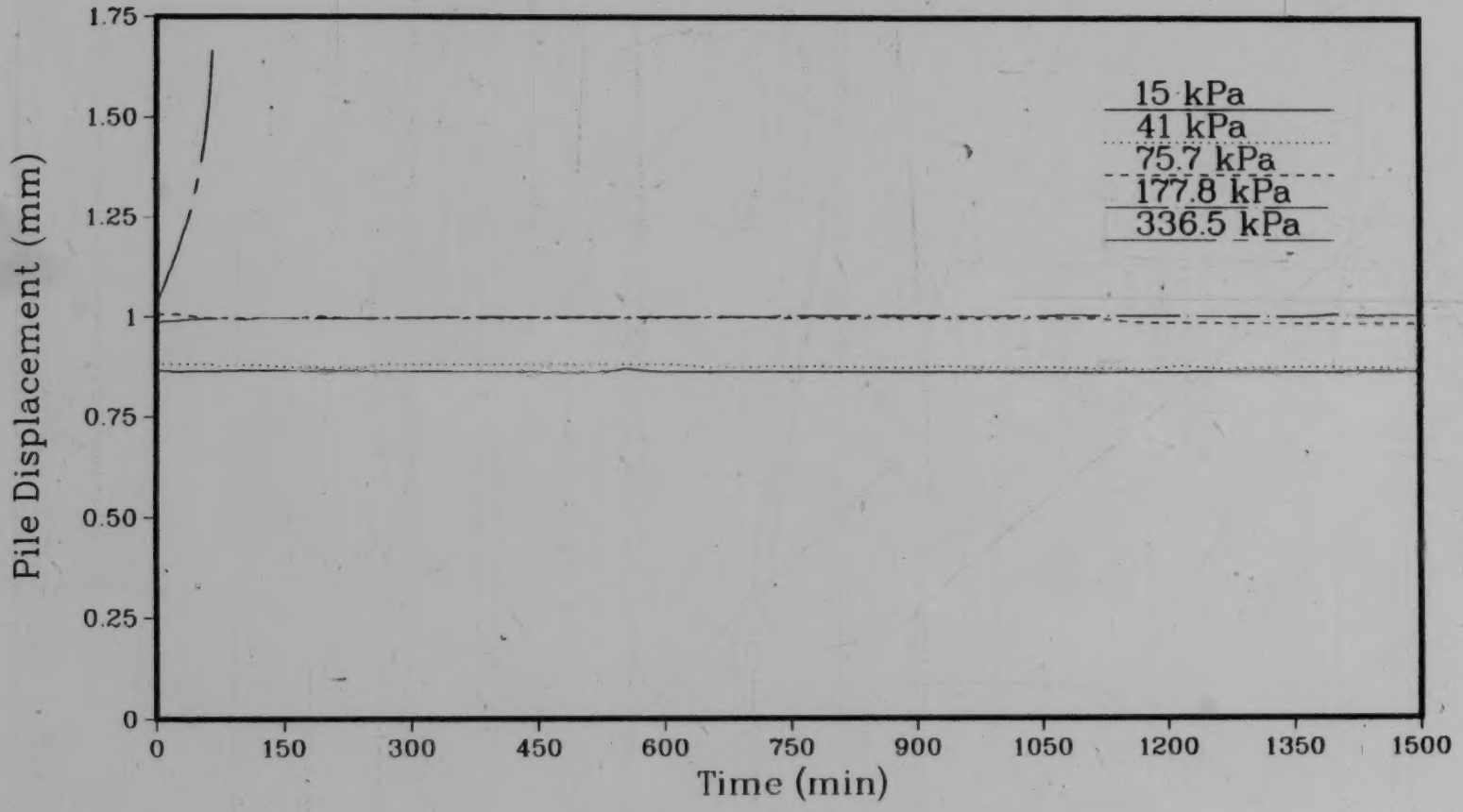

Figure A.27: Pile displacement with time for sample 1.4: silty sand of salinity 15 ppt at −12°C

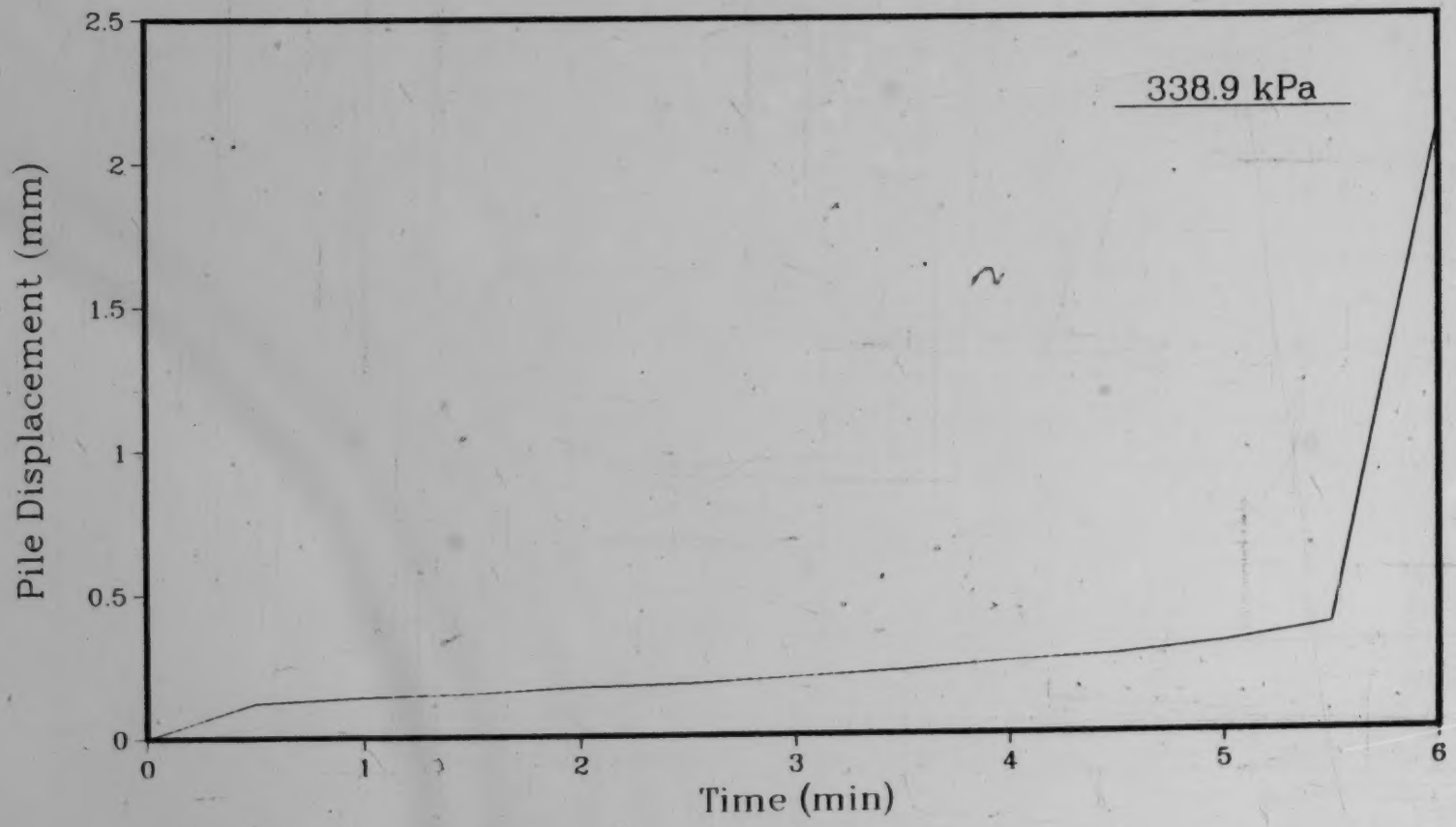

Figure A.28: Pile displacement with time for sample 1.5: silty sand of salinity 15 ppt at −12°C

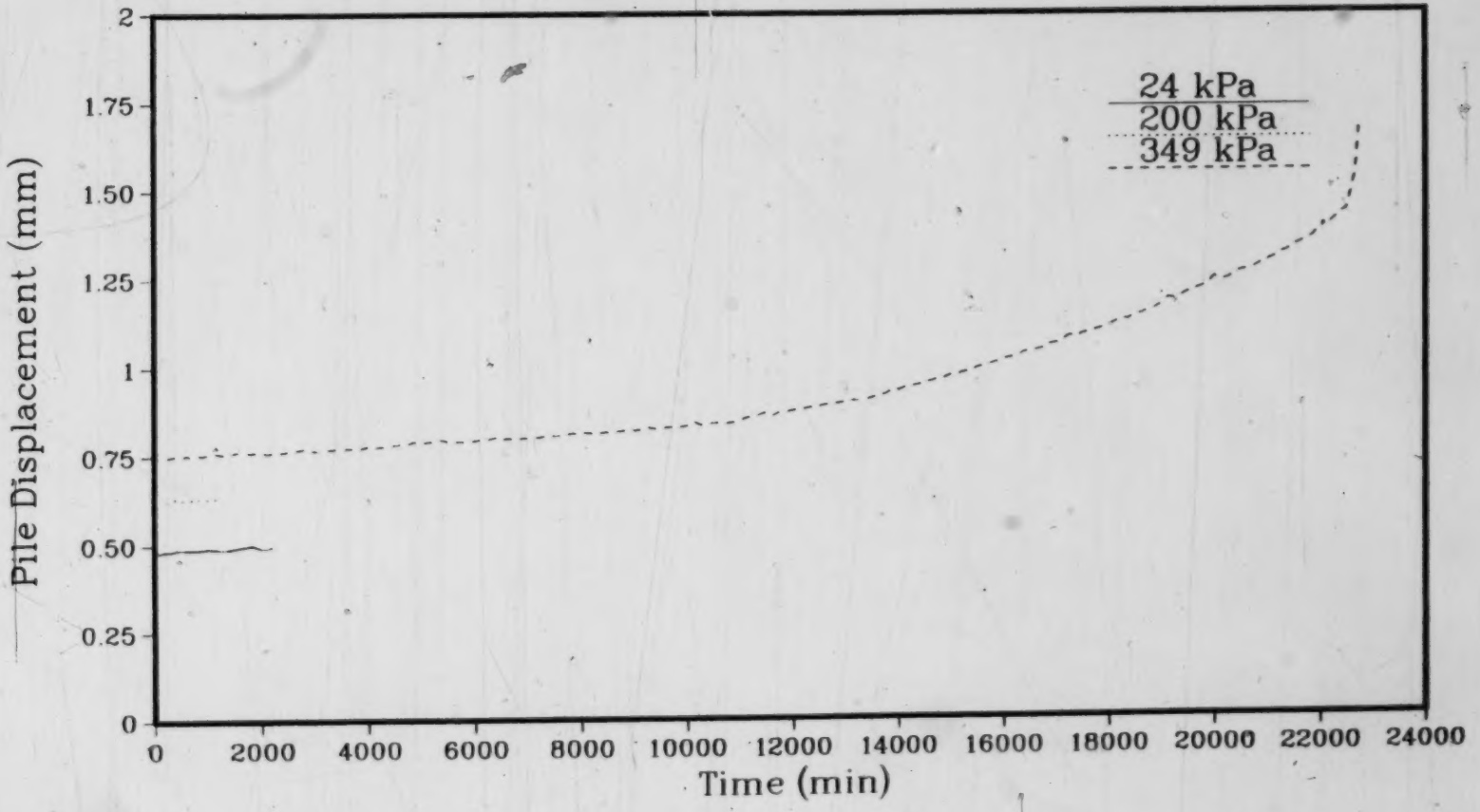

Figure A.29: Pile displacement with time for sample 2.1: fresh water silty sand at −10°C

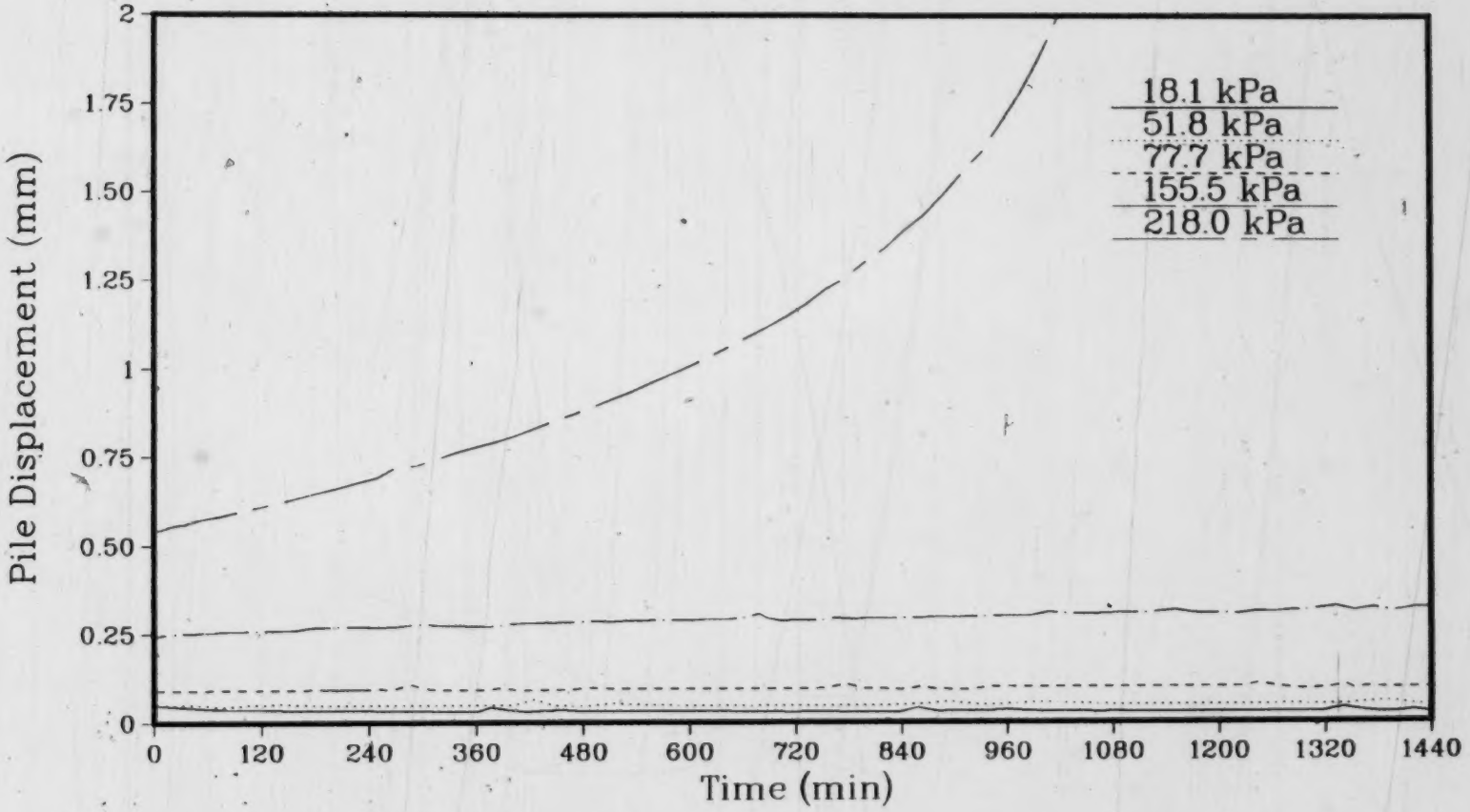

Figure A.30: Pile displacement with time for sample 2.2: silty sand of salinity 5 ppt at −10°C

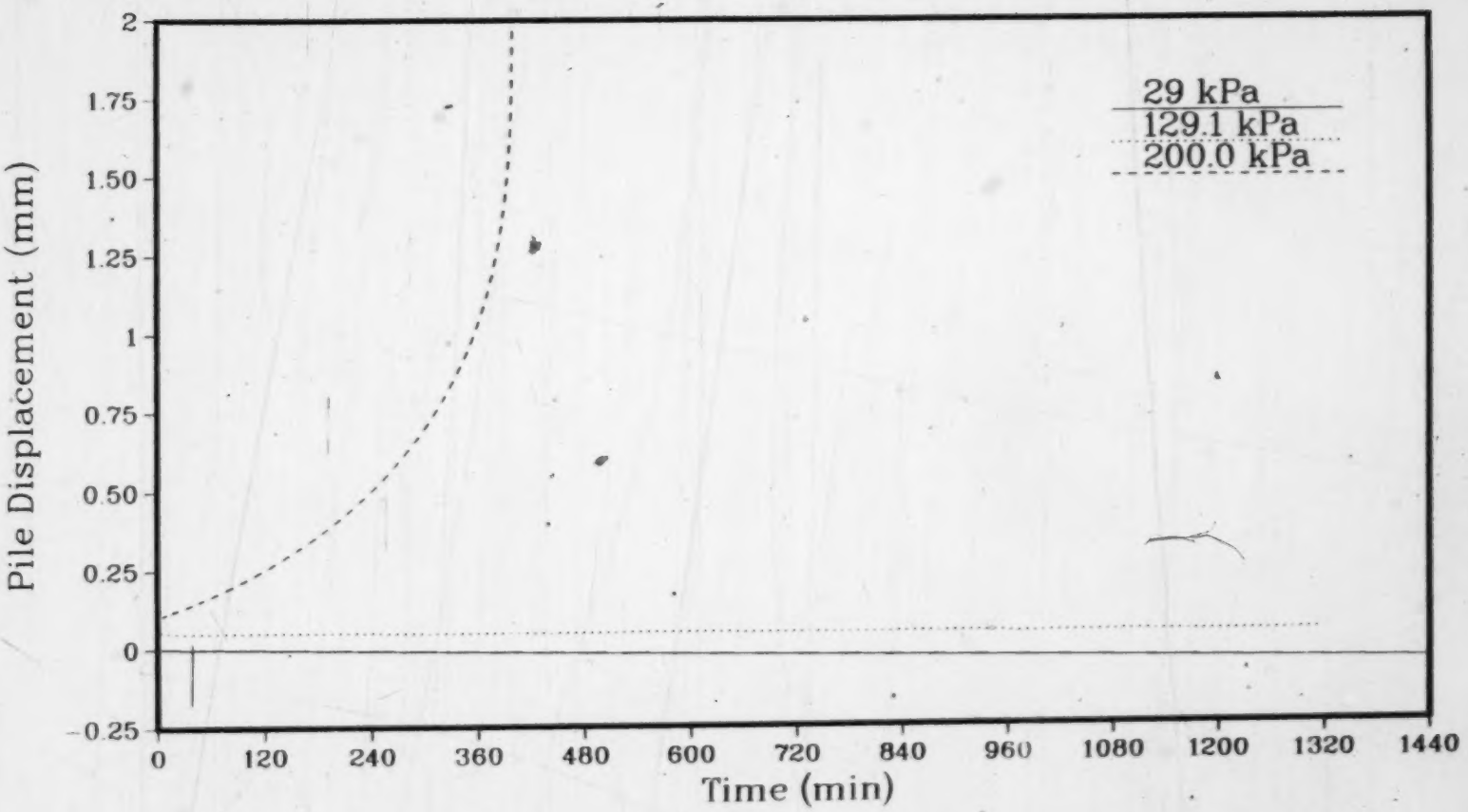

Figure A.31: Pile displacement with time for sample 2.3: silty sand of salinity 10 ppt at −10°C

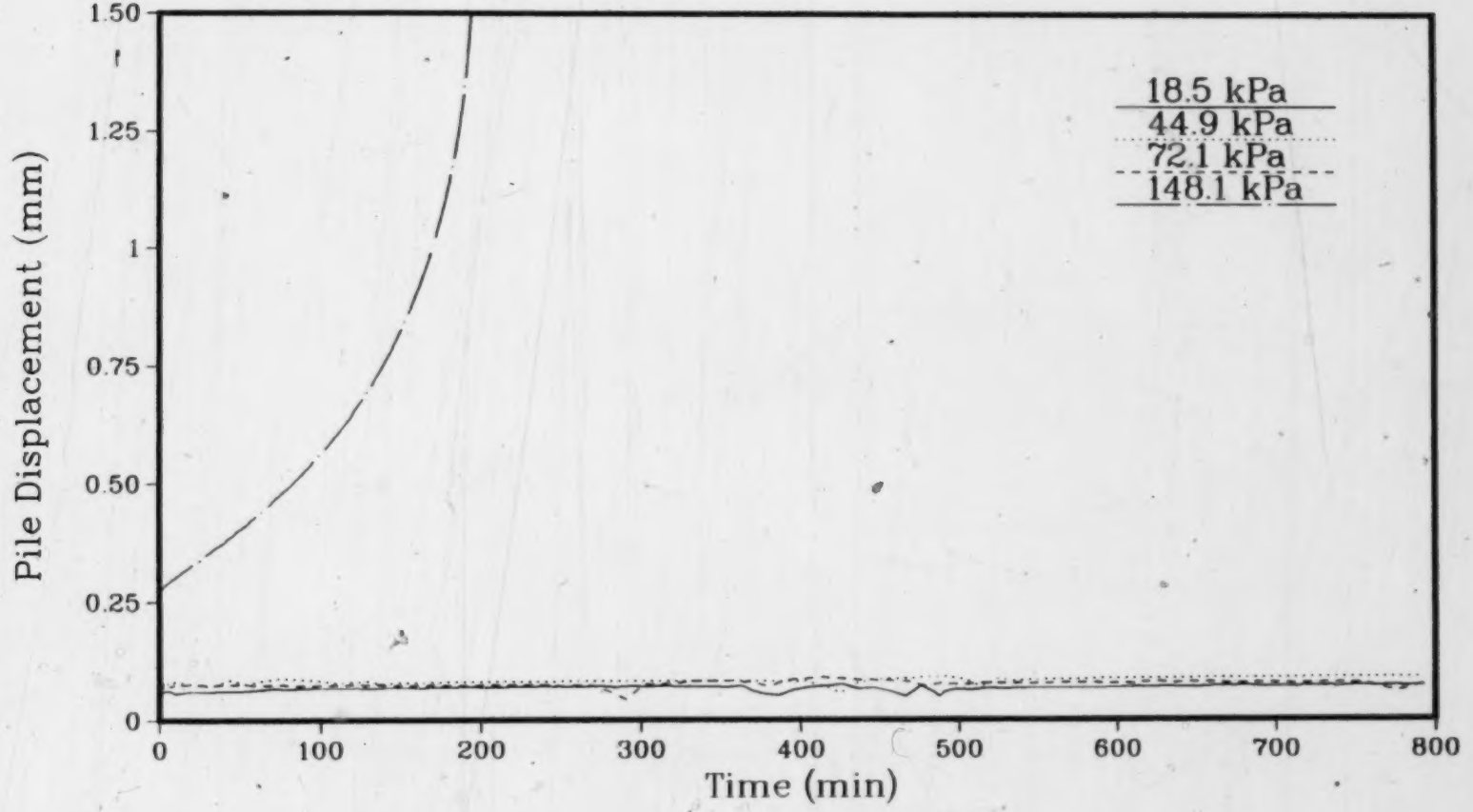

Figure A.32: Pile displacement with time for sample 2.4: silty sand of salinity 10 ppt at −10°C

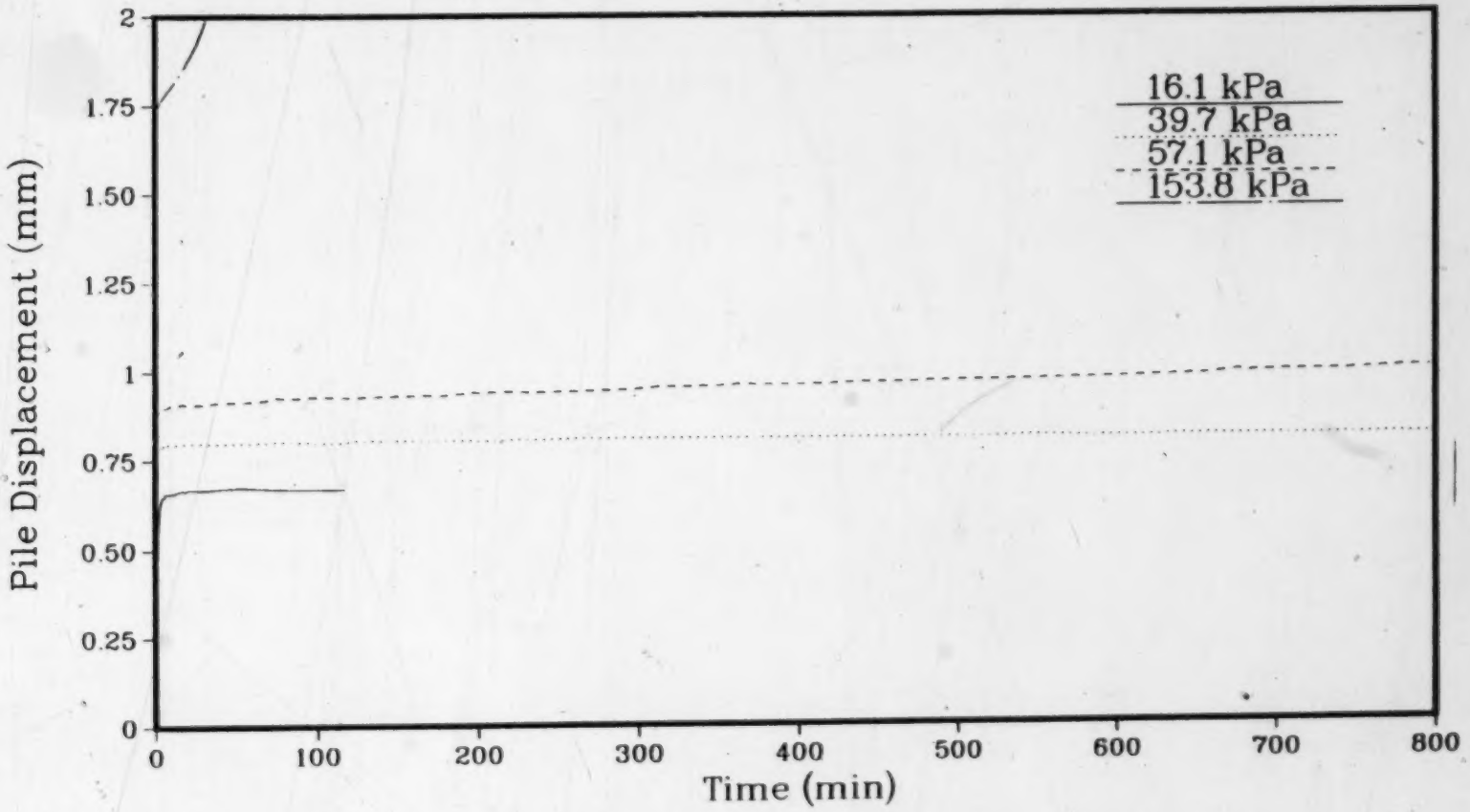

Figure A.33: Pile displacement with time for sample 2.5: silty sand of salinity 15 ppt at −10°C

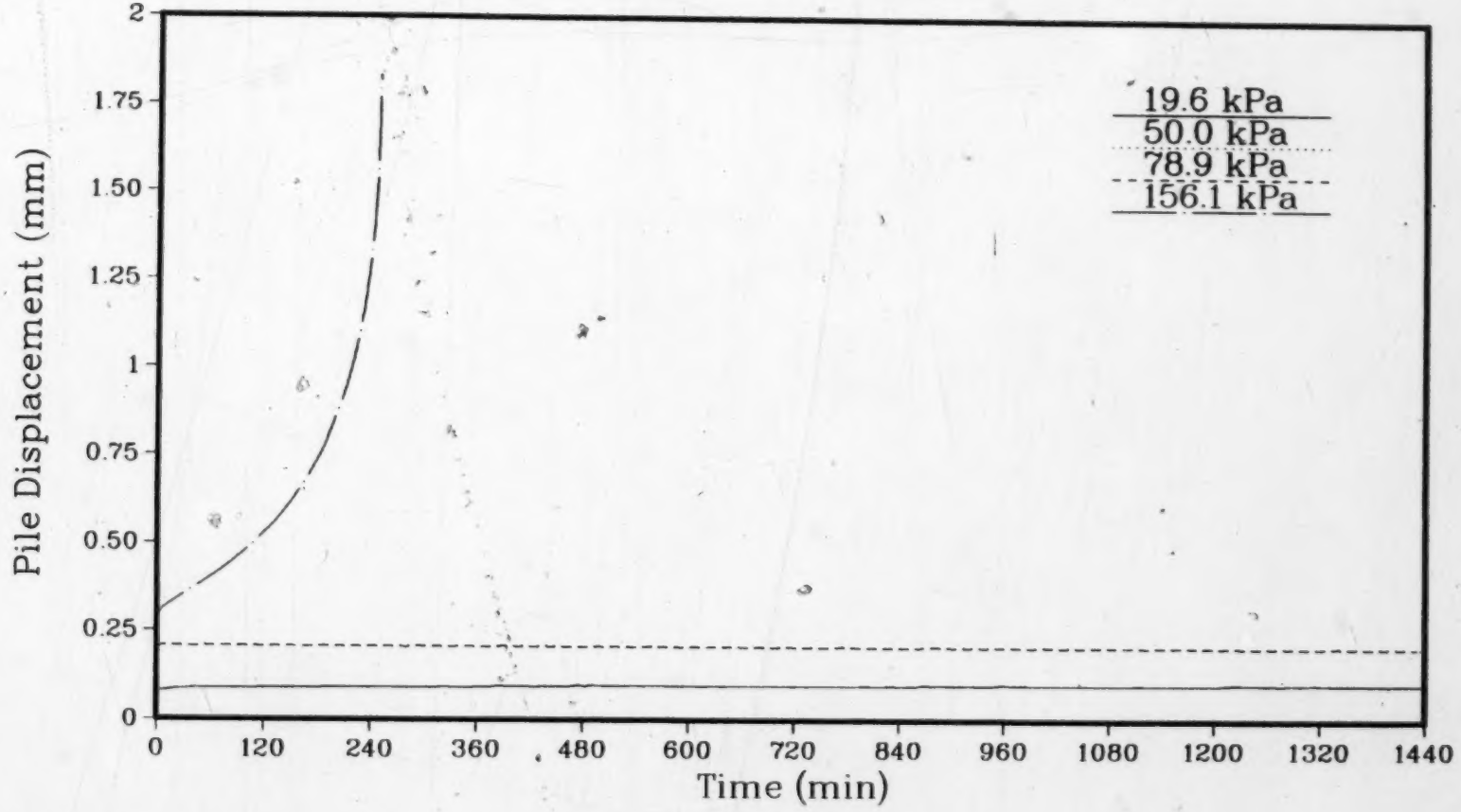

Figure A.34: Pile displacement with time for sample 2.6: silty sand of salinity 15 ppt at −10°C

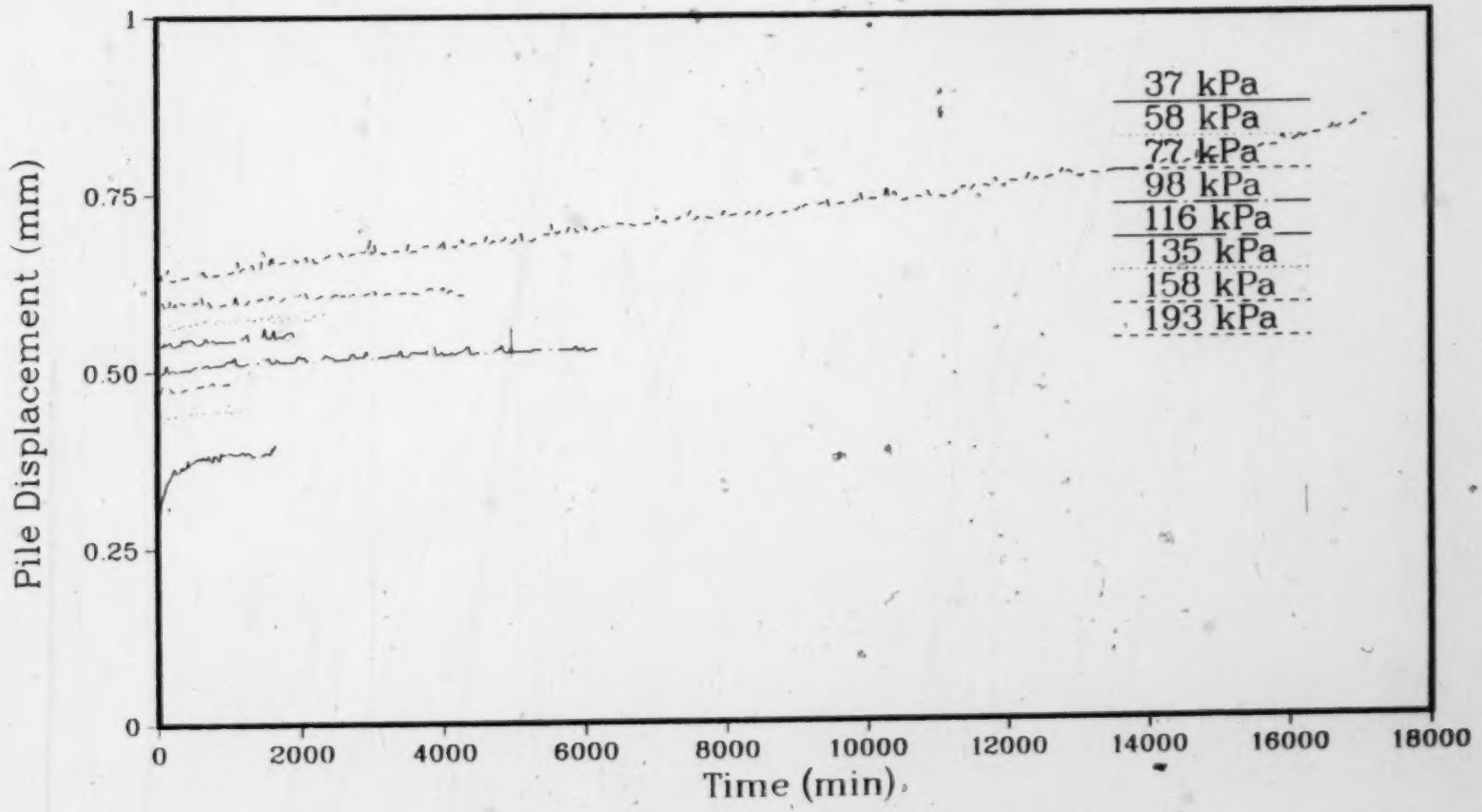

Figure A.35: Pile displacement with time for sample 3.1: fresh water silty sand at −5.1°C

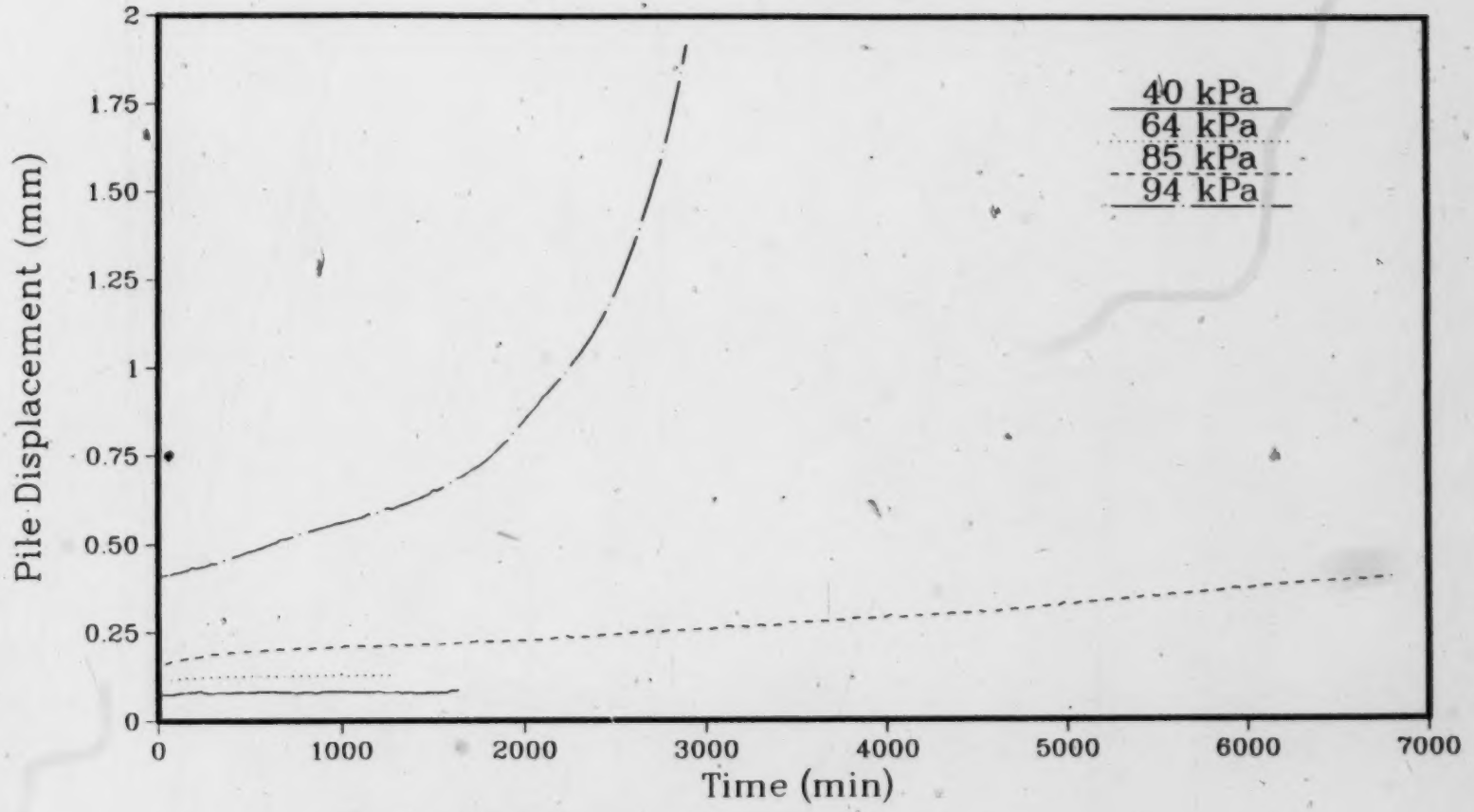

Figure A.36: Pile displacement with time for sample 3.2: silty sand of salinty 5 ppt at −5°C

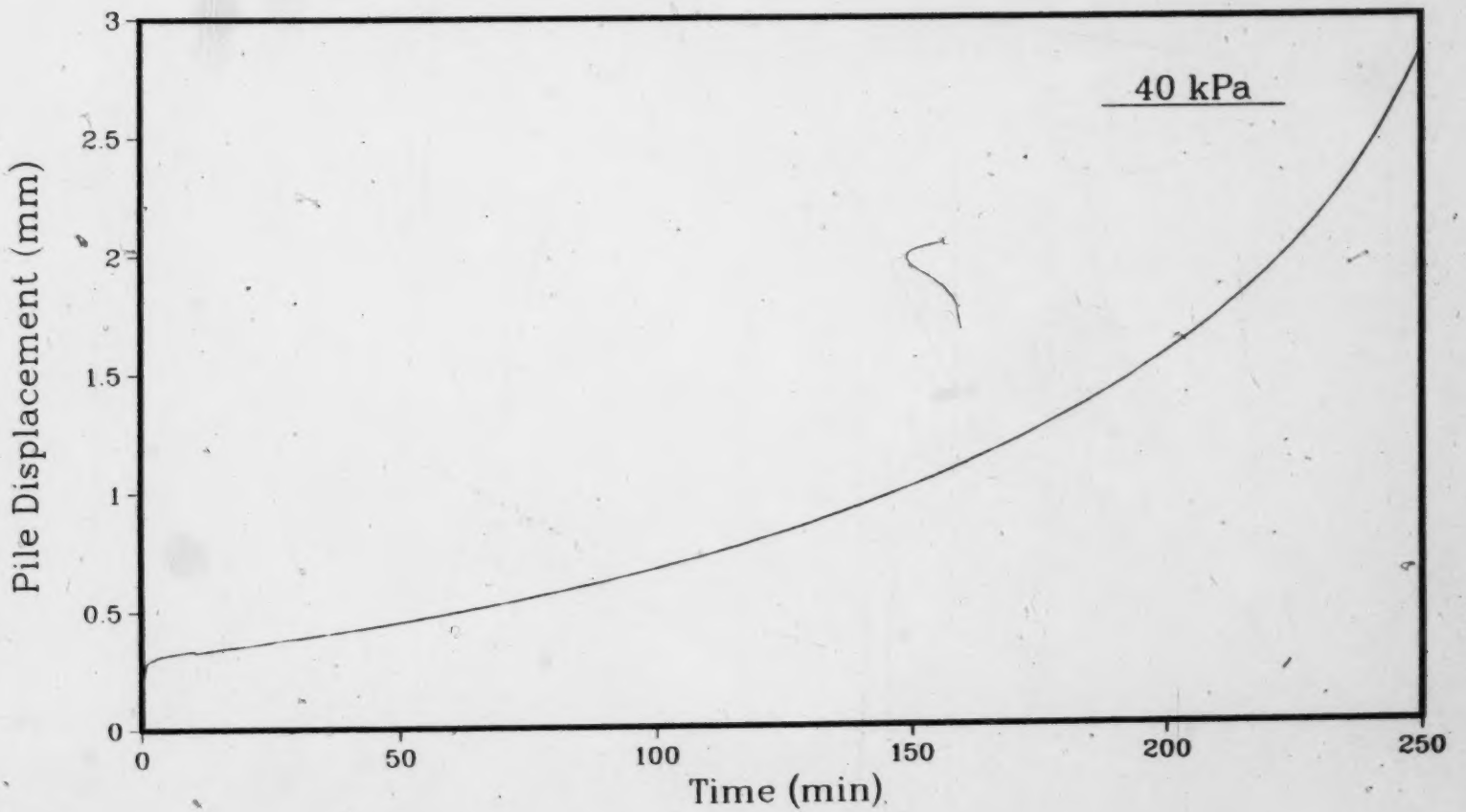

Figure A.37: Pile displacement with time for sample 3.3: silty sand of salinity 10 ppt at −5°C

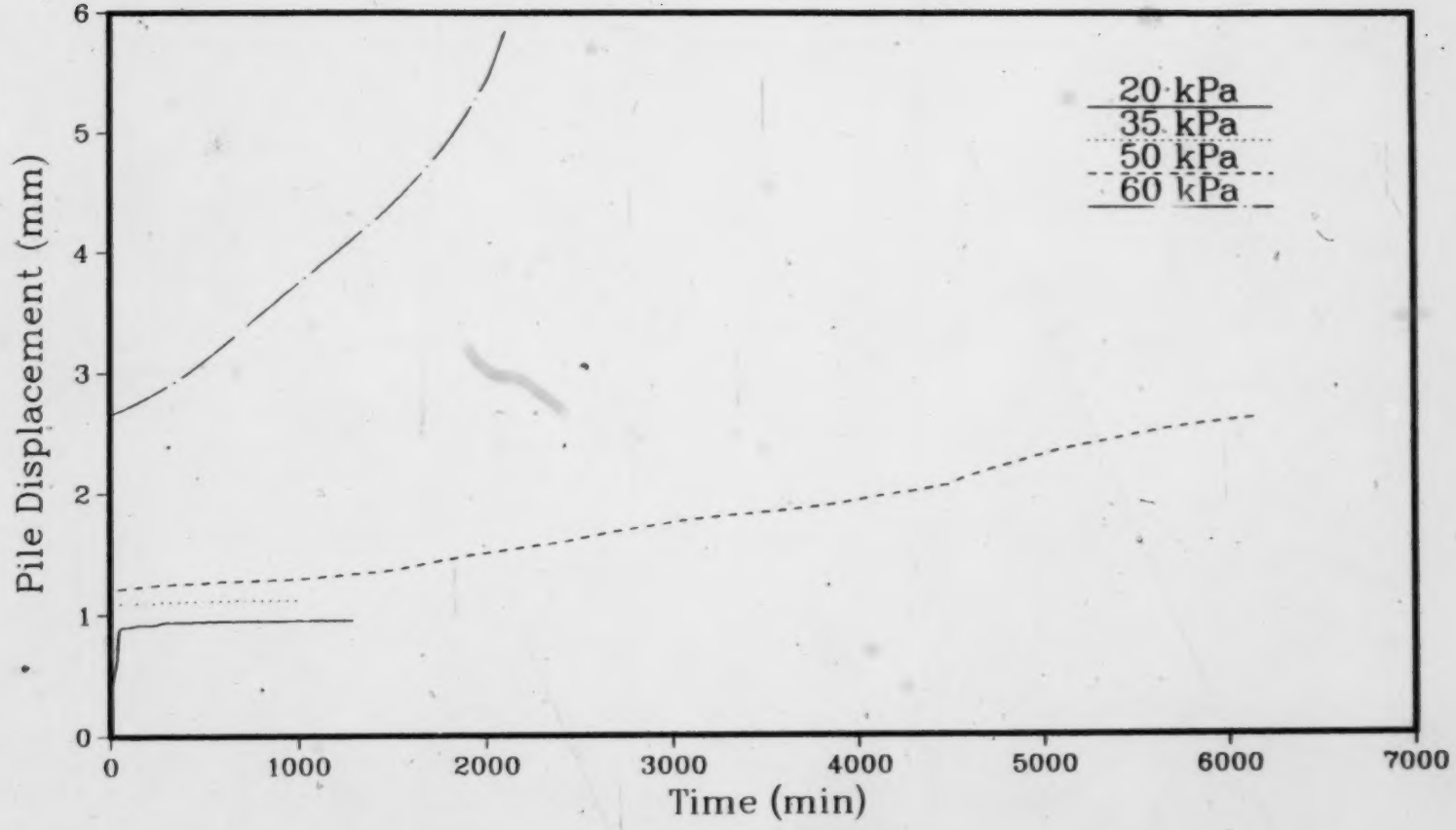

Figure A.38: Pile displacement with time for sample 3.4: silty sand of salinity 10 ppt at −5°C

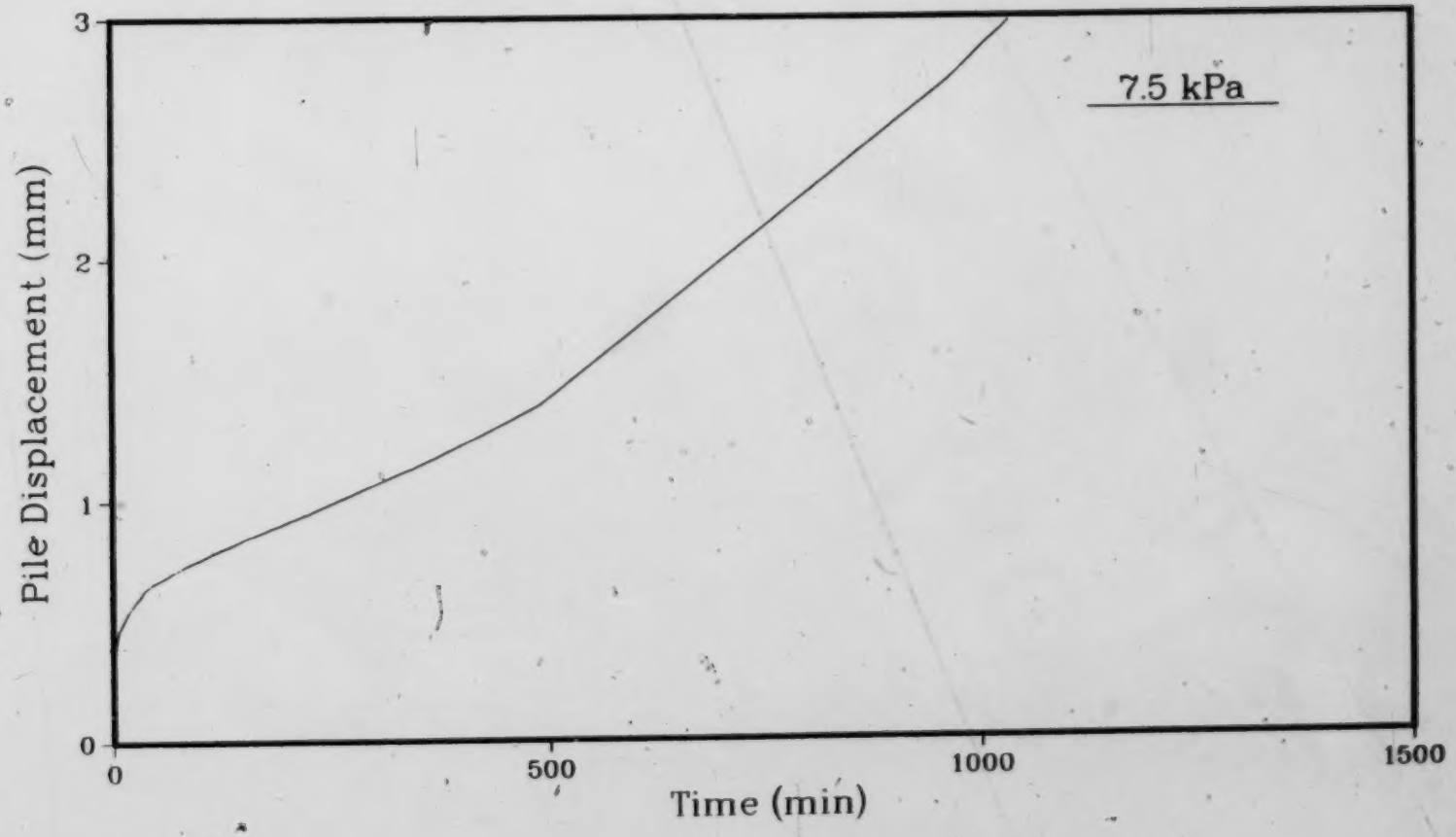

Figure A.39: Pile displacement with time for sample 3.5: silty sand of salinity 15 ppt at −5°C

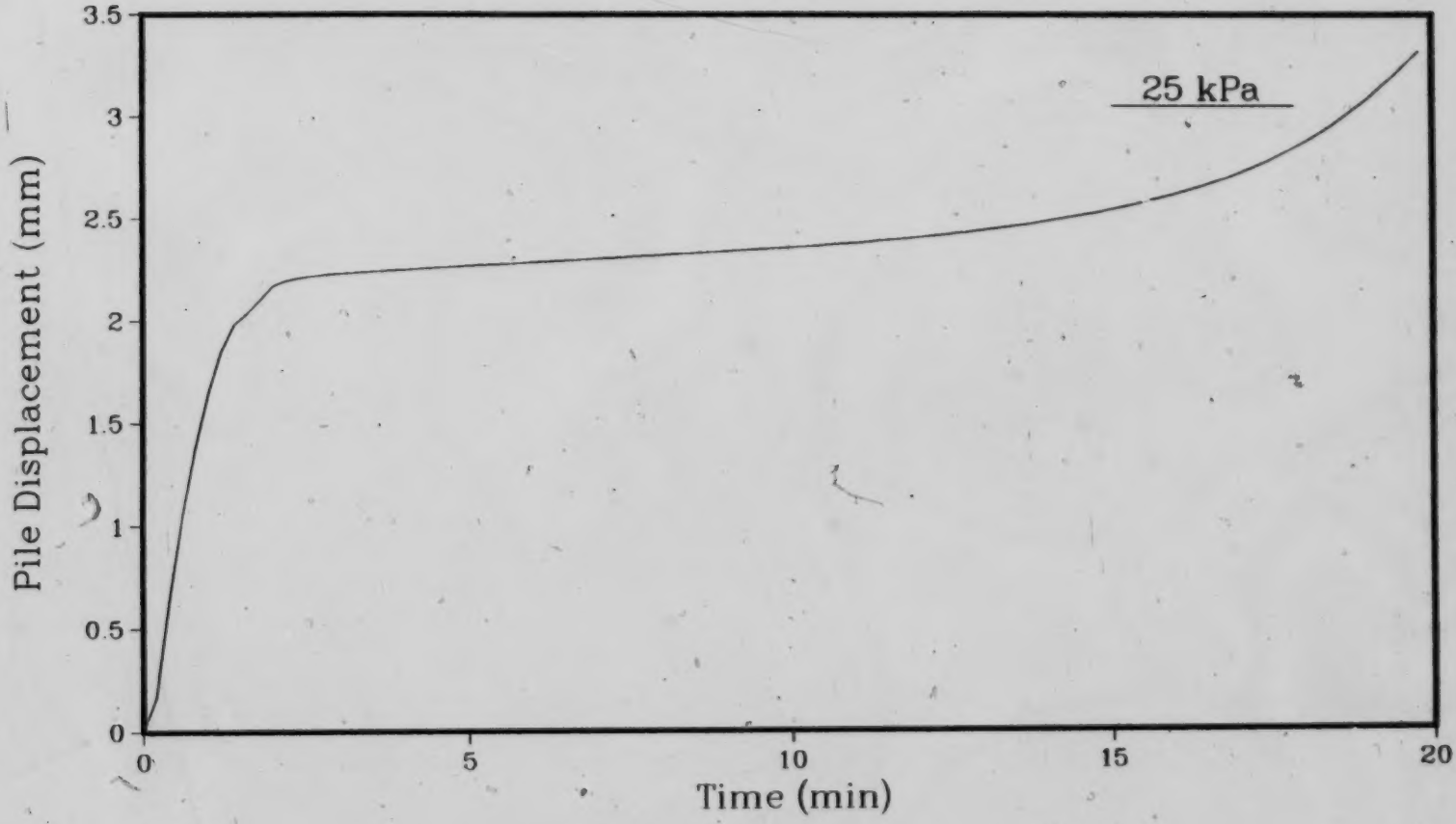

Figure A.40: Pile displacement with time for sample 3.6: silty sand of salinity 15 ppt at −5°C

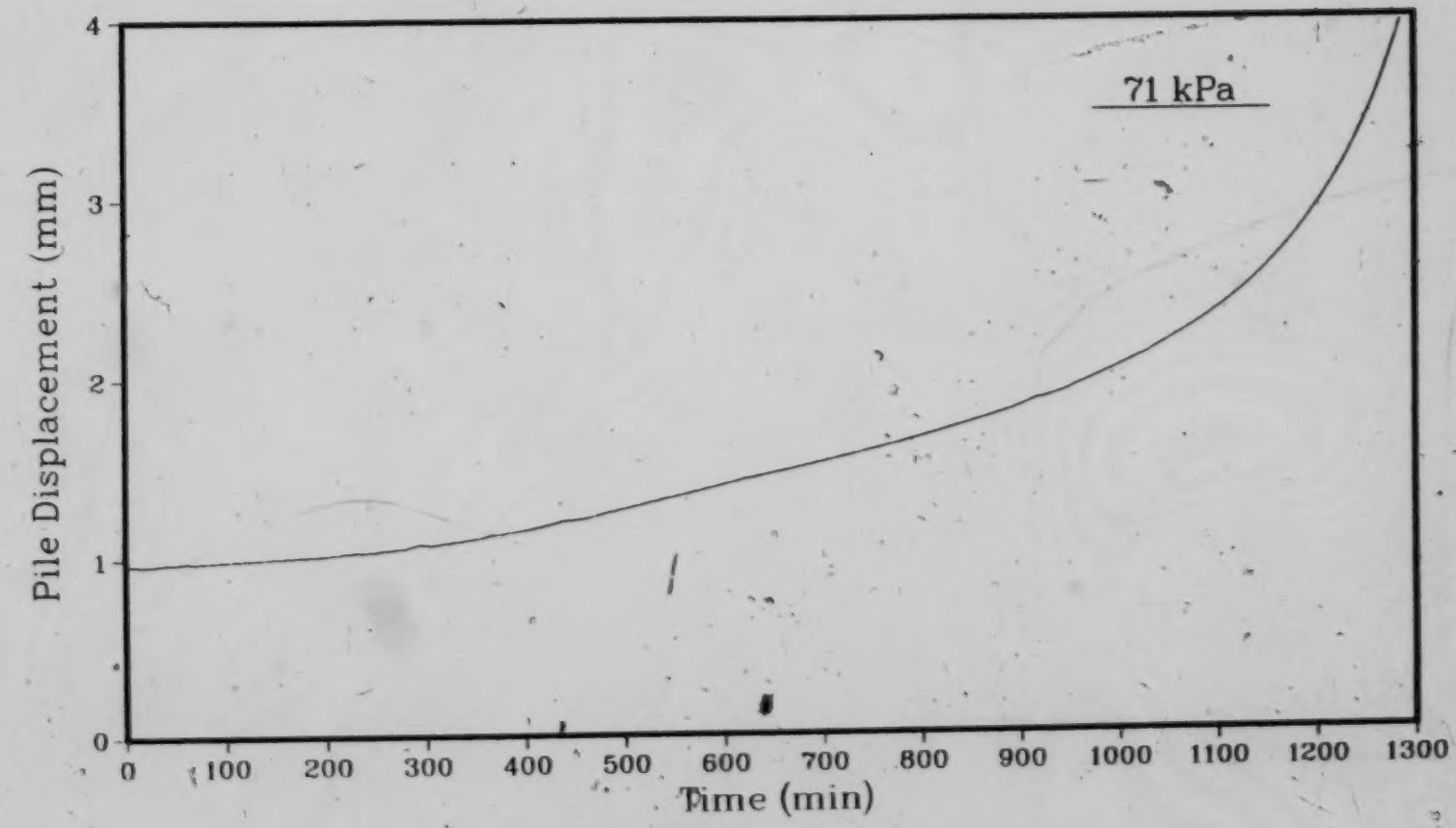

Figure A.41: Pile displacement with time for sample 4.1: silty sand of salinity 5 ppt at −4.7°C

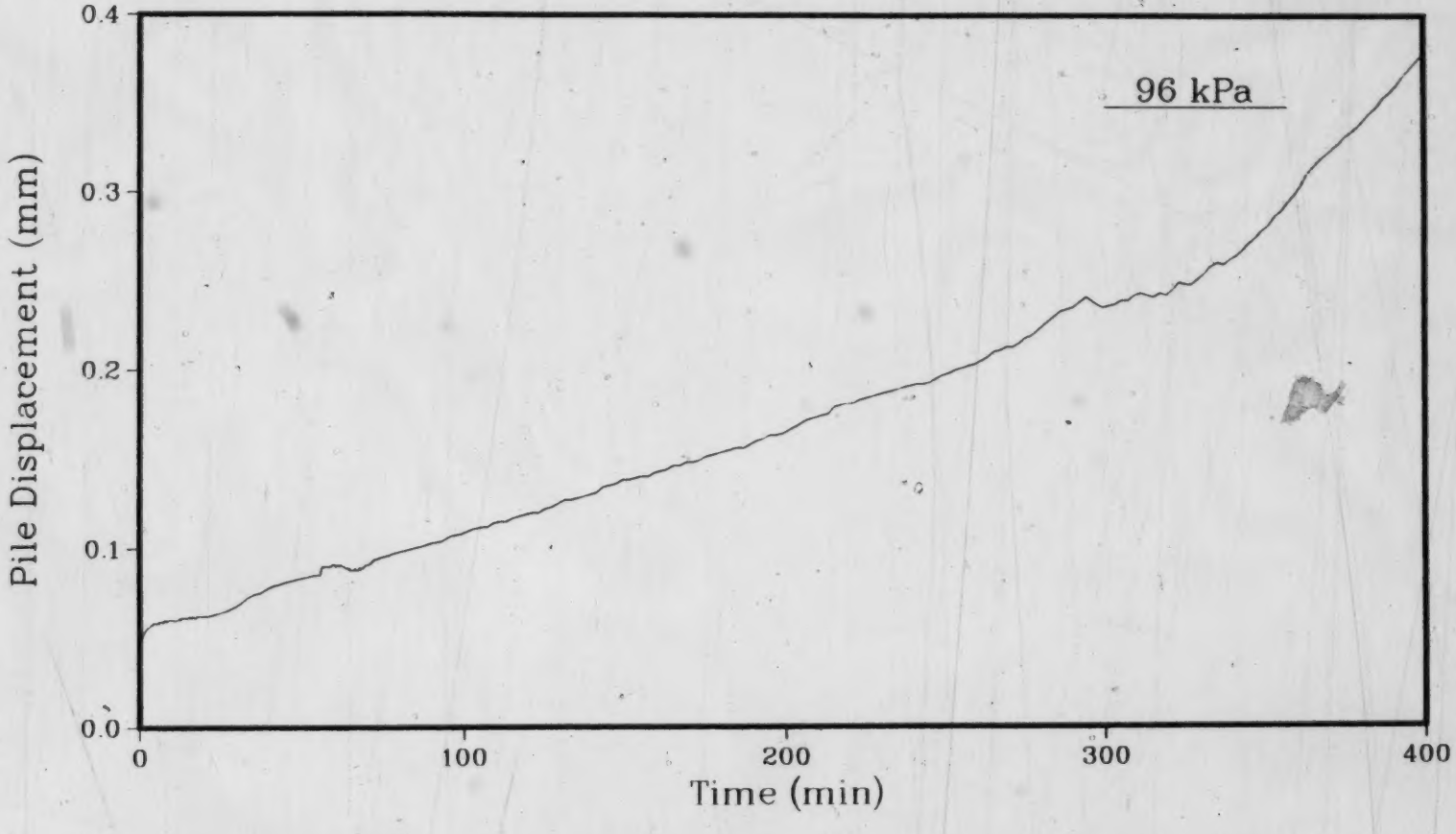

Figure A.42: Pile displacement with time for sample 4.2: silty sand of salinity 5 ppt at −4.8°C

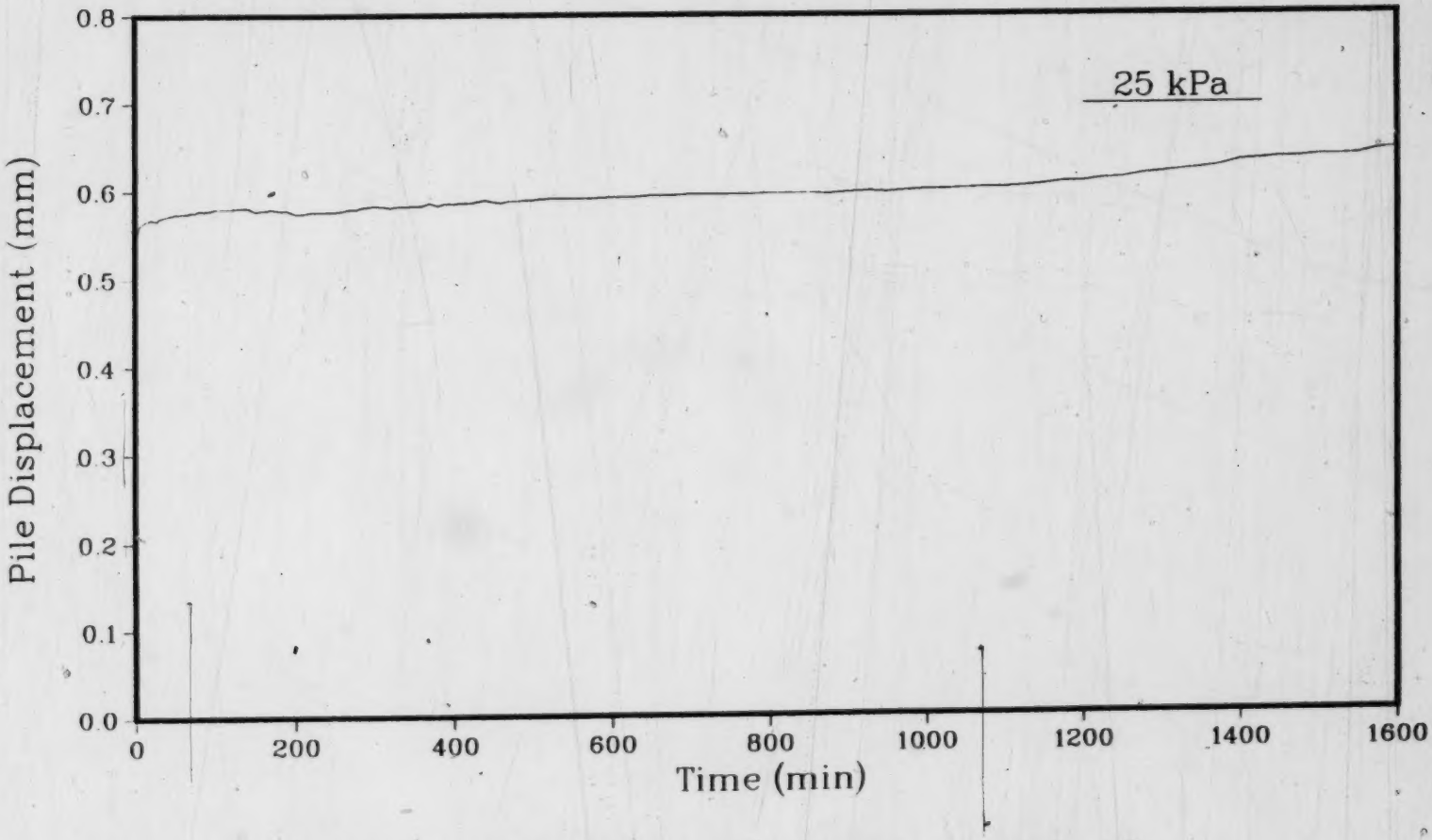

Figure A.43: Pile displacement with time for sample 4.3; silty sand of salinity 10 ppt at −4.7°C

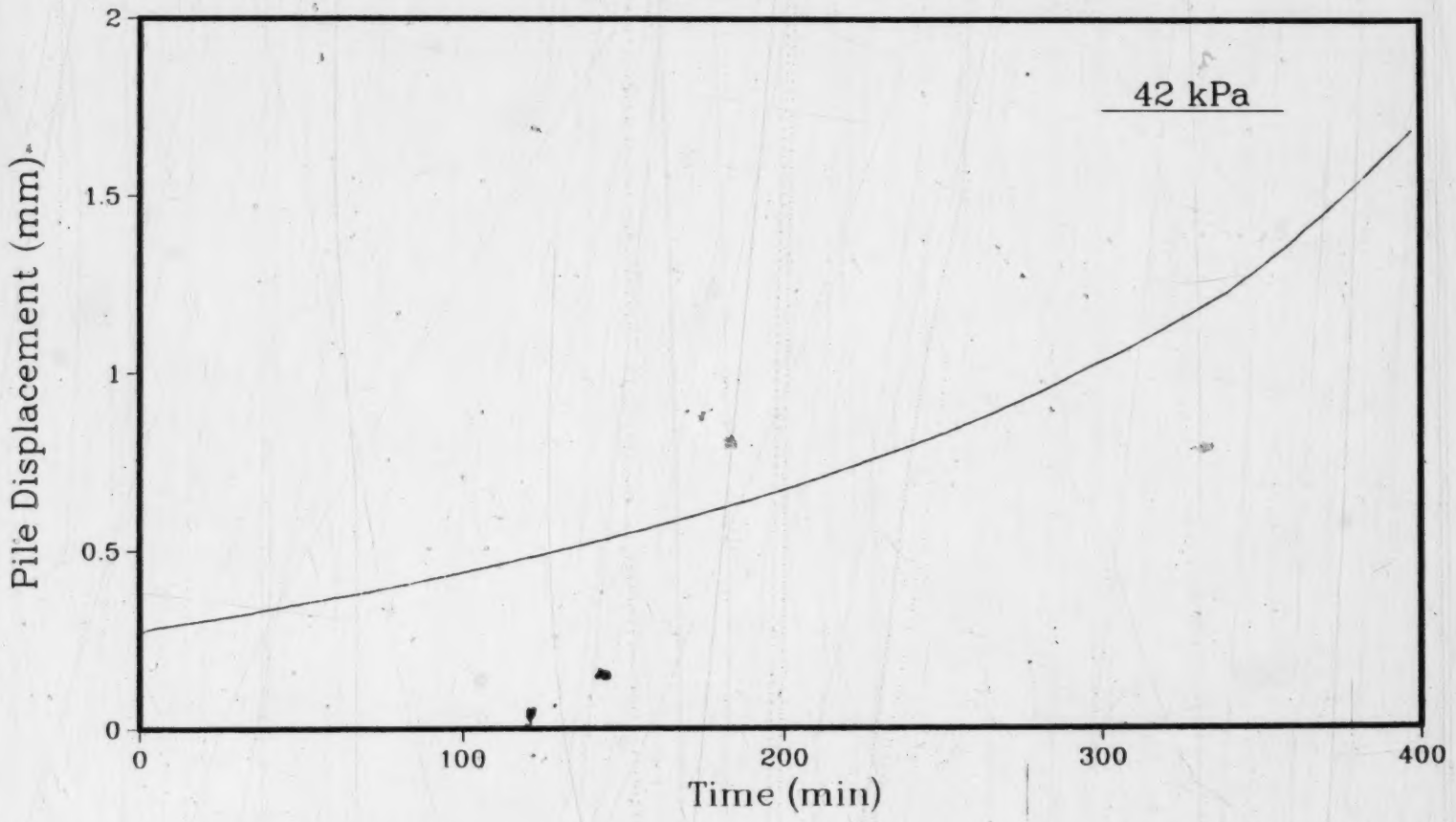

Figure A.44: Pile displacement with time for sample 4.4: silty sand of salinity 10 ppt at −4.6°C

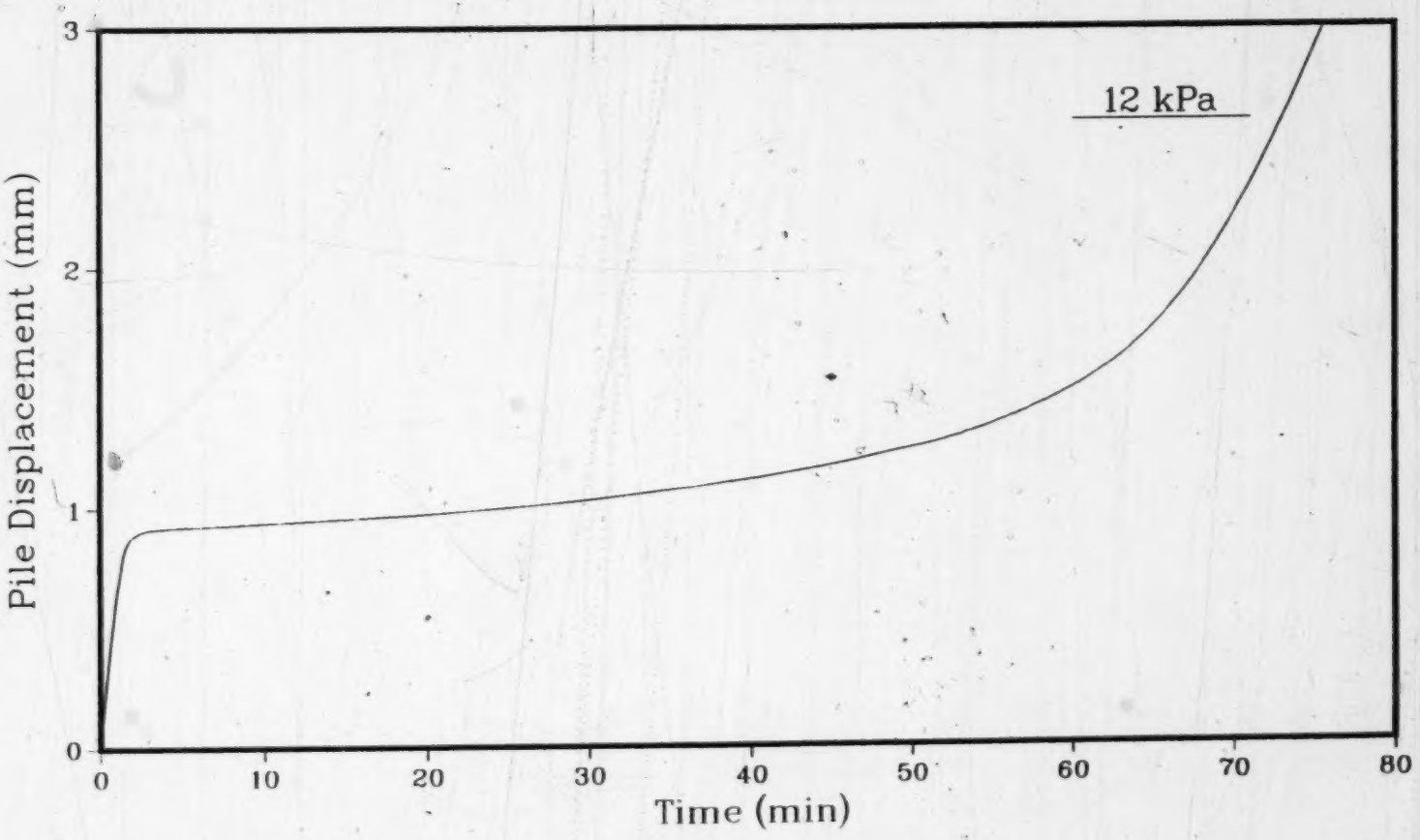

Figure A.45: Pile displacement with time for sample 4.5: silty sand of salinity 15 ppt at −4.5°C

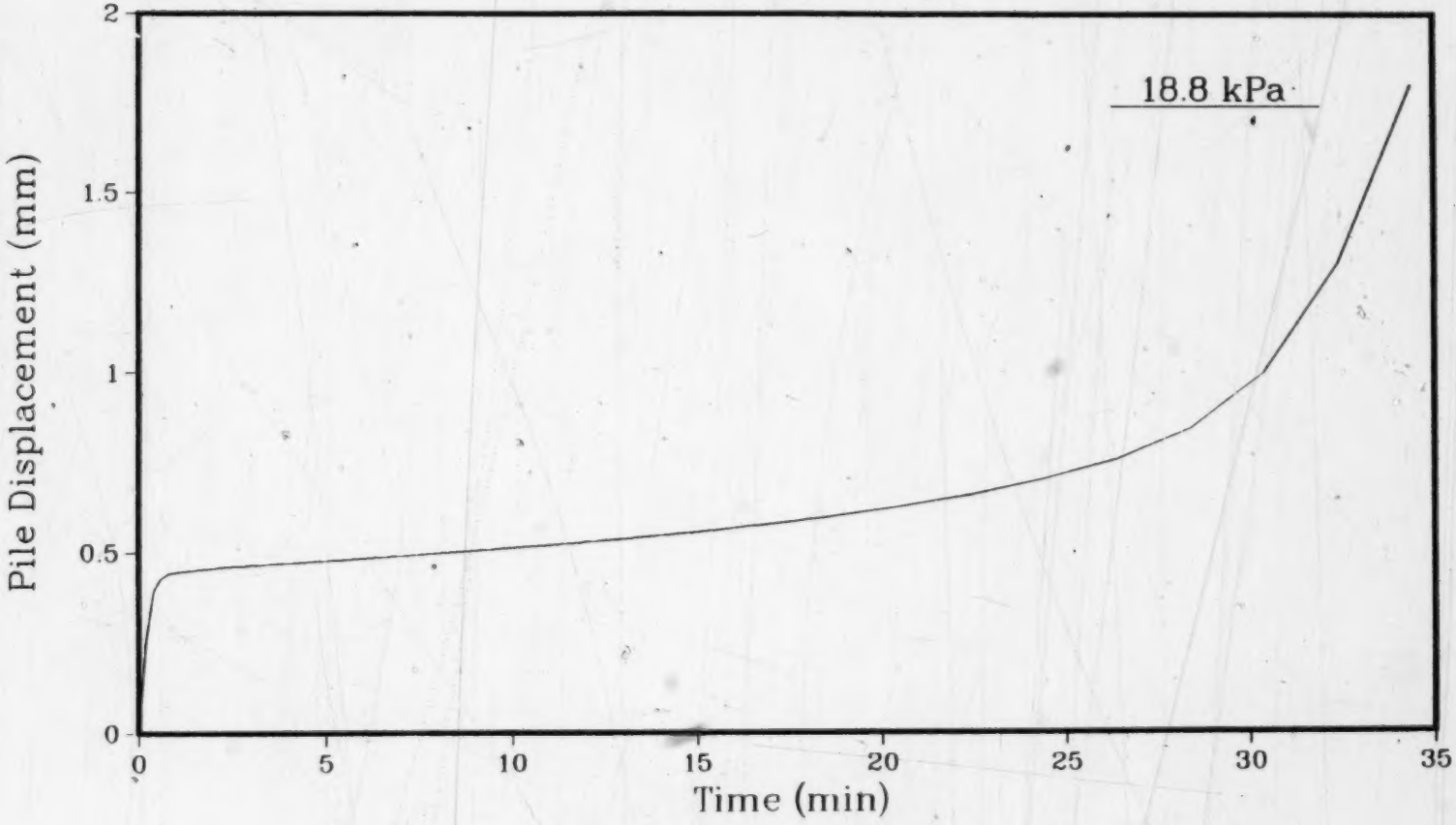

Figure A.46: Pile displacement with time for sample 4.6: silty sand of salinty 15 ppt at −4.6°C

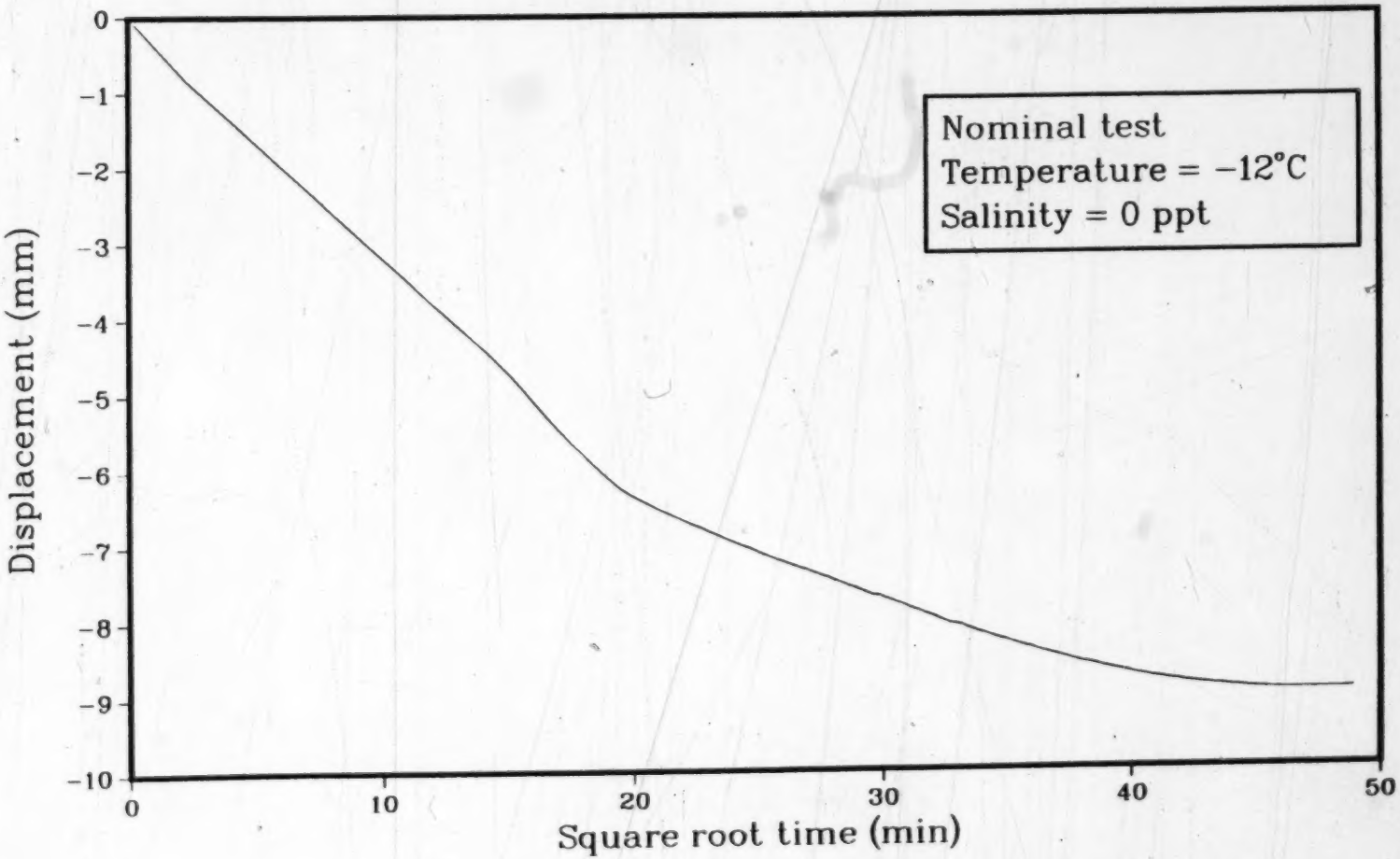

Figure A.47: Consolidation of silty sand sample 1.1

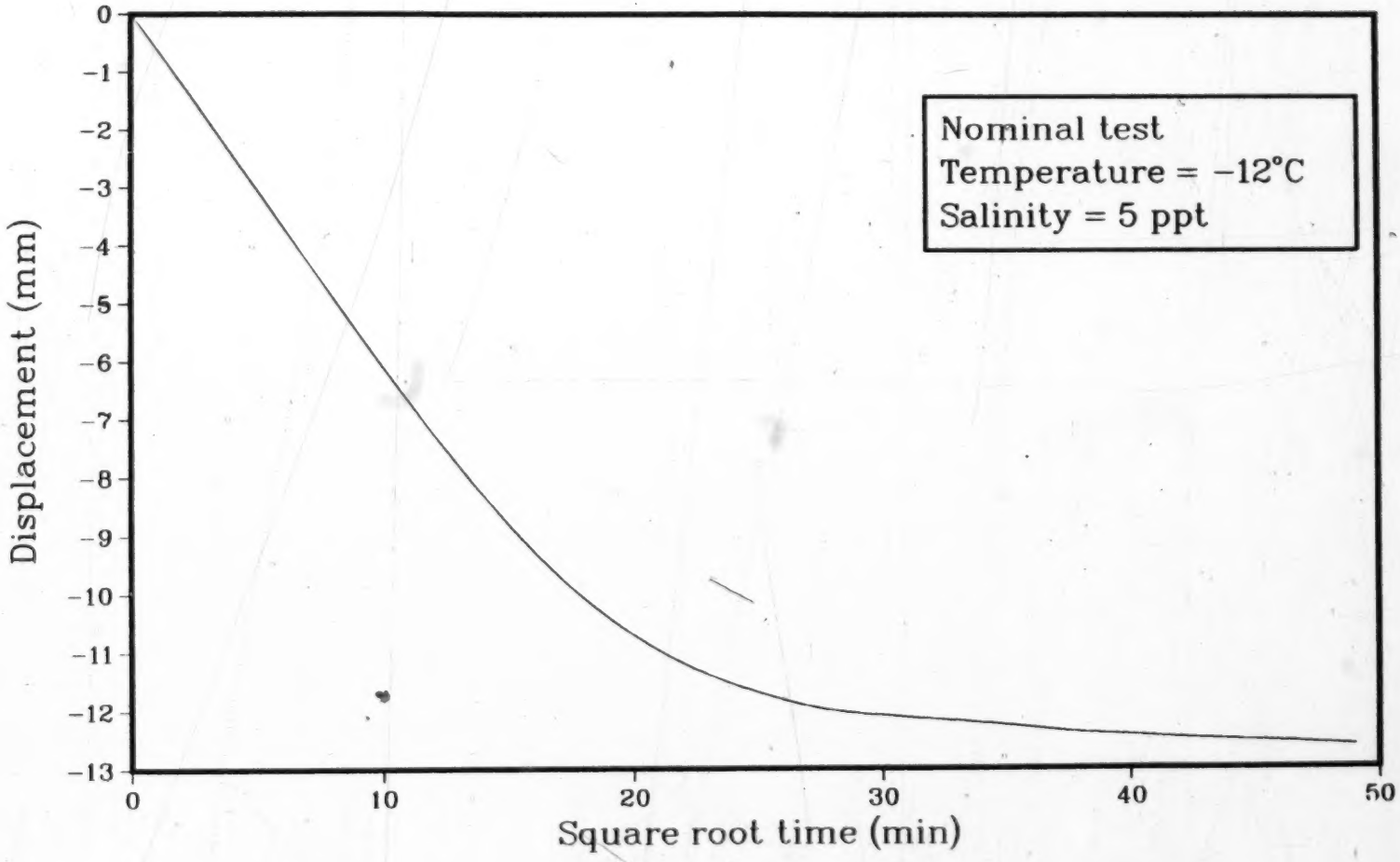

Figure A.48: Consolidation of silty sand sample 1.2

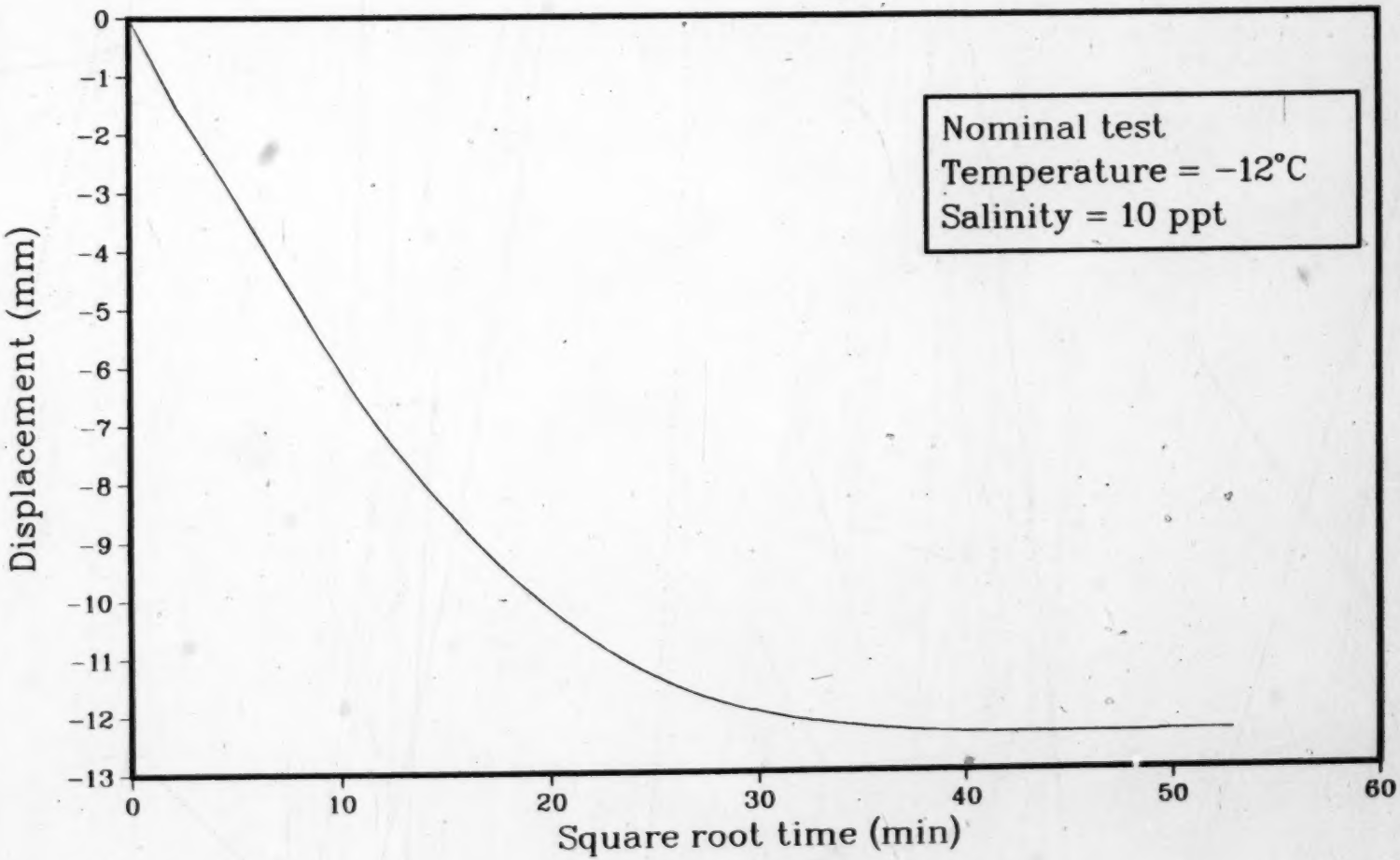

Figure A.49: Consolidation of silty sand sample 1.3

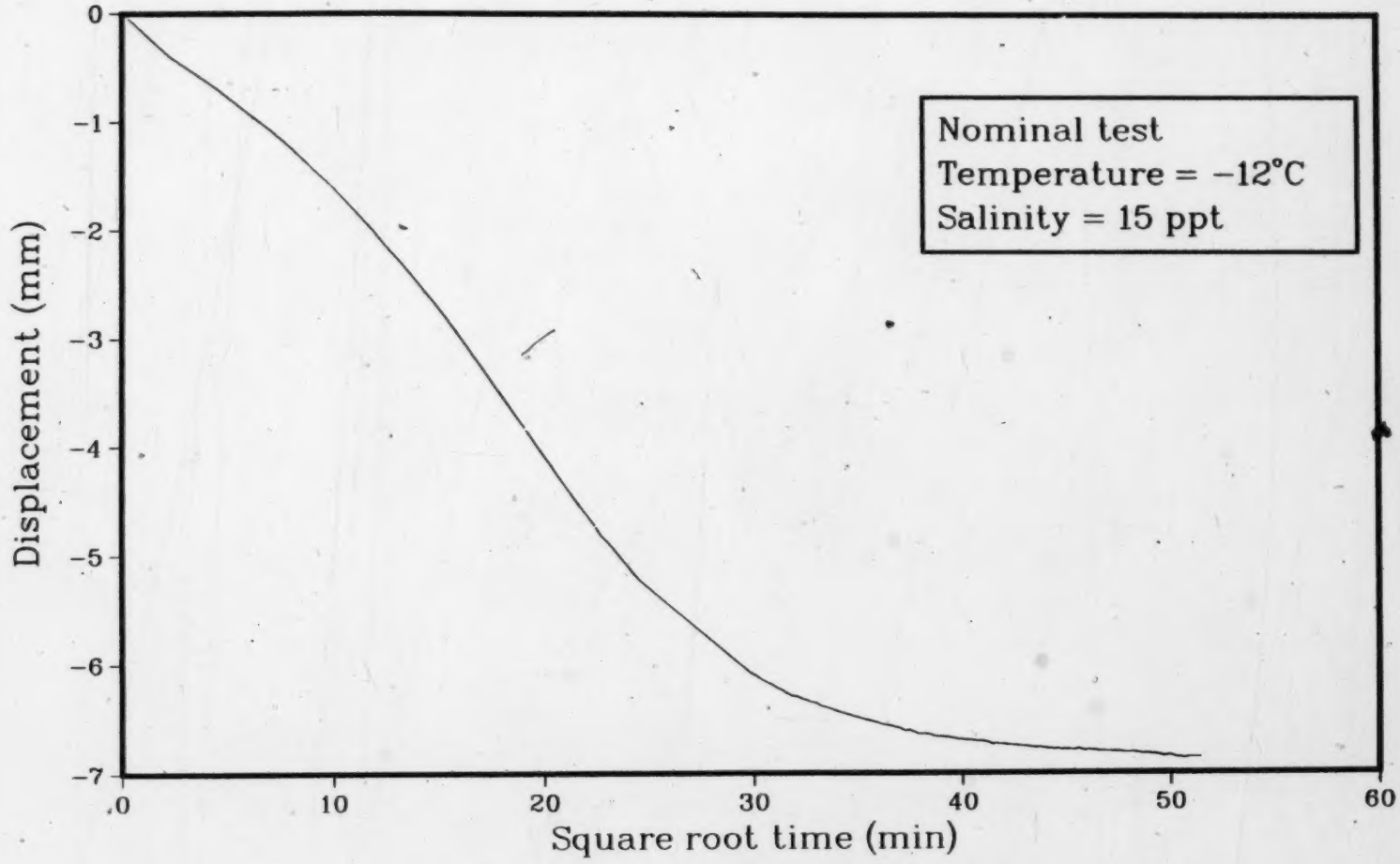

Figure A.50: Consolidation of silty sand sample 1.4

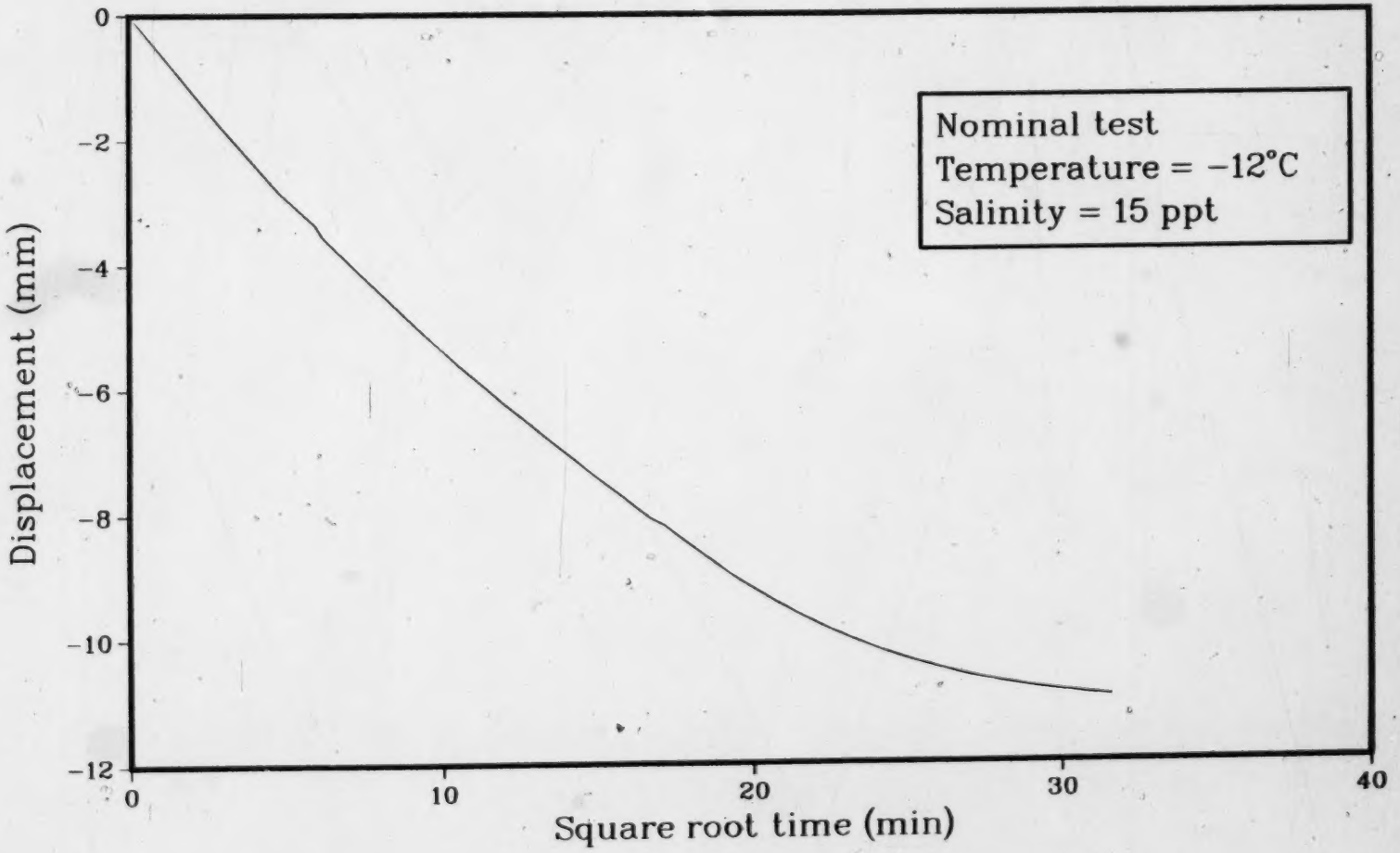

Figure A.51: Consolidation of silty sand sample 1.5

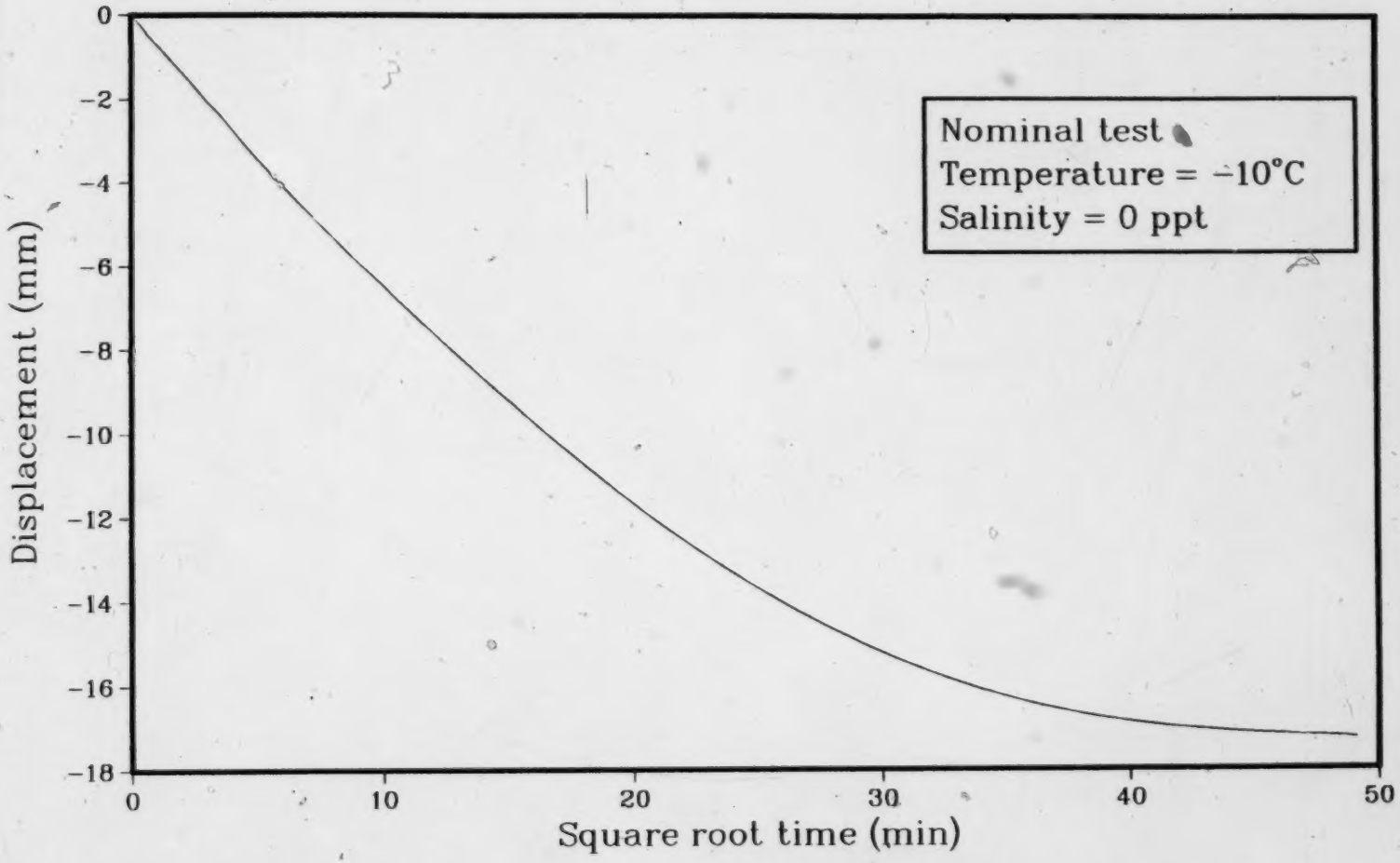

Figure A.52: Consolidation of silty sand sample 2.1

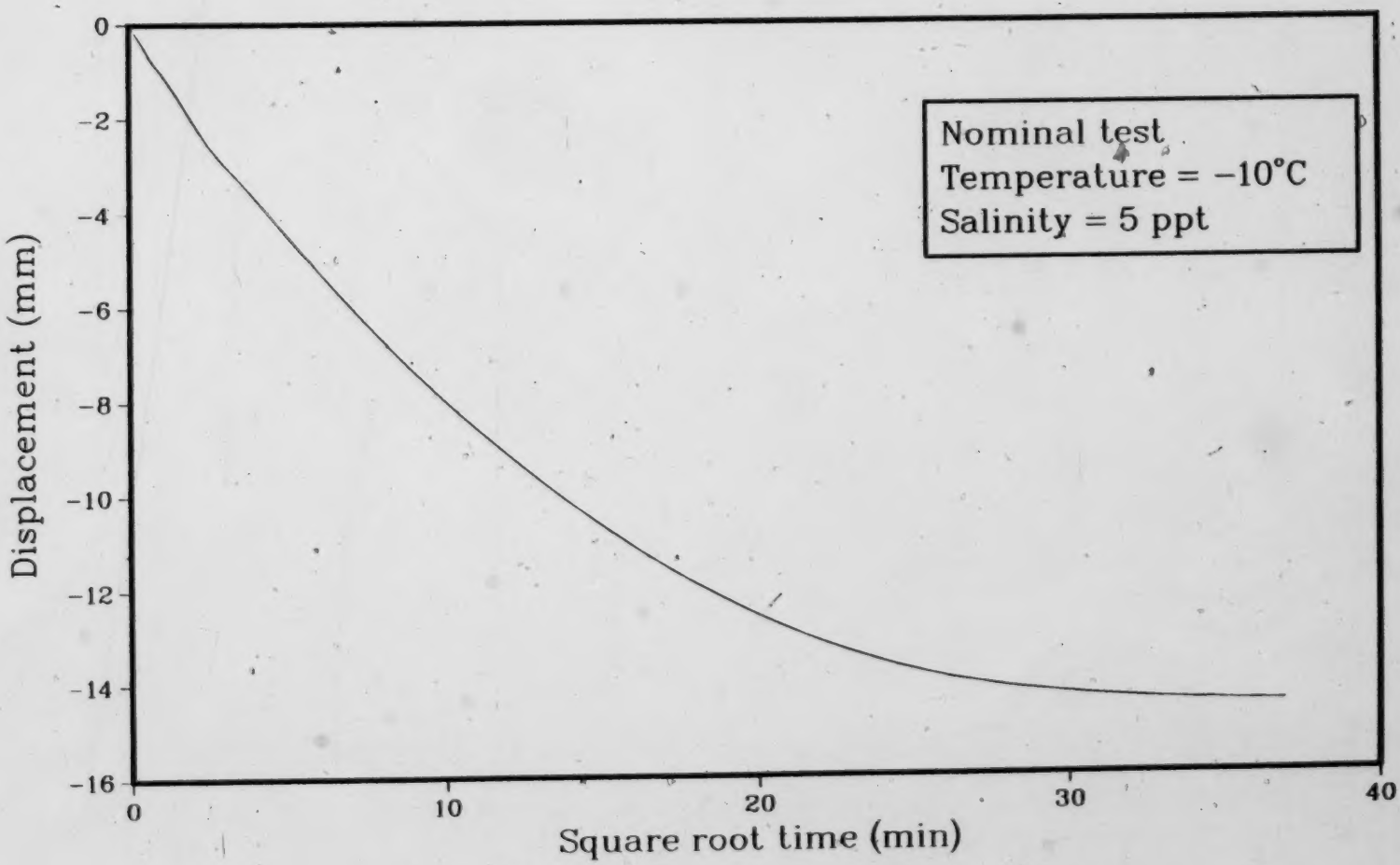

Figure A.53: Consolidation of silty sand sample 2.2

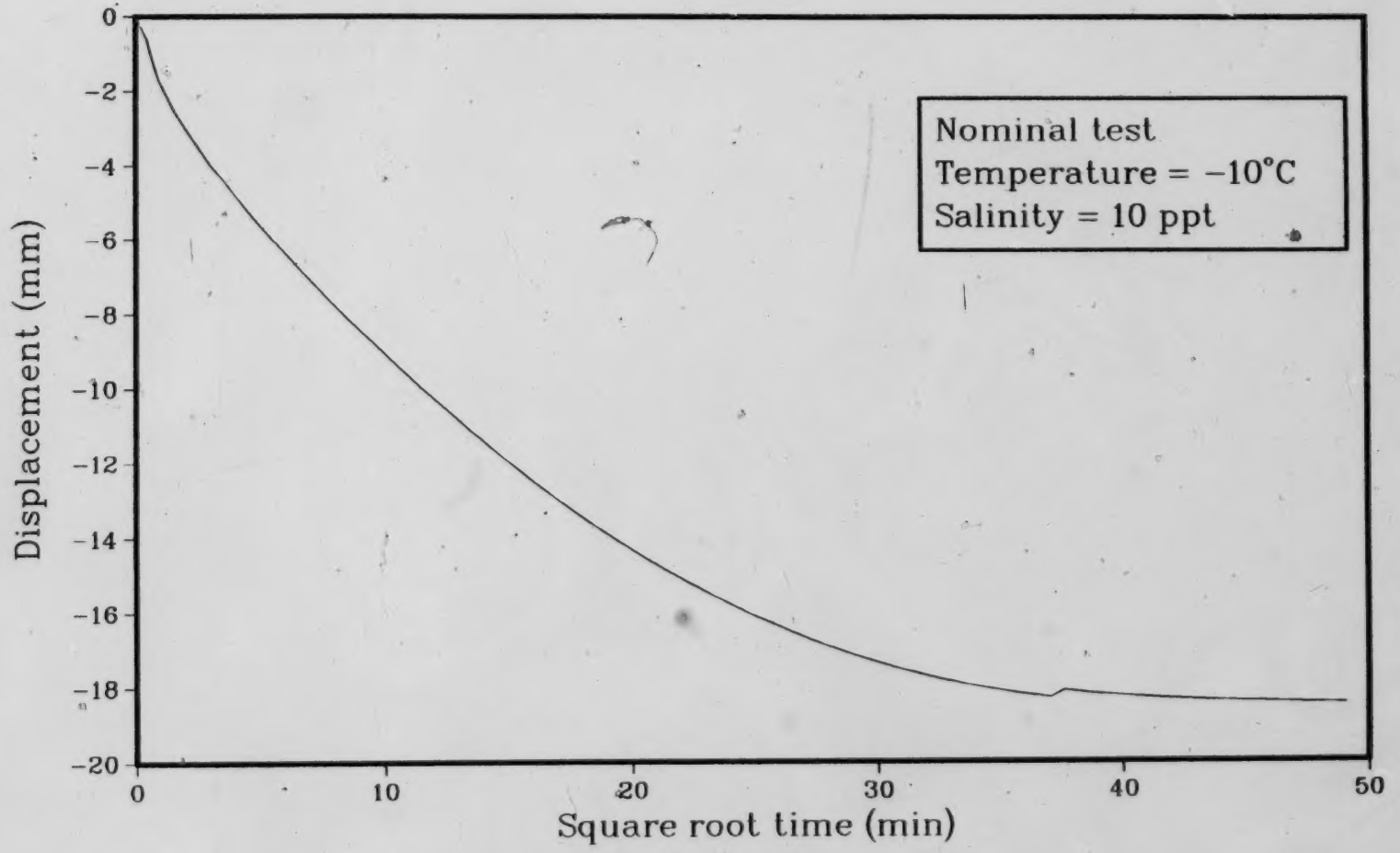

Figure A.54: Consolidation of silty sand sample 2.3

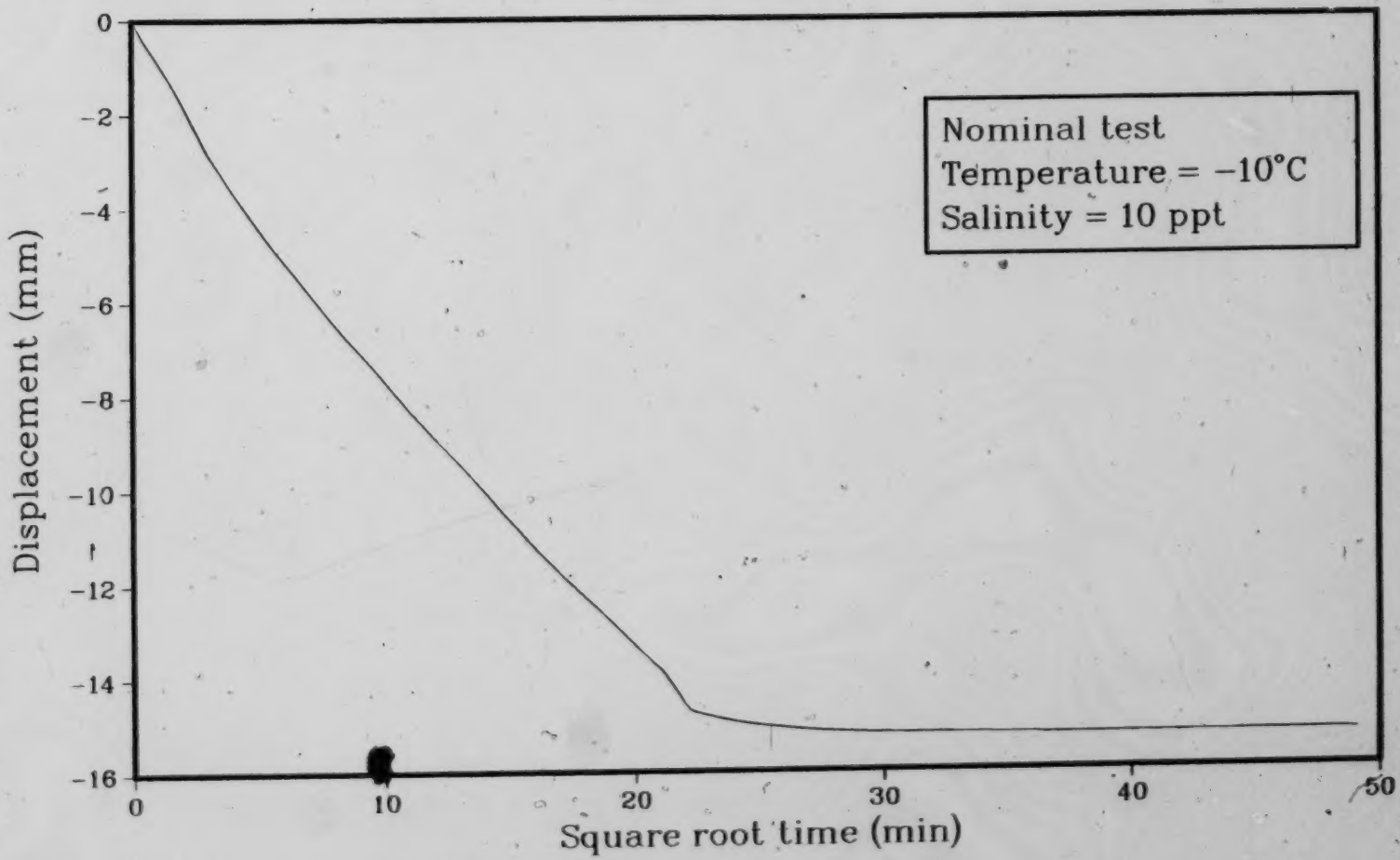

Figure A.55: Consolidation of silty sand sample 2.4

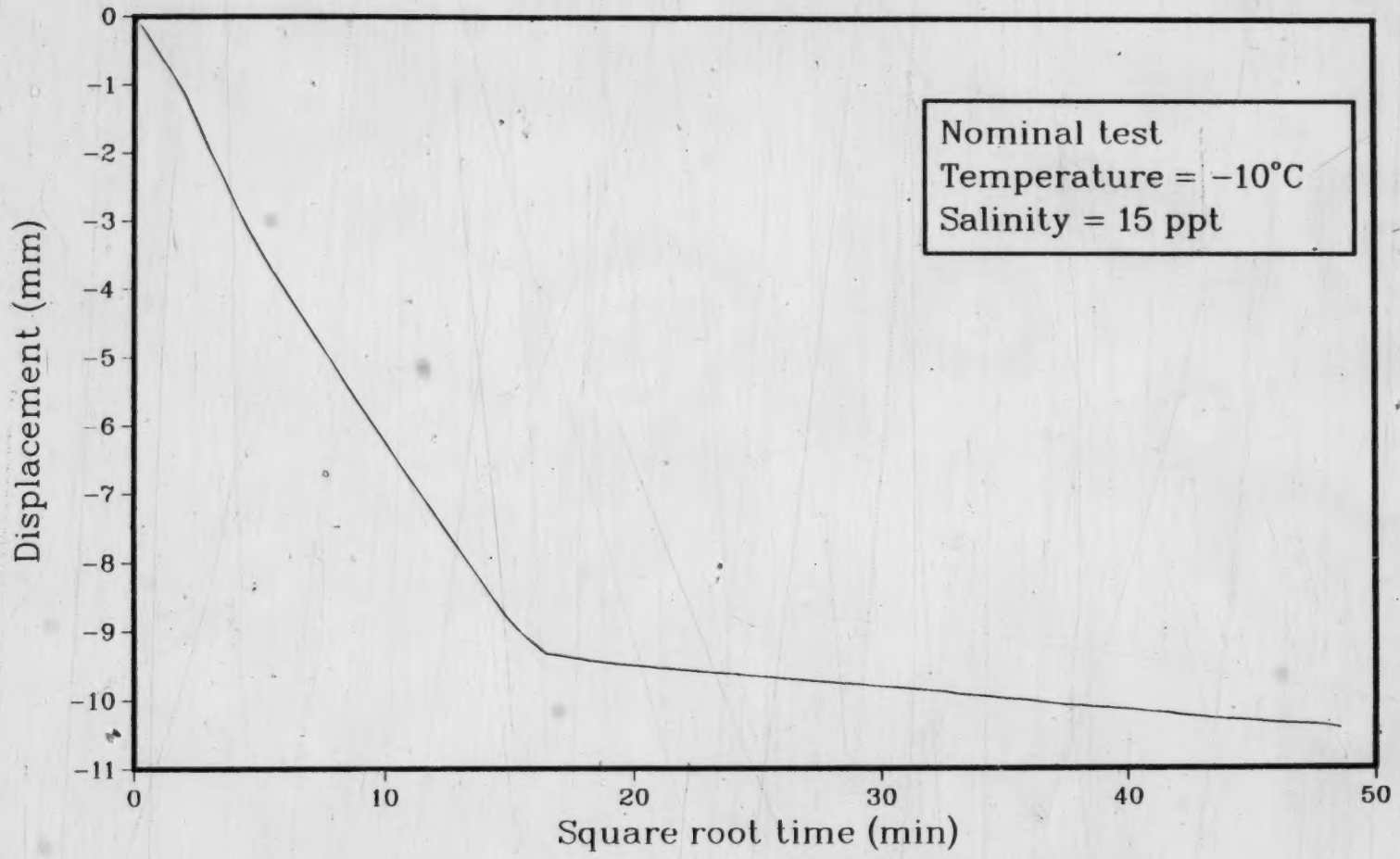

Figure A.56: Consolidation of silty sand sample 2.5

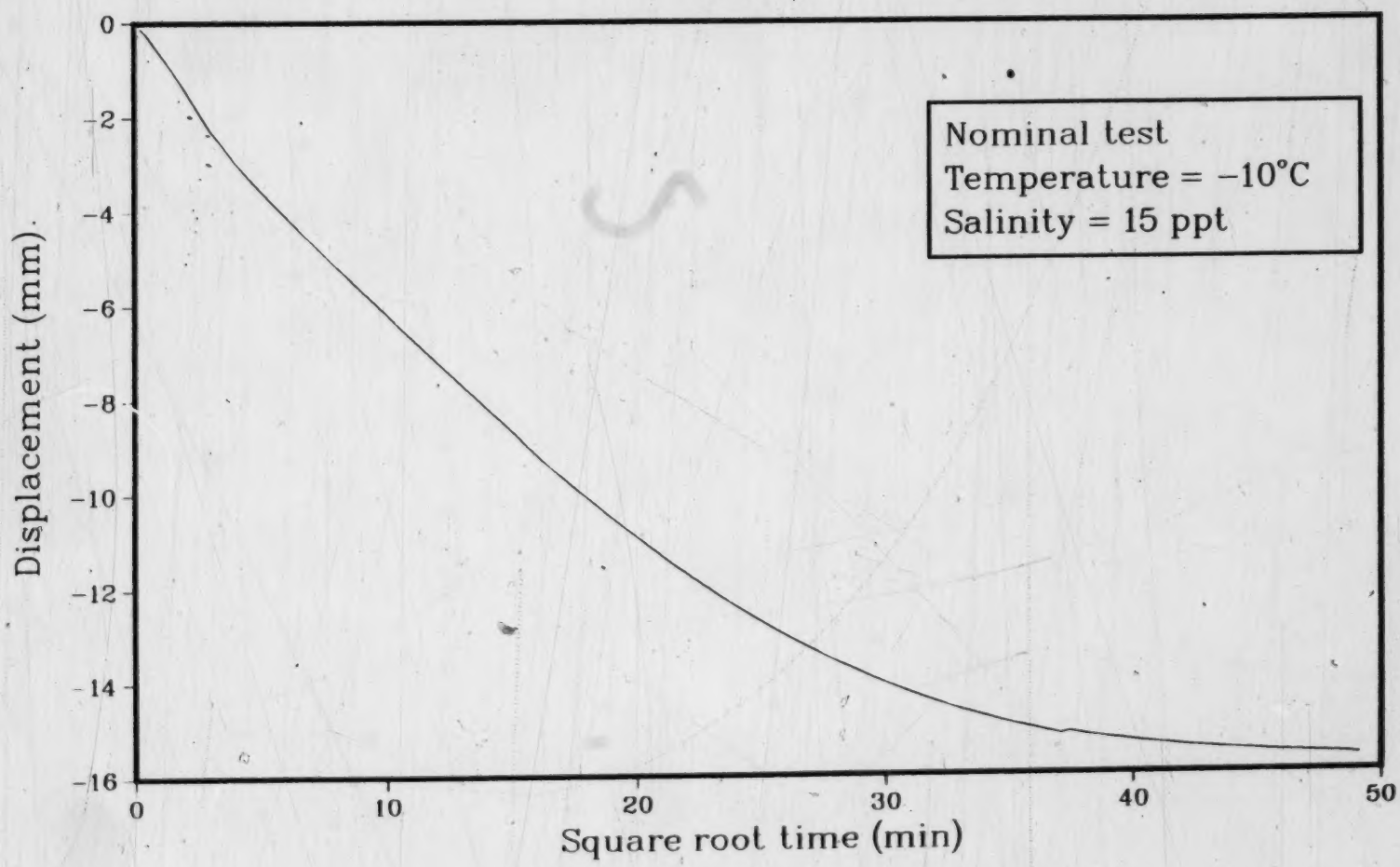

Figure A.57: Consolidation of silty sand sample 2.6

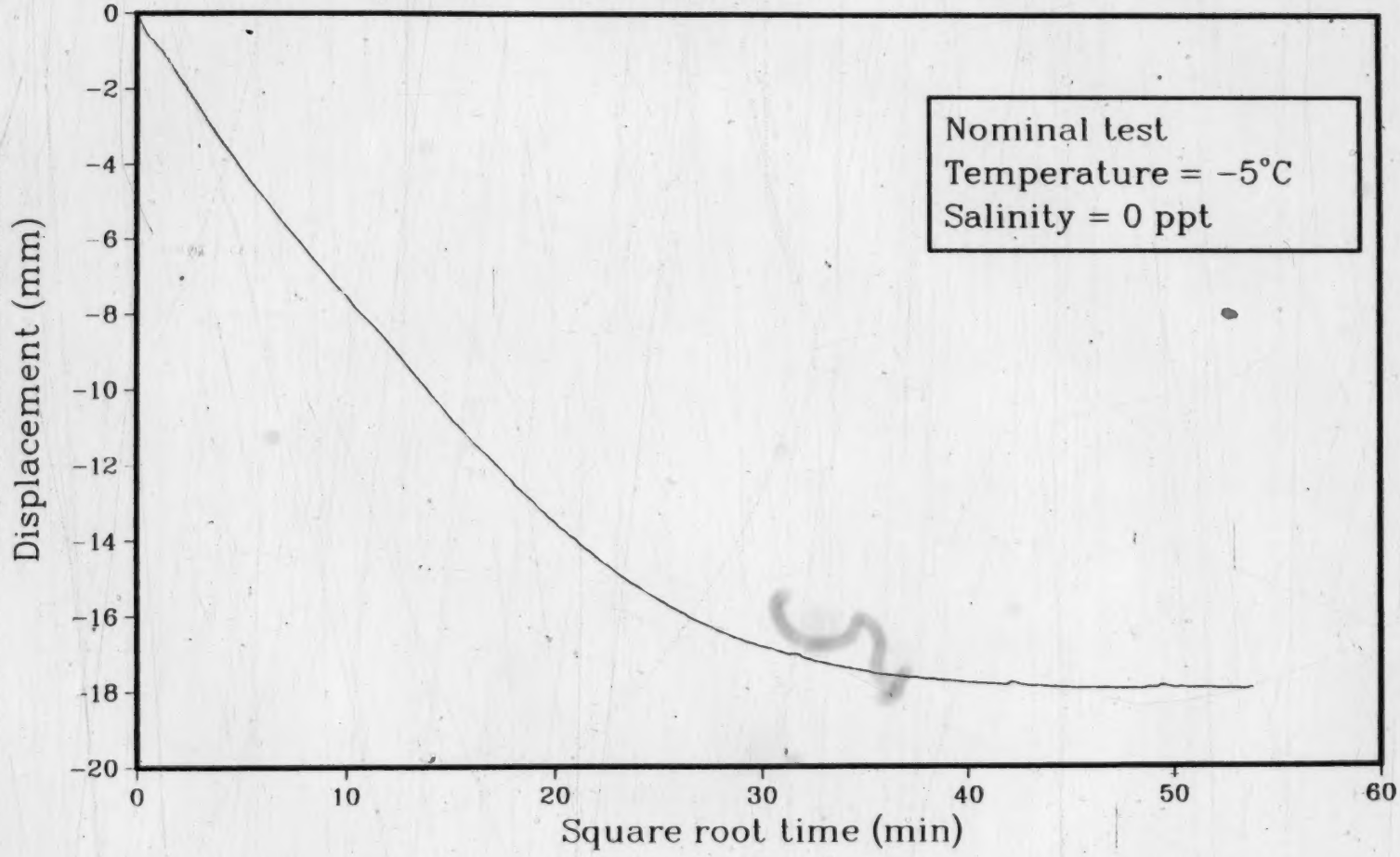

Figure A.58: Consolidation of silty sand sample 3.1

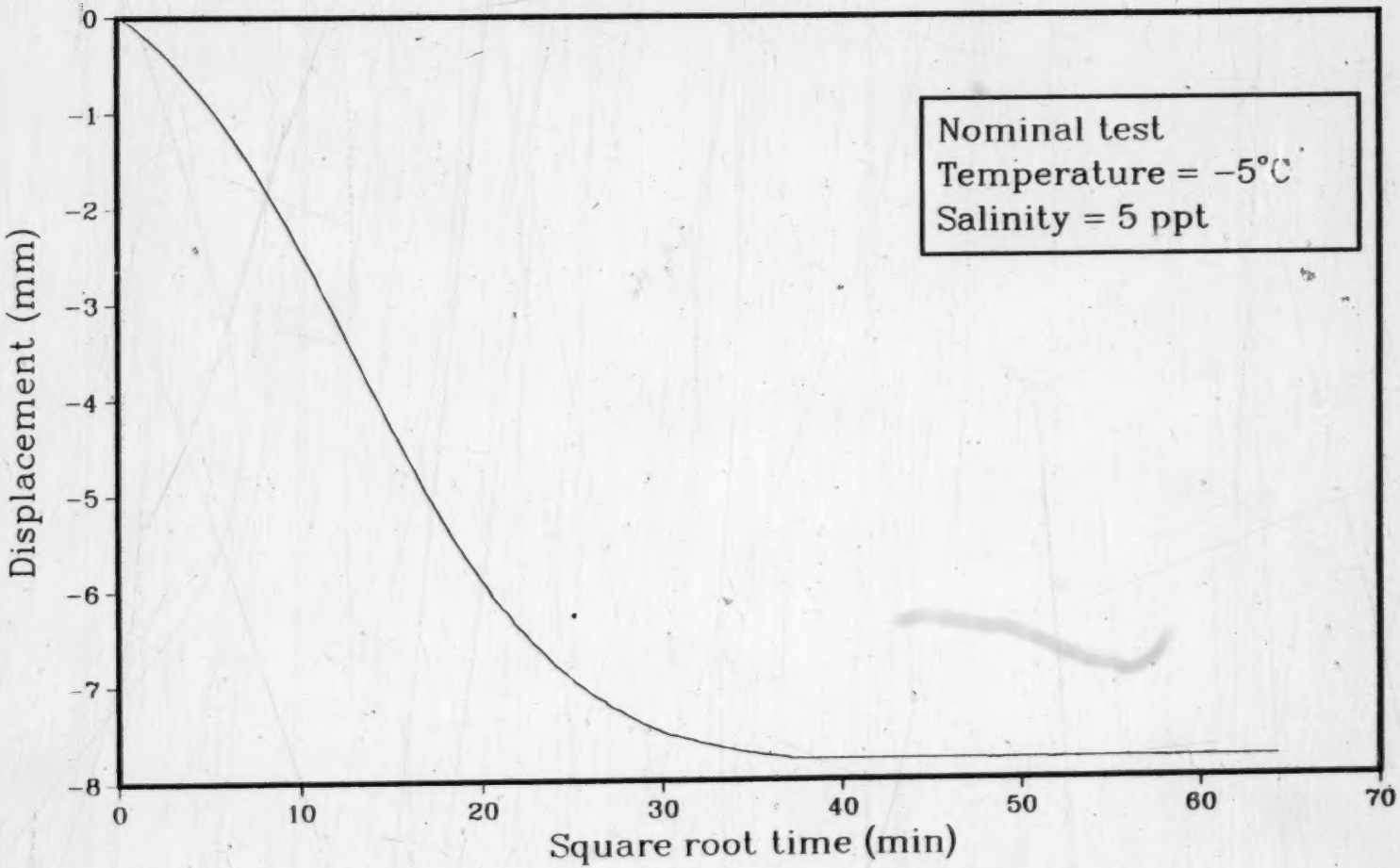

Figure A.59: Consolidation of silty sand sample 3.2

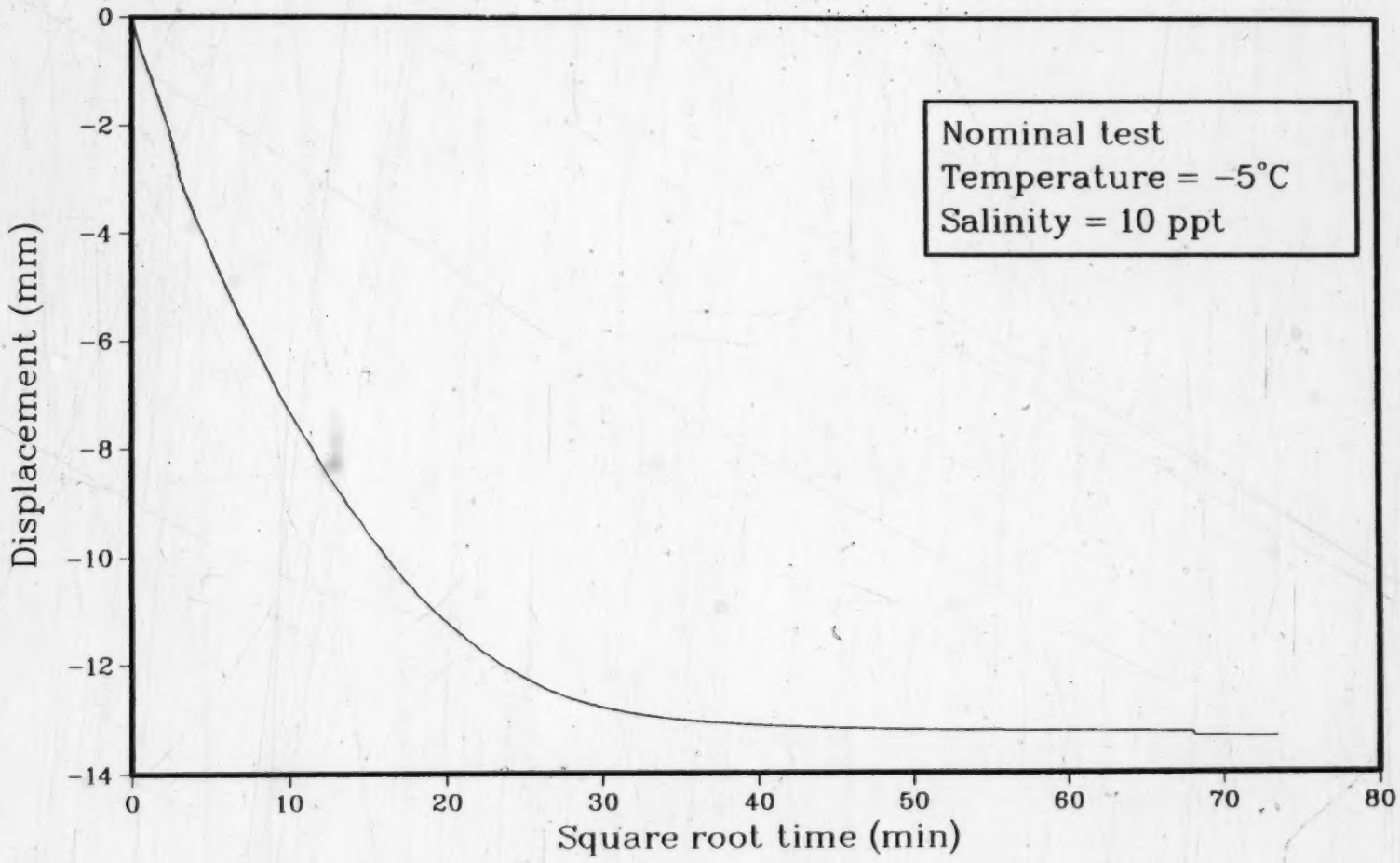

Figure A.60: Consolidation of silty sand sample 3.3

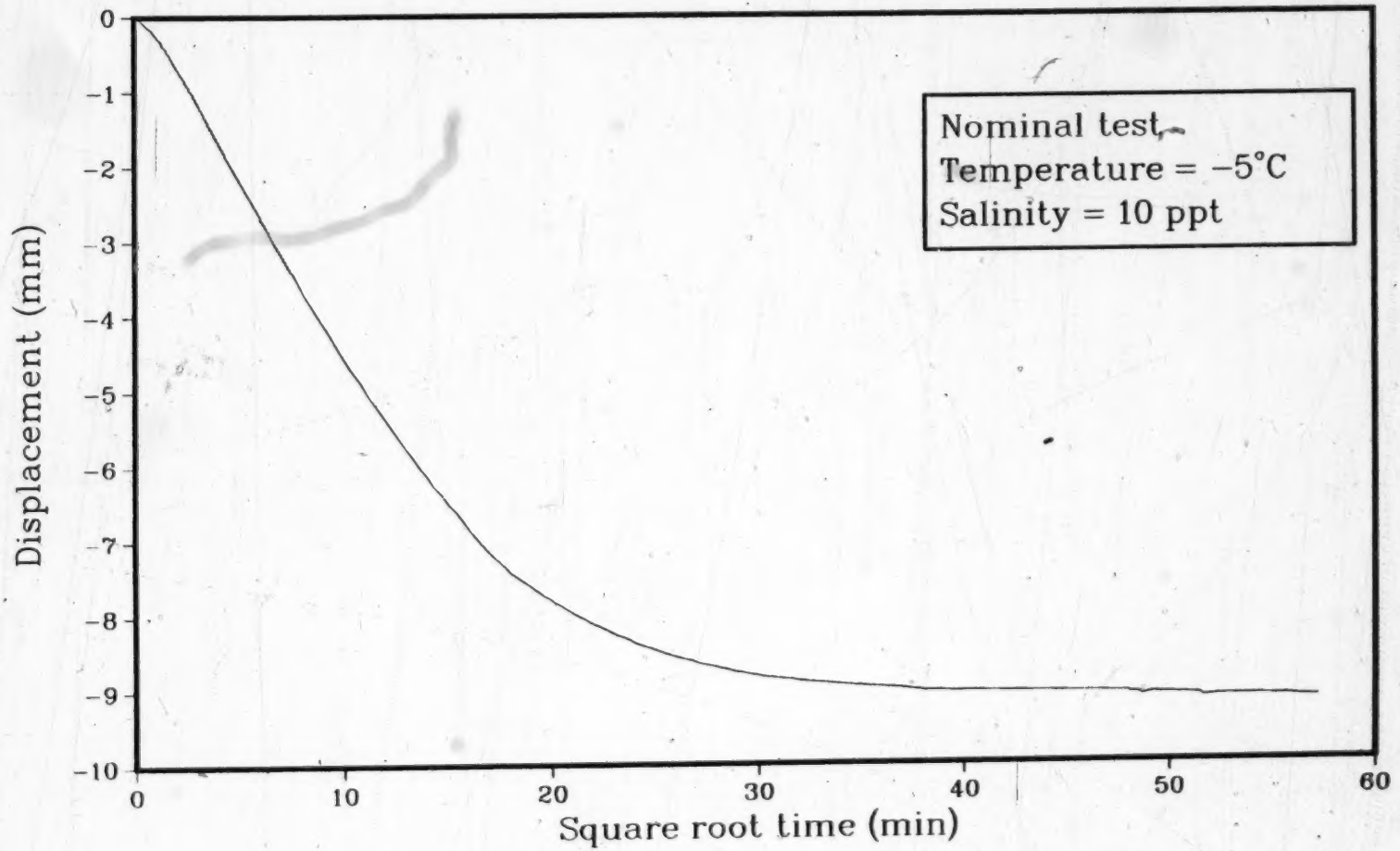

Figure A.61: Consolidation of silty sand sample 3.4

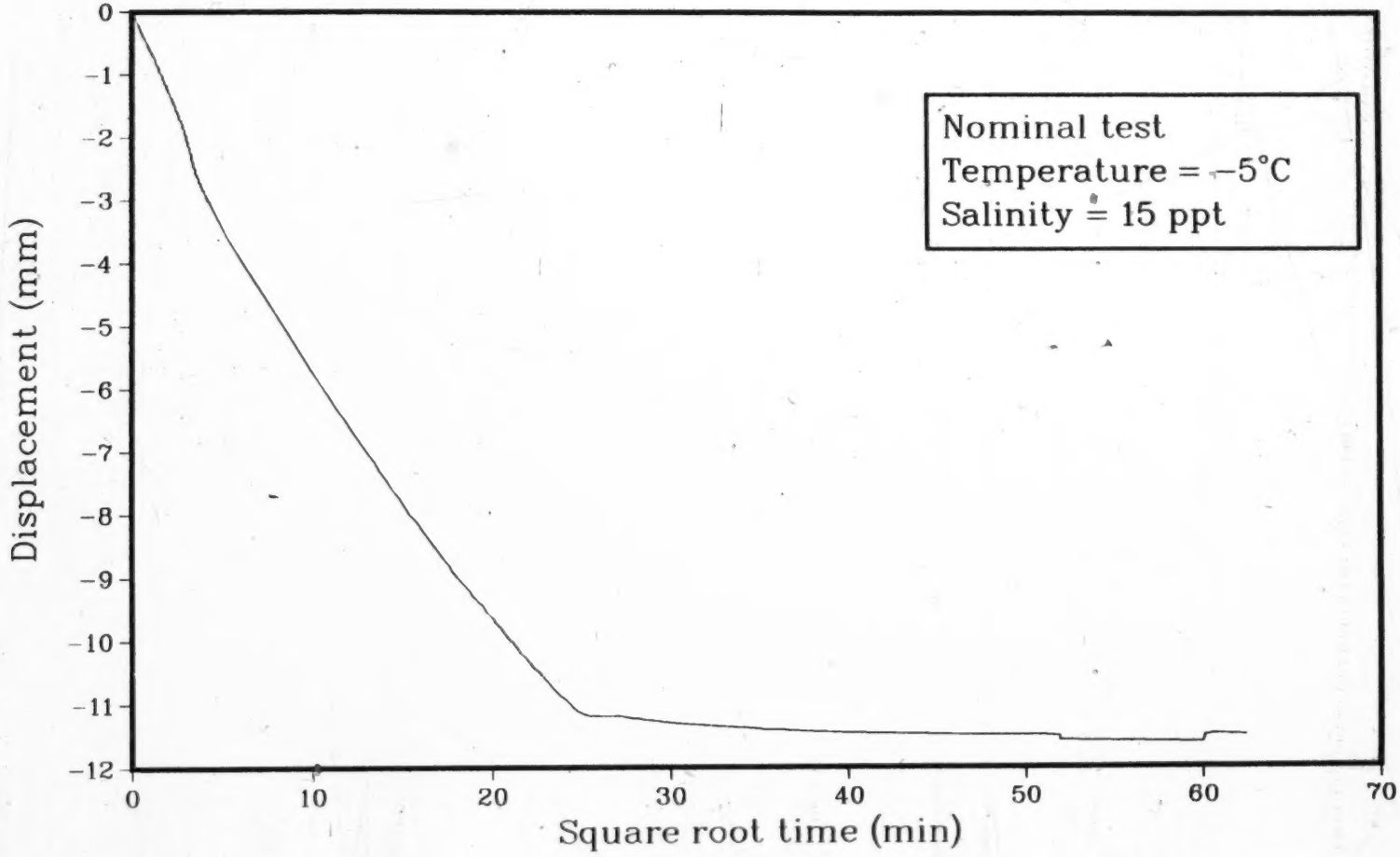

Figure A.62: Consolidation of silty sand sample 3.5

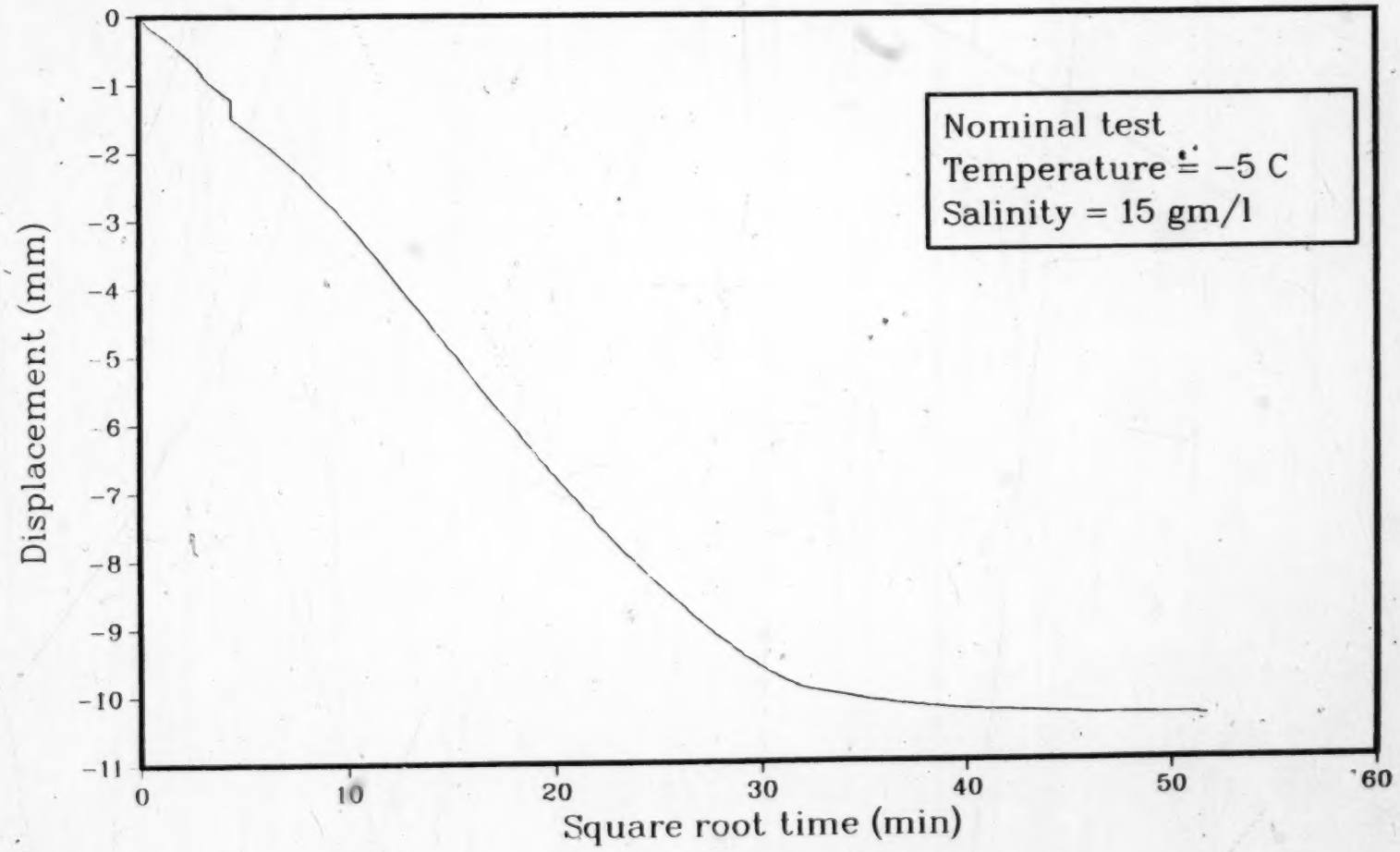

Figure A.63: Consolidation of silty sand sample 3.6

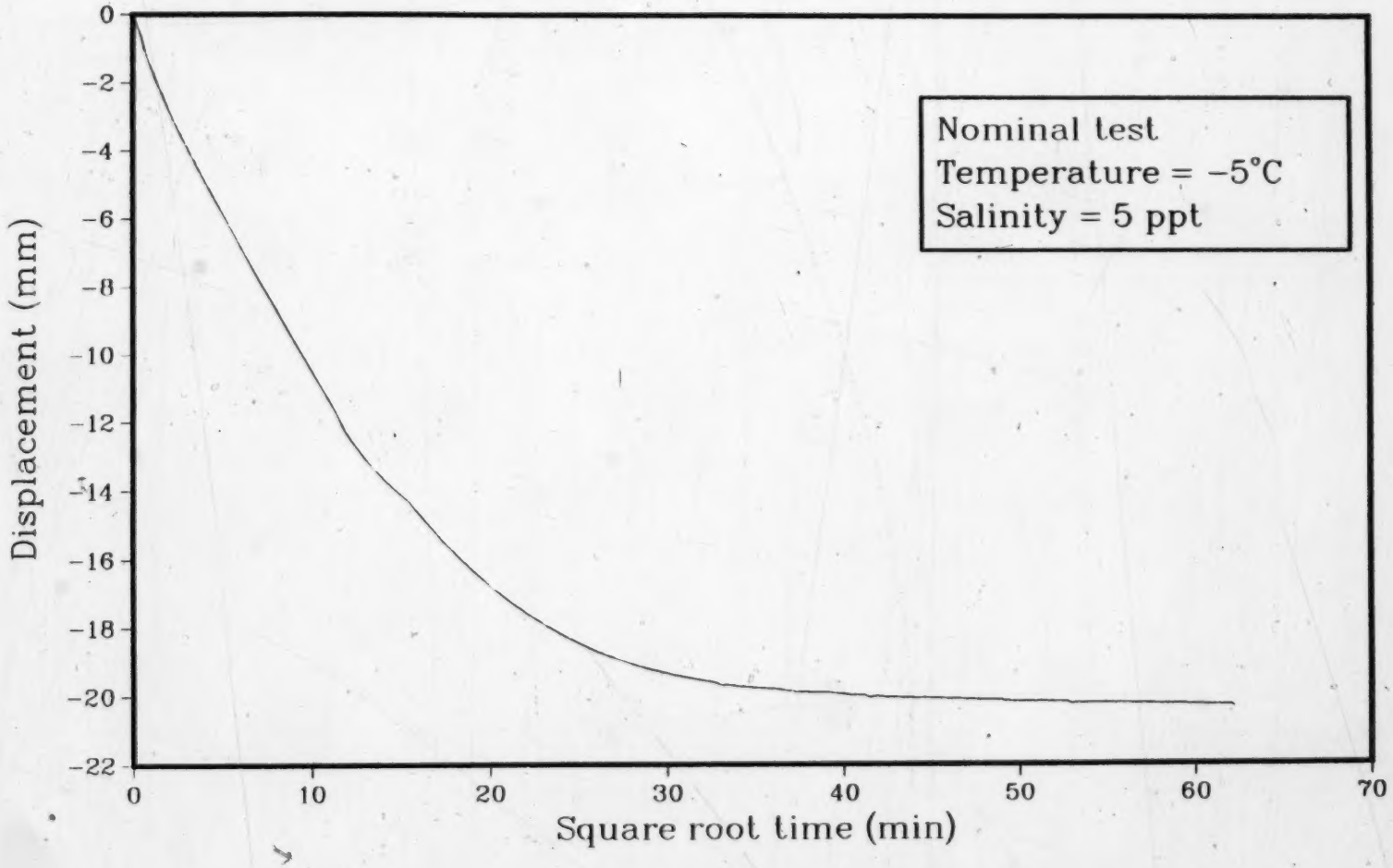

Figure A.64: Consolidation of silty sand sample 4.1

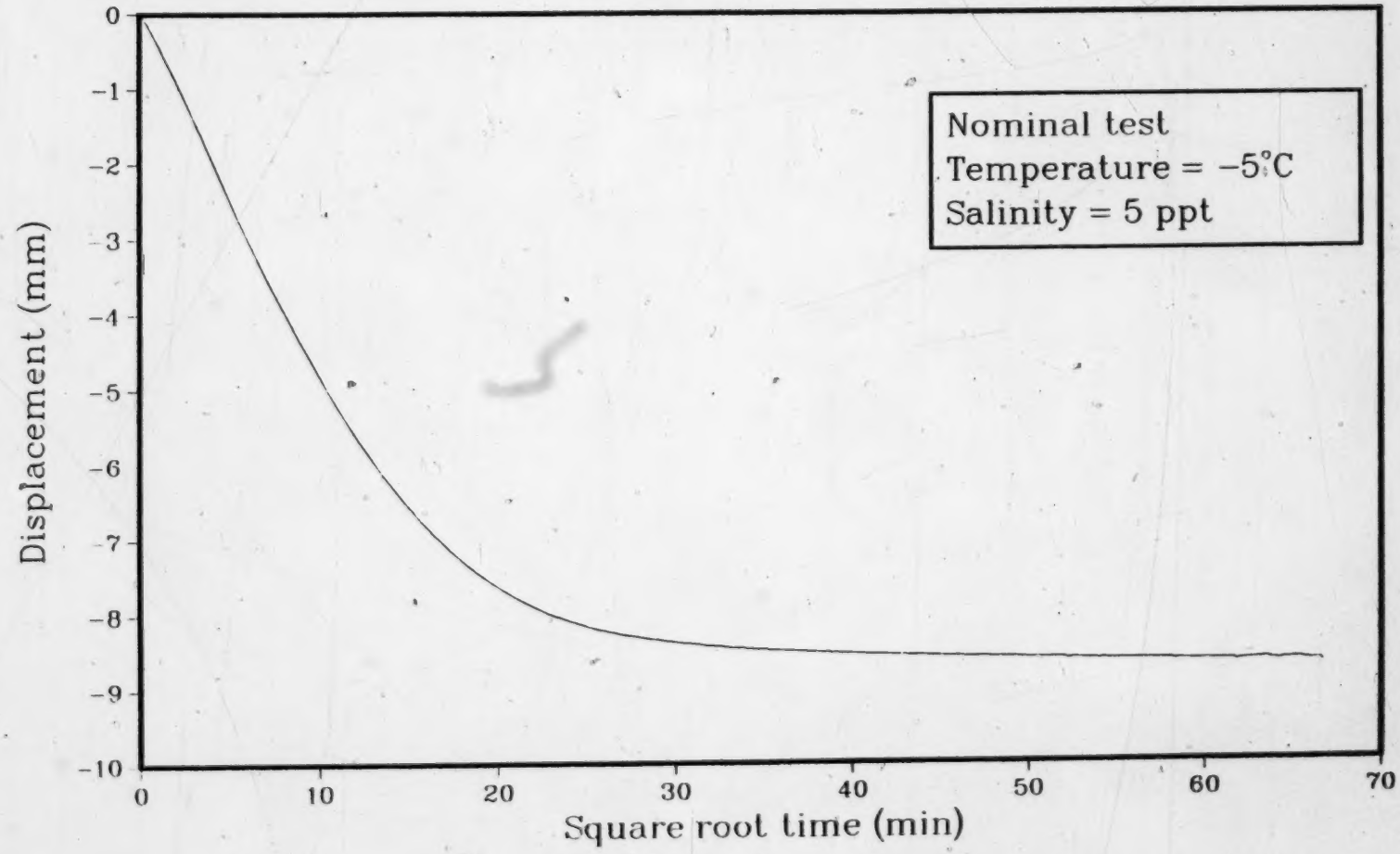

Figure A.65: Consolidation of silty sand sample 4.2

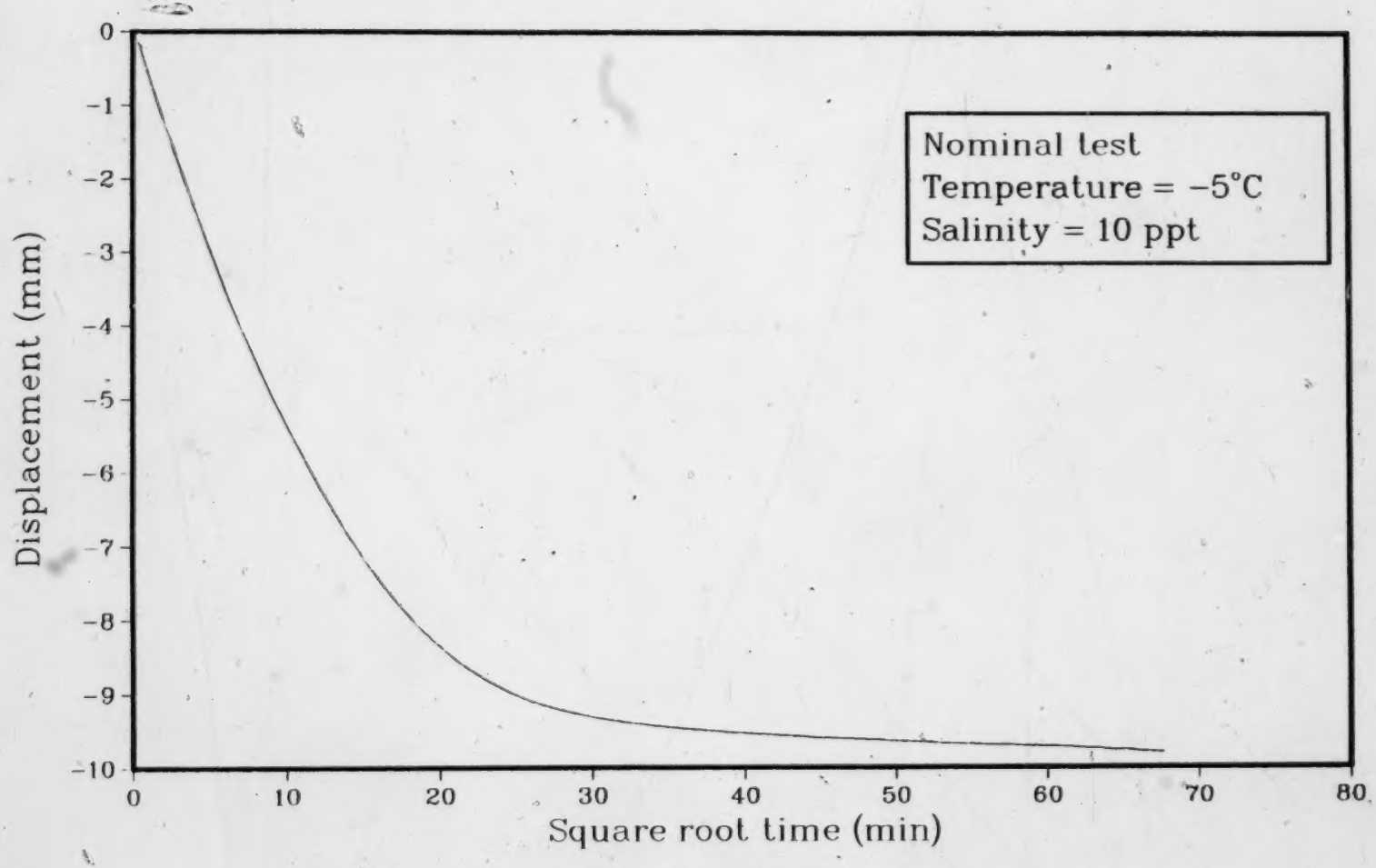

Figure A.66: Consolidation of silty sand sample 4.3

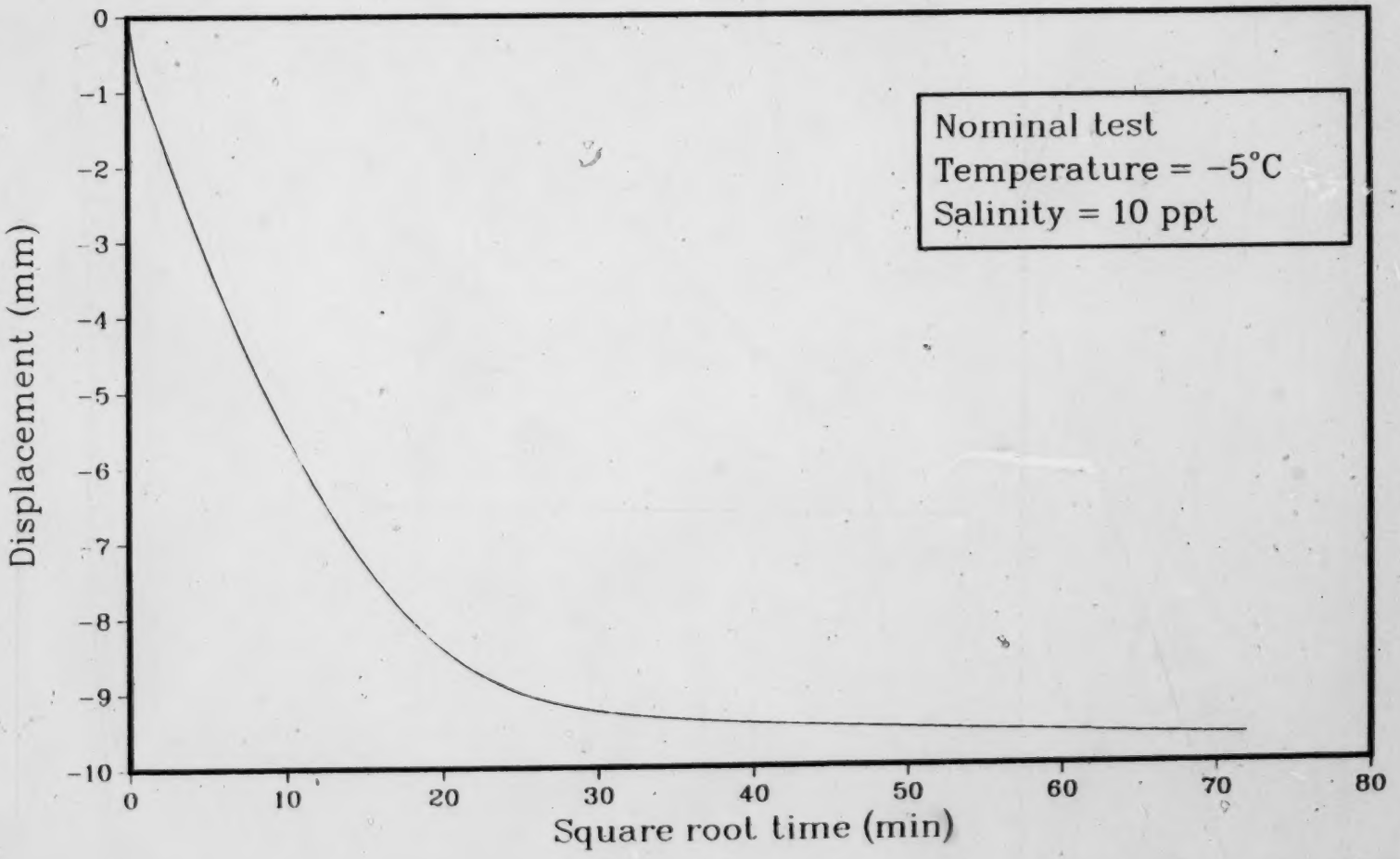

Figure A.67: Consolidation of silty sand sample 4.4

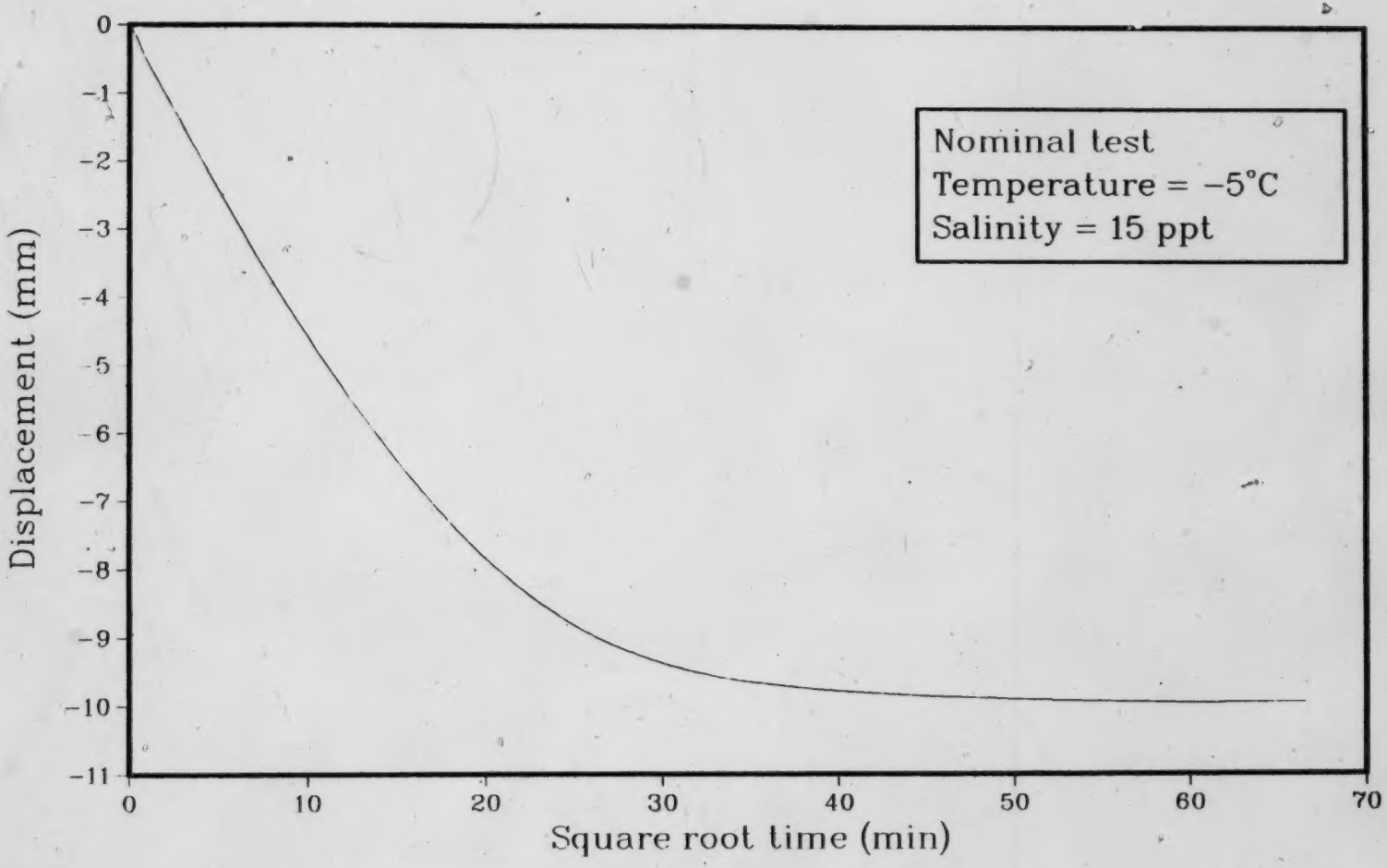

Figure A.68: Consolidation of silty sand sample 4.5

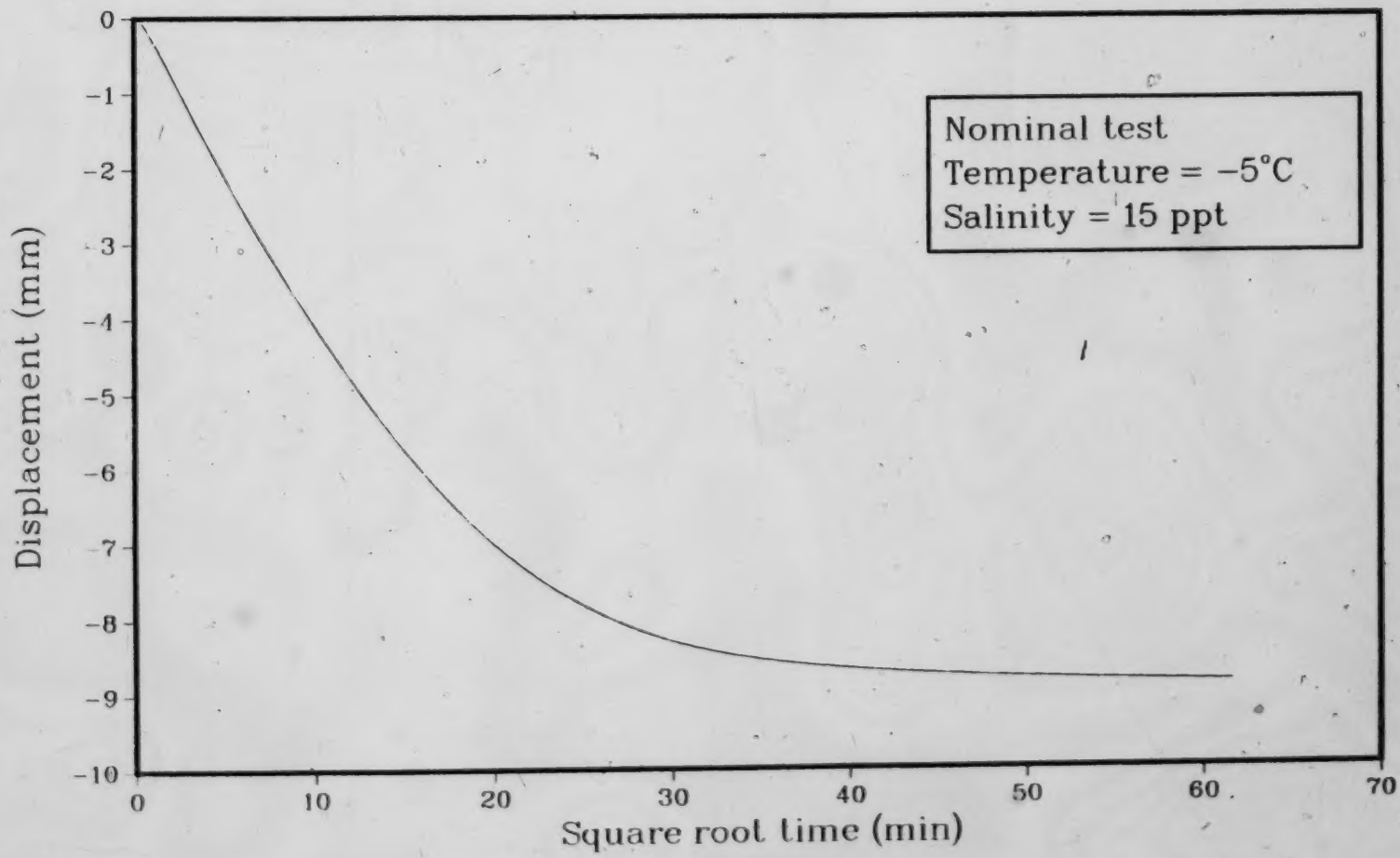

Figure A.69: Consolidation of silty sand sample 4.6

B. Appendix B
Photographs

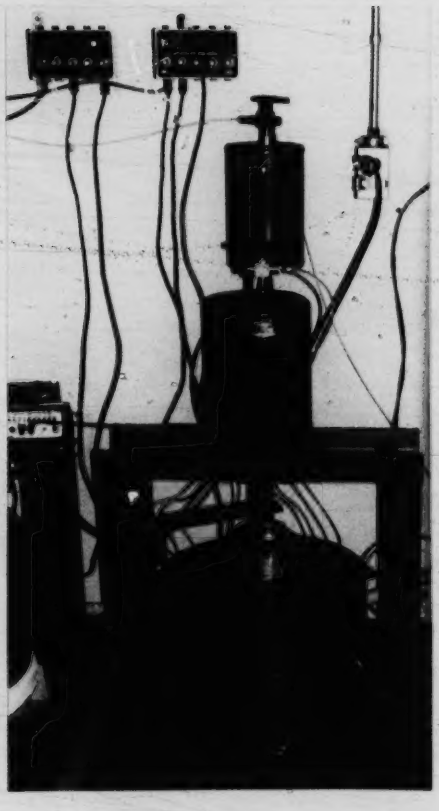

Figure B.1 Consolidation of the soil

Figure B.2 Application of load to the pile

Figure B.3 Pile in Frozen Soil

C. *Appendix C*
Detailed Laboratory Procedure for Testing of Model Piles

C.1 Introduction

The schematic of the apparatus used in this series of experiments is shown in Figure 4.2. Details of the bucket are given in Figure 4.3 and Figure 4.4 shows the apparatus used to freeze the sample.

C.2 Material Preparation

The soil mixture for these tests was chosen to be comparable to soil found beneath the Arctic communities of Pond Inlet, Tuktoyaktuk, Pangnintung and Eskimo Point. The grain size curves for these soils were provided by Mr. Bruce Smith of Thurber Consultants. The average grain size distribution curve of the clean silty sand used in these experiments is shown in Figure 4.1.

C.2.1 Dry Soil Preparation

1. Dry silty sand from Devon and mortar sand from Deep Water Silica in a 55°C oven.
2. Grind the silty sand.
3. Shake the sand through a No 10 seive to break up the soil lumps.
4. Combine the soils in equal parts by weight.
5. Store the soil mixture in a dry bin.

C.2.2 Wet Soil Preparation

1. Place the dry soil in a heavy duty soil mixer.
2. Mix distilled water with the amount of pure sodium chloride required to give the desired salinity.
3. Add the water to the dry soil in approximate proportions: 2 liters to 0.01 m^3 of soil, giving a workable stiff mixture. For ease in mixing, no more than this volume of soil should be placed in the large mixer bowl at one time.
4. Place the wet soil in the buckets as discussed below, or place in plastic buckets with lids to seal and store in the moisture room until ready for use.

C.2.3 Pile Preparation

1. Sand blast the piles, keeping the bottom 2 cm smooth.
2. Profile the piles using a Hobson Talysurf profiler to determine the average roughness.

C.3 Bucket Preparation

1. Clean the buckets prior to each use.
2. Insert the teflon collar into the base of the bucket. Grease all parts of the collar in contact with metal with silicon grease. For the first group of tests at -12°C the teflon collar was inserted from the top of the bucket and so was in contact with the pile throughout the loading procedure. Thereafter, the collar was placed into the base of the bucket from the outside thereby becoming removable.
3. Insert the pile into the teflon collar with the smooth end down. Ensure that the base of the pile is liberally coated with silicon grease.
4. Center the top of pile using the centering collar.
5. Cut a sheet of filter paper to cover the walls of the inner bucket. Cut vertical slots in the paper to facilitate drainage of the expelled pore fluid.
6. Stick the filter paper to the inside of the bucket by wetting it slightly.

C.4 Soil Placement

1. Place the wet soil a spoonfull at a time into the bucket, keeping the surface of the soil horizontal by filling around the pile evenly.
2. Place the contents of one mixer bowl at a time, about 1/3 of the total bucket volume, then rod the soil to remove air pockets.
3. Cut a circle from a double layer of filter paper to fit within the walls of the inner chamber with a hole in the middle to allow the pile to protrude through.
4. Move the bucket to the 0°C cold room and lower into the frame, ensuring that the bucket and pile are resting on a level, smooth surface.
5. Ensure that the pile top is centered and remove the centering bar.
6. Place the circles of filter paper on top of the soil.
7. Insert the pile load cap, to cover the top of the hollow pile.
8. Pour a level 3 cm thick pad of fine sand around the pile, on top of the filter paper.
9. Leave the bucket in the cold room for at least 24 hours, to allow for even distribution of moisture content throughout the soil, self-weight consolidation and stabilization of the soil to 0 °C.

C.5 Consolidation

1. Center the consolidation load plate on top of the sand layer.
2. Place the dimpled load cap and ball bearing on the top of the consolidation plate collar.
3. Attach the LVDT collar to the protruding Bellofram ram.
4. Screw the load cell onto the Bellofram ram and record

the zero voltage reading.
5. Lower the ram until the load cell just touches the ball bearing.
6. Position the LVDT in the collar so that the voltage output is within the linear range and record the zero voltage reading.
7. Set the air pressure to provide an 80 kPa consolidation pressure.
8. Commence data logging, monitoring the time, load and deflection for each bucket.
9. Open the valve at the top of the Bellofram to begin the consolidation process.
10. Monitor the load and deformation until 95% consolidation is achieved.

C.6 Freezing

1. Remove the consolidation pressure by reducing the air pressure to 0 kPa.
2. Remove the LVDT core and retract the Bellofram ram.
3. Remove the consolidation load plate.
4. Zero the RTDs in a bath of ice and water.
5. Insert the short, medium and long RTDs into the soil through the sand layer.
6. Remove the sand around the top of the pile and measure the depth of the silty sand below the top of the pile.
7. Lift the bucket using a crane and place the freezing plate below the bucket.
8. Attach the liquid nitrogen dewar to the inlet of the freezing plate and the outlet of the plate to the cold room exhaust system.
9. Apply low air pressure to the dewar to force the flow of liquid nitrogen through the plate.
10. To prevent wastage of the liquid nitrogen, place a 3 psi check valve at the end of the exhaust line.
11. Allow the liquid nitrogen to flow through the plate until the RTDs indicate that the soil is completely frozen.
12. Once the plate has warmed up, lift the bucket, remove the plate and lower the bucket onto the smooth surface of the frame.

C.7 Establishing Temperature Equilibrium

1. When all of the samples are frozen, set the cold room to approximately -15°C.
2. Allow the samples to equilibrate to the room temperature for 24 hours.
3. Invert the buckets and remove the teflon base collar.
4. Set the cold room to the desired test temperature. Leave the samples for a further 24 hours to allow for temperature equilibration.
5. Ensure that sufficient diluted glycol is stored in the room for at least these 24 hours as well.

6. Using the crane to lift the frozen samples, place the cedar base plates under the buckets. Ensure that the bottom of the pile is aligned with the hole in the base plate.
7. Pour the glycol into the reservior in each bucket.
8. Attach the ends of the copper coil circulation system to the inlet and outlet tubes on the temperature bath.
9. Set the bath controls to the desired temperature and begin fluid circulation.
10. When the RTDs indicate that the samples have stabilized at the test temperature, begin the loading procedure.

C.8 Loading

1. Place the ball bearing on the pile cap.
2. Record the load cell zero voltage.
3. Lower the ram until the load cell is just touching the ball bearing.
4. Position the LVDT within the linear output range, and record the zero reading.
5. Commence data logging monitoring the time, load, displacement, and temperature. Take readings more frequently at the beginning of each load step to ensure adequate data is available for the analysis of primary creep.
6. Calculate the pressure required to load the pile, and set the air pressure using the pressure transducer.
7. Open the valve at the top of the Bellofram.
8. Continue to apply the load steps until failure is indicated by the acceleration of the pile displacement rate.

C.9 Removal of Frozen Soil

1. Remove the LVDT core, retract the ram, unplug the RTDs and remove the pile cap.
2. Using the crane, lift the bucket from the frame, empty the glycol, and lower it onto the trolley.
3. Remove the bucket from the cold room.
4. Circulate warm water through the reservoir surrounding the soil. Once the outer edge of the soil has melted, remove the block of soil from the bucket.
5. Store the soil block in the -25°C cold room overnight.
6. Using a rock saw, cut a wedge of soil from the length of the sample.
7. Wrap the wedge of soil in plastic wrap to prevent ablation of the pore ice, and store in a freezer.
8. Place the remaining soil into a plastic bucket with a sealing lid.
9. Cover the excavated soil in the plastic bucket with water of the same salinity.
10. Store the plastic buckets in the moisture room.
11. Mix the soil and water thoroughly by hand before placing it in the pile test bucket again.

C.10 Measurement of Soil Characteristics

1. Saw the frozen wedge of soil into six slabs. Place all slabs into tightly sealed plastic bags.
2. Store one set in the 4°C moisture room overnight, to allow them to thaw for salinity measurements, and the other set in the -25°C cold room for density measurements.
3. For the salinity measurements, place the thawed soil into the pore water extraction cell. It is imperative that the cell be completely dry and clean prior to use.
4. Apply a small, constant pressure to the ram in the cell.
5. Using a syringe, collect all pore water extracted.
6. Seal the syringe, and store with the needle pointing up, to allow the suspended soil particles to settle out.
7. Once the pore water is clear, use the hand refractometer to determine the salinity.